The Human Coronavirus Nucleocapsid Protein and Its Effects on the Innate Immune Response

The Human Coronavirus Nucleocapsid Protein and Its Effects on the Innate Immune Response

By

Frances W. Lai, B.Sc., M.Sc.

A Thesis Submitted to the School of Graduate Studies in Partial Fulfillment of the Requirements for the Degree of Doctor of Philosophy

McMaster University

DOCTOR OF PHILOSOPHY (2013) McMaster University

(Medical Sciences) Hamilton, Ontario

TITLE:	The Human Coronavirus Nucleocapsid Protein and Its Effects on the Innate Immune Response
AUTHOR:	Frances W. Lai, B.Sc. (McMaster University), M.Sc. (University of Guelph)
SUPERVISOR:	Dr. Brian D. Lichty
NUMBER OF PAGES:	xiii, 192

ABSTRACT

Coronaviruses are the largest known RNA viruses and infect a wide range of hosts. Human coronaviruses traditionally have been known to be the cause of the common cold and have been vastly understudied due to low morbidity and mortality. The emergence of SARS-CoV and MERS-CoV has altered the landscape of coronavirus research and proven the deadly capabilities of human coronaviruses. With two recent zoonotic events, it is increasingly important to understand the molecular biology of human coronaviruses. The coronavirus nucleocapsid protein is an essential structural protein that complexes with the viral genome. Though nucleocapsid formation is the protein's major role, it has also been found to have other functions and effects during infection. The following research aimed to examine how the human coronavirus nucleocapsid protein affects the innate immune response *in vitro*. Modulation of the type I interferon response by the nucleocapsid was first investigated and the nucleocapsids were shown to have the ability to block interferon signalling. Additionally, the nucleocapsid protein was found to cause a dysregulation of transcription factor NFKB1. We propose a novel mechanism of this NFKB1 negative regulation interference. Taken together, we have further characterized the significant role of the coronavirus nucleocapsid protein in innate immune evasion.

ACKNOWLEDGEMENTS

There are many people who have supported me throughout this long journey and deserve my utmost thanks. Although it has been a bumpy road, it was filled with fantastic scenery along the way.

First and foremost, to my supervisor Dr. Brian Lichty, I thank you for all of your continual support over the past several years. I believe that my academic experience would not have been complete without mentoring from someone as intelligent, thought-provoking, and helpful as you. I will never forget all of the mind-bending analogies (or the majority of them, because there were so many) that nobody else would have ever thought of but made so much sense.

To my committee members Drs. Karen Mossman and James Mahony, thank you for all of your ideas and support year after year. As anxious as I was for every meeting, I always came out of them with an enhanced energy for my research. Thank you also to Dr. Dawn Bowdish for taking the time out of your busy schedule to learn about microvesicles with me. Your mentoring during our extended course was invaluable. Karen and Dawn, you are both great inspirations for women in science everywhere.

To my friends and colleagues in the CGT/MIRC, you genuinely made this lengthy journey a more enjoyable experience. I feel truly lucky to have worked alongside countless talented and intellectual people, and to have made so many good friends. Thank you to my labmates Kyle Stephenson, Steve Hanson and Jo Pol for so many laughs (usually at Kyle's expense) and for multitudinous instances of experiment triage. Thank you to Marianne Chew, Amy Gillgrass, Nicole Barra, Amanda Lee, Tamara Krneta, Sarah Reid-Yu, Ryan Shaler, Sarah McCormick, Vera Tang, and Melissa Lawson. Thank you for many cumulative hours of fantastic conversation leading to outrageous (as well as occasionally viable) ideas, both scientific and otherwise. Thank you for your constant cheerleading, complaint listening, and above all, your continual friendship. I could not have made it out with the majority of my sanity had it not been for all of you.

To my parents, Patrick and Elaine Lai, I would not be where I am today without your love and support. Each day, I hope that I have made you proud. Thank you ever so much for equipping me the tools and knowledge that (I hope) have made me a proficient adult. I am also thankful to my grandmother King Chee Lai, who although did not get to see me finish this degree, valued education greatly.

Thank you also to my thesis writing companion Poppy the Great Dane. Lastly, to my husband Graham Stanclik, thank you for sticking with me throughout this adventure. Your love and patience has been above and beyond what anyone could ever ask for. I am truly the lucky one.

TABLE OF CONTENTS

FIGURES AND TABLES

LIST OF ABBREVIATIONS

$3CL^{pro}$	3C-like cysteine protease
α-MEM	Alpha modified Eagle's medium
ACE2	Angiotensin-converting enzyme 2
ADAR	Adenosine deaminase acting on RNA
Ago2	Argonaute 2
APN	Aminopeptidase N
APOBEC3	Apolipoprotein B mRNA-editing enzyme catalytic polypeptide 3
ATCC	American Type Culture Collection
β-gal	Betagalactosidase
BAFF	B-cell activating factor
BAFFR	B-cell activating factor receptor
BCoV	Bovine coronavirus
CARD	Caspase recruitment domain
Cardiff	CARD adaptor inducing IFN-β
CBP	CREB-binding protein
CMV	Cytomegalovirus
CoV	Coronavirus
COX-2	Cyclooxygenase 2
CPE	Cytopathic effects
CTD	C-terminal domain
DAI	DNA-dependent activator of IFN-regulatory factors
d.p.i.	Days post infection
DGCR8	DiGeorge critical region 8
DMEM	Dulbecco's modified Eagle's medium
ds	Double-stranded
E	Envelope
EBV	Epstein Barr virus
EF	Elongation factor
eIF2	Eukaryotic initiation factor 2
ELAM1	Endothelial leukocyte adhesion molecule 1
ER	Endoplasmic reticulum
FADD	Fas associated death domain
FBS	Fetal bovine serum
FIPV	Feline infectious peritonitis virus
G	Glycoprotein
GFP	Green fluorescent protein
GRR	Glycine rich region
HCoV	Human coronaviruses
HCoV-EMC	HCoV Erasmus Medical Center

HCV	Hepatitis C virus
HDAC3	Histone deacetylase 3
HE	Hemagglutinin-esterase
HIV	Human immunodeficiency virus
hnRNP U	Heterogeneous ribonucleoprotein U
HSV	Herpes simplex virus
IBV	Infectious bronchitis virus
ICAM1	Intercellular adhesion molecule 1
IFIT	Interferon-induced proteins with tetratricopeptide repeats
IFN	Interferon
IFNAR1	IFN-α receptor 1
IFNAR2	IFN-α receptor 2
IkBa	Inhibitor of NF-kB alpha
IKK	IκB kinase
IKKi	Inhibitor of NF-κB kinase
IL	Interleukin
iNOS	Inducible nitric oxide synthase
IPS-I	Interferon-beta promoter stimulator 1
IRAK	IL-1 receptor associated kinase
IRF	Interferon regulatory factor
ISG15	Interferon stimulated gene 15
ISGs	IFN-stimulated genes
ISGF3	IFN-stimulated gene factor 3
ISRE	Interferon stimulated response element
IκB	Inhibitor of NF-κB
JAK	Janus Kinase
kDa	Kilodaltons
KSHV	Karposi’s sarcoma-associated herpesvirus
LGP2	Laboratory of Genetics and Physiology 2
LMP1	Latent membrane protein 1
LPS	Lipopolysaccharide
LRR	Leucine-rich region
LRRFIP1	Leucine-rich flightless-interacting proteins 1
LTBR	Lymphotoxin β receptor
LTβ	Lymphotoxin β
Lys	Lysine
M	Membrane
MAVS	Mitochondrial antiviral signalling
MCP-1	Monocyte chemotactic protein 1
MDA5	Melanoma differentiation-associated gene 5

MERS-CoV	Middle Eastern respiratory syndrome coronavirus
MHC I C	Major histocompatibility complex class I C
MHV	Murine hepatitis virus
MIP-1α	Macrophage inflammatory protein 1 alpha
miR-9	microRNA -9
miRNA	microRNA
MOI	Multiplicity of infection
M^{pro}	Main protease
mRNA	Messenger RNA
Mx	Orthomyxovirus resistance protein
MyD88	Myeloid differentiation marker 88
N	Nucleocapsid
NEMO	NF-κB essential modulator
NF-kB	Nuclear factor kappa B
NIK	NF-κB inducing kinase
NK	Natural Killer
NLS	Nuclear localization signal
nm	Nanometer
nsp	Nonstructrual protein
NTD	N-terminal domain
OAS	2’-5’ oligodenylate synthetase
ORFs	Open reading frames
PACT	Protein activator of the IFN-induced protein kinase
PAMPs	Pathogen-associated molecular patterns
PKR	Protein kinase regulated by RNA
PLA2	Phospholipase 2
PLP	Papain-like protease
poly(I:C)	Polyinosinic:polycytidylic acid
pre-miRNA	Precursor miRNA
pri-miRNA	Primary miRNA
PRRs	Pattern recognition receptors
PRRSV	Porcine reproductive and respiratory virus
RANTES	Regulated on activation, normal T cell expressed and secreted
RdRp	RNA-dependent RNA polymerase
RHD	Rel-homology domain
RIG-I	Retinoic acid inducible gene I
RIP	RNA-Immunoprecipitation
RIP1	Receptor interacting protein 1
RIPA	Radioimmunoprecipitation assay
RISC	RNA-induced silencing complex

RLRs	Retinoic acid inducible gene I-like receptors
RNA	Ribonucleic acid
RPMI	Roswell Park Memorial Institute medium
S	Spike
SARS-CoV	Severe acute respiratory syndrome-related coronavirus
SD junction	ssRNA-dsRNA junction
Ser	Serine
sg mRNA	Subgenomic mRNA
SGR	Serine-glycine-arginine-rich region
siRNAs	Small interfering RNAs
SMRT	Silencing mediator of retinoic acid and thyroid hormone receptor
SRD	Serine-arginine-rich domain
SS	Single-stranded
STAT	Signal transducers and activators of transcription
TAB	TAK1-binding protein
TADs	Transactivation domains
TAK1	TGF-β activating kinase 1
TANK	TRAF family member-associated NF-κB-activator
TAR	Trans-activation responsive element
TBK1	TANK-binding kinase 1
TBS	Tris-buffered saline
TCoV	Turkey coronavirus
TGEV	Porcine transmissible gastroenteritis virus
TIR	Toll-interleukin 1 receptor
TLRs	Toll-like receptors
TNFAIP3	TNF-α induced protein 3
TNFR	TNF-α receptor
TNF-α	Tumor necrosis factor alpha
TRAF	TNF receptor-associated factor
TRBP	TAR RNA-binding protein 2
TRIF	TIR-domain-containing adaptor-inducing IFN-β
TRIM	Tripartite motif-containing
TRS	Transcription regulatory sequence
TYK1	Tyrosine kinase 1
UTR	Untranslated region
VCAM1	Vascular cell adhesion molecule 1
VISA	Virus-induced signaling adaptor
VSV	Vesicular stomatitis virus
WNV	West Nile virus
YB1	Y-box binding protein

DECLARATION OF ACADEMIC ACHIEVEMENT

Work described in Chapter 3 has been published as the following:

Frances Lai, Natasha Kazdhan, and Brian D. Lichty. (2008) Using G-deleted vesicular stomatitis virus to probe the innate anti-viral response. Journal of Virological Methods. 153:276-279.

Work in Chapter 3 was presented at the following:

American Society for Virology, 28th Annual Meeting, July 11-15 2009, The University of British Columbia. Abstract Number 915, Board number P12-23. Modulation of antiviral response by human coronavirus nucleocapsid proteins.

Work described in Chapter 4 has been submitted for publication as the following:

Frances Lai, Kyle Stephenson, James Mahony, and Brian D. Lichty. (2013) Human Coronavirus OC43 nucleocapsid protein binds microRNA miR-9 and potentiates NF-κB activation. Journal of Virology (*submitted*).

Chapter 1
Review of Literature

1.1 - The Coronavirus

1.1.1 - Classification and Discoveries

The family *Coronaviridae* is classified in the order *Nidovirales* and contains a vast array of viruses which infect many animals, including cows, poultry, and humans. The order *Nidovirales* also contains the families *Arteriviridae*, *Mesoniviridae*, and *Roniviridae*. *Coronaviridae* is further classified into two subfamilies: *Coronavirinae* and *Torovirinae*. While *Torovirinae* contains a mere two genera with five species of viruses, *Coronavirinae* encompasses 20 species categorized into four genera- *Alphacoronavirus*, *Betacoronavirus*, *Deltacoronavirus*, and *Gammacoronavirus* (Table 1). *Alphacoronavirus*, *Betacoronavirus*, and *Gammacoronavirus* were recently reclassified by the International Committee for Virus Taxonomy from Groups I, II, and III, respectively. Coronaviruses (CoV) are classified according to genetic sequence and antigenicity (1). The alphacoronavirus genus contains the human tropic 229E and NL63 as well as feline infectious peritonitis virus (FIPV) and porcine transmissible gastroenteritis virus (TGEV) which infect cats and pigs, respectively. The remaining human coronaviruses (HCoV) belong to the *Betacoronavirus* genus, including prototypic HCoV OC43 which was recently reclassified as the species Betacoronavirus 1, merging with Bovine coronavirus (BCoV), Human enteric coronavirus, and porcine hemagglutinating encephalomyelitis virus. The remaining HCoVs in the *Betacoronavirus* genus are severe acute respiratory syndrome-related coronavirus (SARS-CoV) and HKU1. The betacoronavirus genus also contains the well-studied murine hepatitis virus (MHV), also known as murine coronavirus. The *Gammacoronavirus* genus contains two poultry viruses, infectious bronchitis virus (IBV) and turkey coronavirus (TCoV) (2). The newest genus, *Deltacoronavirus*, contains several recently discovered avian coronavirus species (3).

Prototypic human coronaviruses OC43 and 229E were first isolated in the 1960's (4-6). OC43 was cultured from laboratory staff that had symptoms of the common cold (5). When the virus was characterized, it was found to be morphologically similar to IBV and had an ability to cause encephalitis in newborn mice (5). Similarly, 229E was isolated from medical students with upper respiratory disease (6). It has been speculated that OC43 split from BCoV quite recently in the late 1800's due to the high sequence similarity between the two viruses (7). This is a prime example of a coronavirus breaking the species barrier, with SARS-CoV being a recent and the most infamous of cross-species jumping. 2003 saw the emergence of SARS-CoV, with higher mortality and

Table 1. Viruses within the Coronaviridae family and their host species.

Genus	Virus	Host
Alphacoronavirus	Alphacoronavirus 1 (Feline coronavirus, Transmissible gastroeneteritis virus)	Cat, pig
	Human Coronavirus 229E	Human
	Human Coronavirus NL63	Human
	Miniopterus bat coronavirus 1	Bat
	Miniopterus bat coronavirus HKU8	Bat
	Porcine epidemic diarrhea virus	Pig
	Rhinolophus bat coronavirus HKU2	Bat
	Scotophilus bat coronavirus 512	Bat
Betacoronavirus	Betacoronavirus 1 (Human Coronavirus OC43, Bovine coronavirus, Human enteric coronavirus, Porcine hemagglutinating encephalomyelitis virus, Equine coronavirus)	Human, cow, pig, horse
	Human Coronavirus HKU1	Human
	Murine coronavirus	Mouse
	Pipistrellus bat coronavirus HKU5	Bat
	Rousettus bat coronavirus HKU9	Bat
	SARS-CoV	Human
	Tylonycteris bat coronavirus HKU4	Bat
Deltacoronavirus	Bulbul coronavirus HKU11	Bird
	Munia coronavirus HKU13	Bird
	Thrush coronavirus HKU12	Bird
Gammacoronavirus	Avian coronavirus (Infectious bronchitis virus, Pheasant coronavirus, Turkey coronavirus, Duck coronavirus, Goose coronavirus, Pigeon coronavirus)	Bird
	Beluga whale coronavirus SW1	Whale

morbidity rates than the conventional cold viruses (8, 9). SARS-CoV originated from bats and infected the first human in Guangdong province, China (10, 11). More recently, human coronaviruses NL63 and HKU1 were identified during the surge of post-SARS coronavirus research (12-14). NL63 was isolated from a young child who was suffering from bronchiolitis in the Netherlands and HKU1 was originally isolated from an elderly man in Hong Kong suffering from pneumonia (13, 14).

In mid-2012 a new coronavirus was isolated from a patient in Saudi Arabia displaying similar symptoms to that of SARS-CoV (15). The HCoV-EMC virus, named after Erasmus Medical Center in the Netherlands where virus was characterized, was identified as a genetically novel coronavirus unrelated to SARS-CoV and classified as a betacoronavirus (15, 16). As of mid-2013, 58 laboratory confirmed cases of HCoV-EMC, also known as Middle Eastern respiratory syndrome coronavirus (MERS-CoV), infection had been reported to the World Health Organization with 33 cases resulting in death (17, 18). As this virus is a recently emerging pathogen and little is known of MERS-CoV, it will not be further discussed in this body of work.

1.1.2. The Virion and Genome

The CoV virion is spherical and enveloped with an average diameter between 100 and 160 nm (Figure 1). The particle's appearance is distinctively crown-like, hence the origin of the family name, as it presents protruding structures consisting of spike protein (S) peplomers. Other structural proteins found in the viral envelope are the membrane (M) protein, envelope (E) protein, and in some betacoronaviruses including OC43 and HKU1, hemagglutinin-esterase (HE) protein. The host-derived envelope encloses a helical nucleocapsid, which consists of the RNA genome complexed with the nucleocapsid protein (N) (2). The nucleocapsid forms long tubular strands when released from the virion by detergent treatment (19).

Coronaviruses are the largest known RNA virus and contain a single-stranded RNA (ssRNA) genome, with HCoV genomes ranging between 27 and 30 kb in size (Figure 2). All HCoV contain 5' and 3' untranslated regions and have similarly organized genomes, with nonstructural protein open reading frames (ORFs) located at the 5' end of the genome which is capped and four ORFs encoding structural proteins (the aforementioned S, M, E, and N) at the 3' end. All HCoV also encode accessory genes, which are variably interspersed

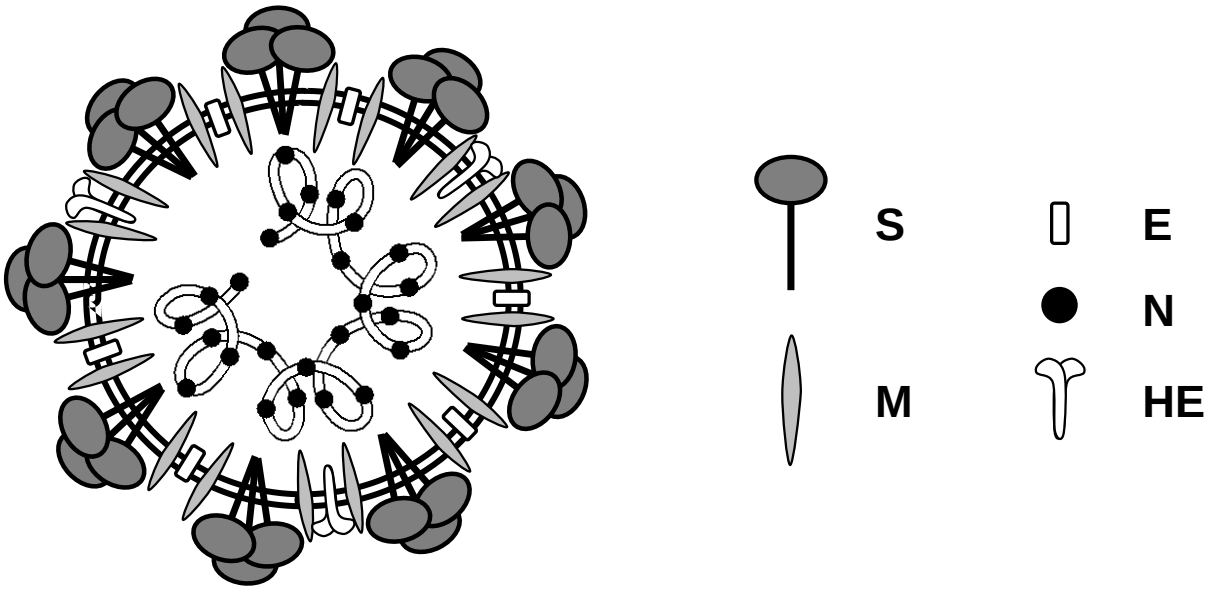
S
E
N
M
HE

Figure 1. Schematic representation of a coronavirus virion.

The spherical particle consists of an envelope embedded with several viral glycoproteins. The S protein forms trimers at the surface and is the most abundant viral protein. M and E are present in lesser quantities. HE can be found in some betacoronavirus particles. The envelope surrounds a helical nucleocapsid consisting of the N protein complexed with ssRNA genome. Figure modified from Field's Virology, 5th Ed. Chapter 36 *Coronaviridae* (20).

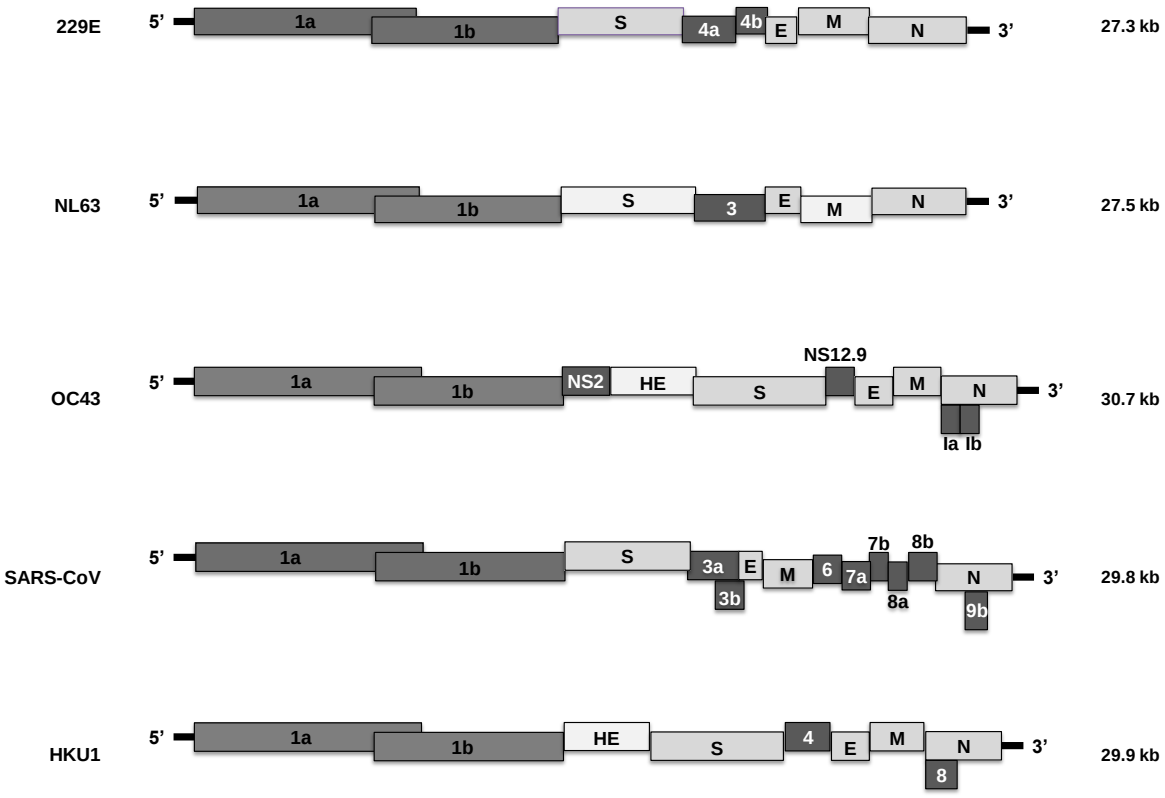
229E
5'
1a
1b
S
4a
4b
E
M
N
3'
27.3 kb
NL63
5'
1a
1b
S
3
E
M
N
3'
27.5 kb
OC43
5'
1a
1b
NS2
HE
S
NS12.9
E
M
N
3'
Ia Ib
30.7 kb
SARS-CoV
5'
1a
1b
S
3a
E
M
6
7a
7b
8a
8b
N
3'
3b
9b
29.8 kb
HKU1
5'
1a
1b
HE
S
4
E
M
N
3'
8
29.9 kb

Figure 2. Schematic representation of human coronavirus genome organization.

All genomes encode overlapping ORFs 1a and 1b and structural proteins spike (S), small envelope (E), membrane (M) and nucleocapsid (N). In addition, OC43 and HKU1 encode hemagglutinin-esterase (HE). Each genome contains small group-specific genes (dark gray shading). SARS-CoV encodes the most group-specific genes at 8, and NL63 only contains 1 group-specific gene. Figure modified from Field's Virology, 5th Ed. Chapter 36 *Coronaviridae*, Vijgen *et al.* (2005), and Perlman *et al.* (2009) (7, 20, 21).

amongst the structural ORFs (2). The small ORFs, while varying between groups of coronaviruses in size and number, are conserved within the group and are termed group-specific genes. These small proteins are generally not essential for virus replication (2). Although the organization is similar between HCoV genomes, there is relatively low sequence homology between the majority of HCoVs.

1.1.3. Structural and nonstructural proteins

The spike protein is a large glycoprotein between 180 and 200 kDa expressed in trimeric form on the surface of the virion (22, reviewed in 23). The type I transmembrane protein mediates binding to the cellular receptor and is a major determinant of host tropism (24-26). After receptor-mediated endocytosis, the subsequent fusion of the virion with the endosomal membrane is catalyzed by S (27-29). It is a class I fusion protein and can cause cell-cell fusion when expressed on the plasma membrane of infected cells (27).

The membrane protein is a small glycoprotein approximately 25 kDa in size located on the surface of the virion (30). Only a small portion of the protein is external to the virion and M contains three major hydrophobic transmembrane domains, resulting in a triple membrane spanning region (31). The M protein has been shown to interact with S, N, E, and M itself and appears to catalyze coronavirus envelope assembly (32-35). Mutations to M have been shown to abolish virion assembly and maturation (32).

The smallest structural protein is the envelope protein, a small integral membrane protein approximately 8 to 12 kDa in size with a single hydrophobic domain (reviewed in 36). The E protein is an ion channel, though the role of its activity is still under investigation (37, 38). It has been speculated that E's ion channel activity is vital in the virion egress through the secretory pathway as deletion of the gene in TGEV results in accumulation of virions in the Golgi (39). It appears that requirements for the E protein vary amongst coronaviruses, as E is not essential for SARS-CoV replication, but an E-deleted SARS-CoV grows to lower titers and is less virulent *in vivo* (40).

Only betacoronaviruses encode HE, and expression can even be variable in certain strains of CoV. The prime example of this inconsistency is MHV, as lab strain A59 lacks HE but neurovirulent strain JHM expresses HE (41). The 70 kDa protein forms disulfide-linked dimers on the virion surface and is thought to play a role in viral entry to the cell (42). In BCoV, HE alone is not sufficient for entry, which appears to rely solely on the S protein (43). Reports have recently been

made, however, that it is necessary for viral entry in HCoV OC43, as viruses lacking HE or containing an enzymatically inactive form of HE did not result in a productive infection (44). Conversely, recombinant A59 strains expressing HE from other MHV strains show reduced fitness compared to recombinant A59 that lacks HE or contains an enzymatically inactive HE, with the HE-containing strain quickly losing expression of HE in serial passaging of the virus (45). Interestingly, the CoV HE shares approximately 30% amino acid sequence homology to the hemagglutinin protein HA1 of influenza C and the CoV HE is speculated to be the product of a recombination event between CoV and influenza (46, 47). Similar to influenza, CoV HE binds to 9-O-acetylated neuraminic acid and possesses acetyl-esterase activity, allowing for reversible binding to sialic acid (48).

The nucleocapsid protein is an essential component to the virion and its primary function is to bind and encapsidate the RNA genome (49, reviewed in 50). The N protein is arguably the most well studied of the CoV structural proteins and will be further discussed in detail in section 1.2.

The nonstructural proteins (nsp) are encoded by a large ORF, ORF1a/b. Translation of this ORF is slightly unconventional as it contains an mRNA pseudoknot between ORF1a and ORF1b which facilitates a -1 ribosomal frameshift during translation (51). Cellular ribosomes translate ORF1a and terminate translation at the stop codon, but a slippery sequence followed by a structured RNA pseudoknot occasionally causes the ribosomes to “wobble” and shift -1 in the reading frame. This yields the ORF1ab polyprotein and both ORF1a and ORF1ab are then proteolytically cleaved into individual nonstructural proteins. The papain-like proteases (PLPs) PL1pro, PL2pro and 3C-like cysteine protease ($3CL^{pro}$), also known as main protease (M^{pro}) encoded within nsp3, nsp4, and nsp5, respectively, process the ORF1a and ORF1ab polyproteins (52, 53). Aside from PLPs, approximately 13 other nps are encoded in the ORF1ab polyprotein. While most CoV encode three PLPs, SARS and IBV only encode one: PLpro encoded in nsp (54, 55). Previously known as the X domain, an ADP-ribose 1”-phosphatase is encoded within nsp3 which is dispensable for replication *in vitro* (56-58). Like many RNA viruses, coronaviruses encode an RNA-dependent RNA polymerase (RdRp), encoded in nsp12 and utilized for genome transcription (7, 58-60). Coronaviruses also encode a 5’ to 3’ helicase in nsp13 and a 3’ to 5’ endonuclease in nsp14 (61-63). Another uridylate-specific endonuclease, NendoU, is encoded in nsp15 (7, 58). Coronavirus nsp16

encodes a 2'-O-methyltransferase, responsible for methylating viral RNA, producing a 5' cap (7, 64).

Lastly, coronaviruses encode a third group of proteins, known as group-specific proteins. Although the group-specific proteins are not necessary for viral replication, it is thought that they have an accessory function (65, 66). These accessory proteins are suspected to serve as virulence factors for the virus. Recent studies showed that when placed into an attenuated strain of MHV, SARS-CoV accessory protein 6 was able to cause an increase in virulence and hastened the progression of infection (67, 68). The group-specific gene 7 of TGEV has also been found to be nonessential for virus replication using a recombinant virus lacking gene 7 (69). This recombinant virus was also highly attenuated, indicating ORF7 had an effect on pathogenicity (69). Along with TGEV, FIPV has also been found to be highly attenuated in cats when clustered ORFs 3a, 3b, and 3c and ORFs 7a and 7b were deleted (70).

SARS-CoV encodes the largest number of accessory genes, at 8 genes interspersed amongst the structural ORFs (reviewed in 71, 72). These accessory genes have also been found to be beneficial for viral replication. Well studied SARS 7a has been shown to inhibit cellular protein synthesis and induces cell cycle arrest at G_0/G_1 (73, 74). SARS 3b also halts cell cycling at G_0/G_1 and additionally induces apoptosis (75). SARS ORF6 and ORF8b have both been found to upregulate DNA synthesis *in vitro* (76, 77). Lastly, SARS accessory protein 3a appears to upregulate intracellular fibrinogen expression in lung cells A549 as well as cause an increase in fibrinogen secretion (78). This is speculated to contribute to viral pathogenesis in the lungs *in vivo*.

1.1.4. Replication

The five HCoVs use a variety of different receptors to enter the target cell. The only two HCoV that utilize the same receptor are SARS-CoV and NL63, which both employ angiotensin-converting enzyme 2 (ACE2) (79, 80). OC43 binds to 9-O acetylated sialic acid and the remaining betacoronavirus HKU1 has been identified to bind major histocompatibility complex class I C (MHC I C) (48, 81). Lastly, the receptor for 229E is aminopeptidase N (APN), also known as CD13 (82).

The viruses enter by receptor mediated endocytosis and release the genome into the cytoplasm where the entire replication cycle occurs (Figure 3). As the positive strand genome contains a 5' cap, it serves as mRNA and initial translation of the nonstructural ORFs 1a and 1b occurs using cellular ribosomes

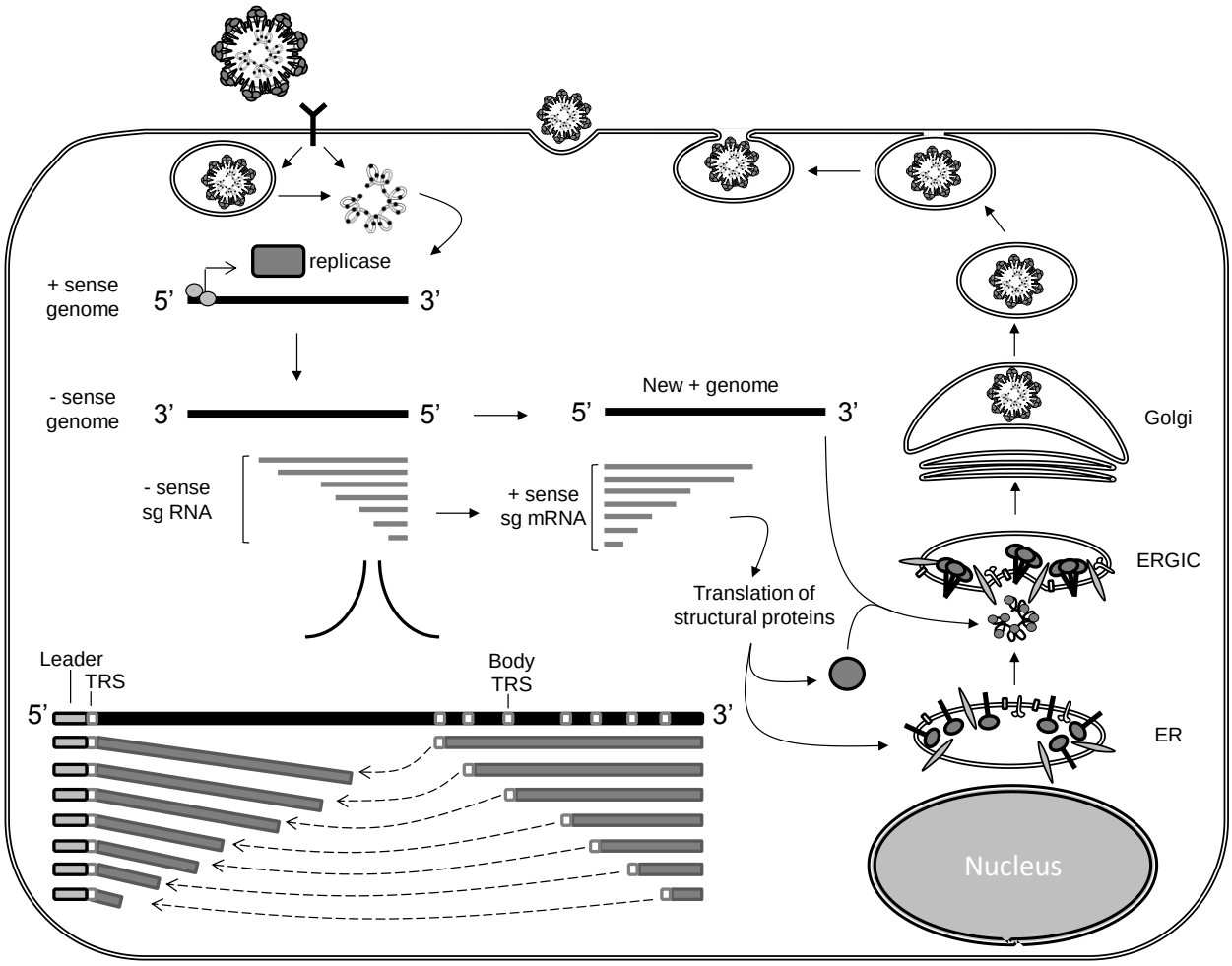
replicase
+ sense genome
5'
3'
- sense genome
3'
5'
5'
New + genome
3'
- sense sg RNA
+ sense sg mRNA
Translation of structural proteins
Leader
TRS
Body TRS
5'
3'
Golgi
ERGIC
ER
Nucleus

Figure 3. Schematic representation of the coronavirus replication cycle.

The coronavirus enters by receptor mediated entry resulting in either direct release of the nucleocapsid into the cytoplasm via fusion of the plasma membrane and viral envelope or release of the nucleocapsid following membrane fusion of the endosome and particle. The replicase proteins are initially translated, followed by negative sense genome and subgenomic (sg) mRNA. Negative sense sg RNA transcription is generated by discontinuous transcription. New positive sense genome and sg mRNA are transcribed from their negative strand counterparts. Translation of structural proteins from sg mRNA occurs, with all proteins except N then localizing to the secretory pathway organelles. N complexes with newly synthesized viral genome and buds into the ERGIC, acquiring its envelope. Egress from the cell occurs by exocytosis. TRS: transcription regulatory sequence. Figure modified from Field's Virology, 5th Ed. Chapter 36 *Coronaviridae* and Sawicki *et al.* (2007) (20, 83).

as discussed above. The viral replicase is encoded in the nonstructural ORFs and once translated, begins to transcribe an anti-sense or negative sense genome using the original positive sense genome as a template. This negative sense genome then serves as the template for new genome to be encapsidated by the nucleocapsid protein. Concurrent to this process of negative sense genome transcription, a unique process of subgenomic mRNA (sg mRNA) generation occurs via discontinuous transcription (Figure 3). The genome encodes a transcription regulatory sequence (TRS) between each structural ORF, as well as one at the 5' end of the genome. When transcription occurs from the genome, the viral RdRp encounters these TRS sequences and a certain proportion of the transcripts continue transcription, but some will terminate transcription at this point and relocate to the 5' TRS and leader sequence where it completes transcription. This process generates a nested set of negative stranded sg RNA which are then transcribed to produce a set of nested positive sg mRNA from which structural proteins are translated. The order was coined Nidovirales after this unique process, (nidus in Latin means nest) and is the method of replication for species within the order.

Once the structural proteins are translated, they enter the secretory pathway by embedding into the endoplasmic reticulum (ER) and Golgi membranes. Newly synthesized genome complexes with the nucleocapsid protein and the complex then buds into the ER where it acquires its viral protein-containing membrane. The new particles egress from the cells by exocytosis.

1.1.5. Coronavirus Pathogenesis and Immune Response

With the exception of SARS-CoV, infection with HCoV does not commonly cause severe disease. As a cause of the common cold, HCoV infection is widespread and usually seasonal, with occurrences mainly in the winter months (84). Respiratory disease, both upper and lower, is the main outcome of infection and disease can progress into pneumonia (85). Typical symptoms of OC43 and 229E infections include fever, rhinorrhea, bronchitis, and otitis media. Coronaviruses may also cause enteric and neurologic disease in animals and possibly humans (86).

Although considerably less mortality occurs with OC43 infection compared to SARS-CoV, morbidity can still be high and outbreaks of the virus can arise. Since 2000, several OC43 outbreaks that occurred in British Columbia, Canada, Normandy, France, and Melbourne, Australia have been analyzed (87-89). The outbreaks in Canada and Australia occurred in long term care facilities where the

majority of those infected were elderly residents. Deaths of residents did occur (8% of the infected patients in both outbreaks), but no infected staff succumbed to the infections. The majority of OC43 infected individuals in the Normandy outbreak were under the age of 2, illustrating that along with the elderly, these two populations are the most susceptible to increased morbidity with OC43 infection. In fact, a longitudinal study was recently published examining the frequency of HCoV infection in children (90). The majority of healthy (non-hospitalized) children tested within 24 months after birth were seropositive for OC43, followed closely by NL63 (90). Children who were hospitalized for respiratory infection tested positive for HCoV infection at a rate of 14%, with OC43 again being the predominant coronavirus, followed by NL63, HKU1, and 229E (90).

OC43 also has neurological implications in mice and is speculated to be linked to neurological disease in humans. Upon isolation in 1967, the virus was initially shown to replicate in the brain of mice and has repeatedly been shown to cause encephalitis upon serial passage in mice (91, 92). Although both OC43 and 229E have been detected in the brains of patients with multiple sclerosis, the link between HCoV infection and multiple sclerosis has remained ambiguous and controversial (93-95).

Aside from the neuroinvasive murine model of OC43 infection, few animal models of HCoV exist (with the exception of SARS-CoV). A transgenic mouse model of 229E infection was established with mice expressing human APN (96). Primary cells from these $APN^{+/+}$ mice were susceptible to 229E *in vitro*, but *in vivo* infections failed to result in detectable viral replication. $APN^{+/+}$ mice that lacked expression of STAT1 ($APN^{+/+}$ $STAT^{-/-}$) were susceptible both *in vitro* and *in vivo* to 229E infection, indicating that perturbation to the IFN pathway was necessary for productive infection (96).

Being the most studied HCoV, SARS-CoV has been established to replicate in numerous animals (reviewed in 97). Small animal models include BALB/c and C57BL/6 mice, Syrian hamsters, and ferrets. A variety of non-human primates have also been infected and resulted in variable disease, manifesting in acute respiratory distress syndrome or alternatively little to no pathology (97). Studies have implicated that pathology in both non-human primates and rodents is age-dependent, with aged animals showing more severe disease than young animals (98, 99).

Some short and long term trials of human coronavirus infections have been conducted in people. Volunteers have been inoculated with 229E and OC43 and monitored for up to a year post-infection. HCoVs were administered intranasally and serum levels of antibodies were monitored. In all cases, infected individuals produced neutralizing antibodies which peaked between 10 and 14 days post infection (d.p.i) which appeared to be negatively correlated with virus shedding (100-102). The antibody levels in sera of volunteers at 52 weeks had further declined and were similar to uninfected individuals (102). These individuals were not protected against re-challenge (102).

The immune responses in SARS-CoV patients have been analyzed, as have those in non-human primates. A large increase in pro-inflammatory cytokines is observed and this cytokine storm leads to the severe lung damage observed in both patients and certain non-human primate models (98, 103, reviewed in 104).

1.2. The Nucleocapsid

1.2.1. Function in infection

Encoding an essential structural protein, the nucleocapsid gene (N) is present in all coronaviral genomes. The nucleocapsid protein complexes with the genomic RNA to form the helical capsid, which during replication buds through the ER and Golgi to acquire the host-derived membrane. As RNA viruses, coronaviruses along with arteriviruses replicate solely in the cytoplasm. An unusual exception consistent across many viruses of the Nidovirus order is the nuclear localization of N. It has been shown that the N proteins of coronaviruses MHV, IBV, TGEV and arterivirus porcine reproductive and respiratory virus (PRRSV) localize to the nucleus and nucleolus (105-107). There have been conflicting reports on the nuclear and nucleolar localization of SARS-CoV N, with some groups reporting a cytoplasmic localization and some reporting presence in the nucleus (108-110). It has also been reported that IBV N nuclear localization is cell-cycle specific (111). The function of this localization is still unknown, though it has been speculated that TGEV and MHV N nucleolar localization induces cell cycle arrest (106). It is known that N is generally a multi-functional protein, as it has been found in IBV to be an RNA chaperone and SARS N has been shown to interact with cellular cyclophilin A, Smad3, and B23 (112-115). Other coronavirus N proteins have also been shown to interact with nucleolar proteins fibrillarin and nucleolin, important in ribosome biogenesis and nucleolar assembly (116).

The phosphorylation of N has also been a point of interest, as more studies have shown that this is an important modification in the life cycle of the virus. Studies of IBV N have shown that phosphorylation may be important in RNA binding in that phosphorylated N bound to viral genomic RNA with a higher affinity as compared to nonviral RNA (117). This may be related to the observation that IBV infectious clones containing phosphorylated N were rescued more efficiently and produced more infectious particles compared to clones containing mutations in the phosphorylation sites of N (118). Phosphorylation may also be important in subcellular localization of N. SARS N has been shown to be phosphorylated in both the cytoplasm and nucleus by different kinases (119, 120). Once SARS N has been phosphorylated in the nucleus, it binds to nuclear export protein 14-3-3 and is shuttled into the cytoplasm (119). Interestingly, a study was done showing that SARS-N binds to B23, a nuclear import shuttle protein, and inhibits phosphorylation of B23 via this interaction (115). B23 is a key nucleolar protein in regulating centrosome duplication, that when phosphorylated disassociates from the centrosome allowing for initiation of duplication (121). In its unphosphorylated form, it remains bound to the centrosome and prevents cell cycle progression (121).

1.2.2. Structural domains of N

The N protein is divided into 3 major domains, the N-terminal domain (NTD), serine-arginine-rich domain (SRD), and the C-terminal domain (CTD) (Figure 4). Some functional studies have been done on each region, though whether these functions are conserved among all coronaviruses is unknown. The exact amino acid positions and sequences of these regions vary between coronaviruses, resulting in non-conserved traits.

The N terminal domain is an important domain for RNA-binding, shown in both SARS-CoV and OC43 nucleocapsid proteins (122-124). Through this interaction, the NTD of SARS N binds genomic RNA resulting in nucleocapsid formation (125). The NTD of IBV N has also been indicated to be imperative for nucleocapsid formation (126). As well, the NTD of SARS-CoV N contains a nuclear localization signal (NLS) motif which allows for truncated NTD mutants to localize exclusively to the nucleus (127). Some CoV N proteins also encode a small 20 residue region 5’ to the NTD, called the serine-glycine-arginine-rich region (SGR) (125).

The centrally located SRD is a major site of phosphorylation in the N protein (128). The SARS N SRD is a region that is essential for robust viral

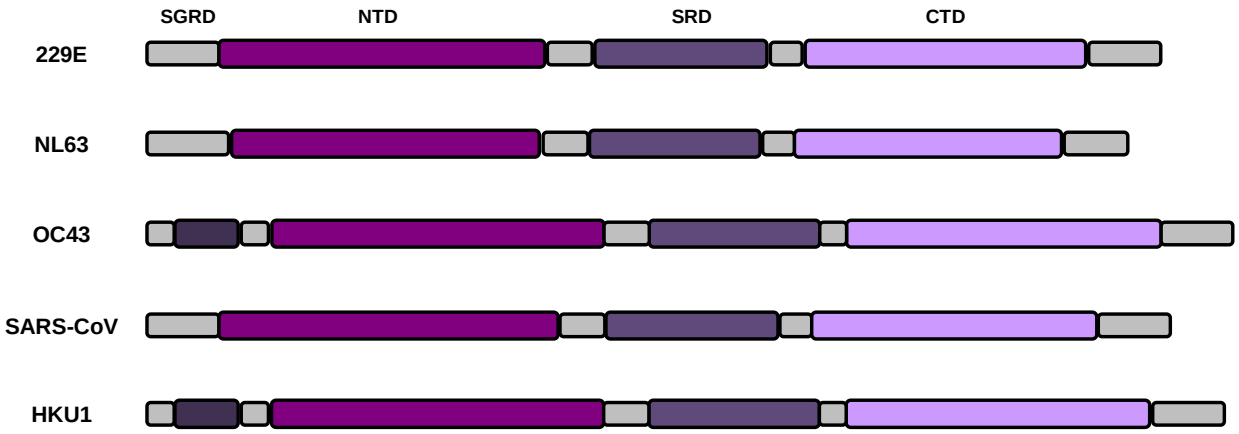
SGRD
NTD
SRD
CTD
229E
NL63
OC43
SARS-CoV
HKU1

Figure 4. Nucleocapsid domains of human coronaviruses.

Each nucleocapsid contains three major domains : NTD, SRD, and CTD. Both OC43 and HUK1 encode an additional region in the NTD, SGRD, which is enriched with serine, glycine and arginine. Figure modified from Saikatendu *et al.* (2007) (125).

replication and contributes to N multimerization (129-131). The SRD of both SARS-CoV and OC43 N, similar to the NTD, binds RNA (122, 123). As the SARS N protein appears to shuttle between the cytoplasm and nucleus, it is predicted that a leucine-rich region (LRR) located in the SRD may act as a nuclear export signal (127).

The CTD of SARS-CoV also binds RNA (122). The region has been consistently shown to be responsible for oligomerization, with N proteins of SARS-CoV, OC43, and 229E all mapping dimerization functions to the CTD (123, 132-134). The nucleocapsid CTD of avian coronavirus IBV has also been implicated in oligomerization (135). In SARS-CoV N, the CTD also encodes two NLS motifs that result in truncated CTD mutants to localize to the nucleolus (127). The CTD of MHV N has been shown to be the region that interacts with M, a major surface glycoprotein, in order to facilitate packaging of the nucleocapsid into the virion (136).

1.3. The Innate Immune Response to Viral Infections

Cells are constantly exposed to microorganisms of varying pathogenicity in the environment. With broad range targeting, the innate immune response is the first line of defense against pathogenic microorganisms. This is often followed by the more specialized adaptive immune response in which effector immune cells and antibodies specifically targeted to the invading pathogen act to clear these microorganisms from the system. The innate immune response has evolved cellular pattern recognition receptors (PRRs) to recognize pathogen-associated molecular patterns (PAMPs), akin to molecular footprints of viruses and bacteria, which are distinct from host cellular proteins and nucleic acids. Binding of PAMPs to PRRs initiates a signalling cascade resulting in the commencement of a cavalcade of anti-microbial mechanisms. This effectively alerts the cell to a potential threat, resulting in an appropriate response including inflammation, apoptosis, inhibition of microbial replication, and induction of the adaptive immune response.

1.3.1. The Interferon Response

1.3.1.1. Interferon and Its Induction

One of the most crucial molecules synthesized in the PAMP-PRR initiated anti-viral response is interferon (IFN). It is often the first induced cytokine in response to a viral infection and is important for the generation of further immune responses. Interferon (IFN) was first discovered in the 1950's by three independent groups (137-141). The cellular product was found to interfere with

viral replication (141). Type I IFN encompasses IFN-α and IFN-β, which are involved in the innate immune response, and type II IFN refers to IFN-γ, which is important in the adaptive immune response. The discovery of type III IFN more recently in the 2000's revealed the third type of IFN, termed IFN-λ, which is induced by viral infection but research in this area is still in its infancy (142). As type I IFN is the most pertinent to the following research relating to innate immunity, this review of literature will focus on this subset of interferons.

In addition to the most extensively studied IFN-β and IFN-α, type I IFN also includes IFN-ε, IFN-κ, IFN-ω, IFN-ν, IFN-ξ, IFN-τ, and IFN-δ, with the latter two found solely in swine and ruminants, respectively (143). IFN-β is encoded by a single gene, while there are 13 different IFN-α genes (IFNA1-8, 10, 14, 16, 17, 21) (reviewed in 144, 145). Initial induction of IFN-β transcription occurs in response to the sensing of pathogen-associated molecular patterns (PAMPs) by various pattern recognition receptors (PRRs). PRRs essential in viral infections are Toll-like receptors (TLRs) and retinoic acid inducible gene I (RIG-I) like receptors (RLRs). In addition, sensors of DNA such as DNA-dependent activator of IFN-regulatory factors (DAI) and leucine-rich flightless-interacting proteins 1 (LRRFIP1) recognize foreign DNA and result in production of type I IFN (reviewed in 146).

Once IFN-β is induced, the cytokine then signals in an autocrine and paracrine manner, resulting in amplification of the antiviral response. Both IFN-β and IFN-α are ligands for the ubiquitously expressed IFN-α receptor 1 (IFNAR1) and IFN-α receptor 2 (IFNAR2) receptor complex. Activation of this pathway leads to expression of interferon-stimulated genes (ISGs) and results in inhibition of viral replication and further amplification of the innate response in part by IFN-α expression. Details in this signalling pathway and its consequences are discussed below.

1.3.1.2. PRRs Pertinent in RNA Virus Detection

There are a multitude of PRRs which play an important role in the innate immune response and vast amounts of information are available about each. Reviews on each of these PRRs are beyond the scope of this thesis. The following will only discuss nucleic acid detectors toll-like receptors and RIGI-like receptors which are most pertinent to this body of work on the human coronavirus.

1.3.1.2.1. Toll-like Receptors

Toll receptors were originally identified in *Drosophila melanogaster*, and human homologs, coined Toll-like receptors, were discovered in the late 1990's (147, 148). Upwards of 10 functional human TLRs have since been identified, TLR1 through TLR10 (149-152). TLRs themselves consist of three structural areas: an extracellular region which binds ligands, a transmembrane domain, and a cytosolic signalling domain which is also known as the Toll-interleukin 1 receptor (TIR) homology domain. Once bound to its specific ligand, most TLRs signal through TIR adapter protein myeloid differentiation marker 88 (MyD88) to recruit IL-1 receptor associated kinase (IRAK) and TNF receptor-associated factor (TRAF) (153). TLR3 is the only TLR to signal independently of MyD88 and signals via TIR-domain-containing adaptor-inducing IFN-β (TRIF).

TLRs are localized to differing areas of the cell and sense distinctive PAMPs accordingly. TLR1, 2, 4, 5, and 6 are located on the cell surface and sense foreign lipids, lipoproteins and proteins. A subset of TLRs consisting of TLR3, 7, 8, and 9 are localized to intracellular vesicles such as endosomes and lysosomes and detect nucleic acid. TLRs can also complex and cooperatively detect and signal. Because such a vast array of PAMPs exists, TLRs have adapted to recognize as many as possible by forming heterodimers to detect different molecules. For example, TLR2 and TLR6 dimerize and detect bacterial cell wall component peptidoglycan (154). However, TLR2 can also recognize bacterial lipoprotein and initiate signalling on its own, and this signalling is enhanced when complexed with TLR1 (154, 155). TLRs that are important in sensing viral PAMPs are TLR3, which detects double stranded RNA (dsRNA), TLR7 and TLR8 which detect ssRNA, and TLR9 which detects CpG motifs in DNA.

TLR3, which recognizes dsRNA, induces both an inflammatory response and type I IFN response through different pathways which activate nuclear factor kappa B (NF-κB) and interferon regulatory factor 3 (IRF-3) (Figure 5A). Once bound to its dsRNA ligand, TLR3 signals through TRIF and TRAF3 to activate TRAF family member-associated NF-κB-activator (TANK)-binding kinase 1 (TBK1) and inhibitor of NF-κB kinase (IKKi) which results in phosphorylation of IRF3. Once IRF3 is phosphorylated, the transcription factor dimerizes and translocates to the nucleus. TLR3 and TRIF also recruit TRAF6 and receptor interacting protein 1 (RIP1) which activate TGF-β activating kinase 1 (TAK1) which in turn activates the IκB kinase (IKK) complex consisting of IKKα, IKKβ, and NF-κB essential modulator (NEMO), leading to the release of NF-κB from its

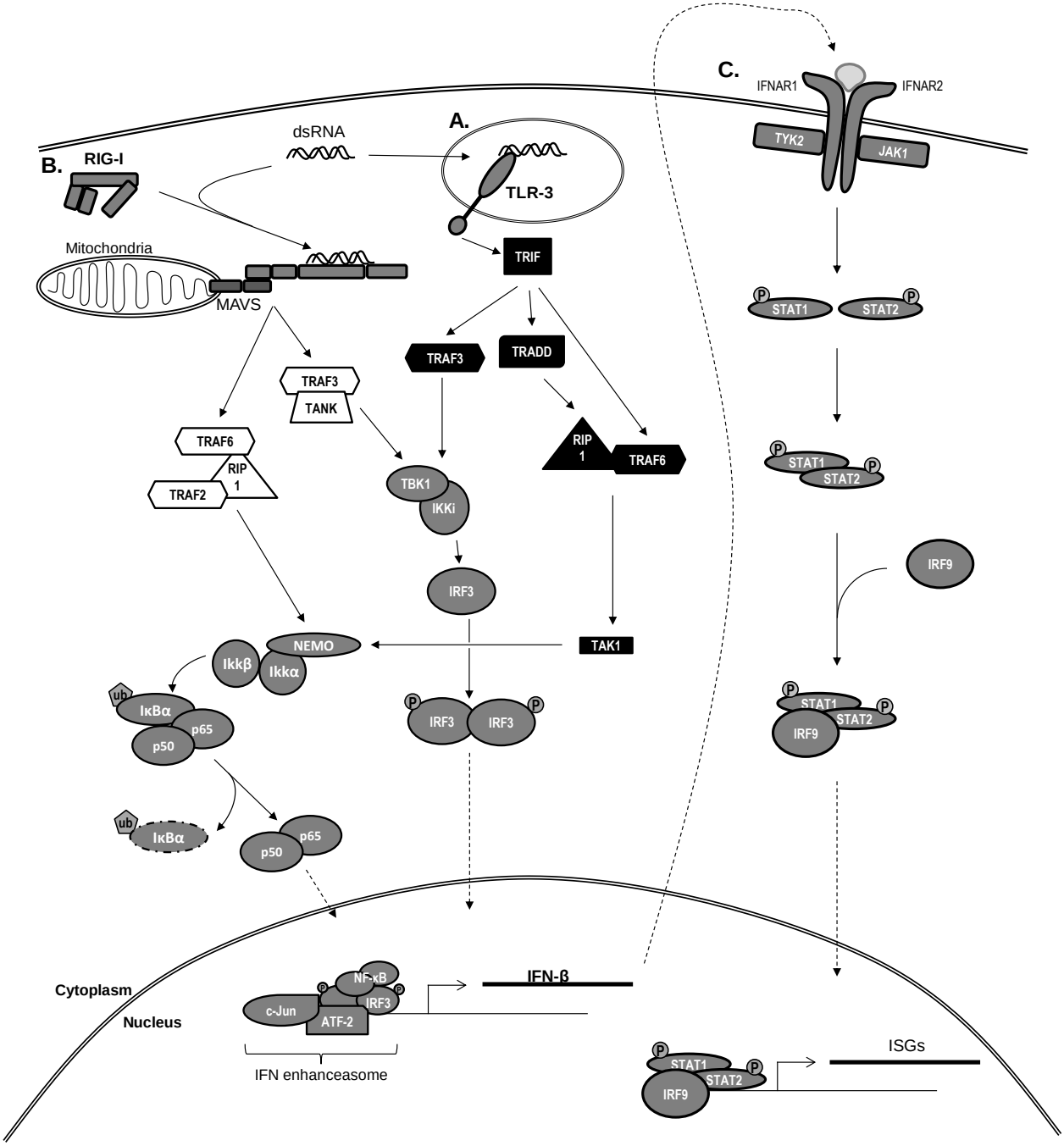
A.
B.
C.
dsRNA
RIG-I
TLR-3
Mitochondria
MAVS
TRIF
TRAF3
TRADD
TRAF3
TANK
TRAF6
RIP 1
TRAF2
TBK1
IKKi
RIP 1
TRAF6
IRF3
TAK1
NEMO
Ikkβ
Ikkα
IκBα
p65
p50
ub
IRF3
IRF3
IκBα
p65
p50
IFNAR1
IFNAR2
TYK2
JAK1
STAT1
STAT2
STAT1
STAT2
IRF9
STAT1
STAT2
IRF9
Cytoplasm
Nucleus
NF-κB
IRF3
c-Jun
ATF-2
IFN-β
IFN enhanceasome
STAT1
STAT2
IRF9
ISGs

Figure 5. A brief synopsis of signalling initiated by dsRNA leading to IFN synthesis and signalling.

(A) Endosomally localized TLR-3 recognizes dsRNA and signals via TRIF to activate both IRF3 and NF-κB, leading to IFN-β gene transcription. (B) RIG-like-receptor RIG-I is present in a conformationally inactive form in the cytoplasm. Once bound to dsRNA, RIG-I becomes conformationally active and interacts with MAVS via CARD domains. MAVS signals via TRAF3 and TRAF2/6 to activate IRF3 and NF-κB, respectively, leading to IFN-β gene transcription. (C) Once IFN-β is translated, it is secreted and signals in an autocrine and paracrine manner by binding to IFNA receptors. This ligand binding initiates the JAK-STAT pathway and leads to transcription of various ISG's. Figure modified from Honda *et al.* (2006) (156).

inhibitor of NF-κB alpha (IκBα) inhibitor. The NF-κB dimer then translocates to the nucleus where it binds to the promoter region of IFN-β.

NF-κB, IRF3, and ATF-2/c-Jun form the IFN-β enhanceasome at the gene's promoter region, binding to positive regulatory domains II, III, and IV, respectively. This initiates IFN-β transcription and its subsequent translation, after which the cytokine signals in a paracrine and autocrine manner.

1.3.1.2.2. RIG-I-like Receptors

In addition to detection by TLR3, dsRNA is also sensed by the PRR RIG-I in the cytoplasm. RIG-I belongs to a subset of PRRs called RIG-I –like receptors, which also includes melanoma differentiation-associated gene 5 (MDA5) and Laboratory of Genetics and Physiology 2 (LGP2), named after where the gene was isolated (157, 158). Both RIG-I and MDA5 receptors consist of two N-terminal caspase recruitment domain (CARD) domains and a central RNA-binding helicase domain (159). The C-terminal domain of RIG-I is responsible for autoinhibition, and once activated the receptor becomes conformationally active (160). LGP2 lacks CARD domains and is thought to be an inhibitor of RIG-I and MDA5 (159, 160). Though both RIG-I and MDA5 bind dsRNA, RIG-I preferentially binds short RNA with 5' triphosphorylated ends and MDA5 preferentially binds higher molecular weight RNA (161, 162).

Binding of RNA by RIG-I and MDA5 also leads to the transcription of IFN-β via IRF3 and NF-κB activation, though through slightly different pathways as compared to TLR3 (Figure 5B). RIG-I and MDA5 are activated upon binding to RNA ligands and interact with mitochondrially localized protein mitochondrial antiviral signalling (MAVS) protein, also known as interferon-beta promoter stimulator 1 (IPS-I), virus-induced signaling adaptor (VISA), and CARD adaptor inducing IFN-β (Cardiff) (163-166). MAVS is anchored in the mitochondria via a transmembrane domain, which is essential to its signalling subsequent to activation (165). The interaction between RIG-I or MDA5 and MAVS occurs between the CARD domains of each protein and triggers the recruitment of TRAF3 to activate TBK1 and IKKi which results in phosphorylation of IRF3. TRAF2, TRAF6 and RIP1 are also recruited, which activate the IKK complex consisting of IKKα, IKKβ, and NEMO, leading to the ubiquitination and degradation of IκBα, releasing NF-κB from its inhibitor and allowing for nuclear translocation. IFN-β transcription is then initiated by binding of NF-κB, IRF3, and ATF-2/c-Jun to the enhanceosome.

1.3.1.3. Downstream IFN signalling

Once translated, IFN-β is secreted and binds the receptor complex of IFN-α receptor 1 (IFNAR1) and IFN-α receptor 2 (IFNAR2) on the IFN-producing cell itself as well as neighbouring cells. This binding initiates signalling via the Janus Kinase (JAK)- signal transducers and activators of transcription (STAT) pathway, leading to phosphorylation of STAT1 and STAT2 by tyrosine kinase 1 (TYK1) and JAK2 (Figure 5C). The activated STATs dimerize, form a complex with IRF9, and translocate to the nucleus where transcription of an array of IFN-stimulated genes (ISGs) is initiated by binding of the STAT1/2/IRF9 complex, also known as IFN-stimulated gene factor 3 (ISGF3) to IFN-stimulated response element (ISRE) promoters. A great number of ISGs have been discovered, though antiviral mechanisms of only a few have been well characterized (reviewed in 167). Paracrine signalling by type I IFN acts to alert and prepare neighbouring cells for potential viral infection.

To further amplify the antiviral response, ISGF3 also induces the expression of the transcription factor IRF7. IRF7 then acts alone or in conjunction with other IRFs, such as IRF3 and IRF5, to initiate transcription of IFN-α as well as to further upregulate IFN-β (168, reviewed in 169). IFN-α can then be secreted and signal through IFNAR receptors, consequently augmenting the antiviral response.

Type I IFN is also an important cytokine in the bridge between innate and adaptive immunity. Type I IFN induces the expression of chemokines in order to recruit immune cells to the site of injury or infection as well as the expression of cytokines that are key in regulating cell function (170). Type I IFN induces IL-15 expression, thus impacting the function of Natural Killer (NK) cells, a lymphocyte important in innate defense, by enhancing the cell's ability to kill target cells as well as promoting NK cell survival and accumulation (171, 172).

IFN supports the differentiation of monocytes to dendritic cells as well as stimulates macrophage antibody dependent toxicity (173, 174). Treatment of dendritic cells with type I IFN also results in increased surface expression of major histocompatibility complex I (MHC I) which results in an increase in the antigen presenting cell's ability to induce a $CD8^+$ T cell immune response (175, 176).

1.3.1.4. Interferon Stimulated Genes

The potent anti-viral activity of IFN is seen in resultant ISGs. Identification of upwards of 1000 ISGs have revealed a high diversity in expression as well as

potency of these antiviral factors. Some ISGs aid in amplification of the IFN response. These include the aforementioned RIG-I and MDA5, as well as the tripartite motif-containing (TRIM) superfamily of proteins (reviewed in 177). Other ISGs are more directly anti-viral and interfere with the virus' ability to replicate in the cell. Some of the best studied include protein kinase regulated by RNA (PKR), 2'-5' oligodenylate synthetase (OAS), RNaseL, and orthomyxovirus resistance (Mx) protein (167).

Some ISGs affect the translation of viral proteins and stability of viral genomes. PKR is activated by dsRNA which leads to the phosphorylation of α subunit of eukaryotic initiation factor (eIF2α), rendering eIF2 inactive and inhibiting translation (178). Additionally, PKR contributes to the stability of IFN mRNA in some viral infections (179). OAS, also activated by dsRNA, polymerizes ATP which in turn activates RNaseL. The cellular endonuclease then degrades all cellular and viral RNA at UU or AA nucleotides (145). Another endonuclease, ISG20, also degrades RNA, specifically single-stranded RNA and is effective in preventing replication of many RNA viruses, including vesicular stomatitis virus (VSV) and influenza (180).

Several ISGs directly interact with viral proteins. Human Mx protein, MxA, confers resistance to many viruses by binding to viral components and preventing function (181). MxA binds to the nucleoprotein of both Thogoto virus and influenza A and while these Mx targets have been determined, a ubiquitous mechanism for this ISG is not clear and the majority of targets in Mx-sensitive viruses are not known (181, 182). ISG15, a ubiquitin-like protein, targets viral proteins by "ISGylation", a comparable process to ubiquitination. The ISG utilizes IFN-inducible E1, E2, and E3 enzymes Ube1L, UbcH8, and HERC5, respectively, to attach itself to target proteins (183). Although the exact antiviral mechanism of this ISGylation is unknown, viral fitness is affected by this process. ISG15 has also been shown to target some cellular proteins including IRF3, which ISG15 prevents from interacting with PIN1, a promoter of IRF3 ubiquitination and degradation (184).

Two ISGs induce mutations into viral genomes, rendering them unstable and leading to decreased viral fitness. Adenosine deaminase acting on RNA (ADAR) acts by replacing AU nucleotide sequences with IU (185). This mutation disrupts base pairing and destabilizes dsRNA. Similarly, apolipoprotein B mRNA-editing enzyme catalytic polypeptide 3 (APOBEC3) is a cytosine deaminase that converts cytidine to uridine in ssDNA viral genomes (145, 186).

The interferon-induced proteins with tetratricopeptide repeats (IFIT) family of proteins consists of IFIT1 (ISG56), IFIT2 (ISG54), IFIT3 (ISG60), and IFIT5 (ISG58) in humans (187). These ISGs are one of the most highly expressed in response to IFN and quickly accumulate after stimulation. The proteins possess several antiviral attributes. IFIT1 and IFIT2 are able to reduce cap-dependent translation by binding to eukaryotic initiation factor 3 (eIF3), a multi-subunit complex involved in translation initiation. This activity effectively blocks Hepatitis C virus (HCV) translation as the virus utilizes eIF3 for translation of its genome (188, 189). IFIT1 also recognizes and binds to viral RNA lacking 2'-O-methylation and although the antiviral mechanism is still unclear, this interaction is able to prevent viral replication. Mutant West Nile virus (WNV), poxviruses, and coronaviruses that lack 2'-O-methylation were attenuated in wild-type cells, but readily replicated in cells lacking IFIT1 (190-192). IFIT1 also recognizes 5'-ppp uncapped RNA and with IFIT2 and IFIT3, forms a complex that prevents viral replication (193). Lastly, IFIT1 has also been shown to bind directly to viral proteins such as human papillomavirus E1 helicase, resulting in reduced viral replication (194, 195).

The ISGs mentioned are merely a handful of known IFN responsive genes. There is a vast list of ISGs of which the scope of this thesis could not possibly cover. Studies are ongoing to identify new ISGs as well as to continue to characterize those previously identified.

1.3.1.5. Viral evasion of IFN

As our immune system has evolved to counter viral infections, viruses have countered with evolutions of their own. This progression is essential to the survival of the virus and occurs most frequently in highly mutable RNA viruses. An important target for viruses is the type I IFN response, as blockage of this early pathway at a key point can allow for profuse viral replication. Many RNA viruses, such as VSV, Hepatitis C virus (HCV), and influenza A, are sensitive to type I IFN, but have developed the ability to circumvent the response.

Viruses target various different components of the IFN pathway and most affect multiple components. Some viruses are able to prevent initiation of the pathway by evading recognition by the PRRs. The NS1 protein of Influenza A binds viral dsRNA, preventing its recognition by PRRs and also binds PKR and prevents its signalling (196, 197). Similarly, the NS5A protein of HCV also inhibits PKR and OAS by directly binding to the ISGs and also inhibits TLR signalling by binding to the adaptor protein MyD88 (198-200).

Downstream PRR signalling is also frequently affected. The NS3-4A protein of HCV inhibits TLR3 signalling by causing degradation of TRIF and preventing IRF3 phosphorylation by TBK1 (201, 202). Additionally, NS3-4A also disrupts RLR signalling by cleaving MAVS at its C-terminal, freeing it from the mitochondria and rendering it ineffective (164, 203).

The IRFs are also a common target of viruses. The ICP0 protein of herpes simplex virus 1 (HSV-1) binds and blocks IRF3 signalling, effectively squelching immune responses mediated by IRF3 (204, 205). The VPR and Vif proteins of HIV also target IRF3 and mediate its ubiquitination, targeting the transcription factor for degradation (206). The rotavirus NSP1 protein similarly targets IRF3 for proteasome-dependent degradation and in addition also induces degradation of IRF5 and IRF7 (207-209).

The Jak-STAT signalling cascade, which is initiated by binding of IFN to IFNAR, is often impinged on. The initiation of the entire cascade is prevented by some poxviruses, such as vaccinia virus, which encode a soluble IFNAR that competitively binds to extracellular IFN (210). STAT proteins are bound by several paramyxovirus V proteins, preventing downstream signalling to occur (211-213).

As the ability to prevent IFN expression and signalling could be the difference between profuse replication and the demise of infection, viruses have evolved many different mechanisms to counteract this host response. The examples stated above have only scratched the surface of the myriad of viral immune evasion tactics and have been extensively reviewed in many excellent publications (211, 214-219).

1.3.2. NF-kB: Role in antiviral response

1.3.2.1. The NF-κB Family

NF-kB is a multifunctional transcription factor and a key player in the innate immune response to virus infection. It is activated via many stimuli (Figure 6) including tumor necrosis factor alpha (TNF-α), interleukin 1 (IL-1), and lipopolysaccharide (LPS), as well as the aforementioned PAMPs (reviewed in 220). There are five mammalian members of the NF-κB family: RelA (p65), RelB, c-Rel, p105/p50 (NFKB1), and p100/p52 (NFKB2). These transcription factors regulate the expression of many genes involved in inflammation, apoptosis, and the innate immune response (reviewed in 221).

All members of the NF-κB family encode an N-terminal Rel-homology domain (RHD) which allows them to bind DNA as well as dimerize (222). Structurally, p65, RelB, and c-Rel are similar and all contain C-terminal transactivation domains (TADs) which allow the proteins to initiate transcription. In contrast, both p105 and p100 lack TADs and are precursors to the subunits p50 and p52, respectively. Initiation of transcription by p50 and p52 can be achieved by dimerization with a TAD-containing NF-κB subunit (222).

Dimers of NF-κB subunits are retained cytoplasmically in an inactive state by inhibitory inhibitor of NF-κB (IκB) proteins in unstimulated cells. Members of the IκB family include IκBα, IκBβ, IκBε, IκBξ, BCL-3, and IκBNS (222, 223). Interaction between IκB proteins and NF-κB dimers is mediated by ankyrin repeats, which all IκB members encode in varying amounts. Additionally, p105 and p100 both encode ankyrin repeats and act as IκB inhibitors.

1.3.2.2. NF-κB Activation Pathways

1.3.2.2.1. The Canonical Pathway

The canonical pathway is the most studied route to NF-κB activation. A wide range of stimuli can initiate the canonical pathway, one example being the cytokine TNF-α upon its binding to the TNF-α receptor (TNFR) (Figure 6A). Recruitment of TRADD, TRAF2, TRAF5, and RIP leads to activation of TAK1 and TAK1-binding protein (TAB) 2 and TAB3. The complex then activates IKKα, IKKβ, and NEMO and follows a similar path to NF-κB activation as with PAMP activation discussed above in section 1.3.1.2. The IKK complex then phosphorylates IκBα at serine (Ser)32 and Ser 36, leading to polyubiquitination at lysine (Lys)21 and Lys22 and targets IκBα for degradation by the 26S proteasome. This results in the release of the NF-κB dimer and allows for nuclear translocation.

The dimer itself can be composed of various NF-κB subunits. The most predominant dimer is that of p50 and p65 and this is often thought of as the classic NF-κB heterodimer. RelB also forms heterodimers with p50 and both RelB and p65 form dimers with p52. As both p50 and p52 lack TADs, it is necessary to dimerize with either p65 or RelB in order for the complex to be transcriptionally active.

Activation of this pathway is also initiated by TLR2 upon binding to its bacterial lipoprotein ligand (Figure 6B). TLR2 signals via MyD88, leading to

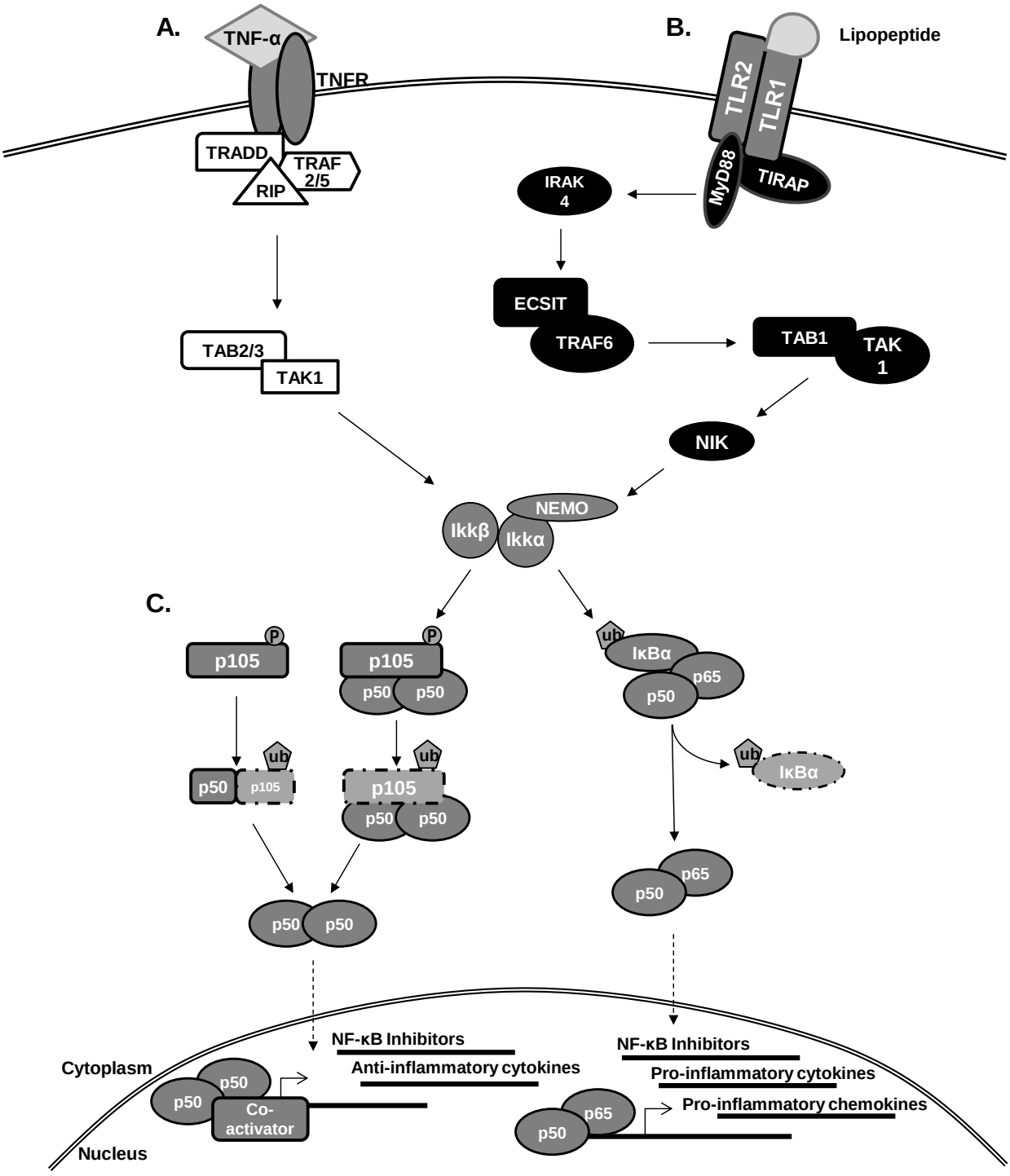
A.
TNF-α
TNFR
TRADD
TRAF 2/5
RIP
B.
Lipopeptide
TLR2
TLR1
MyD88
TIRAP
IRAK 4
ECSIT
TRAF6
TAB1
TAK 1
TAB2/3
TAK1
NIK
NEMO
Ikkβ
Ikkα
C.
p105
P
p50
ub
IκBα
p65
Cytoplasm
Nucleus
Co-activator
NF-κB Inhibitors
Anti-inflammatory cytokines
Pro-inflammatory cytokines
Pro-inflammatory chemokines

Figure 6. Brief synopsis of NF-kB signalling initated by TNF-α and TLR-2.

(A) TNF-α binds to the TNF receptor, initiating a signalling cascade leading to activation of the IKK complex and degradation of inhibitor IκBα, releasing the NF-κB dimer. The dimer translocates to the nucleus where it initiates transcription of various NF-κB responsive genes. (B) Recognition of bacterial lipoprotein by either TLR2 alone or TLR2 in complex with TLR1 leads to MyD88-dependent signalling to activate the IKK complex. (C) Activation of this pathway also leads to phosphorylation of p105, leading to its total degradation or partial processing. p50 homodimers retained by p105 are then released or generated, respectively, and translocate to the nucleus. Homodimers of p50 complex with transcriptional co-activators and initiate transcription. Figure modified from Hayden and Ghosh (2012) (222).

activation of the IKK complex and NF-κB activation. As discussed in 1.3.1, TLR3 signalling also leads to activation of NF-κB.

1.3.2.2.2. The Noncanonical Pathway

More recently, an alternative pathway to NF-κB was discovered (224). The non-canonical pathway mainly is initiated by the TNFR family members lymphotoxin β receptor (LTBR) and B-cell activating factor receptor (BAFFR) binding to ligands lymphotoxin β (LTβ) and B-cell activating factor (BAFF), respectively (reviewed in 225). Receptor binding activates NF-κB inducing kinase (NIK) which then phosphorylates IKKα homodimers. This pathway is dependent upon IKKα and does not require IKKβ or NEMO. Activated IKKα phosphorylates p100, which is then polyubiquitinylated and proteasomally processed to yield p52. The subunit is associated via its rel-homology domain (RHD) with RelB and translocates to the nucleus where it initiates transcription. The non-canonical pathway is initiated by LTβ primarily in lymphocytes and mediates the development of peripheral lymphoid organs. BAFF-mediated signalling induces expression of bcl-2 and bcl-x, which are anti-apoptotic genes, resulting in survival of B cells. The non-canonical pathway is not initiated as a part of the innate immune response to viral infections and will not be discussed further.

1.3.2.3. NFKB1

NFKB1 encodes the p105 subunit of NF-κB which is processed via proteasome to p50 and the subunits are collectively referred to NFKB1. The 20S proteasomal processing of p105 to p50 can occur co-translationally or independently of translation and is both induced by activation and constitutive, though the mechanisms remain controversial (226, 227). Constitutive processing has been speculated to be carried out by the 20S proteasome independently of ubiquitination (226), while others have shown that ubiquitination of p105 is necessary for processing to occur (228-230). Most recently, it was shown that p105 is monoubiquitinated (not a chain of ubiquitin as previously thought) and that multiple monoubiquitins are necessary for processing to occur (231). The processing of p105 requires the glycine rich region (GRR) located between the RHD and Ankyrin repeats, as deletion of this proteasomal stop signal abolishes processing to p50 (232, 233). Post-stimulation, p105 is either processed into p50 or, more predominantly, entirely degraded thereby releasing NF-κB subunits it was bound to which are primarily p50 homodimers (Figure 6C) (234, 235). The process of complete degradation begins with phosphorylation of p105 on Ser927 and Ser932 and recruitment of $SCF^{\beta\text{-}TrCP}$ ubiquitin ligase which leads to

ubiquitination and complete degradation of p105. Enhanced processing of p105 with stimulation occurs and this process is dependent upon IKK phosphorylation followed by ubiquitination. Interestingly, it appears that ubiquitination of a subset of lysine residues results in differential processing as opposed to degradation (236).

The p105 subunit contains an IκB domain which allows it to act as an inhibitor of NF-κB subunits. In a resting cell, it preferentially binds to homodimers of p50, retaining the complex in the cytoplasm (237). As p50 lacks a TAD, it and its homodimers cannot initiate transcription alone. Along with forming dimers with p65, p50 forms homodimers in an unstimulated cell, which also act as transcriptional repressors when complexed with transcriptional co-repressors such as histone deacetylase 3 (HDAC3) and silencing mediator of retinoic acid and thyroid hormone receptor (SMRT) (238). Homodimers of p50 have also been found to be transcriptionally active when complexed with atypical IκB proteins such as IκBζ and BCL-3, resulting in upregulation of ant-inflammatory cytokine IL-10 (239, 240). The p50 subunit can also form dimers with transcriptional co-activators such as CREB-binding protein (CBP) and p65, as mentioned (241). Once the cell has been stimulated resulting in activation of its IKK complex, these NF-κB heterodimers compete with p50 homodimers for κB site binding. Among the multitude of genes whose transcription is initiated is NFKB1 itself, as the promoter region contains a κB consensus sequence that is bound by p65/p50 dimers, thereby initiating transcription (242, 243).

1.3.2.4. NF-κB Responsive Genes

The transcription of a myriad of genes is induced by NF-κB transcription factors. They are involved with a wide range of functions, and products encompass cytokines, chemokines, adhesion molecules, and negative regulators of NF-κB.

NF-κB is traditionally thought of as proinflammatory and this is due to the many chemokines and cytokines induced once the transcription factor is activated. The expression of pro-inflammatory cytokines such as IL-1β, IL-6, and TNF-α are all upregulated (244). Both IL-1β and TNF-α are also activators of NF-κB, leading to a positive autoregulatory loop. The activation of NF-κB by IL-1β also results in the expression of the enzymes cyclooxygenase 2 (COX-2), phospholipase 2 (PLA2), and inducible nitric oxide synthase (iNOS), leading to vasodilation and an increase in inflammation (245). TNF-α signalling through the TNFR can have diverse outcomes, one of which is the activation of NF-κB.

Apoptosis can also occur with TNF-α stimulation if TRADD signals via Fas associated death domain (FADD), leading to activation of the caspase pathway (246, 247). Conversely, the activation of NF-κB by TNF-α can be anti-apoptotic, resulting in the inhibition of caspase-8 (248). IL-6 is a key multifunctional cytokine in the inflammatory response and regulates T cell, B cell, and macrophage differentiation and activation (249).

Chemokines such as IL-8, regulated on activation, normal T cell expressed and secreted (RANTES), macrophage inflammatory protein 1 alpha (MIP-1α), and monocyte chemotactic protein 1 (MCP-1) are also transcribed by activated NF-κB. These result in chemotaxis of immune cells, such as neutrophils, monocytes, T cells, and eosinophils, to the site of insult (250-252). Migration of these cells is also aided by the upregulation of adhesion molecules on endothelial cells, a common result of NF-κB activation. Intercellular adhesion molecule 1 (ICAM1), vascular cell adhesion molecule 1 (VCAM1), and endothelial leukocyte adhesion molecule 1 (ELAM1) are several molecules of which activated NF-κB initiates transcription (244).

The expression and transcriptional activation of NF-κB are tightly regulated. The expression of many negative regulators of NF-κB, such as IκBα and A20 is induced by activation of NF-κB itself (253). The classic mechanism of NF-κB inhibition is retention of the dimers by IκB proteins. Most well studied is the inhibitor IκBα, which binds NF-κB dimers, retaining them cytoplasmically. Once degraded post-activation, IκBα is re-transcribed with the promotion of activated NF-κB and resumes inhibition of NF-κB. There are also many negative regulators of NF-kB including A20 and IkBα, which is constitutively bound to the NF-kB complex prior to stimuli (253). Once activated by phosphorylation, IkBα is degraded, releasing NF-kB which then translocates to the nucleus. In the nucleus, it initiates transcription of many responsive genes, including IkBα (reviewed in 254). Upon translation, IkBα once again binds to NF-kB, removes it from the nucleus and transcription ceases.

A20, also known as TNF-α induced protein 3 (TNFAIP3), is an inhibitor of NF-κB induced by TNF-α-activated NF-κB, highlighting an important self-regulatory loop (255). A20 is a dual ubiquitin editing protein which regulates the activation and degradation of components of the NF-κB signalling cascade by either removing regulatory Lys63-linked ubiquitin or adding Lys48-linked ubiquitin, thus targeting the protein for degradation. It has been shown to de-ubiquitinate the adaptor protein TRAF6 as well as NEMO, thus removing Lys63-

ubiquitin and halting NF-κB signalling (256, 257). A20 has also been shown to both de-ubiquitinate and ubiquitinate the adaptor protein RIP1 (258). RIP1 first is de-ubiquitinated by A20 via removal of regulatory Lys63-linked ubiquitin and subsequently A20 ubiquitinates RIP1 with the addition of Lys48-linked ubiquitin, leading to its proteasomal degradation (258).

Recently, another mechanism of control was found to negatively regulate the expression of NFKB1. A microRNA (miRNA), miR-9, was shown to target the 3'UTR of *NFKB1* and resulted in decreased mRNA expression (259, 260). As with other protein regulators of NFκB, the expression of miR-9 is inducible by stimuli which also activate NFκB, such as TNF-α, LPS, and TLR2 agonists (259).

1.3.2.5. Viral Manipulation of NF-κB

As with other components of the innate immune response, viruses have developed methods to advantageously manipulate NF-κB. As the transcription factor is also important in the initiation of IFN-β transcription, many of the mechanisms affecting NF-κB also have downstream effects on IFN.

The secretion of soluble TNFR by some poxviruses results in sequestering of TNF-α. The T2 protein of myxomavirus selectively interacts with TNF-α and increases virulence in host rabbits (261). This method is limited to DNA viruses with large genomes and no known RNA viruses employ this decoy strategy.

Viral proteins are able to block the initial activation of the IKK complex responsible for phosphorylating inhibitor IκBα, leading to its degradation. The N1L and K1L proteins of vaccinia virus interact with the IKK complex, preventing its activation by phosphorylation (262, 263). The ICP27 protein of HSV-1 also prevents the phosphorylation and ubiquitination of IκBα by directly binding to the inhibitor and stabilizing it (264). NF-κB activation is effectively suppressed by this method.

The process of ubiquitinating IκBα is also targeted by viruses. The E3 ubiquitin ligase $SCF^{\beta\text{-}TrCP}$, which is responsible for ubiquitination of IκBα, is bound by CP77 and A59 of vaccinia virus and Vpu of HIV (265-267). TNF-α treatment was still able to induce phosphorylation of IκBα in cells expressing these viral proteins, but subsequent degradation of the inhibitor did not occur resulting in decreased NF-κB activity (265, 266). The rotavirus protein NSP1 is able to inhibit NF-κB activation by inducing the degradation of β-TrCP, the F-box component of $SCF^{\beta\text{-}TrCP}$ (268).

Targeting of the NF-κB transcription factors themselves is also commonly found in many viruses. The CP77 protein of vaccinia virus, NS1 of West Nile virus, and nucleocapsid protein of Hantaan virus are able to prevent the nuclear localization of p65 (266, 269-271). The nucleocapsid protein of Hantaan virus prevents TNF-α-stimulated NF-κB activation by binding importin-α, which is responsible for p65 nuclear localization (269). The M150 (also known as myxoma nuclear factor) protein of myxomaviruses contain ankyrin repeats, one of which is similar to those found in IκBα (272). This allows the viral protein to bind p65 in the nucleus and prevent its transcriptional activity (272). Similarly, the G1R protein of cowpox virus encodes ankyrin repeats, allowing the viral protein to interact with p105, enabling the blockage of NF-κB activation (273, 274). The myxomavirus protein M013 also interacts with p105 (275). This binding prevents activation and nuclear localization of NF-κB (275).

In addition to inhibiting NF-κB, it is desirable for some viruses to activate it. This is prominent in oncogenic viruses such as hepatitis B virus and Epstein Barr virus (EBV). The hepatitis B protein HBx induces IκBα degradation, leading to constitutive activation of NFκB, promoting hepatocellular carcinoma (276). The latent membrane protein 1 (LMP1) of EBV constitutively activates NF-κB by interacting with TRAF2 and promotes B cell immortalization by suppressing apoptosis (277-279). The core protein of hepatitis C virus binds to the TNFR death domains, resulting in NF-κB activation and an anti-apoptotic response (280). Infection with respiratory syncytial virus leads to persistent inflammation, attributed to activation of NF-κB leading to production of proinflammatory cytokines (281). Interestingly, this activation cannot be inhibited by increased levels of IκBα.

Some viral genomes contain NF-κB binding sites in their promoters and by activating NF-κB, enhance viral transcription (282). The human cytomegalovirus, which contains NF-κB binding sites within its genome, activates NF-κB during infection and the expression of cytomegalovirus immediate early genes is enhanced (277, 283). In addition, the immediate early gene IE1 is itself an activator of NF-κB and perpetuates the activation of NF-κB and expression of immediate early genes (277, 283).

As evidenced above, viruses are adept at targeting each component of the complex pathway surrounding NF-κB. These methods often lead to suppression of the innate immune response to aid in viral evasion, but can also result in cell transformation and uncontrolled inflammation.

1.4. microRNAs

1.4.1. microRNA biogenesis and gene regulation

Once thought to be a matter of transcription and translation, gene regulation on another level was discovered to occur in the early 1990's (284). The revelation that microRNAs existed in *Caenorhabditis elegans* led to the unearthing of thousands of regulatory miRNAs in humans.

In humans, miRNAs are transcribed in the nucleus by DNA-dependent RNA polymerase and when first transcribed are generally several kilobases long with 5' caps and are polyadenlyated. The initial transcript is known as primary miRNA (pri-miRNA), which are hairpin structures containing a terminal loop, a stem of complementary nucleotides, and an unpaired flanking region (Figure 7). The unpaired flanking region is then bound by DiGeorge critical region 8 (DGCR8), a dsRNA binding protein which binds a region approximately 11 bp from the ssRNA-dsRNA junction (SD junction) between the unpaired flanking region and stem of the pri-miRNA (285). DGCR8 is complexed with RNase III protein Drosha, which then cleaves the stem at this location 11 bp from the SD junction, releasing a stem-loop structure known as the precursor miRNA (pre-miRNA) (285). Drosha cleavage leaves a 3' overhang of 2 nucleotides on the pre-miRNA which is the site of recognition for Exportin-5 and Ran-GTP. This protein complex then exports the pre-miRNA to the cytoplasm where it is recognized by Dicer and trans-activation response element (TAR) RNA-binding protein 2 (TRBP), forming the RNA-induced silencing complex (RISC)-loading complex. Dicer then cleaves the pre-miRNA at the terminal loop, yielding a strand of dsRNA approximately 22-23 nt in length with 3' overhangs on both ends. One strand of the dsRNA is then discarded and is selected based on stability as well as 5' terminal nucleotides. Strands that are kept, known as the miRNA guide strand as opposed to discarded strands known as miRNA* (or the passenger strand), usually possess the least stable 5' end (the end with least complementarity between nucleotides) and contain a U or A as the 5' terminal nucleotide (286, 287).

Once the passenger strand has been discarded, the mature miRNA is incorporated in the RISC complex with Argonaute 2 (Ago2) and the miRNA guides the complex towards its mRNA target with complementary base pairing (288). Sequences are contained within the 3' untranslated region (UTR) of the mRNA and although it is uncommon in mammals to have perfect complementarity between miRNA and mRNA, homology of a sequence at

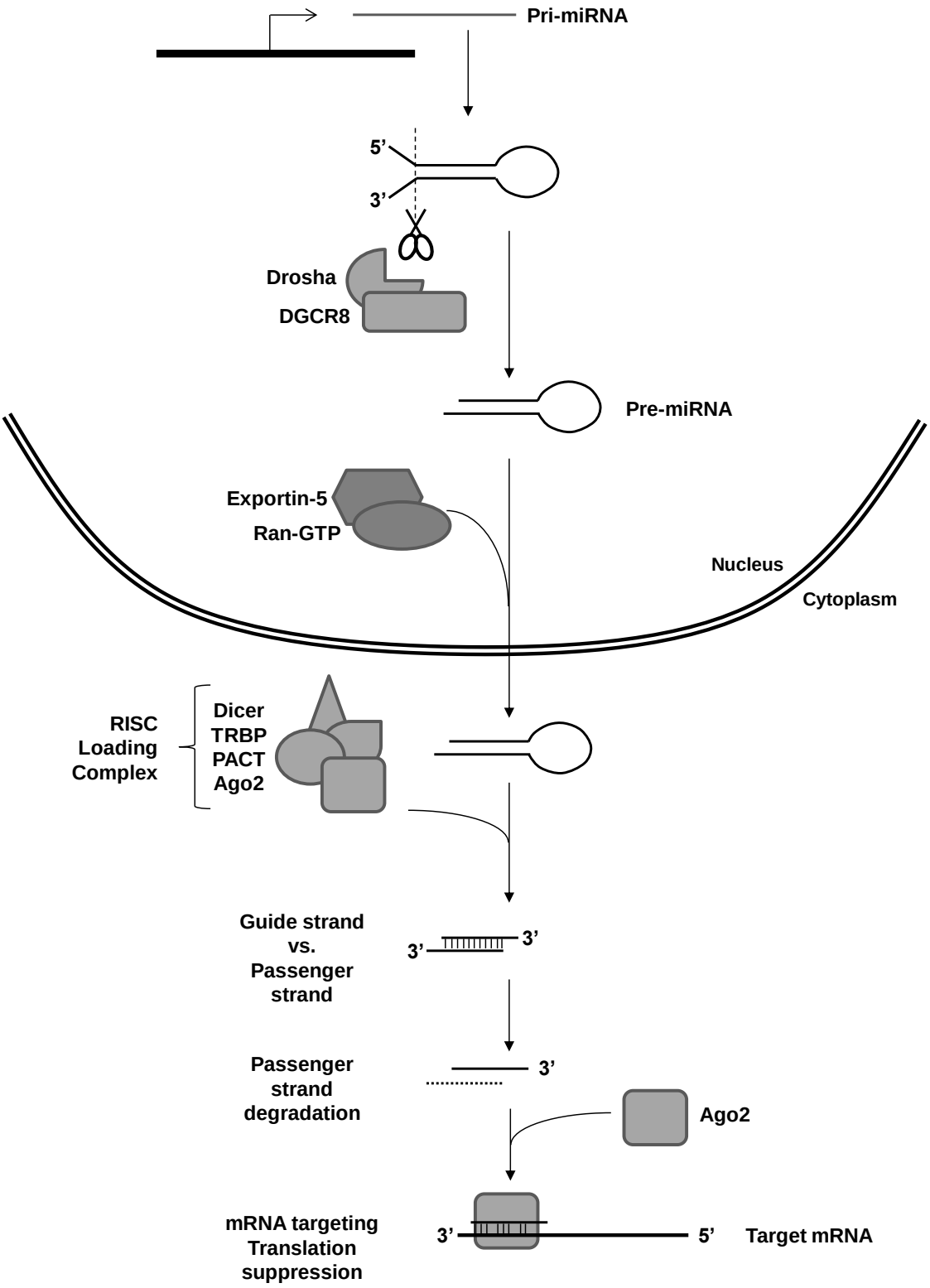
Pri-miRNA
5'
3'
Drosha
DGCR8
Pre-miRNA
Exportin-5
Ran-GTP
Nucleus
Cytoplasm
RISC
Loading
Complex
Dicer
TRBP
PACT
Ago2
Guide strand
vs.
Passenger
strand
3'
3'
Passenger
strand
degradation
3'
Ago2
mRNA targeting
Translation
suppression
3'
5'
Target mRNA

Figure 7. Brief overview of microRNA biogenesis.

Transcription of pri-miRNA occurs in the nucleus and the highly structured RNA is then cleaved by the Drosha/DGCR8 complex to form pre-miRNA. Exportin-5 and Ran-GTP then transports the pre-miRNA to the cytoplasm where it is further processed by the RISC loading complex. Once the terminal loop has been cleaved, the passenger strand of the remaining duplex is degraded, leaving the guide strand. The guide strand directs Ago2 to the target mRNA and prevents translation. DGCR8 (DiGeorge critical region 8), TRBP (trans-activation response element (TAR) RNA-binding protein 2), PACT (protein activator of the IFN-induced protein kinase), Ago2 (Argonaute 2). Figure modified from Filipowicz *et al.* (2008) (289).

positions 2-8 from the 5' end, known as a seed region, is important for this targeting. Regulation of protein expression is then achieved either by inhibition of target translation or destabilization and degradation of the mRNA (290, 291, reviewed in 292).

1.4.2. Current knowledge of viral exploitation of miRNA

As with many cellular mechanisms and processes, viruses have evolved to exploit and manipulate the miRNA pathway. Since the first report of virally encoded miRNA in γ-herpesviruses nearly a decade ago, a multitude of viral miRNAs have been identified in a wide range of viruses (293, 294, reviewed in 295, 296). The sequences of viral miRNAs are generally not perfectly complementary to their targets and this is speculated to be because viruses have evolved miRNAs that target 3'UTR sequences of a few key targets that are not strictly conserved among hosts.

Viruses exploit the miRNA pathway in several different fashions. The viral miRNA may target an important protein in immune signalling such as IRAK1 and MyD88, which are targeted by Karposi's sarcoma-associated herpesvirus (KSHV) encoded miR-K9 and miR-K5, respectively (297). Via expression of these viral miRNAs, KSHV is able to reduce the innate inflammatory response by blocking TLR signalling (297). Virally encoded miRNA also mimic miRNAs expressed by host cells. A well studied example of this is miR-155 which is induced after activation of lymphoid cells with constitutive expression leading to oncogenic transformation of cells (298, 299). KSHV encodes a mimic of miR-155, called miR-K11, and expression of this viral homolog results in the downregulation of genes controlling cellular growth and pro-apoptotic factors (300, 301).

If the miRNA homolog is not encoded in the viral genome, viruses are capable of inducing host expression of the miRNA. The Epstein Barr virus (EBV), like KSHV, is a γ-herpesvirus but unlike KSHV, it does not encode a viral analog to miR-155. EBV encodes a protein, latent membrane protein 1 (LMP1), that activates NF-κB and initiates transcription of miR-155 (302). As a result, cells infected with EBV show increased transformation and immortalization, as expression of miR-155 inhibits apoptosis (303). The human immunodeficiency virus (HIV) has recently been shown to induce miR-132 during infection of T cells, enhancing replication (304). The expression of cellular miRNA has also been shown to be essential to viral growth, as is the case in Hepatitis C virus (HCV) infection (305). The RNA virus belonging to the Flavivirus family relies on the

constitutively expressed liver-specific miR-122 which acts to protect the viral genome (306). While bound to Ago2, miR-122 specifically binds the 5' end of the HCV genome, shielding the 5' terminal triphosphate from recognition by the cell's immune system and allowing for increased viral replication (305-307). Additionally, this interaction between the miR-122/Ago2 complex and HCV RNA appears to stabilize the genome, preventing exoribonuclease decay (307, 308).

Lastly, viruses have been shown to downregulate expression of cellular miRNAs. RNA decoys, encoded by simian herpesvirus saimiri and muring cytomegalovirus, target miR-27 and expression of the viral noncoding RNAs result in degradation of the cellular miRNA (309, 310). Overexpression of miR-27 strongly inhibits viral replication and this evasion technique allows for robust viral growth (309). The expression of all host miRNAs may be prevented by both poxviruses and adenoviruses. The poxvirus vaccinia virus encodes a polyA polymerase which polyadenylates host miRNAs, leading to their degradation (311). The 3' polyadenylation is dependent on the methylation status of the RNA, a post-transcriptional modification used by host cells to differentiate between self and foreign RNA, as small interfering RNAs (siRNAs) which contain a 2'O-methyl group were not degraded (311). The adenovirus prevents miRNA expression at an earlier point in biogenesis than the vaccinia virus. The virally encoded RNA decoy VA1 binds competitively to Exportin-5, preventing the nuclear export of the pre-miRNA and effectively inhibiting miRNA biogenesis (312). The viral RNA also competitively binds Dicer, preventing the processing of cellular miRNAs (313). miRNA processing is also prevented by the Ebola virus proteins VP30 and VP35 which directly interact with pre-miRNA processing proteins Dicer and TRBP effectively preventing miRNA gene silencing (314, 315).

In all of the above illustrations of viral exploitation of the miRNA pathway, the majority of examples cited DNA viruses as the manipulators. Thus far, no RNA virus has been shown to encode a miRNA mimic, although whether HIV encodes miRNA sequences is debatable (316, 317). Certainly, the most apparent disadvantage to RNA viruses encoding miRNA sequences is the likely destruction of the viral genome due to processing by cellular miRNA machinery. Despite the lack of one mechanism for miRNA manipulation, RNA viruses are continually being found to similarly induce miRNAs and block miRNA biogenesis to their advantage as seen by both HIV and Ebola examples.

1.5. Aims

The human coronaviruses have not been extensively studied and while the emergence of SARS-CoV, and more recently MERS-CoV, has reignited interest in these large RNA viruses, much is still unknown. It is known that the nucleocapsid protein is a multifunctional and essential component of CoVs, and in addition, N proteins of MHV and SARS-CoV have been found to suppress the innate immune response. Although the overall amino acid homology between the nucleocapsid proteins of MHV, SARS-CoV and other HCoVs OC43, 229E, and NL63 is low, there are regions that are conserved between them. This indicates that there may be similar functions or an evolutionary advantage to maintaining the sequence in these areas.

It was hypothesized that the N proteins of HCoVs OC43, 229E, and NL63 have a similar ability to suppress the innate immune system. These three viruses were chosen because OC43 and 229E are considered prototypical HCoVs and NL63 is a newly emerged HCoV which served as a good comparison to the two classic HCoVs. The main aim of this research was to investigate the effects of HCoV OC43, 229E, and NL63 nucleocapsid proteins on the innate immune response. The objectives set forth were as follows:

1. Determine whether OC43, 229E, and NL63 nucleocapsid proteins affect the type I interferon response *in vitro*.
    a. Determine the HCoV nucleocapsid point of impact on the IFN signalling pathway.
    b. Roughly map functional regions of the nucleocapsid to determine the responsible region
2. Determine whether OC43, 229E, and NL63 nucleocapsid proteins affect NF-κB activation and signalling *in vitro*.
    a. Determine the HCoV nucleocapsid point of impact on the NF-κB pathway
    b. Determine the mechanism of HCoV nucleocapsid affect on the NF-κB pathway.

Chapter 2
Materials and Methods

2.1. Cells and Viruses.

Vero and A549 cells were maintained in alpha modified Eagle's medium (α-MEM) supplemented with 8% (v/v) fetal bovine serum (FBS), 2 mM L-glutamine, 100U/mL penicillin and 100 µg/mL streptomycin. 293T and HEK293 cells were maintained in Dulbecco's modified Eagle's medium (DMEM) supplemented with 8% (v/v) FCS, 2mM L-gluatamine, 100U/mL penicillin and 100 µg/mL streptomycin. NCI panel of cell lines were maintained in Roswell Park Memorial Institute medium (RPMI) supplemented with 8% (v/v) FBS, 2 mM L-glutamine, 100 U/mL penicillin and 100 µg/mL streptomycin. HCT-8 cells (American Type Culture Collection (ATCC), Manassas, VA, USA) were maintained in RPMI supplemented with 8% (v/v) FCS, 2 mM L-glutamine, 10 mM HEPES, 1 mM sodium pyruvate, 4.5 g/L D-glucose, 1.5 g/L sodium bicarbonate, 100 U/mL penicillin and 100 ug/ml streptomycin. All cells were grown at 37°C in a 5% humidified CO_2 incubator. The vesicular stomatitis virus (VSV) ΔG GFP VSV is a mutant that lacks the glycoprotein (G) gene and contains green fluorescent protein (GFP) in the place of G. Matrix mutant ΔM51 VSV expressing FLAG-tagged OC43 nucleocapsid protein (N-FLAG) was generated by PCR amplification of OC43 N with a FLAG sequence (DYKDDDDK) on the reverse primer, creating a C-terminal FLAG tag (Table 2). OC43 N-FLAG was subcloned into the Δ51 VSV genome between the G and L genes. The resulting virus genome was rescued and amplified in 293T cells. Coronavirus OC43 (ATCC, VR-1558) was a kind gift from Dr. James Mahony. The virus was propagated in HCT-8 cells at 33°C for three days in serum-free RPMI supplemented with 2 mM L-glutamine, 10 mM HEPES, 1 mM sodium pyruvate, 4.5 g/L D-glucose, 1.5 g/L sodium bicarbonate. Supernatants and cell monolayers were collected and freeze thawed. Cell debris was pelleted by centrifugation at 1500 rpm for 10 min.

Table 2. Sequences of primers utilized to amplify OC43 N-FLAG for VSV insertion.

OC43-N Xho Fwd	5'-GCCTCGAGGCCACCATGTCTTTTACTCCTGGTAAGCAAT
OC43-N Xba Rev	5'-GACACCTCAGAAATAGATTACAAGGATGACGACGATAAGTAAT CTAGAGC

2.2. Plasmids.

Coronaviral nucleocapsid (N) genes were amplified via RT-PCR using cDNA generated from coronavirus infected cells (primers listed in Table 3). The amplified genes were FLAG-tagged and subcloned into expression vector pEF. pSG5-G was generated by cloning VSV G into the pSG5 expression vector (Stratagene, Agilent, Santa Clara, CA, USA). Measles V protein was FLAG

tagged and cloned to produce pEF-V-FLAG. Interferon stimulated response element luciferase (ISRE-luc) and ΔRIG-I (ΔRIG-I Myc-pCDNA) plasmids were a kind gift from Dr. John Hiscott. The plasmids containing β-galactosidase (β-gal) and NFκB-luc were kind gifts from Dr. Karen Mossman. Mutant OC43 N genes were PCR amplified using full-length N in pEF-BOS as a template (primers listed in Table 3). Products were subcloned into the pEF vector. pUNO-hTLR2 (Invivogen, San Diego, CA, USA) was a kind gift from Dr. Dawn Bowdish. Empty vectors pCDNA3.1 (pCDNA, Invitrogen, Life Technologies, Carlsbad, CA, USA) and pSG5 were also utilized. The green fluorescent protein (GFP) expression plasmid, pEGFP-N1 (pEGFP) was also utilized (Clontech, Mountain View, CA, USA). The luciferase plasmid luc-NFKB1 was a kind gift from Dr. Massimo Locati.

2.3. In Cell Western for OC43 Titering.

HCT-8 cells were plated in 12-well plates and infected the following day with a dilution series of OC43. After a 60 min incubation, cells were overlayed with serum-free 2xMEM and 1% (w/v) agarose. Plates were incubated at 33°C for two days after which agarose overlays were removed, and cells were fixed with cold acetone:methanol (1:1). Cells were blocked with fish gelatin in tris-buffered saline (TBS) and probed with primary antibody against OC43 N and secondary antibody anti-mouse 800 (Molecular Probes, Invitrogen). Plates were scanned on the Odyssey (Licor, Lincoln, NE, USA).

2.4. Antibodies.

Antibodies against FLAG were obtained from Rockland Immunochemicals Inc. (polyclonal) and Sigma-Aldrich (monoclonal) (Gilbertsville, PA, USA and St. Louis, MO, USA, respectively). Anti-IkBα and anti-p65 NF-kB were both obtained from Santa Cruz Biotechnologies (Santa Cruz, CA, USA). Antibodies against hnRNPU, Ku70, and nucleolin were also obtained from Santa Cruz Biotechnologies. Anti-YB1 was obtained from Cell Signaling (Danvers, MA, USA). Anti-pSTAT1 was obtained from BD Biosciences (San Jose, CA, USA). Anti-β-actin was obtained from Sigma-Aldrich. Anti-NFKB1 was obtained from Santa Cruz Biotechnologies. Anti-OC43 N was obtained from Chemicon (Millipore, Billerica, MA, USA).

Table 3. Sequences of primers utilized for coronavirus nucleocapsid amplification and cloning.

OC43 N Fwd	5’-GCCTCGAGGCCACCATGTCTTTTACTCCTGGTAAGCAATCCA
OC43 N Rev	5’-CGAGATCTTTACTTATCGTCGTCATCCTTGTAATCTATTTCTGAGGTGTCTTCATGATAGG GC
NL63 N Fwd	5’-GCCTCGAGGCCACCATGGCTAGTGTGTAAATTGGGCCGATGACA
NL63 N Rev	5’-CGAGATCTTTACTTATCGTCGTCATCCTTGTAATCATGCAAAACCTCGTTGACAATTTCTATA
229E N Fwd	5’-GCCTCGAGGCCACCATGGCTACAGTCAAATGGGCTGATGCAT
229E N Rev	5’-CGAGATCTTTACTTATCGTCGTCATCCTTGTAATCGTTTACTTCATCAATTATGTCAGTTT CA
OC43 N-FL C-term Fwd	5’-GCGAATTCCGCCACCATGGAGCAAGTAACTAAGCATACTGCCAAAG
OC43 N-FL 916-SR Fwd	5’-AGGCTCAGGAAGGTCTGCTCCTAATGCCTCTAGTGCAGGATCGCGTAGTA
OC43 N-FL dSR Rev	5’-TACTACGCGATCCTGCACTAGAGGCATTAGGAGCAGACCTTCCTGAGCCT
NTD Fwd	5’-GCGAATTCCGCCACCATGGATGGATTACAAGGATGACGACGATAAGAATGTTGTACCCT ACT ATTCTTGG
NTD Rev	5’-GCGAATTCACTCAGACAATGCGATGCAATTTCCTCATTTTATTAGGAAAGGACAGTGGGAGTG GCACCTT CCAGGGTCTTATGAGCCTTCAATATAGTAACCCTG
SGR Fwd	5’-GCGAATTCCGCCACCATGGATGGATTACAAGGATGACGACGATAAGTCTTTTACTCCTG GTAA CAATCC

2.5. Western Blots.

For detection of FLAG-tagged coronaviral N genes, full length and mutant: 293T cells plated in 6-well dishes were transfected with coronaviral plasmids using Lipofectamine 2000 (Invitrogen). Twenty-four hours post-transfection, cells were lysed with radioimmunoprecipitation assay (RIPA) buffer containing a protease inhibitor cocktail (Roche, Penzburg, Germany). Lysates were run on an SDS-PAGE gel and transferred to nitrocellulose membrane (GE Healthcare, Niskayuna, NY, USA). Membranes were blocked with 5% (w/v) milk-TBS and probed with primary polyclonal antibody against FLAG (Rockland). Membranes were then incubated with a secondary antibody, anti-rabbit 680 (Molecular Probes, Invitrogen) and scanned on the Odyssey (Licor).

For detection of phosphorylated STAT1: 293T cells plated in 6-well dishes were transfected with OC43 N or pCDNA using Lipofectamine 2000. Twenty-four hours post-transfection, cells were treated with 500 U/ml of IFN-α and lysed at various time points with RIPA buffer containing a protease inhibitor cocktail as well as a phosphatase inhibitor cocktail (Sigma-Aldrich). Nitrocellulose membranes were blocked with Odyssey Buffer (Licor), probed with primary antibody against phosphorylated STAT1 (BD Biosciences) and anti-mouse 800 (Molecular Probes, Invitrogen). Membranes were scanned on the Odyssey.

For detection of IκBα: 293T cells were plated in 6-well plates and transfected with OC43 N or pCDNA using Lipofectamine 2000. Twenty-four hours post-transfection, cells were treated with 10 ng/ml of TNF-α (Peprotech, Rocky Hill, NJ, USA) and lysed at various time points with RIPA buffer containing a protease inhibitor cocktail. Nitrocellulose membranes were blocked with 5% (w/v) milk-TBS and probed with antibodies against IκBα (Santa Cruz) and β-actin (Sigma-Aldrich). Membranes were incubated with secondary antibodies anti-rabbit 680 and anti-mouse 800 and scanned on the Odyssey.

For detection of NFKB1 (p105/p50): 293T cells were plated in 6-well plates and transfected with OC43 N or pCDNA (for TLR2 variation, cells were also transfected with TLR2 plasmid). Twenty-four hours post-transfection, cells were treated with 10 ng/ml of TNF-α (for TLR2 variation, cells were treated with 100 ng/ml Pam3CSK4 (Invivogen)) and lysed at various time points with RIPA buffer containing a protease inhibitor cocktail. Nitrocellulose membranes were blocked with Odyssey Buffer and probed with antibodies against NFKB1 (Santa Cruz) and β-actin. Membranes were incubated with anti-rabbit 800 and anti-mouse 680 (Molecular Probes, Invitrogen) and scanned on the Odyssey.

For detection of OC43 Nucleocapsid: HCT-8 cells were plated in 60 mm dishes and infected with OC43 at an MOI of 1. Cells were lysed with RIPA buffer containing protease inhibitor cocktail at various days post-infection. Nitrocellulose membranes were blocked with Odyssey Buffer and probed with antibody against OC43 N (Chemicon, Millipore). Membranes were probed with secondary antibody anti-mouse 800 and scanned on the Odyssey.

2.6. VSV G-less Assay.

A549 cells were plated in 6-well plates at a density of $5x10^5$ cells per well. Cells were co-transfected with pSG5-G and the coronaviral gene of interest in pEF using Lipofectamine 2000 (Invitrogen). Empty vector pCDNA3 served as a negative control and pEF-V-FLAG, a measles protein established to be a repressor of IFN, was used as a positive control. Approximately 24 hours post-transfection, cells were infected at an MOI of 5 with ΔG GFP VSV for 45 min at 37°C. Cell monolayers were then thoroughly and repeatedly washed with PBS and incubated overnight. Supernatants from each well were collected the following day and frozen at -80°C. Vero cells were seeded in a 96-well plate at $2x10^4$ cells per well and 24 hours after plating, supernatant from transfected and infected A549 cells was applied in a dilution series. Plates were incubated overnight and then scanned by Typhoon imaging system (GE Healthcare). Production of fluorescence, as an indication of virus replication, was measured by ImageQuant software (GE Healthcare). In the Vero variation of the VSV G-less assay, Vero cells were plated in 6-well plates at a density of $5x10^5$ cells per well. Cells were transfected as above for the A549 variation. The following day post-transfection, cells were treated with a dilution series of IFN-α for 6 hours at 37°C. Cells were then infected at an MOI of 5 with ΔG GFP VSV for 45 min at 37°C. Following infection, cell monolayers were thoroughly and repeatedly washed with PBS, IFN-α of the appropriate dilution was re-applied, and cells were incubated overnight. Supernatants were collected and applied onto Vero cells as described above. Plates were imaged and analyzed as described above.

2.7. Luciferase Reporter Assay.

293T cells were plated in 24-well plates at a density of $1.3x10^5$ cells per well. Cells were co-transfected with a luciferase reporter plasmid (ISRE-luc or NFκB-luc), β-gal plasmid, and coronaviral gene of interest using Lipofectamine 2000. Cells were treated with either IFN-α (50 or 100 U/mL; Peprotech) or tumour necrosis factor alpha (TNF-α, 10 or 20 ng/mL; Peprotech) 24-hours post-transfection. Twenty-four hours after treatment, cells were assayed for luciferase activity using the Enhanced Luciferase Assay Kit (BD Biosciences, Franklin

Lakes, NJ, USA) and β-galactosidase activity using the Luminescent β-gal kit (Clontech). The TLR-2 luciferase assay employed identical methods as the NFκB-luc assay described above, with the exception that the TLR-2 expression plasmid was also co-transfected with NFκB-luc, β-gal, and N gene plasmid. Cells were treated 24-hrs post-transfection with PAM3-CSK4 (100 ng/mL). For assays stimulated with constitutively active RIG-I and IRF3, along with ISRE-luc and β-gal, cells were also co-transfected with either ΔRIG-I or IRF3-5D. Twenty-four hours post transfection, cells were lysed and assayed as above. For OC43 NFκB-luc assays, HCT-8 cells were co-transfected with NF-κB-luc and β-gal plasmids. Twenty-four hours post-transfection, cells were infected with OC43 at an MOI of 1. Cells were lysed as before at 1, 2, and 3 days post-infection. Luciferase and β-galactosidase measurements were taken as above.

2.8. miR-Targeted Luciferase Reporter Assay.

293T cells were plated in 24-well plates at a density of $1.3x10^5$ cells per well and HEK293 cells were plated at a density of $5x10^4$ in 24-well plates. Cells were co-transfected with a luciferase reporter plasmid, NFKB1-luc, OC43-N or empty vector, and miR mimic miR-9 (Sigma-Aldrich) using DharmaFECT Duo (Dharmacon, Lafayette, CO, USA). Cells were assayed for Renilla and Firefly luciferase 2 days post-transfection using the Renilla Luciferase Assay System and Luciferase Assay System (Promega, Madison, WI, USA).

2.9. Immunofluorescence.

For detection of FLAG-tagged coronaviral N genes, full length and mutant: Cells were seeded on glass coverslips and transfected with various coronaviral genes. Twenty-four hours post-transfection, cells were fixed with 4% (v/v) paraformaldehyde and permeablized with 1:1 acetone:methanol. Coverslips were blocked with 1% (w/v) BSA-PBS and incubated with primary antibody against FLAG (Rockland) for 2 hours. Coverslips were washed and incubated with secondary anti-rabbit 488 antibody (Molecular Probes, Invitrogen) for 1 hour. Cell nuclei were stained by incubation with Hoechst and mounted on slides. Cell fluorescence was visualized by fluorescence confocal microscopy (Leica, Wetzlar, Germany).

For detection of p65: 293T cells were seeded on glass coverslips and transfected with OC43 N or pCDNA. Twenty-four hours post-transfection, cells were treated or left untreated with 10 ng/mL TNF-α and fixed with cold 1:1 acetone:methanol. Coverslips were blocked with 5% (v/v) goat serum-PBS and incubated with primary antibody against FLAG (Rockland) to detect OC43 N, and

p65 NF-kB (Santa Cruz Biotechnology). Coverslips were incubated with secondary anti-rabbit 594 and anti-mouse 488 antibodies (Molecular Probes, Invitrogen). Cell nuclei were visualized by incubation with DAPI. Cell fluorescence was visualized by fluorescence confocal microscopy (Leica).

For detection of OC43 N and hnRNPU or Ku70: 293T cells were seeded on glass coverslips and transfected with OC43 N. Twenty-four hours post-transfection, cells were fixed with cold 1:1 acetone:methanol and blocked with 5% (v/v) goat serum-PBS. Cells were co-stained with antibodies against FLAG to detect OC43 N and hnRNPU (Santa Cruz Biotechnology) or Ku70 (Santa Cruz Biotechnology). Coverslips were incubated with secondary anti-rabbit 594 and anti-mouse 488 antibodies and cell nuclei visualized by DAPI. Cell fluorescence was visualized by fluorescence confocal microscopy.

2.10. Quantitative RT-PCR for detection of NFKB1.

293T cells were transfected with OC43 N or pCDNA. Cells were then left untreated or stimulated with 10 ng/ml TNF-α. RNA was extracted with RNeasy Mini Kit (Qiagen, Valencia, CA, USA). cDNA was synthesized using RT^2 First Strand cDNA Kit (SABiosciences, Qiagen) and NFKB1 was amplified by quantitative PCR utilizing SYBR Green Master Mix (SABiosciences, Qiagen) and normalized to β-actin (primers listed in Table 4). Analysis of threshold cycle (C_t) values was carried out by the $\Delta\Delta C_t$ method yielding a fold change of NFKB1 mRNA levels in N transfected cells compared to control cells. For detection of NFKB1 mRNA in OC43 infected cells, HCT-8 cells were infected at an MOI of 1. RNA was extracted at 1, 2, and 3 days post-infection with RNeasy Mini Kit. cDNA synthesis and amplification was as before. Analysis of C_t values was also performed as described above.

Table 4. Sequences of primers utilized for NFKB1 and β-actin amplification.

NFKB1	Fwd	5' CCTGAGACAAATGGGCTACAC
NFKB1	Rev	5' TTTAGGGCTTTGGTTTACACGG
β-actin	Fwd	5’-GGATCCTATGACTTAGTTGCGTTACACCCTTTCTTGACA
β-actin	Rev	5’-AGATCTGAAAGCAATGCTATCACCTCCCCTGTG

2.11. Immunoprecipitation for Protein Interactions.

293T cells were plated in 150 cm dishes and infected with N-FLAG Δ51 VSV or GFP Δ51 VSV, each at MOI 5. Twenty-four hours post-infection, all cells were gathered and lysed in FLAG-IP lysis buffer with protease inhibitor (Roche).

Lysates were incubated on ice for 30 minutes and cell debris was spun out. The resulting supernatant was incubated overnight at 4°C with washed resin pre-conjugated with monoclonal FLAG antibody (Sigma-Aldrich). The resulting resin was then washed and precipitated proteins were eluted by competitive binding. The eluate was then concentrated via spin columns (Millipore). Eluate was run on pre-cast SDS-PAGE gradient gels (Invitrogen) using the Novex Midi Gel system (Invitrogen). Gels were stained for protein using Coomassie Blue Silver stain (318). Gels were scanned on the Odyssey imaging system (Licor). For RNase treatment, identical protocols were followed, however, prior to incubation with FLAG resin, cell lysates were treated with RNase H (150 U; Fermentas) or mock treated at 37°C.

2.12. Real-Time PCR Arrays.

293T cells were transfected with OC43 N-FLAG or pCDNA and subsequently treated with 10 ng/mL of TNF-α. RNA was extracted at 3 hours and 6 hours post treatment using either the RNeasy Mini Kit (Qiagen) for Inflammatory Pathway array or the RT² qPCR-Grade miRNA Isolation Kit (SABiosciences, Qiagen) for miRNome miRNA array. For Inflammatory Pathway arrays, reverse transcription of resulting RNA was performed using the RT² First Strand cDNA Kit and PCR arrays for Human Inflammatory Pathway (PAHS-011C) were performed with RT² SYBR® Green qPCR Master Mix (SABiosciences) on the 7900HT Real-Time PCR System (Applied Biosystems, Life Technologies). For miRNome miRA arrays, reverse transcriptioni of resulting RNA was performed using the RT² miRNA First Strand Kit (SABiosciences). PCR arrays for and Human miRNome miRNA (MAH-100) (SABiosciences) were performed with RT² SYBR® Green qPCR Master Mix (SABiosciences) on the 7900HT Real-Time PCR System (Applied Biosystems, Life Technologies).

2.13. RNA-Immunoprecipitation (RIP).

For OC43 N transfected and N-FL VSV infected cells: 293T cells were either infected with N-FL VSV or GFP VSV or transfected with OC43 N-FL or pEGFP. 24-hours post-infection or tranfection, cells were lysed in FLAG-IP lysis buffer with protease inhibitor (Roche). The same immunoprecipitation procedure previously described using the commercial FLAG-immunoprecipitation kit was followed. After elution, RNA was extracted from eluates using the miRNeasy Mini Kit (Qiagen). Reverse transcription of resulting RNA was performed using the RT² miRNA First Strand Kit (SABiosciences, Qiagen). qPCR was performed with commercial primers for miR-9 (SABiociences, Qiagen) and RT² SYBR® Green qPCR Master Mix (SABiosciences, Qiagen) on the 7900HT Real-Time PCR

System (Applied Biosystems). Analysis of threshold cycle (C_t) values was carried out by the $\Delta\Delta C_t$ method yielding a fold change of miR-9 levels in N expressing cells compared to control cells.

For OC43 infected cells: HCT-8 cells were infected at an MOI of 1 and were lysed at 8 and 20 hours post-infection in immunoprecipitation buffer with protease inhibitor and RNase inhibitor (New England Biolabs). Protein A/G sepharose beads (Pierce, Thermo Scientific, Rockford, IL, USA) were incubated with OC43 N antibody, allowing for binding. Conjugated beads were then incubated with cell lysates. Following supernatant removal, RNA was extracted by applying Qiazol (Qiagen) directly to the beads. The RNA was then extracted as per manufacturer's instructions for the miRNeasy Kit for miRNA extraction (Qiagen). Reverse transcription and qPCR were performed as described above.

2.14. Flow Cytometry.

For NFKB1 detection in OC43 N transfected cells: 293T cells were transfected with N-FLAG or pCDNA. Twenty-four hours post-transfection, cells were treated with 10 ng/mL of TNF-α for 6 hours. Cells were then collected and fixed and permeabilized with Cytofix/Cytoperm Fixation/Permeabilization Solution (BD Biosciences). Cells were incubated with FC block (BD Biosciences), followed by incubation with antibodies against FLAG and NFKB1. Anti-GFP was utilized as an isotype control. Cells were then incubated with secondary antibodies anti-rabbit 649 and anti-mouse 488. Cells were run on LSR II (BD Biosciences) and data analyzed with FlowJo software.

For detection of NFKB1 in OC43 infected cells: HCT-8 cells were infected with OC43 at an MOI of 1. Twenty-four hours post-infection, cells were collected and fixed and permeabilized with Cytofix/Cytoperm Fixation/Permeabilization Solution. Cells were incubated with FC block, followed by incubation with antibodies against OC43 N and NFKB1. Anti-GFP was utilized as isotype control. Cells were then incubated with secondary antibodies anti-rabbit 649 and anti-mouse 488. Cells were run on LSR II (BD Biosciences) and data analyzed with FlowJo software (Ashland, OR). .

Chapter 3
Coronavirus Nucleocapsid Modification of the Interferon Response

3.1. Introduction

3.1.1. Current knowledge in the field of coronavirus modification of IFN

Numerous studies have been conducted illuminating the impact of CoV on the type I IFN response, with several different coronaviral proteins possessing abilities to suppress this pathway. Like most other aspects of human coronaviruses, extensive investigations into SARS and IFN have been made since the 2003 outbreak, but a negligible number of studies have been done on gene function and properties of the remaining human coronaviruses.

In general, SARS-CoV infection fails to induce an IFN response both *in vivo* and *in vitro* (103, reviewed in 104, 319). Several proteins have been linked to the repression of type I IFN and all appear to target different points of the pathway. As previously discussed, accessory genes are not necessary for viral replication, but are thought to be virulence factors. The accessory proteins ORF3b and ORF6 have been shown to be IFN antagonists (320). Both ORF3b and ORF6 inhibit IRF3 phosphorylation and nuclear translocation, while ORF6 also prevents STAT1 nuclear translocation (320). Interestingly, ORF6 does not impede phosphorylation of STAT1, but instead retains nuclear import factors responsible for STAT1 nuclear localization in the ER/Golgi (321). The accessory protein 3a induces the degradation of IFNAR1, leading to decreased receptor expression and contributing to IFN resistance (322). Two non-structural proteins have also been implicated in IFN antagonism. Nonstructrual protein 1 (nsp1) induces host cell mRNA degradation, resulting in global decreased protein expression, including IFN, and it also has been shown to downregulate STAT1 phosphorylation (323-325). The protein responsible for processing ORF1a and ORF1ab polyproteins, the papain-like protease (PLP), is a potent inhibitor of IRF3 phosphorylation (326, 327). In addition, structural proteins M and N are also IFN antagonists. The M protein acts upstream in the IFN pathway and prevents the formation of the signalling complex of TRAF3, TANK, TBK1, and IKKi by binding RIG-I, TBK1, IKKi, and TRAF3 (328). The N protein of SARS-CoV interferes with IFN signalling in a stimulation-dependent manner. N is able to prevent Sendai virus and poly(I:C)-induced IRF3 phosphorylation and nuclear localization as well as IFN synthesis, but not IFN-β signalling (320, 329). The exact mechanism of how SARS-CoV N suppresses IFN is unknown, but is speculated to be due to N's RNA-binding ability (329, 330).

The murine coronavirus, formerly murine hepatitis virus (MHV) and most frequently still referred to as such, also possesses IFN antagonistic properties. Thus far, only one of MHV's accessory genes, 5a, has been found to antagonize interferon (331). The mechanisms of 5a interferon suppression are unknown. Similar to SARS-CoV, the MHV PLP has also been implicated in interference with the IFN response. MHV PLP, which is encoded by nsp3, acts in several manners

to target IRF3 activation. PLP binds and deubiquitinates IRF3, effectively preventing and reversing its activation (332). Furthermore, PLP also targets TBK1, an upstream activator of IRF3, and deubiquitinates TBK1 resulting in deactivation (333). Lastly, the nucleocapsid of MHV is an IFN antagonist, allowing an IFN-sensitive vaccinia virus to replicate in the presence of IFN (334). Additionally, N is able to interfere with the activity of 2'-5' oligodenylate synthetase (OAS) and RNase L, as indicated by the rescuing of protein translation in infections with IFN-sensitive vaccinia virus expressing MHV N (334).

Compared to SARS-CoV, very little research has been performed on other human coronaviruses in the area of the innate immune response to infection. It is known that infection of human alveolar macrophages with HCoV 229E results in robust TNF-α production, but a suppression in IFN-β mRNA is observed (335). Additionally, the PLP of NL63 prevents IFN signalling, similar to SARS-CoV PLP (327). NL63 PLP, similar to MHV PLP, is a deubiquitinating protein, and acts to deconjugate ubiquitin and interferon stimulated gene 15 (ISG15) from substrates though this activity is not directly responsible for its IFN antagonism (52, 336). No studies to date have examined proteins of OC43 and their ability (or lack thereof) to alter the IFN response.

3.1.2. VSV and the G-less Assay

In the study of interferon, an extremely useful virological tool is *Vesicular stomatitis virus* (VSV). VSV is a member of the order *Mononegavirales*, family *Rhabdoviridae*, genus *Vesiculovirus* (reviewed in 337). Primarily a livestock pathogen, infection with the virus results in lesions of the mouth and hooves. Human infection is non-fatal and causes influenza-like symptoms (338). The small, enveloped, bullet-shaped virus has a negative sense single stranded 11 kb RNA genome composed of 5 genes, nucleocapsid (N), phosphoprotein (P), matrix (M), glycoprotein (G), and large protein (L) (Figure 8) (339). Once the virus has entered the cell by receptor-mediated endocytosis via G protein, L and P proteins, which encode the viral polymerase, begin subgenomic mRNA transcription. Once translated, G protein localizes to the plasma membrane via the secretory pathway (339). N, P, and L form the nucleocapsid, and along with M are transported to the cell membrane and interact with membrane-embedded G protein. The virus is then assembled and progeny virus buds from the cell (339). During this replication cycle, VSV suppresses the host IFN response via

A.

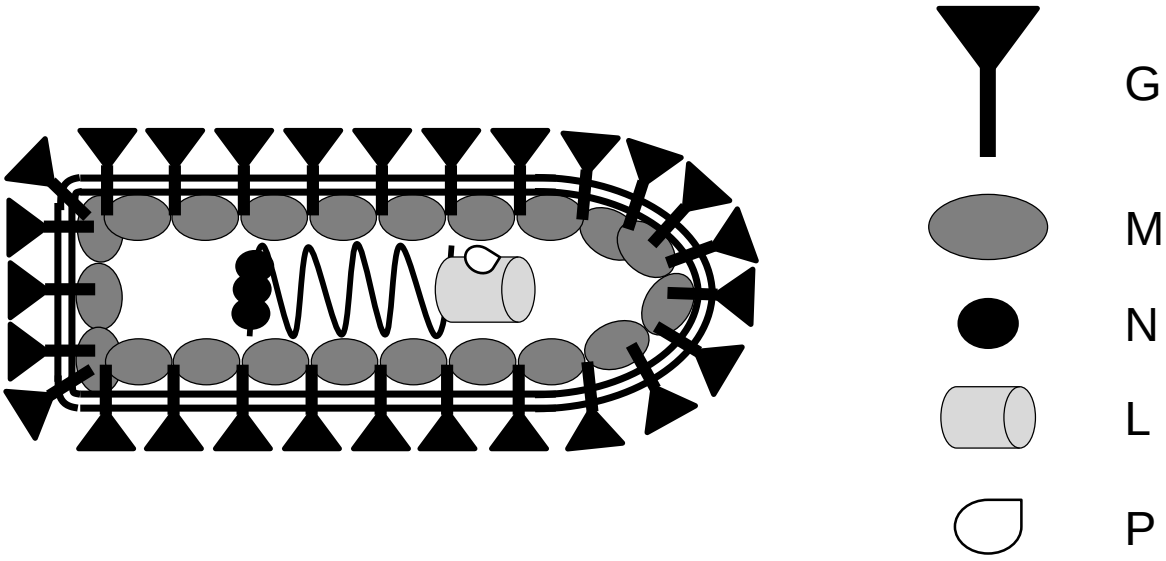

B.

Figure 8. The vesicular stomatitis virus particle and genome organization.

(A) VSV is a bullet-shaped enveloped particle with glycoprotein G embedded in its host-derived membrane. (B) VSV encodes an 11 kb ssRNA genome composed of 5 proteins. N (nucleocapsid), P (phosphoprotein), M (matrix), G (Glycoprotein), and L (large protein). Figure modified from Lichty *et al.* (2004) (340).

its matrix protein (341). The M protein prevents mRNA transport out of the nucleus via interaction with the nuclear pore complex, effectively stopping cellular protein synthesis (342-344). This ability has been pinpointed to the methionine at position 51 of M (345-348). A mutation at M51 renders the virus unable to inhibit the IFN response (344, 349). Wild-type VSV is able to stop the IFN response, but it is severely sensitive to IFN. It is this sensitivity that makes it a valuable aid in the study of the IFN response to other viruses.

The VSV G-less assay is advantageous in transient transfection settings to examine effects on the IFN response (350). As implied by the name, this assay utilizes a G-deleted VSV, ΔG VSV, that although replication competent, progeny virions are noninfectious due to lack of glycoprotein. Propagation of this virus occurs in cells that express G on their surface by either transient transfection or stable expression. Thus production of infectious particles only occurs from cells previously transfected by G. By employing ΔG VSV, it is possible to examine the IFN response in cells that have been transfected only, as those will express the viral G protein, and are the only source of infectious progeny.

As summarized in Figure 9, the G-less assay relies on the induction of type I IFN (and an antiviral state) upon co-transfection of A549 cells with VSV-G and the gene of interest. Subsequent infection with ΔG VSV expressing GFP (ΔG GFP VSV) yields two possible outcomes. Firstly, if the gene of interest does not have an effect on the antiviral response, IFN will be produced and ΔG GFP VSV infection is prevented and these transfected cells produce no progeny despite the presence of transfected G. Alternatively, if the gene of interest is able to suppress the antiviral response, ΔG GFP VSV will infect the transfected cells and replicate, producing viral progeny as these cells provide G protein expressed in trans. As readout, the supernatants from the transfected and infected cells are collected and passaged onto Vero cells. GFP is measured as an indication of ΔG GFP VSV infectivity and an inference can be made of the gene of interest's effect on the antiviral response. Supernatants are passaged onto Vero cells in serial dilution as subtleties in differences between candidates can be obscured in undiluted supernatants that contain large amounts of VSV.

A second variation on this assay utilizes Vero cells as the recipient of transfected VSV-G and gene of interest. These cells do not have the ability to produce IFN-β as they lack the gene (351, 352). However, the cell line can respond to IFN and induce an antiviral state. The Vero variation of the G-less assay therefore also begins with co-transfection of VSV-G and the gene of interest, but prior to ΔG VSV infection, the cells are treated with exogenous IFN to induce an antiviral state. The outcomes of the assay are analogous to the A549 G-less assay.

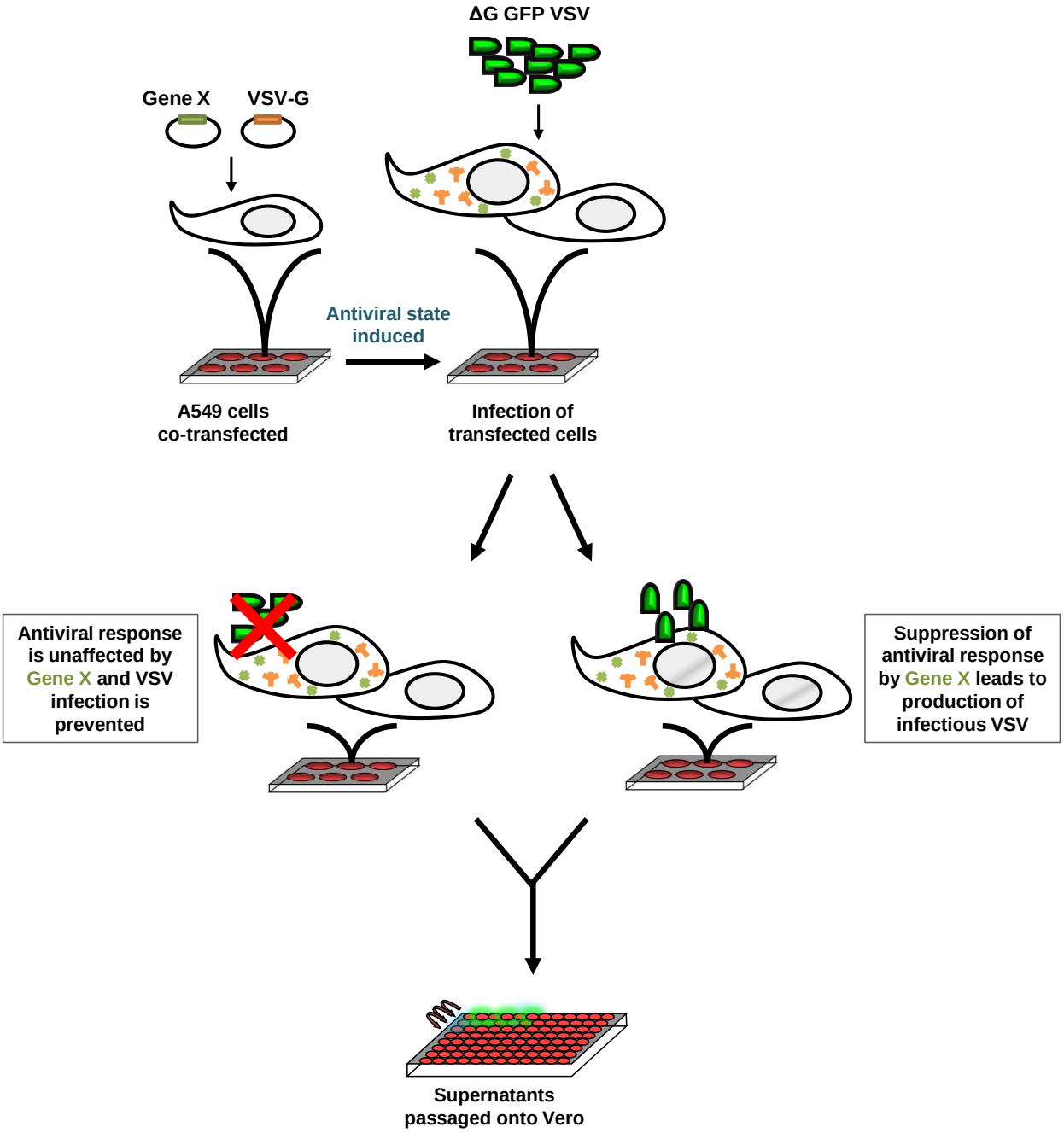
ΔG GFP VSV
Gene X
VSV-G
Antiviral state induced
A549 cells co-transfected
Infection of transfected cells
Antiviral response is unaffected by Gene X and VSV infection is prevented
Suppression of antiviral response by Gene X leads to production of infectious VSV
Supernatants passaged onto Vero

Figure 9. Schematic representation of the VSV G-less assay.

Alterations of the innate antiviral response can be assessed using this innovative assay. An individual gene co-transfected with VSV-G either alters the antiviral response or leaves the response untouched. This outcome can be seen in the production of infectious virus particles or lack thereof and is quantified by GFP fluorescence.

3.1.3. Objectives

The evidence discussed above in 3.1.1. as well as other studies reporting modulation of IFN by various proteins of related arteriviruses such as porcine respiratory and reproductive syndrome virus and equine arteritis virus can be utilized to form hypotheses about HCoV and their own proteins (353-357). Additionally, as the nucleocapsid of SARS has been shown to downregulate type I IFN, the other human coronavirus N proteins potentially act in the same manner (320). Although several accessory proteins of SARS-CoV have been shown to suppress the production and signalling of type I IFN, we chose to examine the nucleocapsid, as it is an essential protein common to all CoV, as opposed to the accessory proteins which vary greatly between viruses. The objectives of the following research were to establish whether the N proteins of HCoV OC43, 229E, and NL63 interfered with the innate IFN response and elucidate the mechanism of this antagonism.

3.2. Results

3.2.1. The nucleocapsid dampens the host antiviral response

As aforementioned, other coronaviral nucleocapsid proteins have been shown to antagonize the type I interferon response. It was probable that the N proteins of human coronaviruses OC43, 229E, and NL63 also affected the IFN response and to initially test this hypothesis, these viral proteins were utilized in the VSV G-less assay.

The three HCoV nucleocapsid genes were first FLAG-tagged and cloned into mammalian expression vector pEF and expression of the resulting plasmids pEF OC43 N-FLAG, pEF 229E N-FLAG, and pEF NL63 N-FLAG, was first confirmed. Strong expression of all N genes was observed by western blot of transfected cells (Figure 10A). By western blot, doublet bands were detected in both NL63 and OC43 lanes, indicating that these proteins had most likely been post-translationally modified by phosphorylation. Cellular localization was also examined by immunofluorescence (Figure 10B). Once again, expression of all FLAG-tagged N proteins was strong, but most of the N expression was excluded from the nucleus.

The three HCoV N genes were subjected to the VSV G-less assay to assess their abilities to affect the antiviral response. Briefly, A549 cells were co-transfected with a VSV-G expression vector and either one of the three HCoV N gene vectors, empty vector pCDNA or positive control vector pEF V-FLAG. The pEF V-FLAG positive control vector expresses a FLAG-tagged Measles virus V

A.

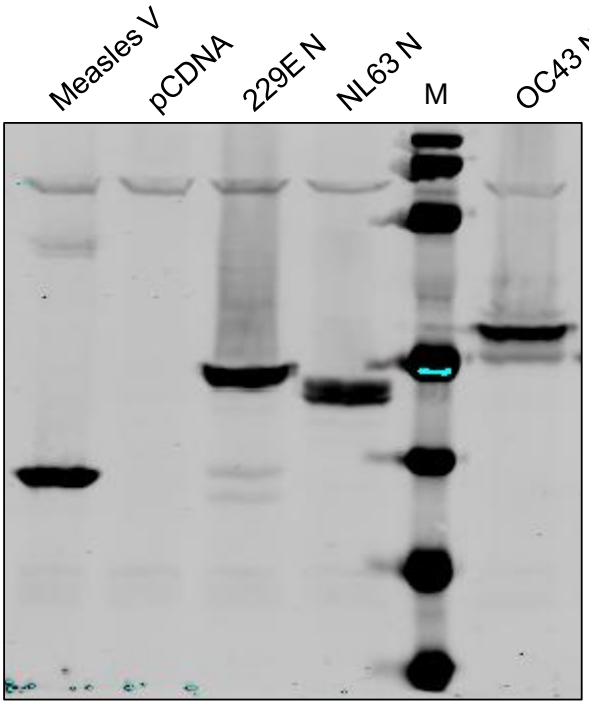
Measles V
pCDNA
229E N
NL63 N
M
OC43 N

B.

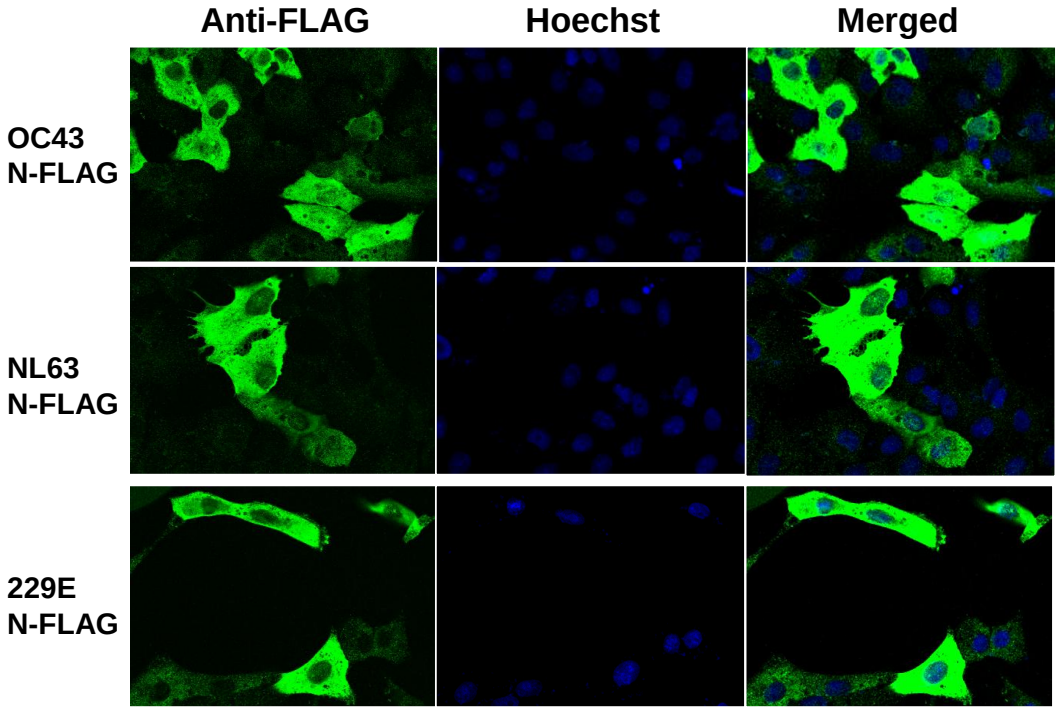
Anti-FLAG
Hoechst
Merged
OC43
N-FLAG
NL63
N-FLAG
229E
N-FLAG

Figure 10. Detection of coronavirus N protein expression.

(A) 293T cells were transfected with expression plasmids containing FLAG-tagged OC43, 229E, and NL63 N genes. Cell lysates were separated on an SDS-PAGE gel and probed with a FLAG antibody. Positive control measles V was seen at the expected size of approximately 37 kD. 229E-N and NL63-N were detected at expected sizes 44 kD and 42 kD, respectively. OC43-N, migrating comparatively more slowly, was detected at the expected size of 55 kD. (B) Vero cells were transfected with expression plasmids containing FLAG-tagged OC43, 229E, and NL63 N genes. Cells were fixed and stained with anti-FLAG, followed by a 488-conjugated secondary. Fluorescence was visualized by confocal microscopy.

A.

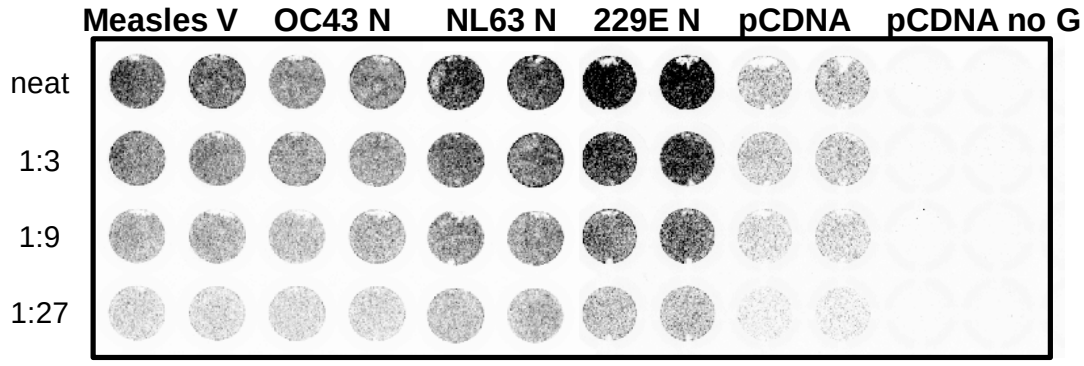
Measles V
OC43 N
NL63 N
229E N
pCDNA
pCDNA no G
neat
1:3
1:9
1:27

B.

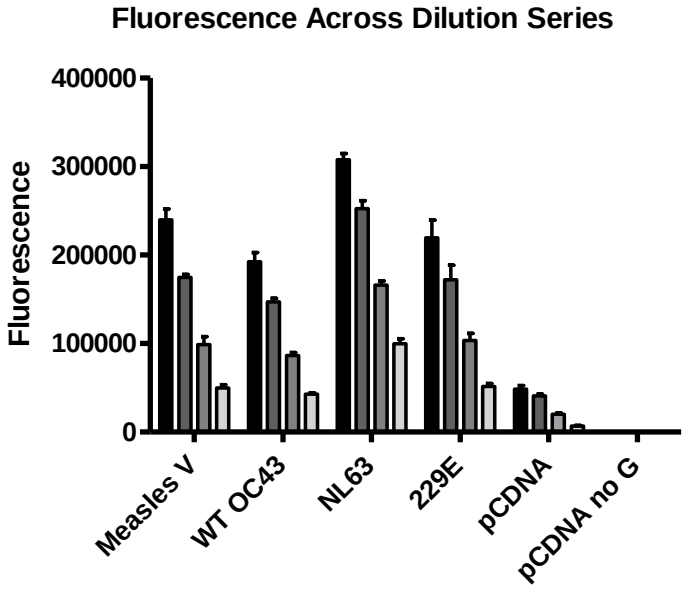
Fluorescence Across Dilution Series
Fluorescence
400000
300000
200000
100000
0
Measles V
WT OC43
NL63
229E
pCDNA
pCDNA no G

Figure 11. Human coronavirus N genes negatively impact the innate antiviral response *in vitro*.

The N genes were assayed for impact on the antiviral response via the G-less VSV assay. (A) Positive control measles V-FLAG showed increased GFP and therefore increased viral replication. Empty vector pCDNA served as a negative control and allowed for minimal viral replication. Empty vector without VSV-G served as a control for carryover of input virus. OC43, NL63, and 229E N genes all showed an elevated level of GFP, indicating an increase in viral replication.
(B) Graphic representation of the quantified GFP measurements illustrate that all 3 N genes allow for increase viral replication as compared to negative control pCDNA.

protein, which is a potent suppressor of the IFN response (358-360). A further negative control used was empty vector transfected alone without VSV-G. 24 hours after transfection, cells were infected with ΔG GFP VSV and supernatants collected the day following infection. These supernatants were then applied in serial dilution to Vero cells and GFP, an indication of viral infection, was measured 24 hours post infection. After visualization by Typhoon scanner, it was clear that all three CoV N proteins strongly impaired the antiviral response in A549 cells (Figure 11A). Further, the fluorescence was quantified from each well and confirmed that cells transfected with OC43 N-FLAG, 229E N-FLAG, and NL63 N-FLAG allowed for more viral replication as compared to empty vector control pCDNA (Figure 11B). Negative control pCDNA allowed for minimal levels of VSV replication and without VSV-G, no replication was observed. As expected, positive control Measles V allowed for high levels of VSV replication. This data indicated that all three HCoV N proteins were able to negatively affect the antiviral response.

The other variation of the VSV G-less assay that employs Vero cells was used to further establish the ability of HCoV N proteins to hinder the IFN response. In this assay, Vero cells were co-transfected with a VSV-G expression vector and either one of the three HCoV N gene vectors, empty vector pCDNA or positive control vector pEF V-FLAG. Following transfection, cells were treated with a series of IFN-α concentrations and subsequently were infected with ΔG GFP VSV. Supernatants were then passaged onto Vero cells in serial dilution. Typhoon scans of the cells showed that in the pCDNA control, VSV infection was strong in untreated cells, but quickly diminished with increasing IFN-α (Figure 12A). As was observed in the A549 G-less assay, Vero cells that were transfected with all three HCoV N genes were permissive to ΔG GFP VSV infection despite treatment with IFN-α (Figure 12A). At higher concentrations of IFN-α (300 and 600 U/ml), VSV infection appears to wane. Measles V was again used as a positive control and cells transfected with this gene were permissive to VSV infection even at higher concentrations of IFN-α. As before, the intensity of GFP was measured and represented in graphical form (Figure 12B). The graph represents data collected from the third dilution (a 1:9 dilution from neat) in the series, as at this level of dilution, subtle differences between samples are more evident. This data corroborates with the A549 G-less assay in that the HCoV N proteins were able to negatively affect the innate antiviral response in Vero cells.

A.

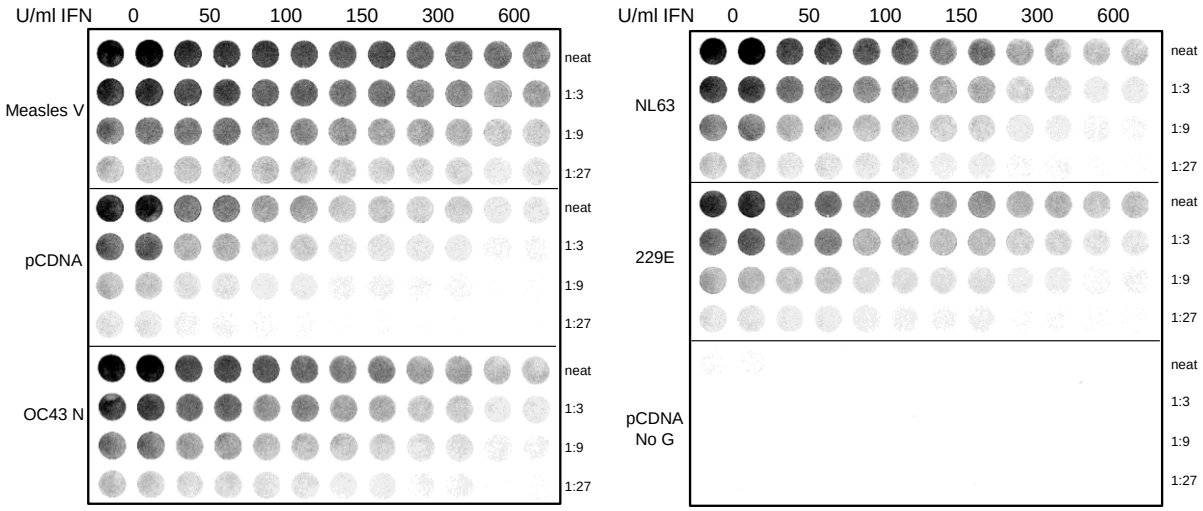
U/ml IFN 0 50 100 150 300 600
Measles V
pCDNA
OC43 N
NL63
229E
pCDNA No G
neat
1:3
1:9
1:27

B.

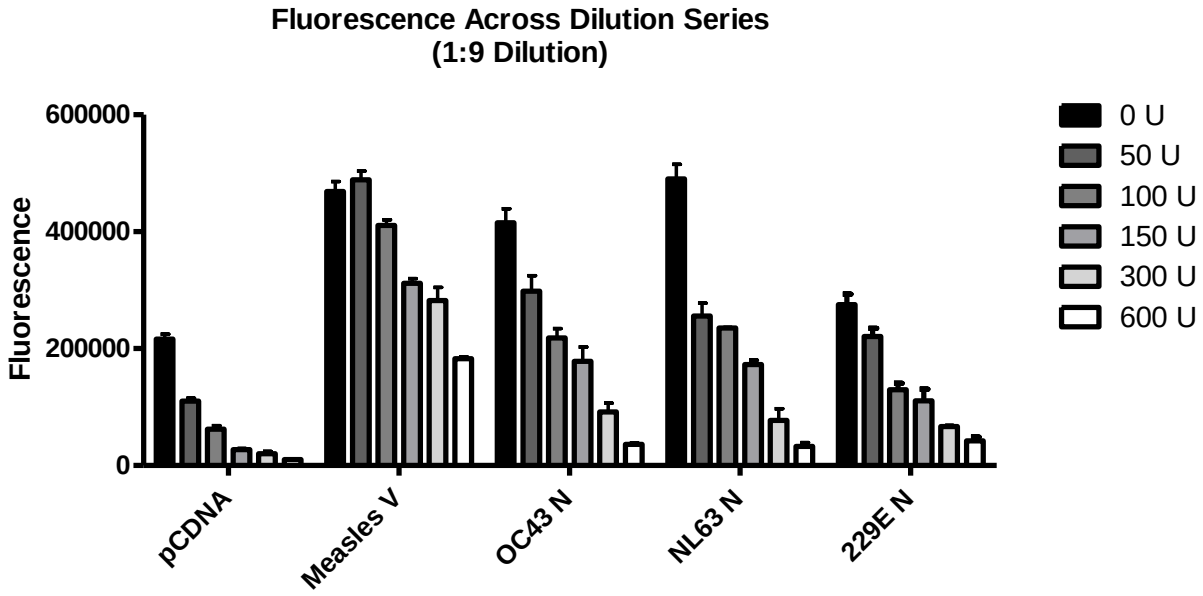
Fluorescence Across Dilution Series (1:9 Dilution)
Fluorescence
600000
400000
200000
0
pCDNA
Measles V
OC43 N
NL63 N
229E N
0 U
50 U
100 U
150 U
300 U
600 U

Figure 12. Human coronavirus nucleocapsid proteins impede IFN-induced antiviral responses in Vero cells.

The N genes were assayed for impact on the antiviral response via the G-less VSV assay in Vero cells. (A) V-FLAG transfected cells showed consistent resistance to IFN at all concentrations. Negative control pCDNA allowed for minimal infectivity with IFN treatment. All OC43, NL63, and 229E N genes all showed an elevated level of GFP despite IFN treatment, indicating an increase in viral replication. At the highest concentrations of IFN, HCoV N genes were less capable of antiviral suppression. Empty vector without VSV-G served as a control for carryover of input virus. (B) Graphic representation of the quantified GFP measurements from the 1:9 dilution illustrate that all 3 N genes allow for increase viral replication as compared to negative control pCDNA.

3.2.2. The nucleocapsid impairs the interferon signaling pathway

In order to further dissect the IFN pathway, the three HCoV N genes were subjected to a series of luciferase assays. A luciferase reporter plasmid containing Firefly luciferase under the control of an interferon stimulated response element (ISRE) promoter, ISRE-luc, and internal control plasmid expressing Betagalactosidase (β-gal) were co-transfected into 293T cells with either one of the three HCoV N gene vectors, empty vector pCDNA or positive control vector pEF V-FLAG. Cells were subsequently stimulated with either 10 or 100 U/ml of IFN-α to drive luciferase expression or left untreated. Upon measurement of luciferase levels, a high level of luciferase was stimulated by IFN-α treatment in pCDNA transfected cells and as expected, minimal luciferase expression was induced in Measles V transfected cells (Figure 13). The HCoV N genes affected IFN-α-stimulated luciferase to varying degrees. OC43 N appeared to have the greatest negative effect, followed by NL63 N. 229E N had a minimal effect on IFN-α-stimulated luciferase compared to the pCDNA control. The membrane protein (M) of OC43 also served as a negative control. This viral protein did not prevent IFN-stimulated luciferase expression, highlighting that suppression of IFN signalling in this luciferase assay is not a general effect of viral proteins. This assay gave further confirmation that HCoV N was impacting the IFN-α signalling pathway.

Next, impact of coroanviral N on RIG-I signalling was investigated by luciferase assay. A vector expressing a constitutively active RIG-I, ΔRIG-I, was utilized to drive the ISRE-luc reporter plasmid. This form of RIG-I consists of its two CARD domains and lacks the autoinhibitory domain (361). Two different amounts of ΔRIG-I were co-transfected with ISRE-luc, β-gal, and coronaviral N plasmids or control plasmids pCDNA and pEF V-FLAG. 24 hours post-transfection, luciferase was measured. The ΔRIG-I vector stimulated luciferase expression in pCDNA transfected cells and measles V was able to dampen the effects of ΔRIG-I by approximately 50% (Figure 14). However, none of the coronaviral N genes were able to block ΔRIG-I stimulation of luicferase expression to any statistically significant level. From this data, it was concluded that HCoV N did not affect RIG-I mediated signalling.

Lastly, in order to investigate effects of HCoV N on interferon regulatory factor 3 (IRF-3), a vector expressing a dominant negative (constitutively active) IRF-3, IRF3-5D, was utilized to drive the ISRE-luc reporter plasmid. IRF3-5D contains five serine to aspartic acid substitutions in its key C-terminal region of phosphorylation which mimics phosphorylated and activated IRF3 (362). Once

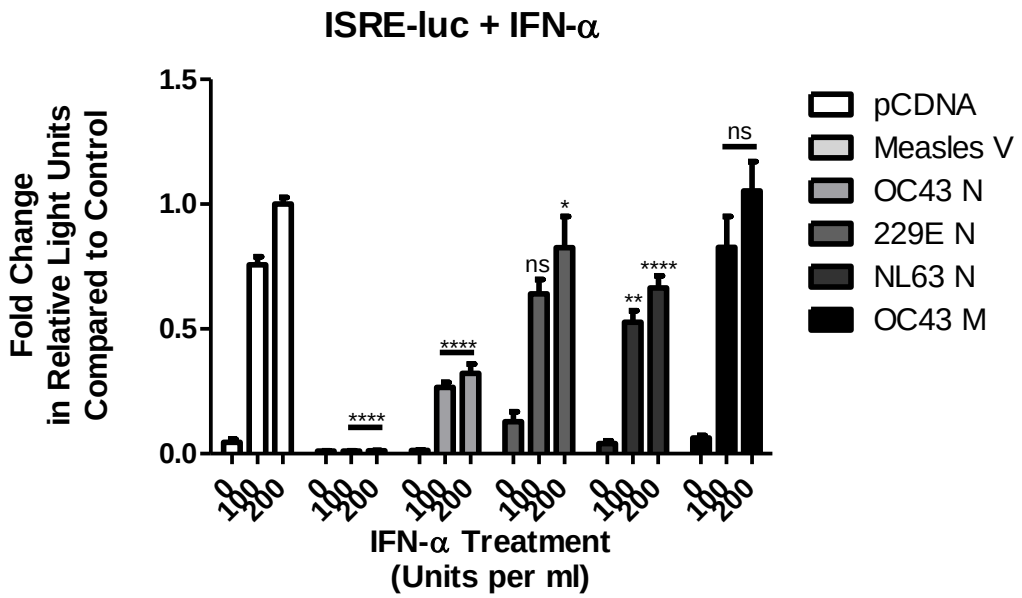
ISRE-luc + IFN-α
Fold Change in Relative Light Units Compared to Control
1.5
1.0
0.5
0.0
ns
****
****
*
ns
**
****
100
200
IFN-α Treatment (Units per ml)
pCDNA
Measles V
OC43 N
229E N
NL63 N
OC43 M

Figure 13. Human coronavirus N proteins negatively impact IFN signalling.

293T cells were co-transfected with each CoV-N gene and reporter plasmid ISRE-luc and subsequently stimulated with IFN-α. While OC43 N reduced luciferase expression by more than half compared to pCDNA control, 229E N did not have as significant an effect. NL63 N also significantly interfered with IFN signalling, but not as dramatically as OC43 N. Negative control OC43 M protein did not affect IFN signalling. All luciferase measurements were normalized to β-galactosidase and compared to negative control pCDNA, which was set to 1. pCDNA, measles V, and OC43 N data represents four independent experiments, each performed in duplicate. 229E N and NL63 N data represents three independent experiments, each performed in duplicate. OC43 M data represents one experiment performed in duplicate. Error bars represent standard error of the mean. * $p < 0.1$, ** $p < 0.01$, **** $p < 0.0001$, ns – not significant.

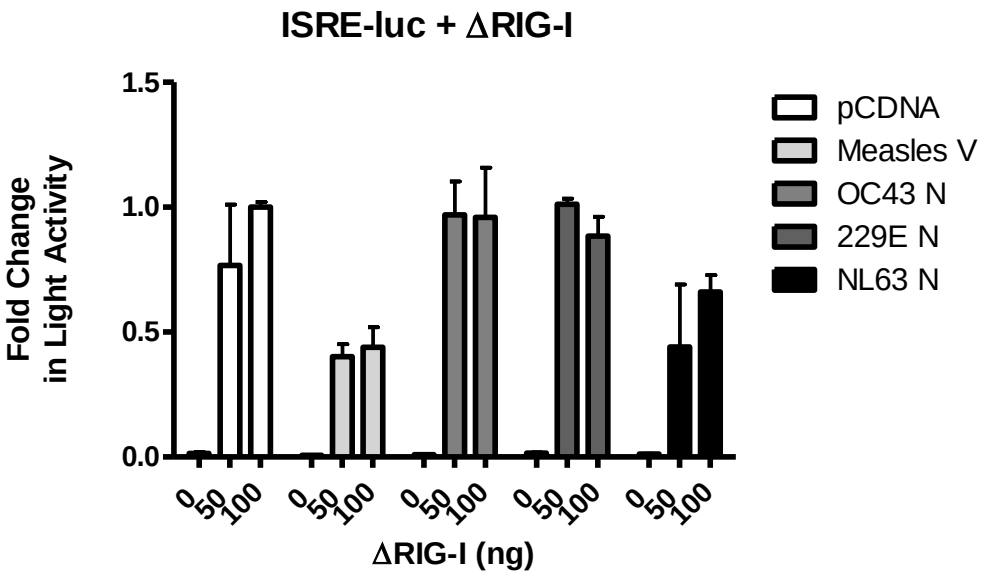
ISRE-luc + ΔRIG-I
Fold Change in Light Activity
1.5
1.0
0.5
0.0
0
50
100
ΔRIG-I (ng)
pCDNA
Measles V
OC43 N
229E N
NL63 N

Figure 14. Human coronavirus N proteins do not interfere with RIG-I signalling.

293T cells were co-transfected with each HCoV N gene, constitutively active construct ΔRIG-I and reporter plasmid ISRE-luc. No significant reduction in luciferase activity was observed in HCoV N expressing cells compared to empty vector control. All luciferase measurements were normalized to β-galactosidase. Data represents two independent experiments, each performed in duplicate. Error bars represent standard error of the mean. * $p < 0.1$.

again, two different amounts of IRF3-5D were co-transfected with ISRE-luc, β-gal, and HCoV N vectors or control plasmids pCDNA and pEF V-FLAG. 24 hours post-transfection, luciferase was measured. Measles V was able to significantly reduce luciferase expression as compared to control vector pCDNA (Figure 15). While the HCoV N genes did not appear to have a dramatic effect on IRF-3 driven luciferase expression, OC43 N dampened luciferase activity at lower concentrations of IRF3-5D (Figure 15). 229E N also lessened luciferase activity driven by IRF3-5D to a level that was significantly lower, statistically, than the pCDNA control. No significant reduction was observed in cells expressing NL63 N. It was concluded that OC43 N and 229E N have minimal effects on IRF-3 signalling.

The state of STAT1 phosphorylation was examined in N-transfected cells via western blot. Cells were transfected with OC43 N and subsequently treated with IFN-α. The state of STAT1 was detected at several times post-IFN treatment with a phospho-specific STAT1 antibody. Untreated cells did not contain phosphorylated STAT1 (Figure 16). STAT1 was rapidly phosphorylated with IFN stimulation in both empty vector and N-transfected cells. There did not appear to be any differences in STAT1 phosphorylation between control and N-expressing cells, indicating that STAT1 is not the point at which N impedes IFN signalling.

3.2.3. Functional mapping of the nucleocapsid via mutational analysis

As discussed in section 1.2.2., the CoV N protein has several functional domains which serve various purposes during coronaviral infection. In an attempt to dissect which domain was responsible for interference with the antiviral response, several mutants of N were constructed. OC43 N was chosen for mutant construction and continuing research as it consistently had effects in both the G-less and luciferase assays.

The N mutants were constructed based on previous research of functional regions (125). Four mutants were constructed by PCR mutagenesis (Figure 17). Mutants consisting of the N-terminal domain (NTD) and C-terminal domain (CTD) of N were constructed, as well as a mutant lacking the central serine arginine (SR) rich domain (ΔSR). Lastly, an additional N-terminal mutant was constructed which contained an adjacent serine, glycine, arginine rich (SGR) domain, SGR-NTD. All mutants were FLAG-tagged for detection purposes.

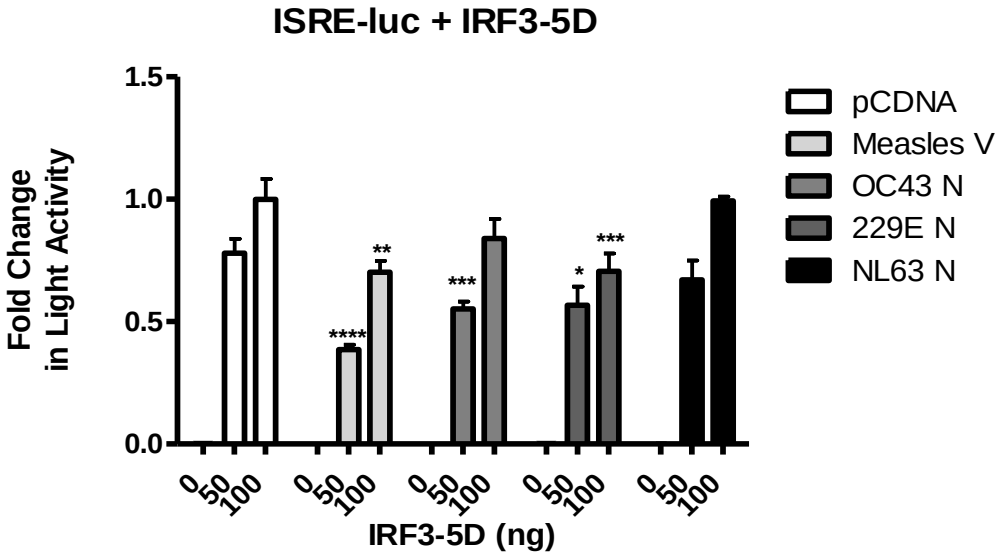
ISRE-luc + IRF3-5D
Fold Change in Light Activity
1.5
1.0
0.5
0.0
****
**
***
*
***
0
50
100
IRF3-5D (ng)
pCDNA
Measles V
OC43 N
229E N
NL63 N

Figure 15. Human coronavirus N proteins negatively effect IRF3 signalling.

293T cells were co-transfected with each HCoV N gene, constitutively active construct IRF3-5D and reporter plasmid ISRE-luc. Significant reduction in luciferase activity was observed in both OC43 N and 229E N expressing cells compared to empty vector control. NL63 N did not significantly impact IRF3 stimulated luciferase. All luciferase measurements were normalized to β-galactosidase. Data represents two independent experiments, each performed in duplicate. Error bars represent standard error of the mean. * $p < 0.1$, ** $p < 0.01$, *** $p < 0.001$, **** $p < 0.0001$.

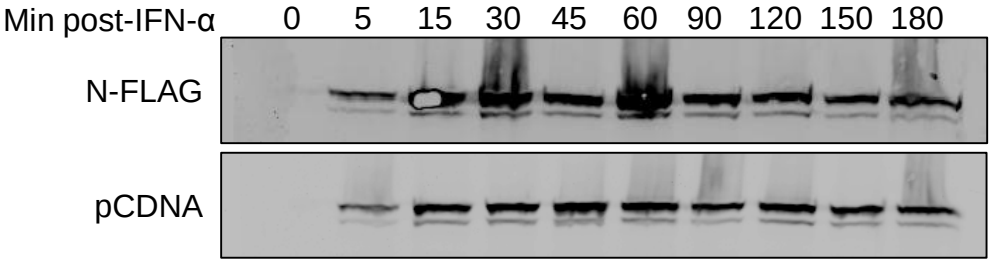
Min post-IFN-α
0
5
15
30
45
60
90
120
150
180
N-FLAG
pCDNA

Figure 16. OC43 N does not prevent STAT1 phosphorylation in response to IFN.

293T cells were transfected with OC43 N or empty vector pCDNA and subsequently stimulated with IFN-α. STAT1 phosphorylation was detected at various timepoints post-IFN treatment. STAT1 in both N and pCDNA transfected cells was phosphorylated as early as 5 min post-treatment and remained phosphorylated up to 180 min post-treatment. OC43 N does not interfere with IFN-induced STAT1 phosphorylation.

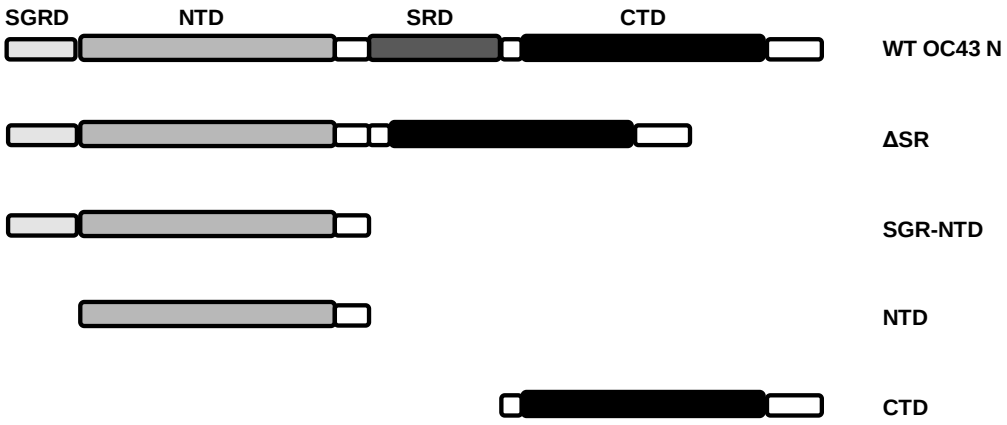
SGRD
NTD
SRD
CTD
WT OC43 N
ΔSR
SGR-NTD
NTD
CTD

Figure 17. Schematic of mutant N genes generated.

A total of 4 truncated N mutants were created. ΔSR consists of OC43 N with a deletion of its SR domain. The SGR-NTD mutant contains the SGR domain and NTD, whereas the NTD mutant solely contains the N-terminal region of the gene. Mutant CTD consists of the C-terminal domain of the gene.

After construction of the mutants, expression of the truncated N proteins were verified by western blot. Both ΔSR and CTD mutants were easily detected from transfected cells (Figure 18A). As the central SR region is a major site of phosphorylation, the ΔSR mutant was not detected as a doublet as seen in wild type N indicating that post-translational phosphorylation had not taken place. Both were expected sizes of approximately 53 kDa (ΔSR) and 23 kDa (CTD). The two N terminal mutants, NTD and SGR-NTD, were not detected by western blot. Although protein levels were undetectable in NTD and SGR-NTD transfected cells, it was a possibility that they were being transcribed but not translated or the proteins were unstable and being degraded. The mRNA expression of NTD and SGR-NTD in transfected cells was assessed by RT-PCR. mRNA was detected from both NTD and SGR-NTD transfected cells, though expression of SGR-NTD appeared to be stronger than NTD (Figure 18B). This confirmed that transcription of both mutants was occurring, though protein expression was not detectable.

Subcellular localization as well as expression of the NTD mutant was examined in transfected cells by immunofluorescence. Numerous cells expressed the CTD and ΔSR mutants well and expression was mostly cytoplasmic (Figure 19). Expression of the NTD mutant was extremely low in frequency, with the number of cells on one slide expressing NTD in the single digits.

The ability of the mutants to inhibit the innate immune response was tested utilizing the VSV G-less assay. A549 cells were co-transfected with VSV-G and the mutant N genes ΔSR, NTD, SGF-NTD, CTD, or control plasmids pCDNA and pEF V-FLAG. Transfected cells were then infected with ΔG GFP VSV as before, and supernatants were subsequently passaged onto Vero cells. When the Vero cells were scanned for GFP fluorescence indicating VSV infection, surprisingly all the mutants transfected allowed for significant ΔG VSV replication (Figure 20). The level of permissiveness was on par with both measles V and WT N.

The ISRE luciferase assay was performed with the mutant N genes. 293T cells were co-transfected with ISRE-luc, β-gal, and the mutant N genes ΔSR, NTD, SGF-NTD, CTD or control plasmids pCDNA and pEF V-FLAG. Transfected cells were subsequently stimulated with IFN-α. Resultant luciferase levels reflected what was observed in the G-less assay. All N mutants blocked IFN-α

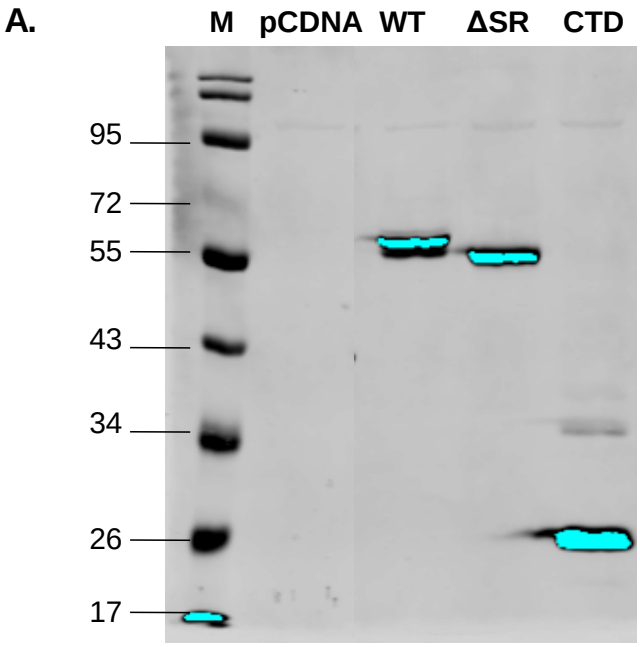
A.
M
pCDNA
WT
ΔSR
CTD
95
72
55
43
34
26
17

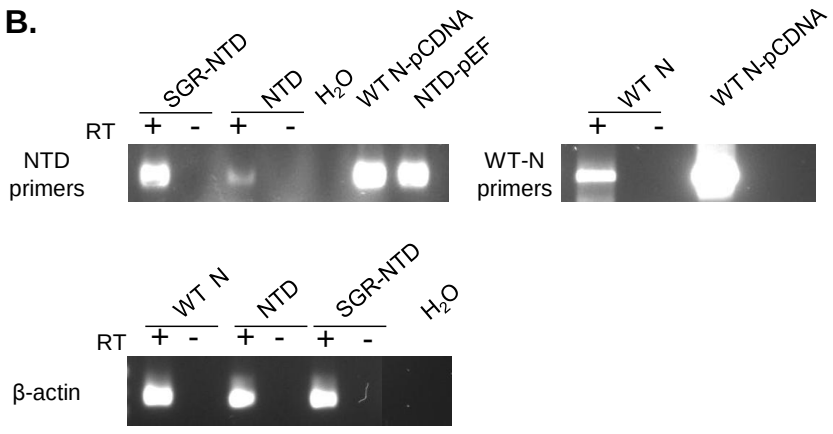
B.
SGR-NTD
NTD
H2O
WT N-pCDNA
NTD-pEF
RT
+ - + -
NTD primers
WT N
WT N-pCDNA
+ -
WT-N primers
WT N
NTD
SGR-NTD
H2O
RT
+ - + - + -
β-actin

Figure 18. Expression of N mutant proteins.

(A) 293T cells were transfected with each WT OC43-N, ΔSR, CTD, NTD, SGR-NTD, and pCDNA. Mutant N proteins were detected by western blot. WT OC43-N was detected at its expected size of 55 kD, with a doublet as seen previously. The mutant ΔSR was detected as a single band at around 55 kD. The CTD mutant was detected around its expected size of 23 kD. The 2 NTD mutants, NTD and SGR-NTD, were not able to be detected by Western (not shown). (B) RT-PCR from SGR-NTD and NTD transfected cells revealed that mRNA from both constructs were expressed.

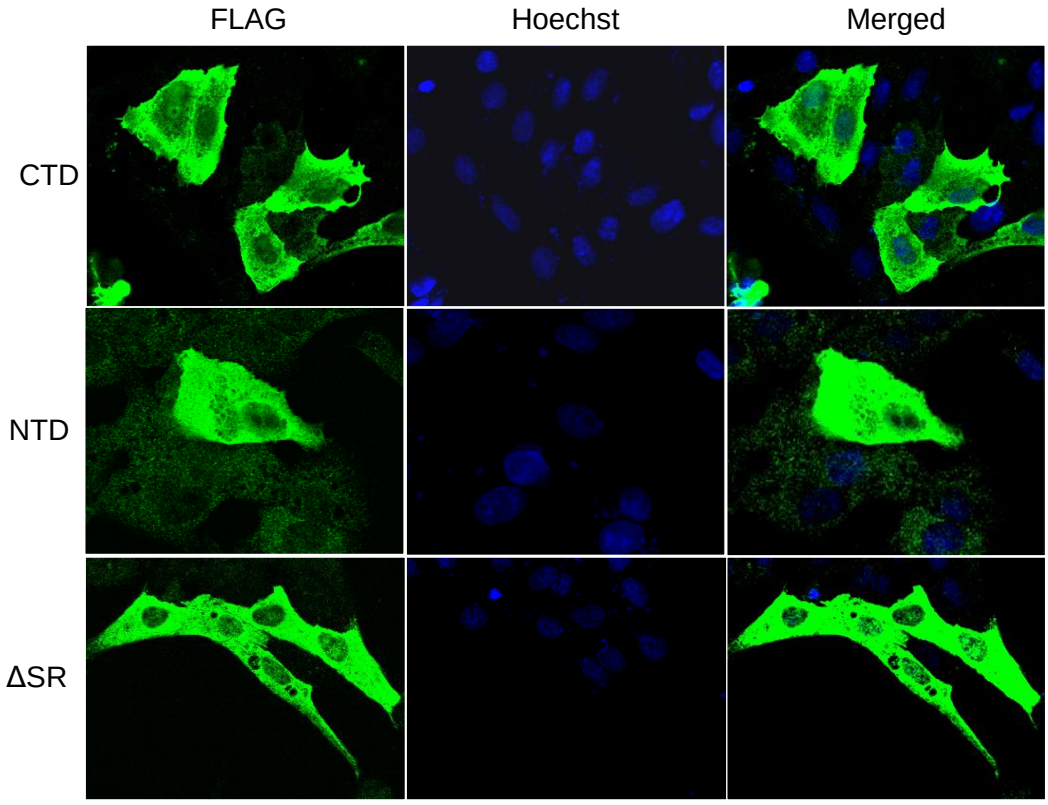
FLAG
Hoechst
Merged
CTD
NTD
ΔSR

Figure 19. Truncated N proteins show cytoplasmic distribution.

Vero cells were transfected with OC43 N truncated mutant constructs, fixed and stained with an antibody against FLAG. Hoechst was utilized to visualize the nucleus. All three mutants were visualized primarily in the cytoplasm.

A.

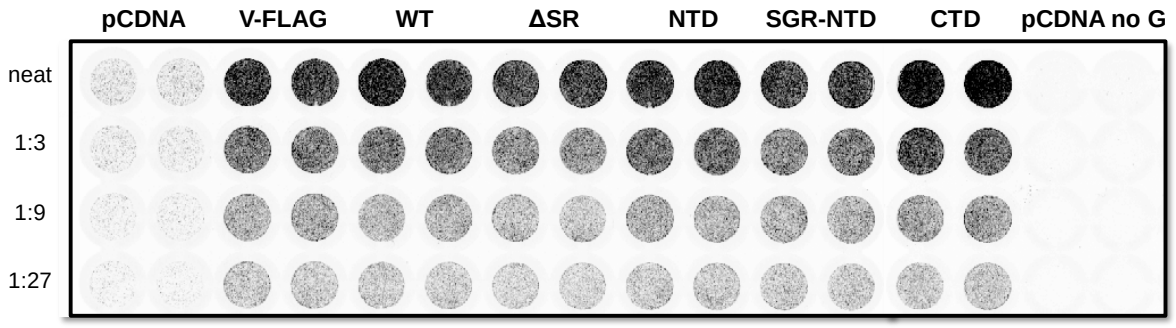
pCDNA
V-FLAG
WT
ΔSR
NTD
SGR-NTD
CTD
pCDNA no G
neat
1:3
1:9
1:27

B.

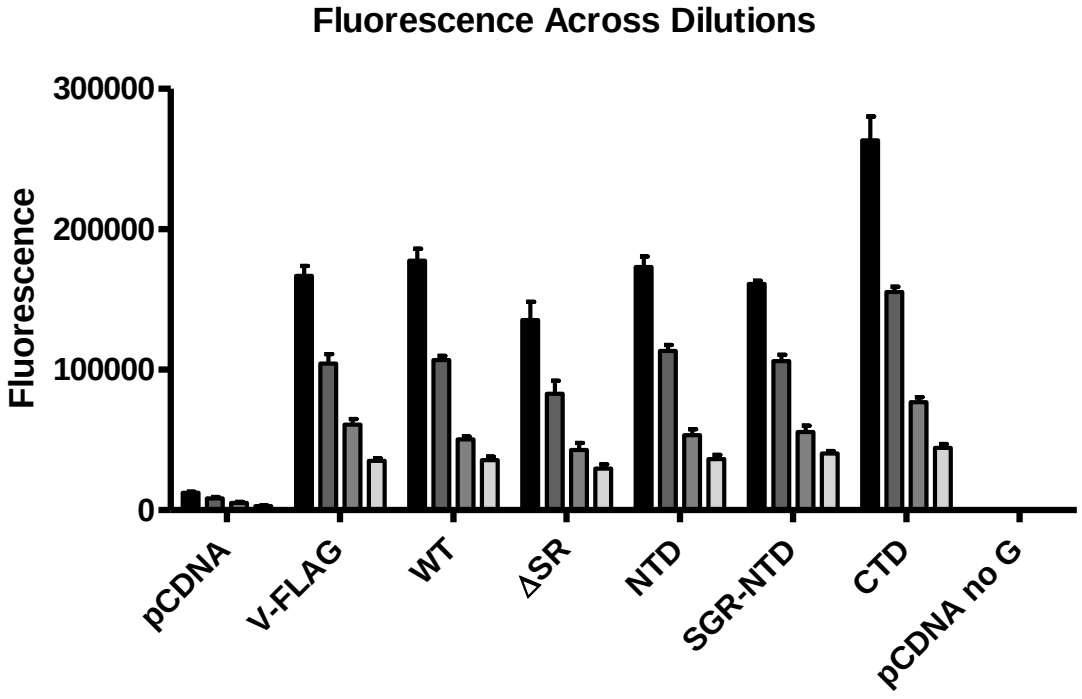
Fluorescence Across Dilutions
Fluorescence
300000
200000
100000
0
pCDNA
V-FLAG
WT
ΔSR
NTD
SGR-NTD
CTD
pCDNA no G

Figure 20. Truncated N genes impede the innate antiviral response.

Mutant N genes were assayed for differing ability to impact the innate antiviral response *in vitro* via VSV G-less assay. (A) As compared to the negative control pCDNA, all mutant N genes appeared to allow for increased VSV replication. (B) Graphical representation of the quantified GFP.

signalling, resulting in lower luciferase levels compared to pCDNA control (Figure 21).

Lastly, the other plasmid stimulants of ISRE-luc, ΔRIG-I and IRF3-5D, were also used to determine if the mutant N genes had an effect on RIG-I and IRF-3 signalling. Cells were co-transfected as before, and luciferase measured. No significant suppression by mutant N genes was observed in ΔRIG-I stimulated luciferase (Figure 22). When ISRE-luc was driven by IRF3-5D, both ΔSR and CTD mutants suppressed luciferase activity and less of an effect was observed in cells transfected with NTD and SGR-NTD (Figure 23).

3.3. Discussion

The nucleocapsid proteins of coronaviruses have been shown to be multifunctional, as they play a major role in virion formation along with possessing immune modulatory properties. The immune modulatory properties of human coronaviruses OC43, 229E, and NL63 had not previously been explored. By analogy to other nidovirus nucleocapsid proteins, it was hypothesized that these three HCoV N proteins would retain similar properties of IFN antagonism.

The N genes of OC43, 229E, and NL63 were initially investigated for effects on the innate antiviral response via the VSV G-less assay. The advantages of this assay are numerous for investigation of individual proteins in a transient transfection situation. As ΔG GFP VSV can only be produced from cells transfected with VSV-G which would also be transfected with the gene of interest, HCoV N in this case, only the innate immune response generated in the transfected cells will be measured. ΔG GFP VSV will also only replicate in cells if the innate immune response has been compromised by the co-transfected gene of interest. The hypothesis that HCoV N is able to affect the innate immune response was confirmed via our G-less assay. The N proteins were able to prevent an innate immune response from being generated in A549 cells in response to transfection. In the other variation of the VSV G-less assay which employs transfected Vero cells treated with IFN, all HCoV N genes allowed for ΔG GFP VSV replication post-IFN-α-treatment. VSV infection and replication did decline as IFN-α concentrations increased, revealing a dose response and implying a threshold for inhibition by HCoV N. The positive control measles V protein is more potent inhibitor of type I IFN compared to N, reflected in the sustained VSV infection in measles V transfected cells despite increases in IFN-α

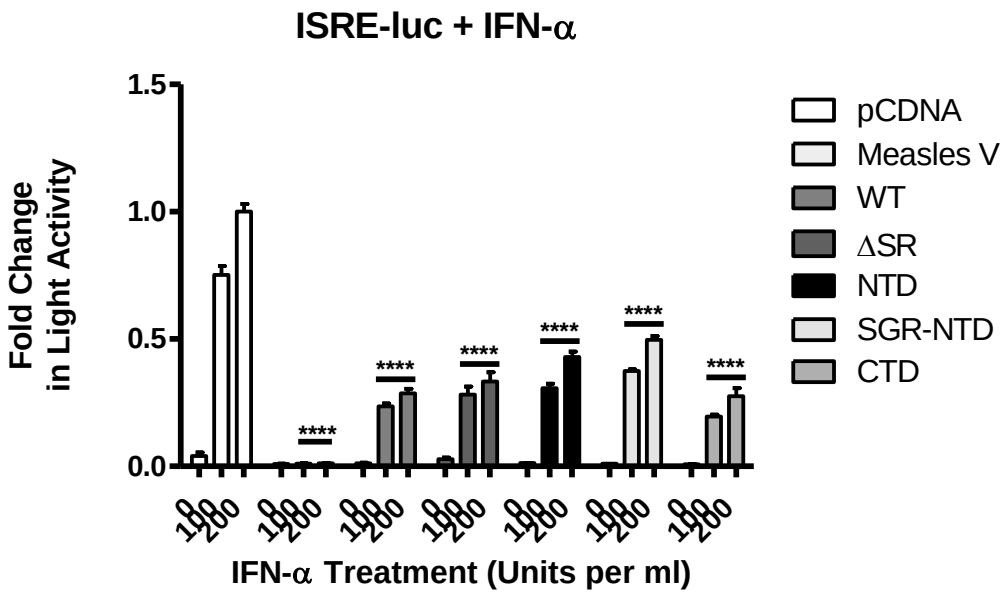
ISRE-luc + IFN-α
Fold Change in Light Activity
1.5
1.0
0.5
0.0
****
pCDNA
Measles V
WT
ΔSR
NTD
SGR-NTD
CTD
100
200
IFN-α Treatment (Units per ml)

Figure 21. Mutant N genes impact IFN-stimulated signaling.

293T cells were co-transfected with each mutant N gene and reporter plasmid ISRE-luc and subsequently stimulated with IFN-α. All mutant genes had a negative effect on the expression of IFN-α stimulated ISRE-luciferase. All luciferase measurements were normalized to β-galactosidase. Data from pCDNA, measles V, wild-type N, and ΔSR mutant represents four independent experiments, each performed in duplicate. CTD mutant data represents two independent experiments, each performed in duplicate. NTD and SGR-NTD mutant data represents one experiment performed in duplicate. Error bars represent standard error of the mean. **** $p < 0.0001$.

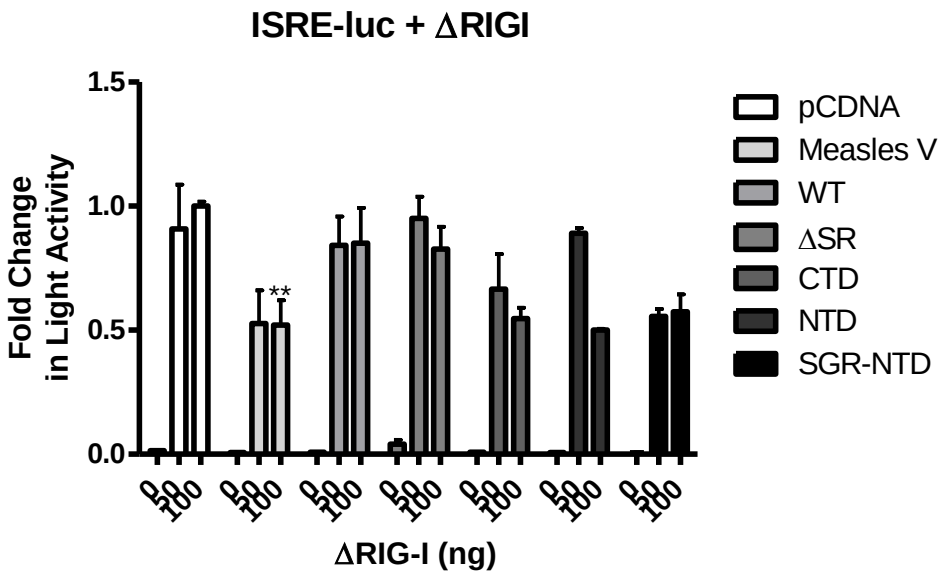
ISRE-luc + ΔRIGI
Fold Change in Light Activity
1.5
1.0
0.5
0.0
**
0
50
100
ΔRIG-I (ng)
pCDNA
Measles V
WT
ΔSR
CTD
NTD
SGR-NTD

Figure 22. Mutant N genes do not impact RIG-I mediated signaling.

293T cells were co-transfected with each mutant N gene, constitutively active construct ΔRIG-I and reporter plasmid ISRE-luc. No significant differences in luciferase activity were observed between cells transfected with empty vector control pCDNA and mutant N genes. All luciferase measurements were normalized to β-galactosidase. Data from pCDNA, measles V, wild-type N, and ΔSR mutant represents three independent experiments, each performed in duplicate. Data from CTD, SGR-NTD, and SGR mutants represents one experiment performed in duplicate. Error bars represent standard error of the mean. ** $p < 0.01$.

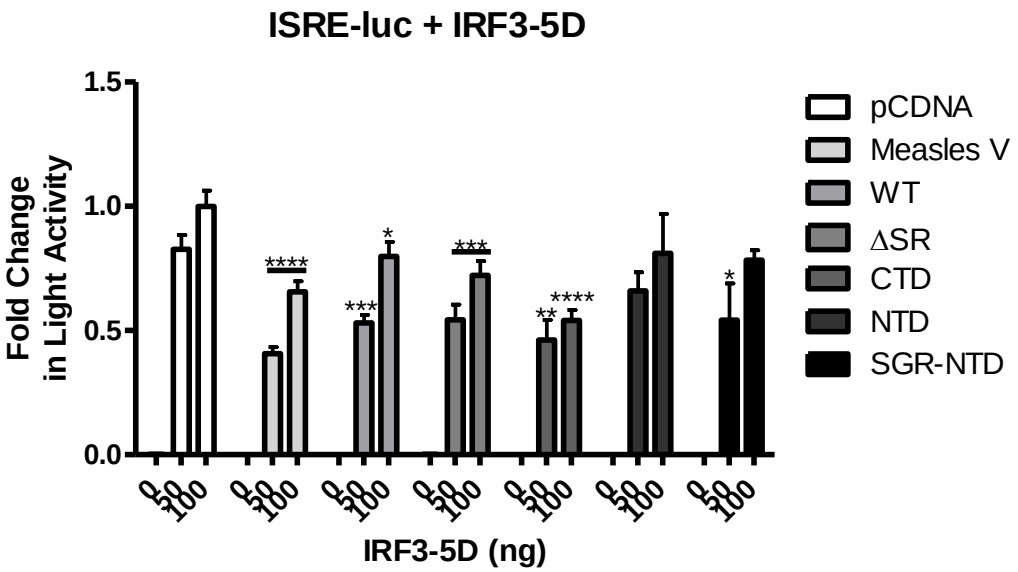
ISRE-luc + IRF3-5D
Fold Change in Light Activity
1.5
1.0
0.5
0.0
****
*
***
***
**
****
*
0
50
100
IRF3-5D (ng)
pCDNA
Measles V
WT
ΔSR
CTD
NTD
SGR-NTD

Figure 23. CTD and ΔSR mutant N proteins negatively impact IRF3 signalling.

293T cells were co-transfected with each mutant N gene, constitutively active construct IRF3-5D and reporter plasmid ISRE-luc. Consistent with previous results, full-length N significantly prevented IRF3-induced luciferase at lower concentrations of IRF3-5D. Both ΔSR and CTD mutants were also able to significantly interfere with IRF3 signalling. All luciferase measurements were normalized to β-galactosidase. Data from pCDNA, measles V, wild-type N, and ΔSR mutant represents three independent experiments, each performed in duplicate. Data from CTD, NTD, and SGR-NTD mutants represents one experiment performed in duplicate. Error bars represent standard error of the mean. * $p < 0.1$, ** $p < 0.01$, *** $p < 0.001$, **** $p < 0.0001$.

treatment. Taken together, this implicated that the HCoV N proteins were impacting the cell's ability to generate and respond to antiviral signals.

One potential difficulty in studying individual proteins by transfection is expression variations between cells and efficiency of transfection itself, which also varies depending on cell line. This was encountered with initial experiments using HCoV N genes which were originally cloned into the pCDNA mammalian expression vector. Protein overexpression typically yields relatively robust levels of the foreign protein, however N genes expressed from pCDNA vectors were barely detectable. This was mirrored by VSV G-less assays in which cells transfected with N genes showed similar levels of ΔG VSV susceptibility to that of pCDNA control. Even though the VSV G-less assay somewhat neutralizes the variation experienced in transfection-based assays (in terms of efficiency oftransfection), transcription levels and subsequent protein levels of the exogenous protein remain significant. This expression issue was resolved by subcloning the HCoV N genes into another expression vector, pEF, in which the V-FLAG positive control was cloned. One major difference between pCDNA and pEF is the promoter, human cytomegalovirus (CMV) immediate-early versus elongation factor (EF), respectively. As excellent expression was always seen with V-FLAG, it was expected that the N genes would also be vigorously expressed in the pEF vector.

Another factor impacting expression is contamination of the prepared DNA with endotoxin or lipopolysaccharide (LPS), a bacterial component that can remain from the bacteria used to propagate the plasmid. It has been long known that LPS contamination could lead to lower transfection efficiencies, though the level of endotoxin necessary is debatable (363, 364). This can be eliminated by using endotoxin-free reagents, commercially available, to prepare all plasmid DNA. This tactic was employed to ensure that optimal levels of protein expression were being obtained. This was also important in that innate immune signalling was being examined and LPS is a stimulant of innate immunity.

The HCoV N genes were confirmed to interfere with the IFN response via the luciferase assay employed. The reporter plasmid utilized consisted of an ISRE promoter, which can be driven by various stimuli. In cells transfected with HCoV N, IFN-α stimulated luciferase expressed was negatively affected. This corroborated with the effects seen in the VSV G-less assay. To attempt to further dissect the point of intervention in the IFN pathway, different stimuli were employed. Two plasmids encoding constitutively active RIG-I (ΔRIG-I) and IRF3

(IRF3-5D) were co-transfected with HCoV N genes to drive the expression of luciferase. No repression of ΔRIG-I-induced luciferase was observed in HCoV N expressing cells, while the positive control Measles V had some effect. While the most obvious conclusion that can be made from this data is that HCoV N is not able to block downstream signalling of RIG-I, it is also possible that the activity of ΔRIG-I was too strong to overcome. Overexpression of the constitutively active protein would lead to high levels of ΔRIG-I which could have overwhelmed the mechanism by which HCoV N inhibits.

HCoV N genes appeared to be more effective at interfering with IRF3-5D stimulation of ISRE-luc, with both OC43-N and 229E-N having statistically significant impacts on luciferase expression. As previously discussed, the RIG-I pathway leads to IRF3 activation, which seems contradictory to the luciferase results when considered together. Many pathways lead to IRF3 activation, however, such as the pathway initiated by TLR3. Downstream pathways also differ, as RIG-I activation results in the activation of not only IRF3, but also NF-κB. Utilizing a reporter with a promoter that is further upstream in the pathway, such as the IFN-β promoter, could help further distinguish which point in the pathway HCoV N is affecting.

Mutational analysis was undertaken using OC43 N in attempts to dissect the active region of the nucleocapsid protein in the IFN suppression. The generation of deletion mutants was based on previous reports of CoV N regional analyses. The C-terminal mutant (CTD) and mutant lacking the central SR-rich region (ΔSR) were robustly expressed, but the N-terminal mutants (NTD and SGR-NTD) were not detected via western blot. Both NTD and SGR-NTD were confirmed to express their respective mRNAs, indicating the expression problem lay within protein translation or stability. Further investigation by immunoflourescence of N-terminal mutant transfected cells revealed that the protein was being expressed, but the expression was only detectable in a minimal number of cells. As endotoxin contamination can inhibit transfection, all DNA plasmids were prepared endotoxin-free, but expression levels did not change.

Mutants were screened for effects on antiviral innate immunity via the VSV G-less assay. Surprisingly, all of the mutants were able to suppress the antiviral response, allowing for ΔG GFP VSV permissiveness. This result was echoed in the ISRE luciferase assay when stimulated with IFN-α. Most surprising was that the low-expressing N-terminal mutants had an effect as well. It is unknown why

the NTD mutants had effects on the antiviral response, as the protein expression level was so low. While these assays do somewhat control for variations in transfection efficiency, it does not entirely explain why such a large effect was observed.

Subsequent to the completion of this research, a report was published detailing the functional regions of OC43 N specifically (123). Prior to this study, no research on the elucidation of OC43 N regions had been published. The domains described varied from our created mutants as we also considered linker-regions between domains. More recently, this same group has further published on the OC43 N N-terminal and this region is more in line with our N-terminal mutant (365, 366). Our mutant constructs classified the N-terminal domain between amino acids 1-191, SR-rich domain between amino acids 197-208, and the C-terminal domain between amino acids 253-448. The published study defined these domains between amino acids 1-173, 174-300, and 301-448, respectively, which results in both our NTD and CTD domains to overlap with the published SR domain. These discrepancies between our constructs and published regional divisions could account for the identical effects between N mutants in the VSV G-less assay and luciferase assays, assuming that there is a single region responsible for IFN antagonism.

No concrete mechanisms have been reported for the downregulation of the type I IFN response by CoV-N as of yet. One recent report on SARS-CoV N gave evidence to support that the point of interference was upstream of RIG-I (329). While N could prevent poly(I:C) and Sendai virus-induced IFN, N could not prevent the induction of IFN by RIG-I, MAVS, TRIF, TBK1 or IKKi (329). This indicated that the point of interference was upstream of these components of the signalling pathway. Furthermore, SARS-CoV N inhibited synthetic dsRNA analog polyinosinic:polycytidylic
acid (poly(I:C)) induced IRF3 nuclear localization, but was not able to prevent IRF3 activation via the MAVS pathway. In addition, the authors determined that the C-terminal of SARS-CoV N was essential for the suppression of IFN and correlated with the RNA-binding abilities of the C-terminal to this immune evasion. The authors speculated that SARS-CoV N masks the recognition of RNA via interaction. The RNA-binding regions of SARS-CoV N originally were thought to be solely located in the N-terminal, with the C-terminal solely responsible for oligomerization, but more evidence points towards the C-terminal possessing RNA-binding capabilities equivalent to or greater than the N-terminal (122, 367, 368). These results corroborate with a previous study by Kopecky-

Bromburg *et al.* which showed SARS-CoV N suppresses IFN response induced by Sendai virus, a strong IFN inducer, and prevents the phosphorylation and nuclear localization of IRF3 (320). SARS-CoV N does not, however, inhibit IFN-β signalling, as STAT1 was phosphorylated and an ISRE-luc reporter assay showed equivalent activation to control.

Although no mechanism was elucidated for OC43 N, 229E N, and NL63 N in the suppression of IFN, it appears that they act differently than that of SARS-CoV N. Our data indicates that the three HCoV N proteins are able to suppress IFN signalling, whereas SARS-CoV N does not. The ability of SARS-CoV N to bind and mask RNA from innate immune recognition may apply to the remaining HCoV N proteins, but one can only speculate as although N-transfected cells were challenged with VSV, they were not stimulated with poly(I:C). The N proteins are all known RNA binding proteins and this interaction could contribute to IFN suppression in addition to another unknown mechanism.

Chapter 4
Coronavirus Nucleocapsid Modification of the NF-κB Activation Pathway

4.1. Introduction

4.1.1. Current knowledge of effects of coronaviral N on NF-κB

Currently, limited published studies have reported the relationship between coronaviral infection and the transcription factor NF-κB. Even fewer have addressed the effects of human coronaviruses, with the exception of SARS-CoV, on NF-κB.

Several proteins of SARS-CoV have been shown to effect NF-κB activation. In transfected cells, the structural spike protein (S) activates the p65 subunit of NF-κB, leading to increased expression of proinflammatory cytokines Il-6, TNF-α, and IL-8 (369, 370). Conversely, the membrane protein binds IκB kinase β (IKKβ) in transfected cells, and as a result suppresses NF-κB activation (371). Nonstructural proteins of SARS-CoV also have an effect on NF-κB. The papain-like protease (PLP) antagonizes NF-κB activation, while non-structural protein 1 (nsp 1) activates NF-κB (327, 372). Two of SARS-CoV accessory proteins, 3a and 7a, are also activators of NF-κB which leads to an increase in IL-8 expression (373).

Few other coronaviruses have been examined for effects on NF-κB. Transmissible gastroenteritis virus (TGEV), which infects pigs, has been shown to activate NF-κB during *in vitro* infection, leading to apoptosis (374). Conflicting evidence has been published concerning the prototypic coronavirus, murine hepatitis virus (MHV) and its effects on NF-κB activation. A study reported the extensively studied strain MHV-A59 activates the p65 NF-κB, though this activation was not necessary for MHV-induced TNF-α production (375). Contrary to this publication, it was previously reported that neither MHV-A59 nor MHV strain JHM activate NF-κB and cannot prevent its activation via synthetic dsRNA poly (I:C) (376). Lastly, the PLP of human coronavirus NL63 was examined for effects on NF-κB activation and similarly to the SARS-CoV PLP, it also blocks signalling and activation of NF-κB (327).

No studies have been published examining HCoV nucleocapsid proteins and their effect on NF-κB activation. The one exception to that statement is SARS-CoV, which since its emergence in 2003 has reinstated interest in the coronavirus field. In addition to the aforementioned research on various viral proteins, several publications on the nucleocapsid (N) of SARS-CoV have explored the affects of this essential structural protein on NF-κB. SARS-CoV N has been the most extensively studied structural protein in its impact on NF-κB, with varying results. Some studies have reported that the N protein activates NF-

κB and binds to the NF-κB promoter binding site, leading to an increase in IL-6 expression (377-379). Opposing studies report that N does not activate NF-κB and furthermore can suppress NF-κB activation when challenged with a stimulus (320, 380).

4.1.2. microRNA: Regulation of NF-κB

As discussed in section 1.3.2, NF-κB can be negatively regulated in a multitude of methods. In the canonical pathway, the inhibitory protein IκBα is proteasomally degraded upon phosphorylation by inhibitory κB kinase β (IKKβ) thereby releasing the p65:p50 dimer, allowing for its nuclear localization and subsequent initiation of transcription. Several of the genes transcribed encode inhibitors of NF-κB, including IκBα and A20, also known as TNF-α induced protein 3 (TNFAIP3). Once translated, these proteins complete the negative feedback loop by binding to NF-κB and re-sequestering the dimer in the cytoplasm (in the case of IκBα) and inhibiting the NF-κB activators IKK (in the case of A20).

In addition to these protein inhibitors, microRNAs also negatively regulate NF-κB. Specifically, miR-9 targets the 3'UTR of *NFKB1*, which encodes the NF-κB subunits p105 and p50. Currently, only a handful of publications have addressed the regulation of NFKB1 by miR-9 and are primarily in the context of cancer. These studies have shown that miR-9 is able to hinder cancer cell growth and metastasis by targeting NFKB1 and preventing its expression (260, 381, 382). The reduction in NFKB1 expression attributed to miR-9 has also been correlated with increased sensitivity of cancer cells to gamma irradiation (383). Similar to protein mechanisms in place for negative regulation of NFKB1, miR-9 is also an inducible negative regulator. Its transcription is initiated upon TLR2 and TLR7/8 activation as well as stimulation with TLR4 ligand lipopolysaccharide (LPS), TNF-α and IL-1β (259).

4.1.3. Objectives

As several viruses, including coronaviruses, have been shown to affect the NF-κB pathway, the objectives of the following research were to establish whether the N proteins of HCoV OC43, 229E, and NL63 affected NF-κB activity. Elucidation of the mechanism of this interference was also attempted.

4.2. Results

4.2.1. The nucleocapsid causes potentiation of NF-κB activation

Initially, to examine the state of NF-κB activation in the presence of HCoV N proteins, luciferase assays were employed. The plasmids containing HCoV N proteins of OC43, NL63, and 229E were co-transfected into 293T cells with a luciferase reporter plasmid containing firefly luciferase under the control of an NF-κB DNA-binding domain, NF-κB-luc. These cells were subsequently either stimulated with TNF-α or left untreated. Unexpectedly, while untreated cells expressing N yielded luciferase levels similar to control plasmids, those stimulated with TNF-α showed a hyperactivation of NF-κB with luciferase measurements ten-fold higher than the control (Figure 24A). This effect was observed with all three HCoVs, but not negative control viral protein OC43 M.

A decision was made to continue solely focusing on the N protein of OC43. Mainly this was due to the immense affects of the protein on the IFN response (Chapter 3). All data presented from this point onwards is exclusively of OC43 N. All references to N will indicate OC43 N unless otherwise stated.

To determine if this phenomenon was TNF-α dependent, another pathway that initiates NF-κB activation was examined. The toll-like receptor 2 (TLR-2) pathway is well characterized and activates NF-κB as a result of binding various ligands, one of which is Pam3CSK4, a synthetic lipoprotein. This commercially available synthetic ligand is analogous to the amino terminus of bacterial lipoproteins, which are cell wall components known to be proinflammatory and are ligands for TLR-2 (384). As 293T cells do not express TLR-2, a plasmid containing TLR-2 was also co-transfected in addition to N and NF-κB luciferase plasmids. As observed with TNF-α stimulation, inclusion of the N protein expression plasmid led to a greater than ten-fold enhancement in the NF-κB response to stimulation (Figure 24B). This signified that the phenomenon of potentiated NF-κB activation in the presence of OC43 N occurs via multiple pathways.

It had been noted in the luciferase assay that the potentiation of NF-κB activation in the presence of N solely occurred following stimulation by either TNF-α or Pam3CSK4. This discernment led to the hypothesis that the mechanism by which N was affecting NF-κB was by interfering with a negative regulator of the transcription factor. By preventing the effective “shut-off” of NF-κB, N expression would lead to a perpetually active NF-κB after stimulation, but not in the absence of an activator when NF-κB is in its inhibited state In the

A.

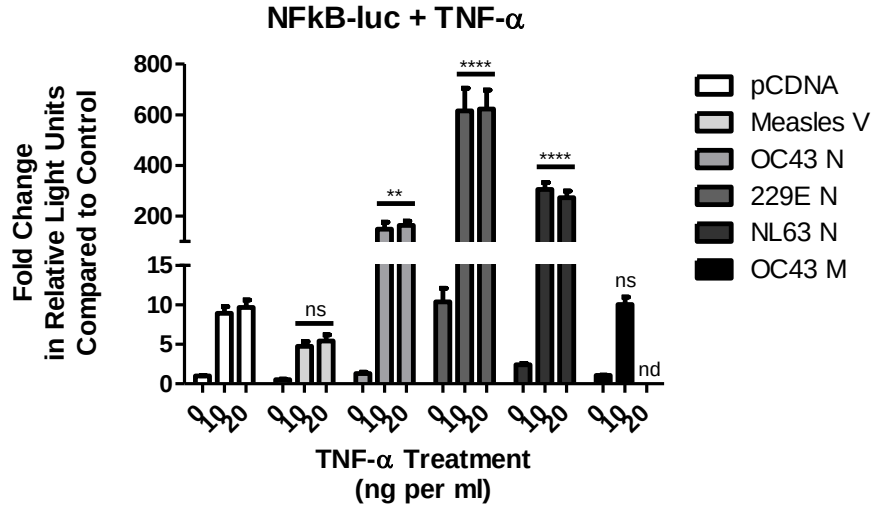
NFkB-luc + TNF-α
Fold Change in Relative Light Units Compared to Control
800
600
400
200
15
10
5
0
**
****
****
ns
ns
nd
0
1
20
TNF-α Treatment (ng per ml)
pCDNA
Measles V
OC43 N
229E N
NL63 N
OC43 M

B.

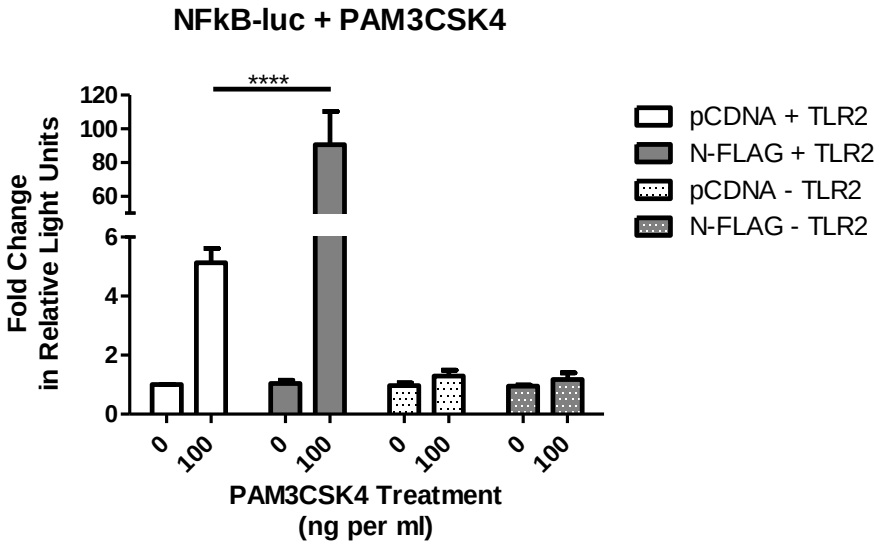
NFkB-luc + PAM3CSK4
Fold Change in Relative Light Units
120
100
80
60
6
4
2
0
****
0
100
PAM3CSK4 Treatment (ng per ml)
pCDNA + TLR2
N-FLAG + TLR2
pCDNA - TLR2
N-FLAG - TLR2

Figure 24. NF-κB activation is potentiated in the presence of OC43-N upon stimulation.

(A) A luciferase reporter assay using a reporter vector (NF-κB-luc) with an NF-κB DNA-binding site promoter was used to examine NF-κB activation. Cells were stimulated with TNF-α for 24 hours prior to measurement. All luciferase measurements were normalized to β-galactosidase and compared to negative control pCDNA, which was set to 1. pCDNA, measles V, and OC43 N data represents five independent experiments, each performed in duplicate. 229E N and NL63 N data represents three independent experiments, each performed in duplicate. OC43 M data represents one experiment performed in duplicate. Error bars represent standard error of the mean. (B) A TLR2-expressing plasmid was co-transfected with NF-κB-luc and OC43 N or empty vector and cells were stimulated with PAM3CSK4 for 24 hours prior to measurement. Cells were also co-transfected with empty vector and NF-κB-luc to ensure any response seen was due to TLR2 signalling. All luciferase measurements were normalized to β-galactosidase and compared to untreated pCDNA, which was set to 1. Data represents 2 independent experiments, each performed in triplicate. Error bars represent standard error of the mean. ** $p < 0.01$, **** $p < 0.0001$, ns – not significant, nd – not determined.

canonical NF-κB signalling pathway, the p65 and p50 dimers are retained in the nucleus by the inhibitory IκBα. This protein becomes ubiquitinated and degraded, leading to the release of the NF-κB dimer. NF-κB is then able to localize to the nucleus and bind its DNA consensus site, initiating transcription.

It was hypothesized that the point of interference in this negative regulatory pathway was IκBα and its target p65. Therefore, the p65 subunit of NF-κB was first examined for prolonged activation in the presence of N. Cells grown on coverslips were transfected with OC43 N expression plasmid or empty vector and subsequently treated with TNF-α. Cells were fixed with methanol at various times post-TNF-α treatment and co-stained with antibodies against FLAG (to detect FLAG-tagged OC43 N) and p65. When examined via confocal microscopy, no differences were observed between cells expressing N and empty vector (Figure 25). p65 localized to the nucleus as early as 15 minutes post-treatment and began to re-localize to the cytoplasm by 90 minutes post-treatment. Localization was examined up to 210 min post-TNF-α treatment but p65 staining in N and empty vector transfected cells were similar (Figure 25).

Concurrently, the degradation kinetics of IκBα were examined via western blot. Cells were transfected with OC43 N expression plasmid or empty vector, subsequently treated with TNF-α, and lysed at various time points. By western blot, the kinetics of IκBα degradation were indistinguishable between cells transfected with N and cells transfected with empty vector (Figure 26). Together, these data indicate that OC43 N does not interfere with p65 activation nor IκBα degradation.

4.2.2. N interactions with cellular proteins

As the initial hypothesis that OC43 N was affecting the p65 subunit and/or its inhibitor IκBα was incorrect, another approach was employed to deduce the negative inhibitor of NF-κB that was being affected by N. One direct approach was to identify cellular proteins with which N was interacting by co-immunoprecipitation. In order to achieve sufficient N protein expression, a vesicular stomatitis virus was generated expressing a FLAG-tagged N gene.

The generation of the VSV expressing N, designated N-FLAG VSV, was carried out by PCR amplification of a FLAG-tagged N gene followed by ligation into the Δ51 mutant VSV genome, between G and L (Figure 27A). The genome was co-transfected into cells with VSV helper plasmids and the resulting virus was collected. Expression of N-FLAG was checked by infecting cells with N-FLAG VSV and immunoprecipitating subsequent cell lysates with an antibody

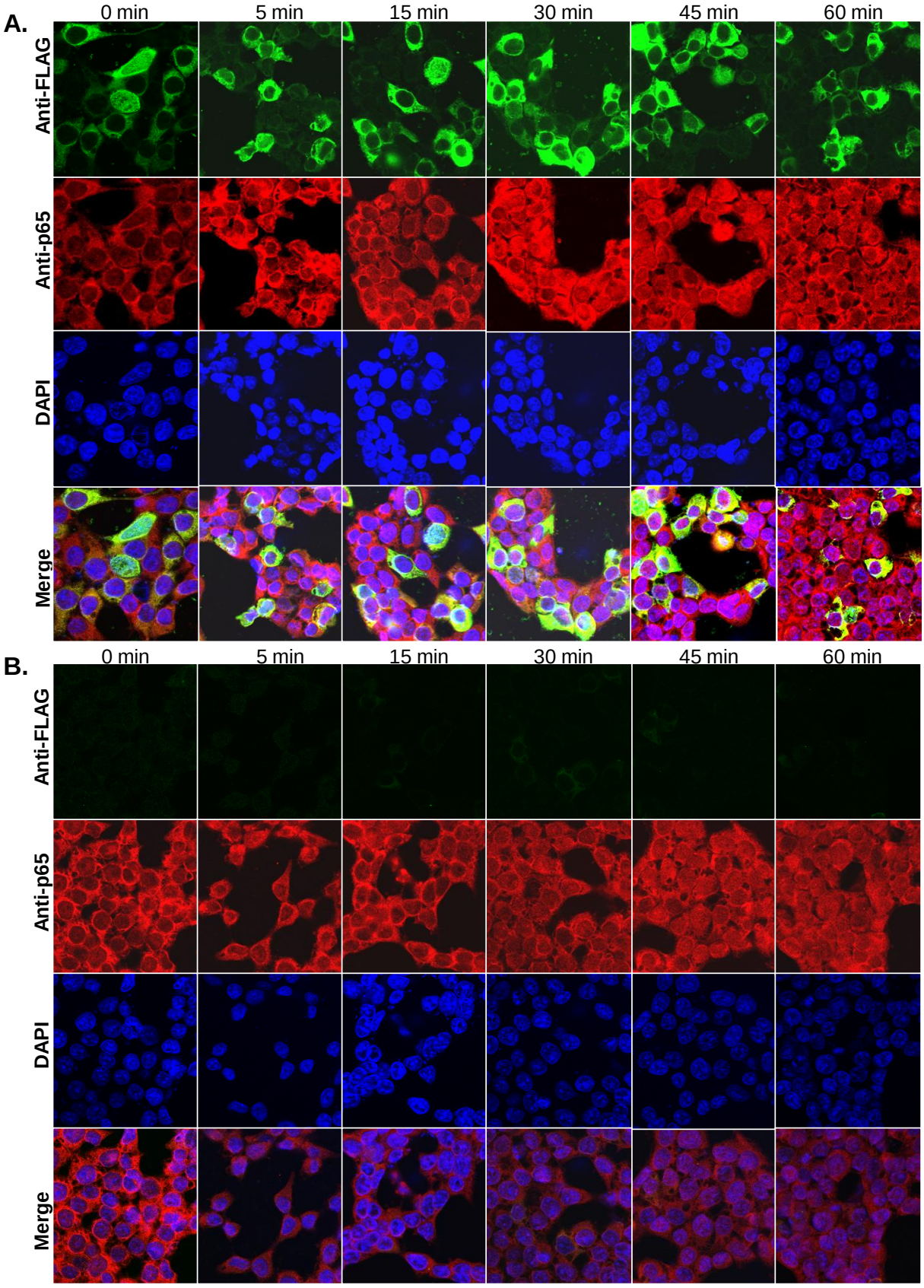
A.
0 min
5 min
15 min
30 min
45 min
60 min
Anti-FLAG
Anti-p65
DAPI
Merge
B.
0 min
5 min
15 min
30 min
45 min
60 min
Anti-FLAG
Anti-p65
DAPI
Merge

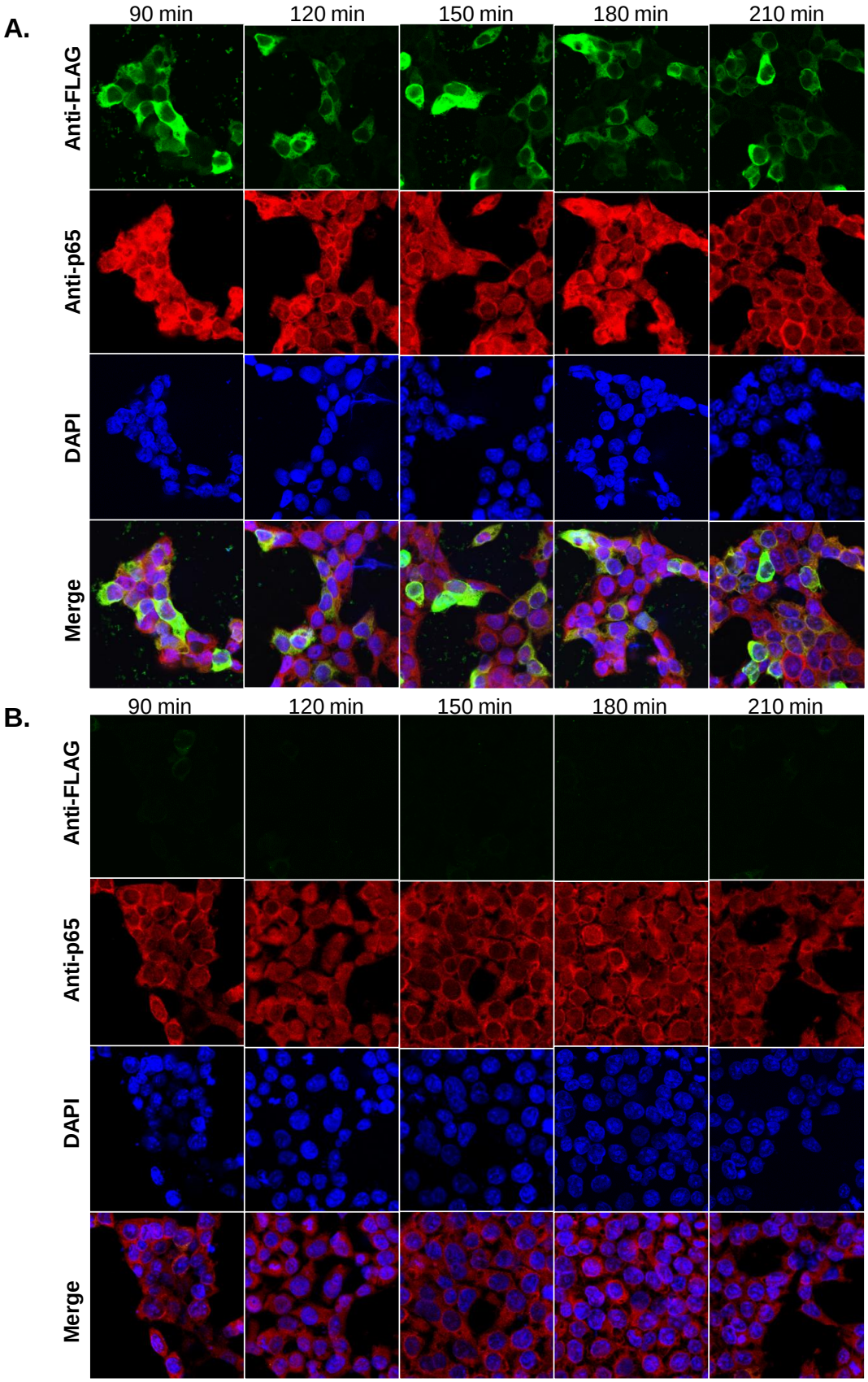
A.
90 min
120 min
150 min
180 min
210 min
Anti-FLAG
Anti-p65
DAPI
Merge
B.
90 min
120 min
150 min
180 min
210 min
Anti-FLAG
Anti-p65
DAPI
Merge

Figure 25. OC43 N does not alter the kinetics of p65 activation.

Cells transfected with pCDNA or N-FLAG were treated with TNF-α for varying lengths of time. Nuclear localization of NF-κB subunit p65 was tracked by immunofluorescence. Cells were co-stained with antibodies against FLAG and p65 and nuclei were visualized by DAPI. No kinetic differences in p65 activation were observed between cells transfected with N-FLAG (A) and cells transfected with pCDNA (B).

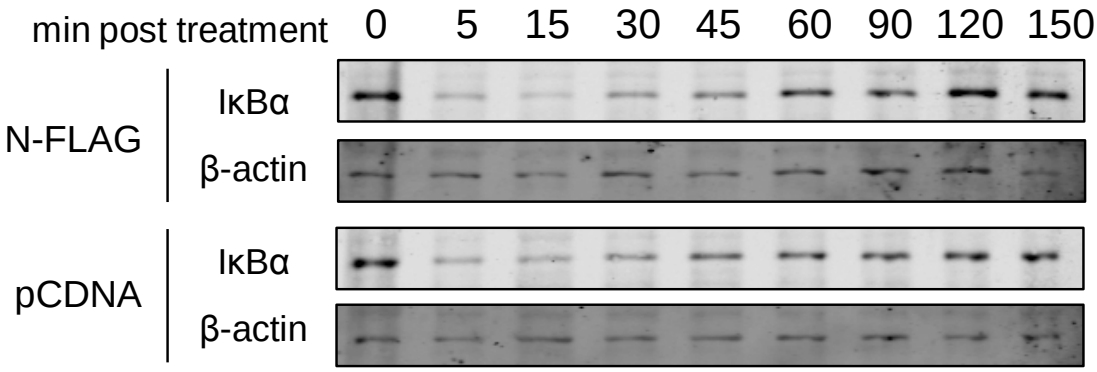
min post treatment
0
5
15
30
45
60
90
120
150
N-FLAG
IκBα
β-actin
pCDNA
IκBα
β-actin

Figure 26. OC43 N does not alter the kinetics of IκBα degradation.

Cells transfected with pCDNA or N-FLAG were treated with TNF-α for varying lengths of time. IkBα degradation examined via western blot did not reveal any kinetic differences between N and pCDNA transfected cells.

A.

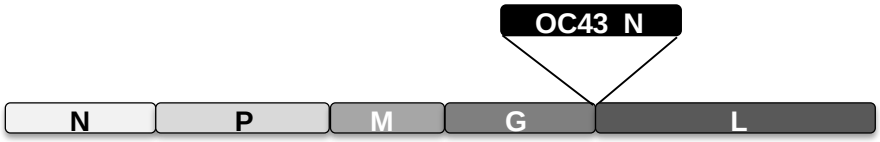

B.

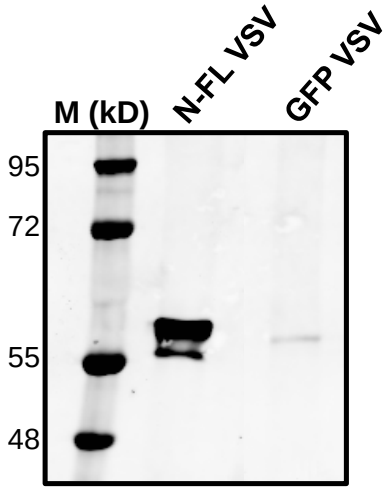

Figure 27. Construction of VSV expressing OC43 N.

(A) Schematic representation of the VSV genome with location of OC43 N insertion. (B) Expression of N-FLAG by N-FL VSV was confirmed by FLAG immunoprecipitation and western blot. GFP VSV was utilized as a negative control.

against FLAG. A western blot confirmed expression and proper FLAG-tagging of N (Figure 27B).

A large number of 293T cells were infected with N-FLAG VSV and control virus GFP VSV. Lysates of these infected cells were then immunoprecipitated with an antibody against FLAG, run on gradient SDS-PAGE gels and proteins co-immunoprecipitated with N were identified by mass spectrometry (Figure 28A). Numerous cellular proteins were pulled down with N and unique bands were sequenced. Although no NF-κB inhibitors were identified, it was confirmed that analogous to the majority of Nidoviral nucleocapsid proteins examined, OC43 N interacts with the nucleolar protein nucleolin (Figure 28B). Upon review, a trend emerged amongst the interacting proteins–virtually all possessed the ability to bind RNA.

In a coronaviral infection, the N protein complexes with the RNA genome to form the nucleocapsid, which indicates that it is an RNA-binding protein. Other studies, as previously mentioned, have identified that coronaviral N is an RNA-chaperone. The protein has clearly been shown to have the ability to bind RNA and given that the majority of the proteins identified to interact with N are also RNA-binding proteins, it led to the inquiry of whether these interactions were direct or occurring via RNA.

In order to test this possibility, cells were infected as before, but prior to co-immunoprecipitation with the FLAG-conjugated beads, lysates were treated with RNase or mock treated. The immunoprecipitates were then run on a gradient SDS-PAGE gel and coomassie stained as before. Compared to untreated cells infected with N-FLAG VSV, samples treated with RNase co-immunoprecipitated dramatically fewer proteins (Figure 29A). Furthermore, interactions with several cellular proteins that had been specifically confirmed by western blot were eliminated with RNase treatment (Figure 29B). Interactions between N and nucleolin, Y-box binding protein (YB1), heterogeneous ribonucleoprotein U (hnRNP U), and Ku70 were ablated with RNase (Figure 29B). These data indicated that interactions between N and cellular proteins were mediated through RNA.

It remained a possibility that although N interactions were RNA-dependent, N was having an effect on the cellular proteins by re-localization. To examine the subcellular localization of hnRNP U and Ku70 in the presence of N, cells grown on coversilps were transfected with N expression plasmid and fixed with

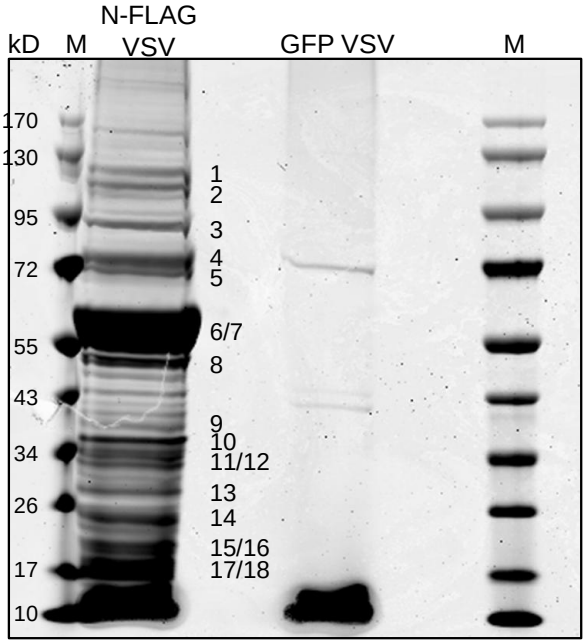

Band	Identified Protein	Protein Description	RNA Binding
1	HNRNPU protein	Component of nuclear matrix scaffold	Y
2	Nucleolin	Nucleolar protein	Y
3	Nuclear factor IV (p80 of Ku)	p80 of Ku, nucleolar protein involved in DNA repair	Y
4	G22P1 (p70 of Ku)	p70 of Ku, nucleolar protein involved in DNA repair	Y
	Poly(A) binding protein, cytoplasmic 1	Binds to cytoplasmic mRNA, shuttles between nucleus & cytoplasm	Y
5	HSP70-1	Heat shock protein, expression is induced by stress, contributres to DNA stability	Y
6/7	HCoV Nucleocapsid	Nucleocapsid protein of OC43	Y
8	Y box binding protein-1	Cold-shock protein, binds Y-box motif, transcriptional repressor or activator	Y
9	HNRNPA1 protein	Shuttles to and from nucleus, bound to mRNA, involved in mRNA splicing	Y
10	Histone cluster 1, H1d	Nuclear protein, 1of the 4 core histone proteins	N
11-14	No Identification	N/A	N/A
15/16	RPL26 (Ribosomal protein LL26)	Regulation of p53 mRNA translation via interaction with Mdm2	Y
17/18	Ribosomal protein S19	Component of 40S ribosomal subunit	Y

Figure 28. Proteins identified to co-immunoprecipitate with OC43-N.

(A) Lysates of N-FL VSV and GFP VSV infected cells were immunoprecipitated with an anti-FLAG antibody and resulting precipitates were coomassie stained. (B) Proteins co-immunoprecipitated with N-FL were identified by mass spectrometry. Numbered bands correspond with numbered bands in (A).

A.

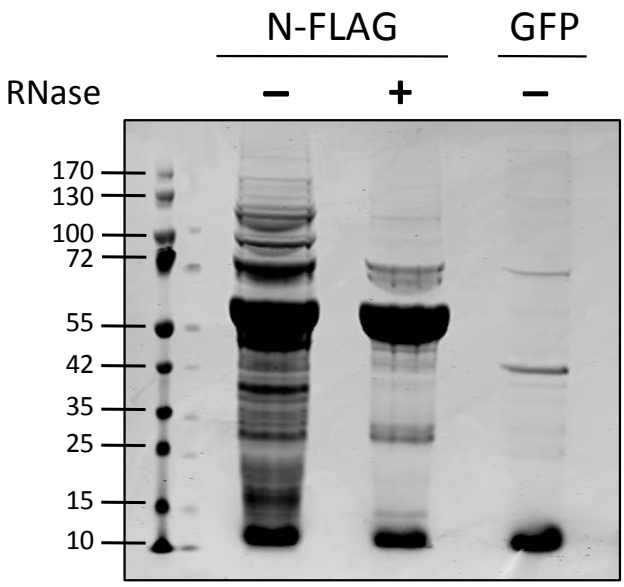
N-FLAG
GFP
RNase
–
+
–
170
130
100
72
55
42
35
25
15
10

B.

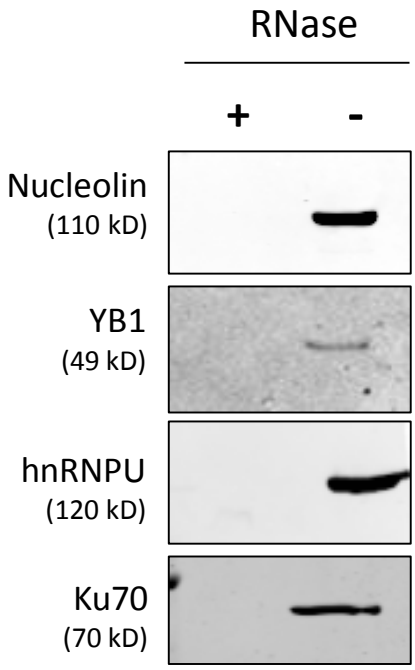
RNase
+
-
Nucleolin
(110 kD)
YB1
(49 kD)
hnRNPU
(120 kD)
Ku70
(70 kD)

Figure 29. OC43-N interacts with many cellular proteins in an RNA-dependent manner.

(A) Cells lysates of N-FL VSV infected cells were treated with RNase or left untreated prior to FLAG-immunoprecipitation. GFP VSV infected cell lysates were again FLAG-immunoprecipitated as a control. (B) Several proteins identified via mass spectrometry to interact with N-FL were confirmed to be pulled down with N. These interactions were eliminated when lysates were treated with RNase prior to immunoprecipitation

methanol. The fixed cells were co-stained with antibodies against FLAG to detect N and hnRNP U or Ku70, and visualized by confocal microscopy. Neither hnRNP U or Ku70 were re-localized from their nuclear positions in the presence of N (Figure 30). Thus, although N interacted with these proteins in an RNA-dependent fashion, it had no effect on the subcellular localization of either protein.

4.2.3. N interference in miR-9 negative regulation of NFKB1

The demonstration that N was binding cellular proteins via RNA resulted in speculation that it may be binding microRNA (miRNA). Initially, effects of N on cellular miRNAs were assessed by PCR array, allowing for 384 miRNAs to be screened. 293T cells were transfected with OC43 N or empty vector, followed by TNF-α stimulation. In the presence of N, a myriad of miRNA levels were altered and miR-9 expression, in particular, showed over a 3-fold increase as compared to empty vector (Figure 31). Upon further investigation into published literature, it was revealed that miR-9 targets *NFKB1* (259, 383). NFKB1 encodes the NF-κB subunit p105, which is then proteasomally processed to form the p50 subunit (226). This information led to the postulation that N could be functionally hindering the negative regulation of NFKB1 by interacting with miR-9. To test this hypothesis, N was expressed in cells both by transfection with N expression plasmid and infection with N-FLAG VSV, lysates were immunoprecipitated as before with anti-FLAG, and the resulting immunoprecipitates were subjected to RNA extraction. By both conventional and quantitative PCR, miR-9 was detected in immunoprecipitates from cells expressing N, but not the control plasmid (Figure 32). This confirmed that OC43 N binds miR-9 and supported the hypothesis that N was sequestering this negative regulator of NF-κB.

As miR-9 prevents the translation of NFKB1, if N was preventing miR-9 function it would be logical to expect an increase in NFKB1 subunits p105 and p50 in cells that were expressing N. The protein expression of NFKB1 was then examined by western blot. Cells were transfected with N expression vector or empty vector, and subsequently treated with TNF-α. Several timepoints post-treatment were scrutinized for NFKB1 expression. Both p105 and p50 subunits were detected, quantified, and compared between samples. Protein expression of both p105 and p50 were elevated in cells transfected with N plasmid when compared to empty vector (Figure 33). The total protein levels of NFKB1 remained consistently higher in N expressing cells throughout the timecourse. Similarly, when cells were co-transfected with N and TLR-2 expression vectors and subsequently stimulated with TLR-2 ligand Pam3CSK4, total protein levels of

A.

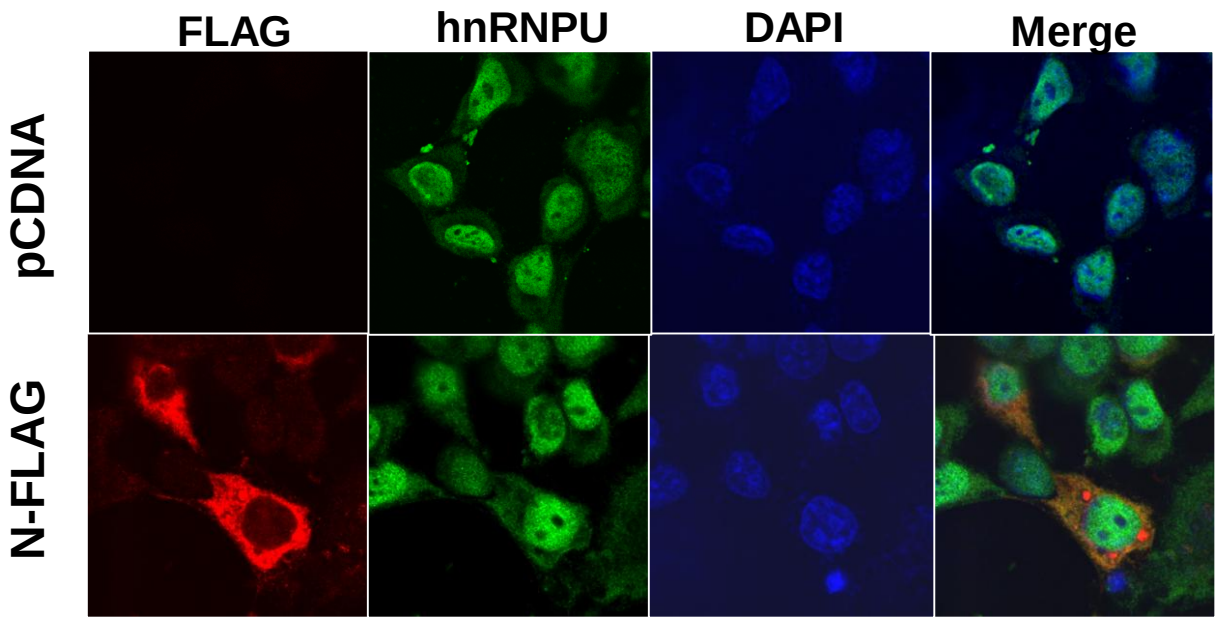
FLAG
hnRNPU
DAPI
Merge
pCDNA
N-FLAG

B.

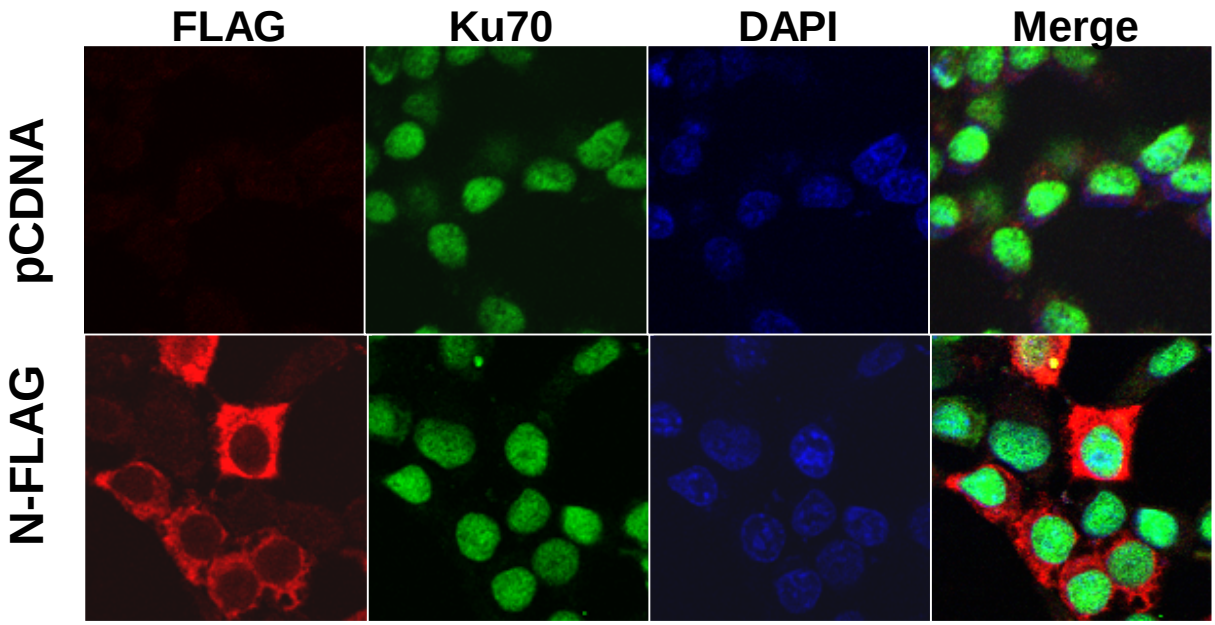
FLAG
Ku70
DAPI
Merge
pCDNA
N-FLAG

Figure 30. OC43 N does not relocalize cellular proteins.

Cells were transfected with OC43 N expression vector, fixed and stained with antibodies against FLAG and hnRNPU (A) or Ku70 (B). Nuclei were visualized by DAPI. No relocalization of cellular proteins was observed.

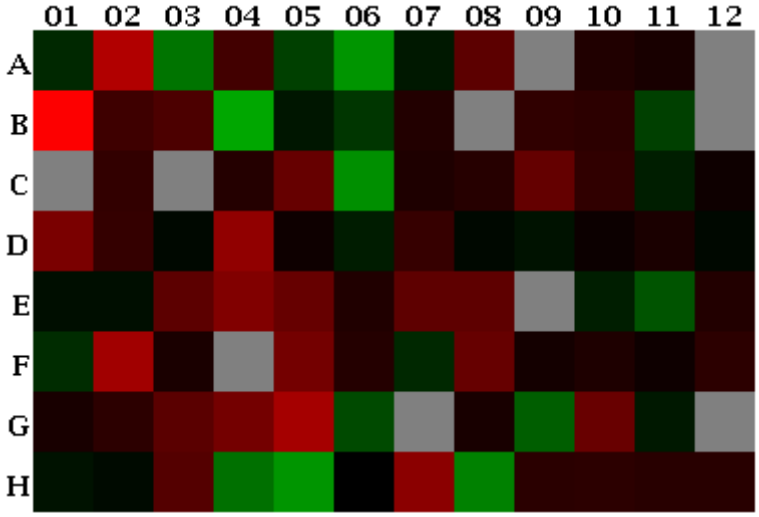

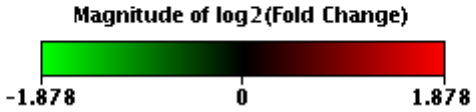

	1	2	3	4	5	6	7	8	9	10	11	12
A	hsa-miR-142-5p **-1.23**	hsa-miR-16 **2.49**	hsa-miR-142-3p **-1.81**	hsa-miR-21 **1.41**	hsa-miR-15a **-1.39**	hsa-miR-29b **-2.15**	hsa-let-7a **-1.13**	hsa-miR-126 **1.59**	hsa-miR-143 **1.26**	hsa-let-7b **1.18**	hsa-miR-27a **1.13**	hsa-let-7f **1.26**
B	hsa-miR-9 **3.68**	hsa-miR-26a **1.38**	hsa-miR-24 **1.48**	hsa-miR-30e **-2.36**	hsa-miR-181a **-1.11**	hsa-miR-29a **-1.32**	hsa-miR-124 **1.19**	hsa-miR-144 **1.26**	hsa-miR-30d **1.28**	hsa-miR-19b **1.25**	hsa-miR-22 **-1.38**	hsa-miR-122 **1.26**
C	hsa-miR-150 **1.26**	hsa-miR-32 **1.29**	hsa-miR-155 **1.26**	hsa-miR-140-5p **1.21**	hsa-miR-125b **1.68**	hsa-miR-141 **-2.09**	hsa-miR-92a **1.17**	hsa-miR-424 **1.21**	hsa-miR-191 **1.67**	hsa-miR-17 **1.28**	hsa-miR-130a **-1.17**	hsa-miR-20a **1.08**
D	hsa-miR-27b **1.87**	hsa-miR-26b **1.3**	hsa-miR-146a **-1.04**	hsa-miR-200c **2.11**	hsa-miR-99a **1.07**	hsa-miR-19a **-1.16**	hsa-miR-23a **1.31**	hsa-miR-30a **-1.04**	hsa-let-7i **-1.1**	hsa-miR-93 **1.07**	hsa-let-7c **1.14**	hsa-miR-106b **-1.04**
E	hsa-miR-101 **-1.08**	hsa-let-7g **-1.07**	hsa-miR-425 **1.6**	hsa-miR-15b **1.93**	hsa-miR-28-5p **1.69**	hsa-miR-18a **1.17**	hsa-miR-25 **1.62**	hsa-miR-23b **1.61**	hsa-miR-302a **1.26**	hsa-miR-186 **-1.16**	hsa-miR-29c **-1.54**	hsa-miR-7 **1.19**
F	hsa-let-7d **-1.26**	hsa-miR-30c **2.28**	hsa-miR-181b **1.14**	hsa-miR-223 **1.26**	hsa-miR-320a **1.81**	hsa-miR-374a **1.21**	hsa-let-7e **-1.23**	hsa-miR-151-5p **1.68**	hsa-miR-374b **1.1**	hsa-miR-196b **1.17**	hsa-miR-140-3p **1.08**	hsa-miR-100 **1.26**
G	hsa-miR-103 **1.13**	hsa-miR-96 **1.25**	hsa-miR-302b **1.58**	hsa-miR-194 **1.81**	hsa-miR-125a-5p **2.33**	hsa-miR-423-5p **-1.46**	hsa-miR-376c **1.26**	hsa-miR-195 **1.13**	hsa-miR-222 **-1.62**	hsa-miR-28-3p **1.71**	hsa-miR-128 **-1.13**	hsa-miR-302c **1.26**
H	hsa-miR-423-3p **-1.1**	hsa-miR-185 **-1.05**	hsa-miR-30b **1.54**	hsa-miR-210 **-1.76**	SNORD48 **-2.15**	SNORD47 **-1**	SNORD44 **2.04**	RNU6-2 **-1.95**	miRTC **1.24**	miRTC **1.25**	PPC **1.23**	PPC **1.22**

Figure 31. Profiling of human miRNA expression indicates OC43 N effects miR-9 levels.

A heat map of human miRNA PCR array comparing cells transfected with N-FLAG to pCDNA transfected cells, both treated with TNF-α, shows various miR that are affected by N-FLAG. Of particular interest is hsa-miR-9 (B2), which is over 3-fold higher in N-FLAG cells as compared to pCDNA. Gray squares – unamplified.

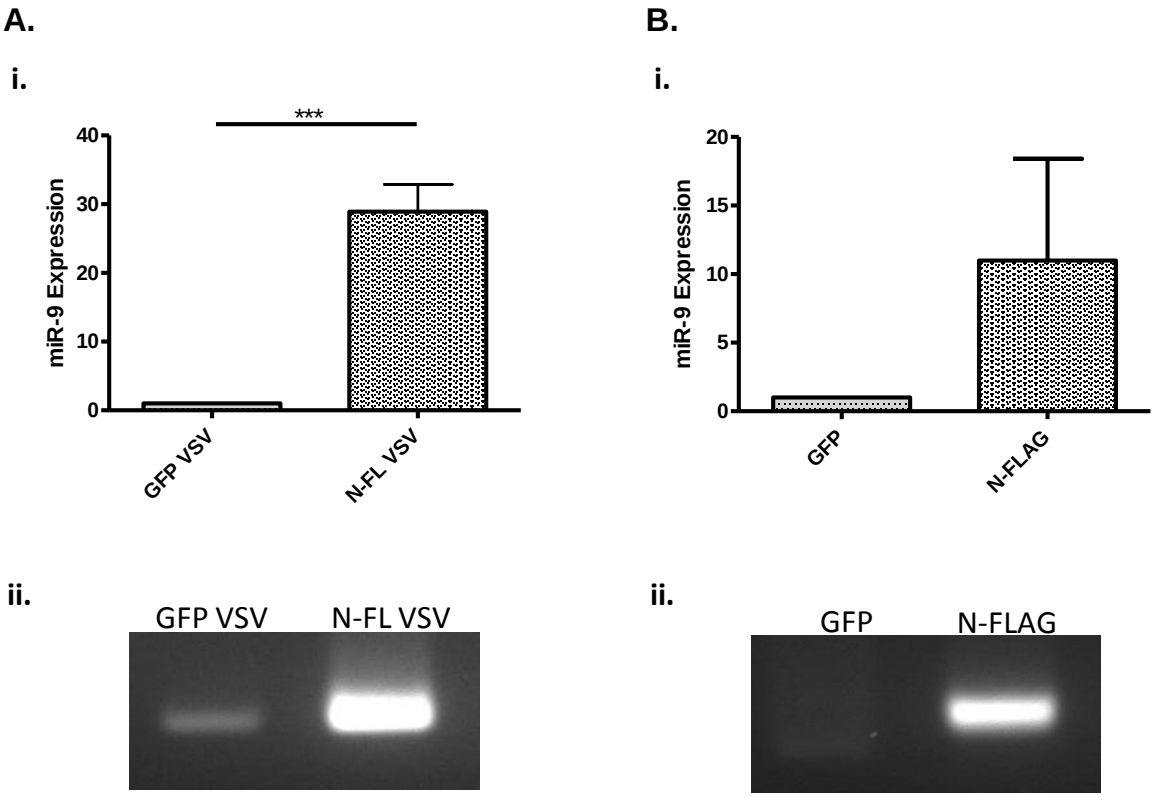
A.
i.
***
40
30
20
10
0
miR-9 Expression
GFP VSV
N-FL VSV
ii.
GFP VSV
N-FL VSV
B.
i.
20
15
10
5
0
miR-9 Expression
GFP
N-FLAG
ii.
GFP
N-FLAG

Figure 32. OC43 N interacts with miR-9.

FLAG immunoprecipitation was performed on cells (A) infected with N-FL VSV or GFP VSV and (B) transfected with N-FLAG or GFP. miR-9 was detected in N-containing immunoprecipitate by qRT-PCR (i) and also by conventional RT-PCR (ii). Error bars represent standard error of the mean. *** $p < 0.001$.

A.

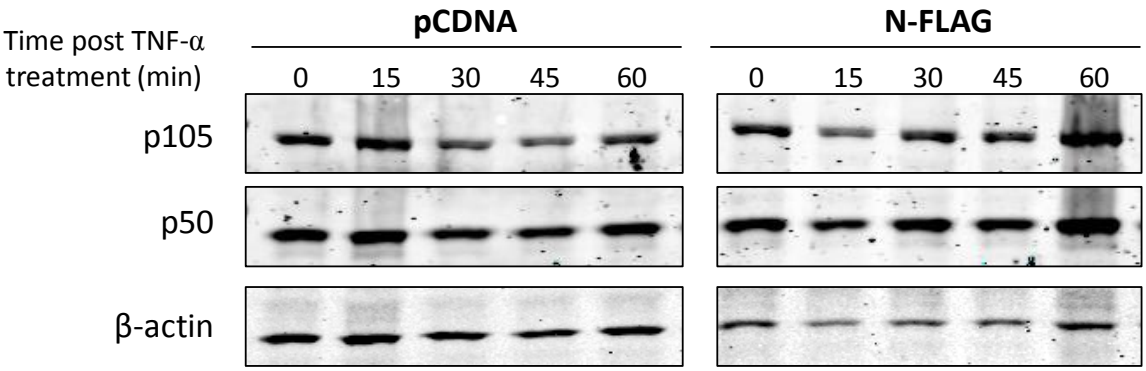
Time post TNF-α treatment (min)
pCDNA
N-FLAG
0
15
30
45
60
0
15
30
45
60
p105
p50
β-actin

B.

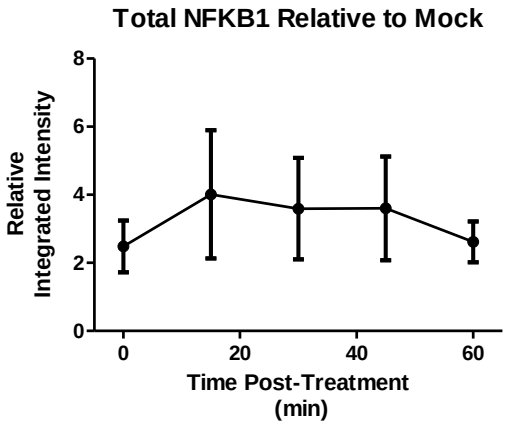
Total NFKB1 Relative to Mock
Relative Integrated Intensity
0
2
4
6
8
0
20
40
60
Time Post-Treatment (min)

Figure 33. Presence of OC43 N results in elevated expression of NFKB1.

(A) Western blot detecting NFKB1 products p105 and p50 in cells transfected with pCDNA or N-FLAG and treated with TNF-α for various lengths of time. Representative blot is shown. (B) Quantification of the both p105 and p50 bands show that NFKB1 protein is more highly expressed in cells transfected with OC43 N. Values were normalized to β-actin. Data represents three independent experiments. Error bars represent standard error of the mean.

NFKB1 were higher in cells expressing N compared to empty vector (Figure 34A, B).

To delineate effects in cells specifically expressing N, cells were examined via flow cytometry. This allowed for consideration of only those cells expressing N, as opposed to the entire population which includes untransfected cells. Transfected 293T cells were stained with antibodies against FLAG and NFKB1. As is commonly found in transient transfection, N-transfected cells contained populations of cells with varying levels of N expression. These two groups of cells were designated N_{hi} and N_{lo}, which expressed high levels and low levels of N protein, respectively (Figure 35A). While cells expressing low levels of N did not display enhanced NFKB1 levels, those that strongly expressed N did, indicating that the steady-state level of NFKB1 correlated with N protein expression levels (Figure 35B, C). This corroborated with the previous observation that in the cells expressing N, an elevated NFKB1 protein level is seen.

It would be expected that if N disrupted the negative feedback cycle of miR-9, an increase in NFKB1 mRNA would also occur. The addition of pathway stimulation, such as TNF-α, would result in elevated transcription of NFKB1. A further augmentation of NFKB1 mRNA would be observed with the addition of N to the system. Quantitative RT-PCR was employed to investigate the mRNA levels in N-transfected cells stimulated with TNF-α. A modest increase of NFKB1 mRNA was observed in unstimulated N-transfected cells compared to empty vector (Figure 36). In cells stimulated with TNF-α, however, a more pronounced difference in NFKB1 mRNA was apparent between N and empty vector transfected cells (Figure 36). Thus, these data further supported the hypothesis that OC43 N was perturbing the negative feedback mechanism of miR-9 resulting in increases in both mRNA and protein levels of NFKB1.

Though the previous assays showed that in the presence of N, both NFKB1 protein and mRNA levels were increased, it had not been confirmed whether N could directly functionally impair miR-9. A luciferase assay that allowed for assessment of miR-9 function was employed. This assay, specifically designed for detection of miRNA function, consists of a luciferase reporter vector containing Renilla luciferase with a 3'UTR of the mRNA targeted by the miRNA of interest (Figure 37A). Thus, if the miRNA targets the 3'UTR expressed with luciferase, translation of luciferase will not occur. If the miRNA does not target

A.

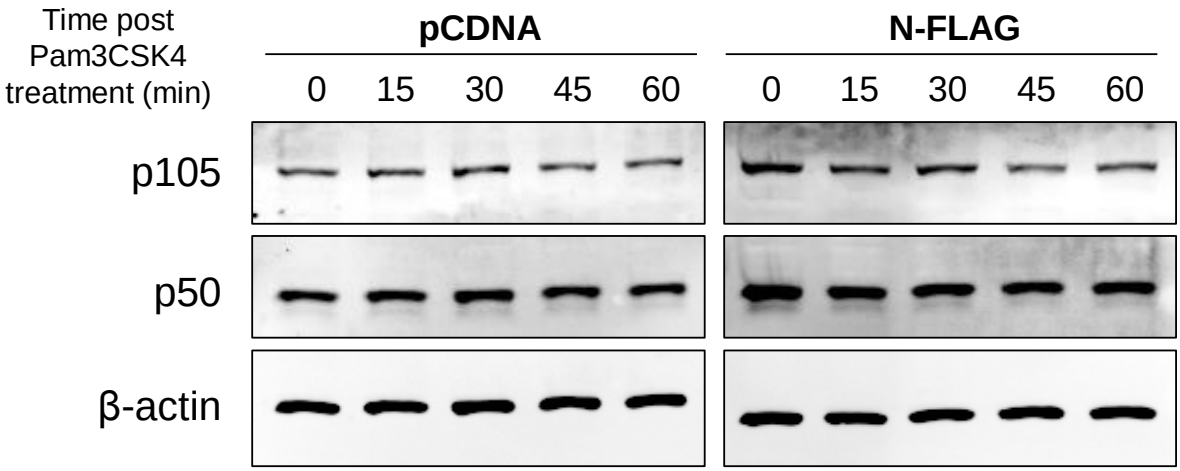
Time post Pam3CSK4 treatment (min)
pCDNA
N-FLAG
0 15 30 45 60
0 15 30 45 60
p105
p50
β-actin

B.

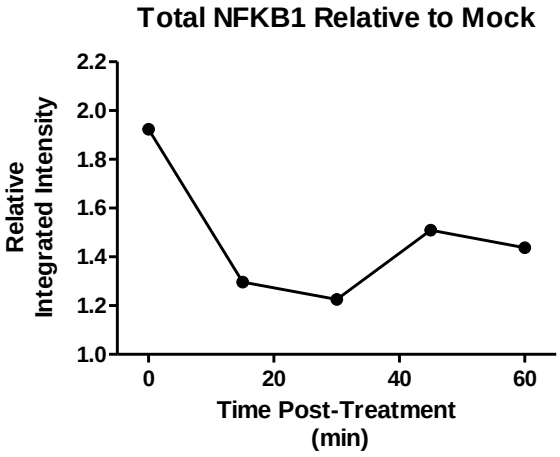
Total NFKB1 Relative to Mock
Relative Integrated Intensity
2.2
2.0
1.8
1.6
1.4
1.2
1.0
0
20
40
60
Time Post-Treatment (min)

Figure 34. An elevation in NFKB1 is observed in cells co-transfected with TLR2 and OC43 N.

(A) Western blot detecting NFKB1 products p105 and p50 in cells co-transfected with pCDNA or N-FLAG and TLR2 and treated with Pam3CSK4 for various lengths of time. (B) Quantification of the both p105 and p50 bands show that NFKB1 protein is more highly expressed in cells transfected with OC43 N. Values were normalized to β-actin.

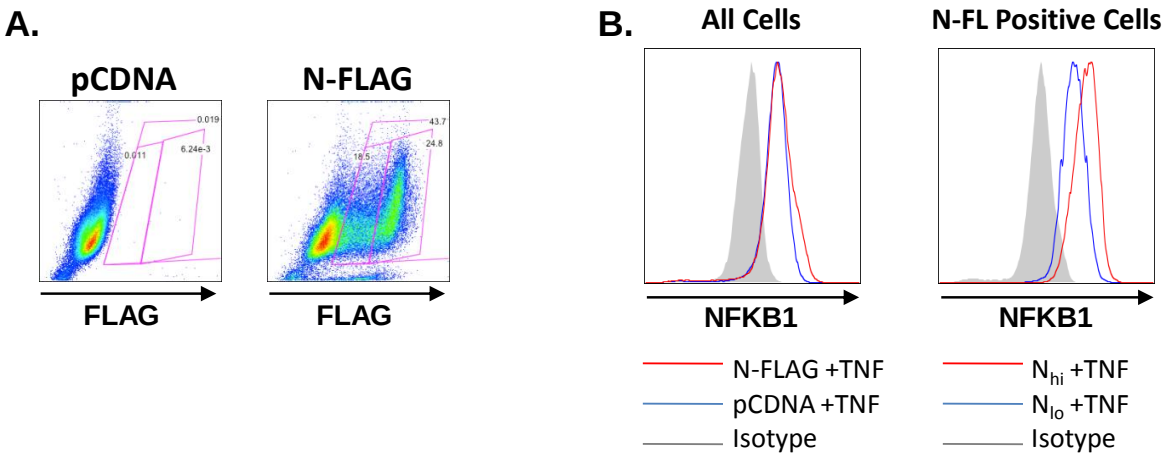
A.
pCDNA
N-FLAG
0.019
0.011
6.24e-3
43.7
24.8
18.5
FLAG
FLAG
B.
All Cells
N-FL Positive Cells
NFKB1
NFKB1
N-FLAG +TNF
pCDNA +TNF
Isotype
N$_{hi}$ +TNF
N$_{lo}$ +TNF
Isotype

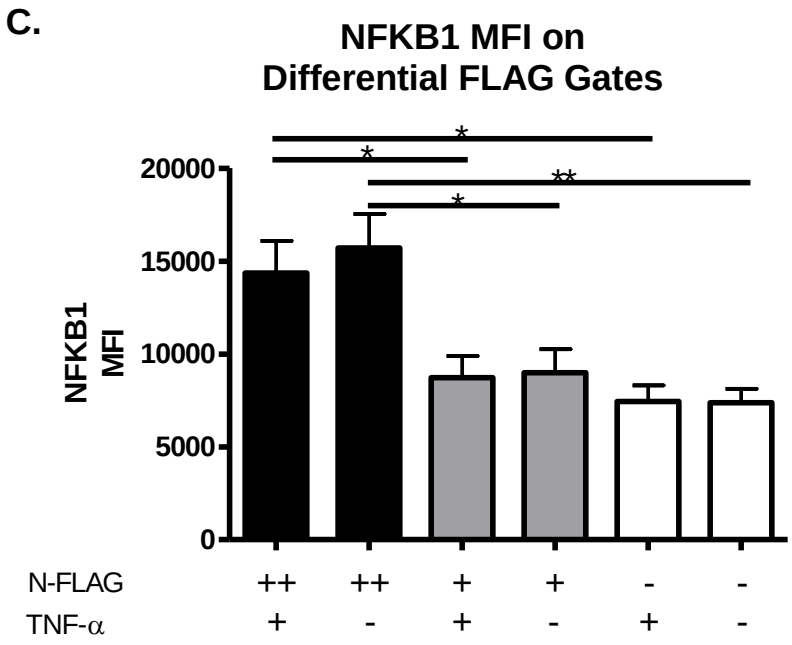
C.
NFKB1 MFI on
Differential FLAG Gates
NFKB1
MFI
20000
15000
10000
5000
0
*
*
**
*
N-FLAG ++ ++ + + - -
TNF-α + - + - + -

Figure 35. Elevated expression of NFKB1 is observed in cells expressing OC43 N.

Cells were transfected with N-FLAG or pCDNA and then treated with TNF-α or left untreated. Cells were then co-stained with antibodies against NFKB1 and FLAG and protein expression was examined by flow cytometry. (A) FLAG staining specifically stained cells transfected with OC43-N. Two different populations of FLAG positive cells were seen with varying expression levels of FLAG, N_{hi} and N_{lo}. (B) Comparison of NFKB1 levels in the total population of cells (left). No difference was observed between N-FLAG and pCDNA transfected cells. Comparison of NFKB1 levels in cells both positive for FLAG and NFKB1 show a difference in staining intensity between N_{hi} and N_{lo} cells (right). Anti-GFP was utilized as an isotype control. (C) Graphical representation of mean fluorescent intensity of NFKB1 staining. In N_{hi} cells (++), the expression of NFKB1 is significantly higher than that of N_{lo} (+) and pCDNA (-) transfected cells. Data represents two independent experiments, each performed in triplicate. Error bars represent standard error of the mean. * $p < 0.05$, ** $p < 0.01$.

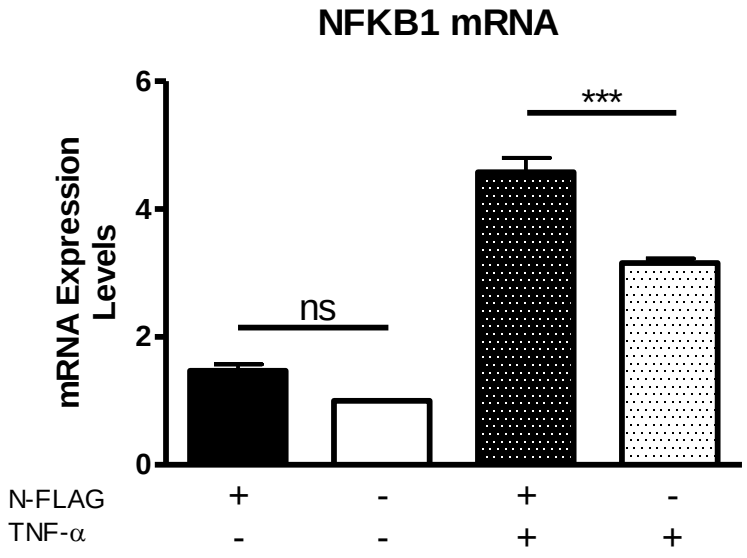
NFKB1 mRNA
mRNA Expression Levels
6
4
2
0
***
ns
N-FLAG + - + -
TNF-α - - + +

Figure 36. NFKB1 mRNA levels are elevated in cells expressing N.

NFKB1 mRNA was detected by qRT-PCR in cells transfected with pCDNA or N-FLAG and either treated with TNF-α or left untreated. In cells transfected with OC43-N, NFKB1 mRNA levels were increased as compared to pCDNA transfected cells. Data represents the fold change of NFKB1 mRNA amplified in relation to untreated pCDNA NFKB1 (negative control), which was set to 1. All NFKB1 mRNA levels were normalized to housekeeping gene GAPDH. Error bars represent standard error of the mean. *** $p < 0.001$.

A.

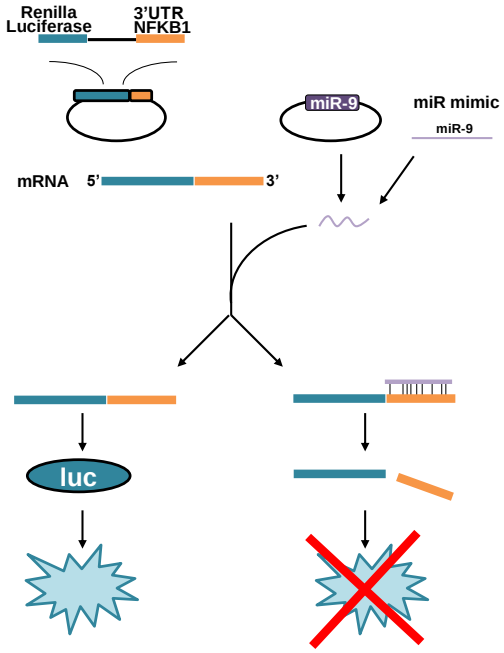
Renilla Luciferase
3'UTR NFKB1
miR-9
miR mimic
miR-9
mRNA 5'
3'
luc

B.

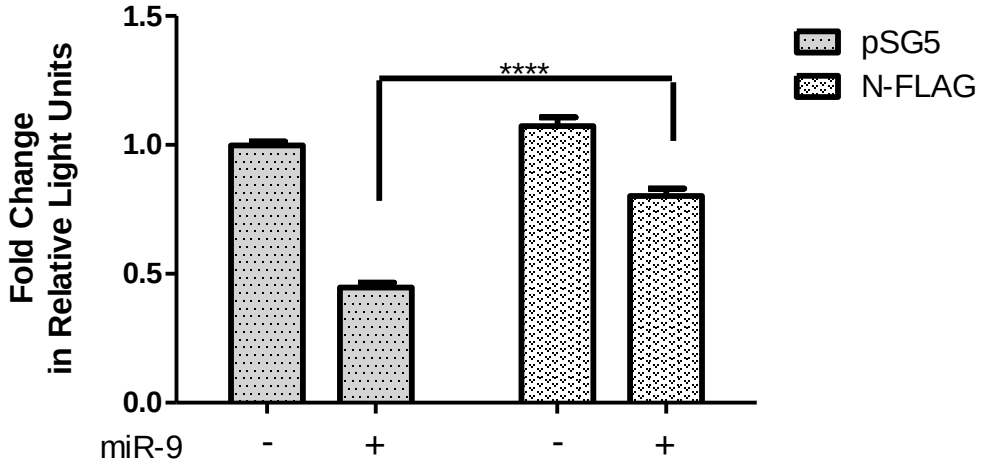
Fold Change in Relative Light Units
1.5
1.0
0.5
0.0
****
pSG5
N-FLAG
miR-9
-
+
-
+

Figure 37. OC43-N prevents miR-9 negative regulation of NFKB1.

(A) Schematic of the luciferase assay shows possible outcomes of the assay. Figure modified from www.promega.ca. (B) The NFKB1 luciferase construct, NFKB1-luc, was co-transfected with either empty vector pSG5 or N-FLAG and with or without miR-9. When transfected with empty vector, a basal level of luciferase is observed. With the addition of miR-9, luciferase levels are reduced. The presence of N-FLAG blunts the effect of miR-9 on luciferase levels. All renilla luciferase measurements were normalized to firefly luciferase and subsequently compared to empty vector without miR-9 which was set to 1. Data represents three independent experiments. Error bars represent standard error of the mean. **** $p < 0.0001$.

the 3'UTR of the predicted target, then translation will be allowed to occur and a measurable amount of luciferase will be present in the cell (Figure 37A).

For the purposes of this research, a luciferase expression construct luc-NFKB1, which contains the NFKB1 3'UTR, was co-transfected into 293T cells with either the N expression vector or empty vector, with or without miR-9. As expected, in cells transfected with empty vector, the level of luciferase decreased with the addition of miR-9. With the addition of N, the ability of miR-9 to suppress luciferase expression was obstructed (Figure 37B). This signified that by binding to miR-9, N was able to prevent its function in the negative regulation of NFKB1.

4.2.4. Phenomena in OC43 viral infection

As all data gathered thus far utilized a transient transfection system, whether analogous phenomena occurred in the context of a coronaviral infection was unknown. Upon attaining the OC43 virus, strain VR-1558, characterization of the growth characteristics and establishment of a virus titering protocol was necessary. Initial inoculation of susceptible cell line HCT-8 at a low multiplicity of infection (MOI) resulted in clear visualization of cytopathic effects (CPE) at 4 days post infection (dpi) (Figure 38A). Although literature states that growth of OC43 *in vitro* should occur at 37°C which is the conventional tissue culturing temperature, American Type Culture Collection (ATCC), the original source of VR-1558, states virus growth should occur at 33°C. A direct comparison was performed by growth of OC43 at both temperatures, harvesting the virus, and titering to investigate under which temperature resulted in superior virus growth. Virus that was grown at 33°C reached a titer greater than one log higher than the virus grown at 37°C (Figure 38B). A growth curve was also performed to establish the optimal day post infection for harvesting (Figure 38C). Lastly, a western blot of infected HCT-8 cells was performed and OC43 N was detected at 1, 2, and 3 days post infection (Figure 38D).

Initially, the binding of N to miR-9 during OC43 infection was investigated. HCT-8 cells were infected with OC43 or mock infected and cells were lysed at 8 and 20 hours post infection. Subsequent lysates were immunoprecipitated with an anti-OC43 N antibody and resulting immunoprecipitates were subjected to RNA extraction. miR-9 was amplified by quantitative PCR at as early as 8 h.p.i. indicating that during OC43 infection, N bound miR-9 (Figure 39).

Next, it was sought to establish whether there was an increase in NFKB1 protein expression during OC43 infection. Cells were infected with OC43 or

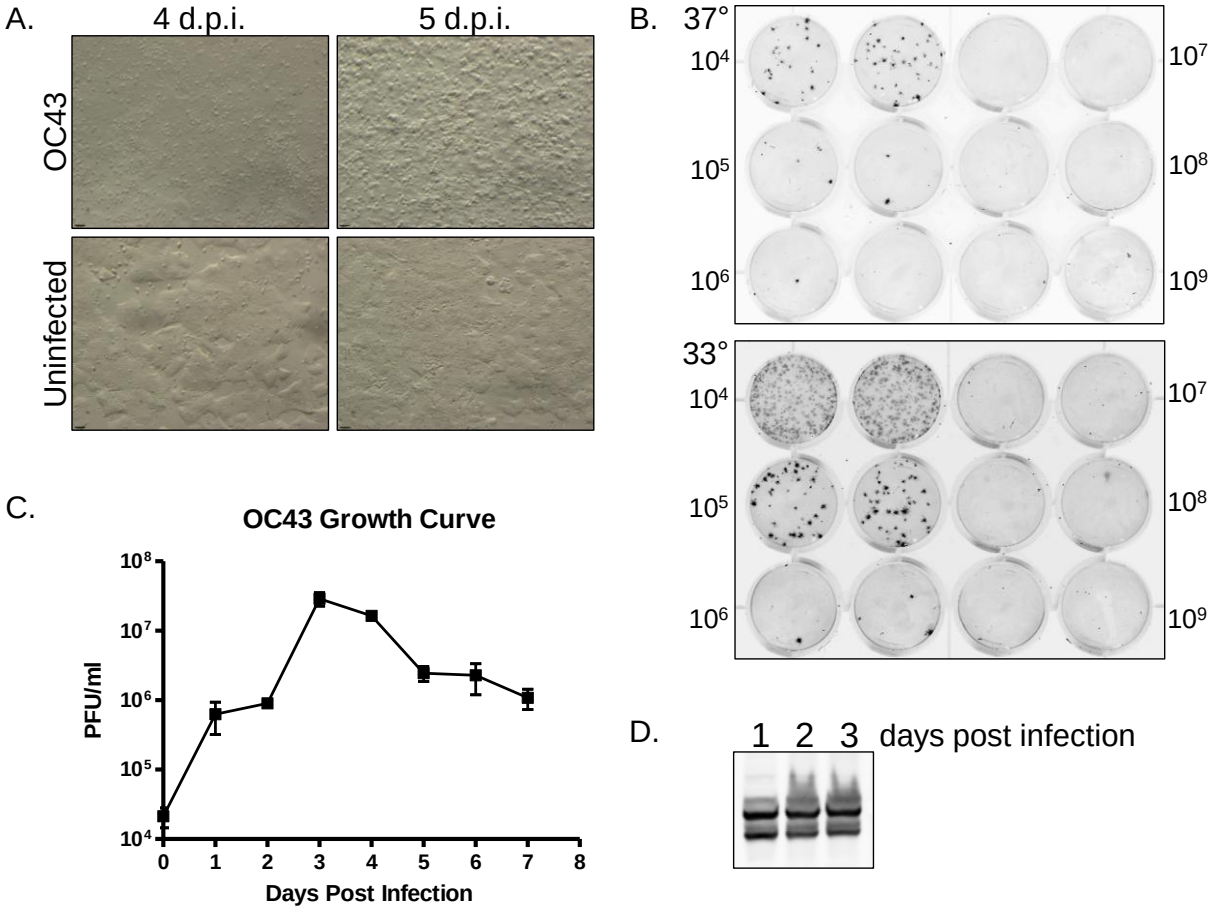
A.
4 d.p.i.
5 d.p.i.
OC43
Uninfected
B.
37°
10^4
10^5
10^6
10^7
10^8
10^9
33°
10^4
10^5
10^6
10^7
10^8
10^9
C.
OC43 Growth Curve
PFU/ml
10^8
10^7
10^6
10^5
10^4
0 1 2 3 4 5 6 7 8
Days Post Infection
D.
1 2 3 days post infection

Figure 38. Characterization and optimization of OC43 growth.

After obtaining OC43, characterization of its growth in HCT-8 cells was carried out. (A) CPE was visible after infection at 4 days post infection, with more prominent CPE appearing at 5 days post infection. (B) A comparison of propagation of OC43 at 33°C and 37°C revealed growth to a higher titer at the lower temperature. (C) A growth curve of OC43 indicated peak titers are reached at 3 days post infection after initial inoculation at MOI 1. Error bars represent standard error of the mean. (D) A western blot for detection of N shows strong expression at 1 day post infection.

A.

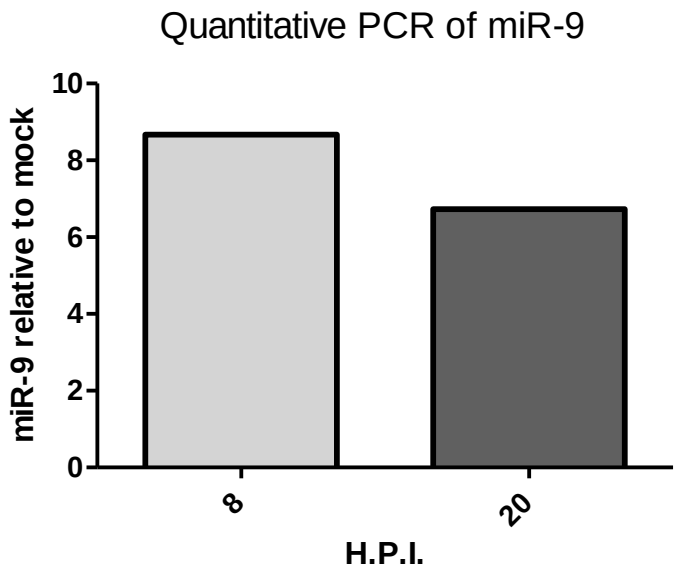
Quantitative PCR of miR-9
miR-9 relative to mock
10
8
6
4
2
0
8
20
H.P.I.

B.

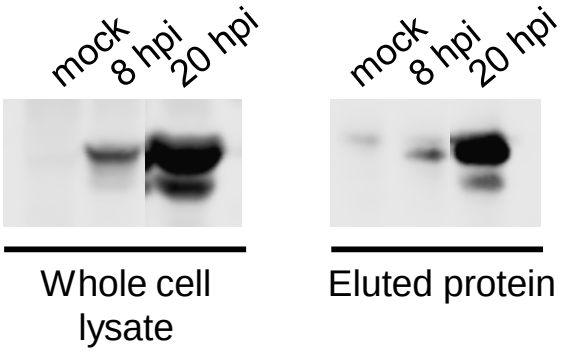
mock
8 hpi
20 hpi
mock
8 hpi
20 hpi
Whole cell lysate
Eluted protein

Figure 39. N interacts with miR-9 during infection with OC43.

HCT-8 cells infected with OC43 were subjected to immunoprecipitation with antibody against N. (A) miR-9 was amplified by qPCR from RNA extracted from immunoprecipitates. Amplified miR-9 is expressed as fold change relative to mock. Data is averaged from triplicates. Each sample was amplified in triplicate. (B) Representative portion of OC43 N expression at various time points during infection both from entire lysates pre-immunoprecipitation (left) and immunoprecipiatate (right).

mock infected and lysed at various times post-infection. Lysates were run on SDS-PAGE gel and subjected to western blotting for the NFKB1 subunits p105 and p50. As expected, in OC43 infected cells, the protein expression of NFKB1 was significantly higher than in mock infected cells (Figure 40A, B). Infected cells were also subjected to flow cytometry to examine NFKB1 protein expression solely in cells infected with OC43. Cells, OC43 infected and mock infected, were co-stained with anti-OC43 N and anti-NFKB1 antibody and in cells infected with OC43, the level of NFKB1 protein was significantly higher than in mock infected cells (Figure 40C). This confirmed that NFKB1 protein expression was augmented in cells infected with OC43.

The mRNA level of NFKB1 was also examined during OC43 infection. Cells were infected with OC43 and RNA was extracted at 1, 2, and 3 days post infection. At all timepoints, NFKB1 mRNA was increased in OC43 infected cells versus mock infected cells (Figure 41).

Lastly, the activation of NF-κB during OC43 infection was examined via luciferase assay. HCT-8 cells were transfected with the reporter construct NF-κB-luc and subsequently infected with OC43 or mock infected. At 1, 2, and 3 days post infection, NF-κB activation in OC43 infected cells was higher than mock infected cells (Figure 42). Taken all together, these data indicate that similar phenomena occur in the context of an OC43 infection as does when the nucleocapsid is overexpressed in cells.

4.3. Discussion

The above findings illustrate a novel method by which viruses can modify the host immune response. Although many viruses have been found to modulate signalling and subsequently activate NF-κB (reviewed in 385), human coronaviruses other than SARS-CoV have not been identified to interfere with this pathway. SARS-CoV membrane protein and papain-like protease (PLP) have been found to block NF-κB signalling whereas the spike protein has been found to activate NF-κB (327, 369, 371). As aforementioned, one study reported that the N protein of SARS-CoV inhibited NF-κB activation via luciferase reporter assay (320) while others reported NF-κB activation by the nucleocapsid (377, 378). No mechanisms of interference were proposed in these reports.

The unexpected observation that the three HCoV N proteins significantly potentiated NF-κB activation following cytokine or TLR ligand stimulation initiated interest in the interaction between viral N and this important signalling pathway.

A.

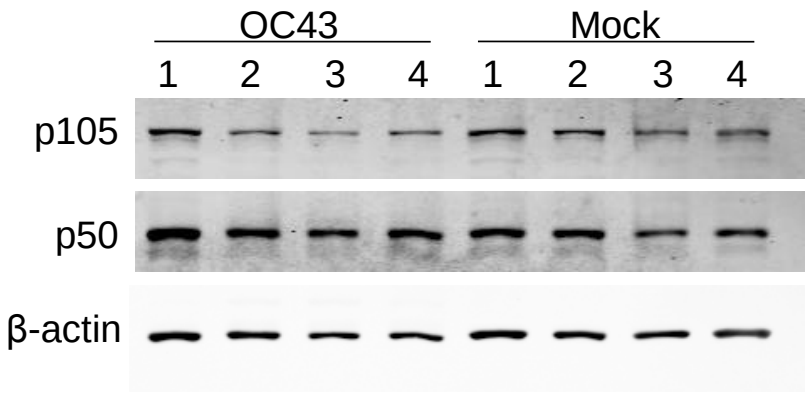
OC43
Mock
1 2 3 4 1 2 3 4
Days Post Infection
p105
p50
β-actin

B.

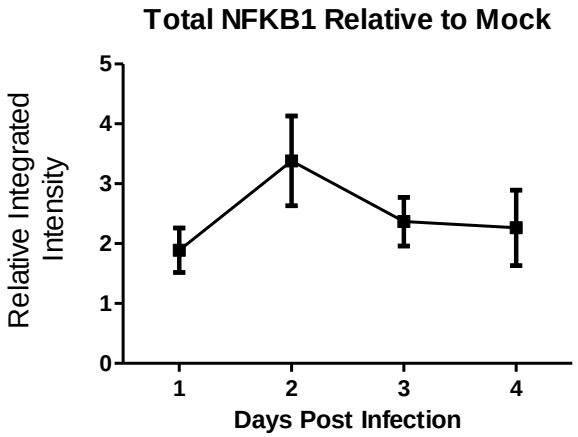
Total NFKB1 Relative to Mock
Relative Integrated Intensity
0
1
2
3
4
5
1
2
3
4
Days Post Infection

C.

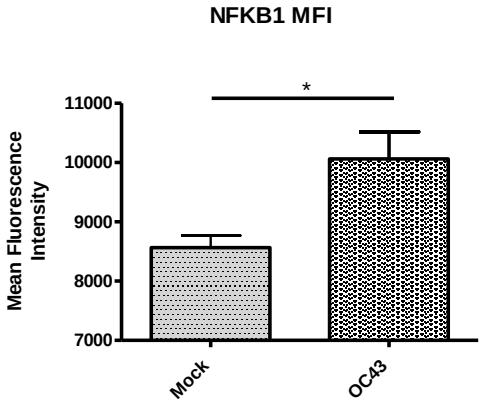
NFKB1 MFI
Mean Fluorescence Intensity
7000
8000
9000
10000
11000
*
Mock
OC43

Figure 40. Infection with OC43 results in elevated expression of NFKB1.

(A) Western blot detecting NFKB1 products p105 and p50 in cells infected with OC43 for various lengths of time compared to uninfected cells. (B) Quantification of total NFKB1 in infected cells relative to mock. All NFKB1 intensities were normalized to β-actin. Data represents 3 independent experiments. Error bars represent standard error of the mean. (C) Flow cytometric analysis of OC43 infected cells compared to mock at 1 day post infection. Cells were co-stained with antibodies against NFKB1 and OC43-N protein. The mean fluorescence intensity of NFKB1 was significantly higher in infected cells as compared to mock. Error bars represent standard error of the mean. * $p < 0.05$

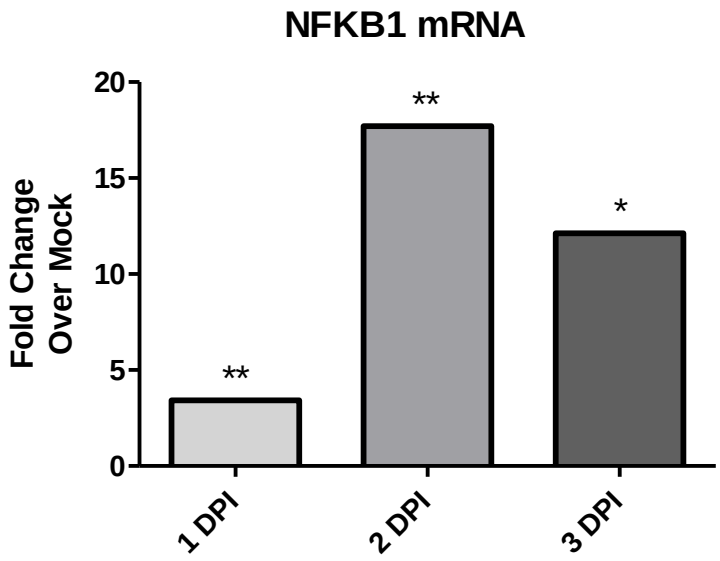

* $p < 0.05$
** $p < 0.01$

Figure 41. NFKB1 mRNA levels are elevated in OC43 infected cells.

Cells were infected with OC43 and RNA was extracted at 1, 2, and 3 days post infection. Quantitative PCR detecting NFKB1 mRNA showed an increase in NFKB1 mRNA in infected cells compared to mock.

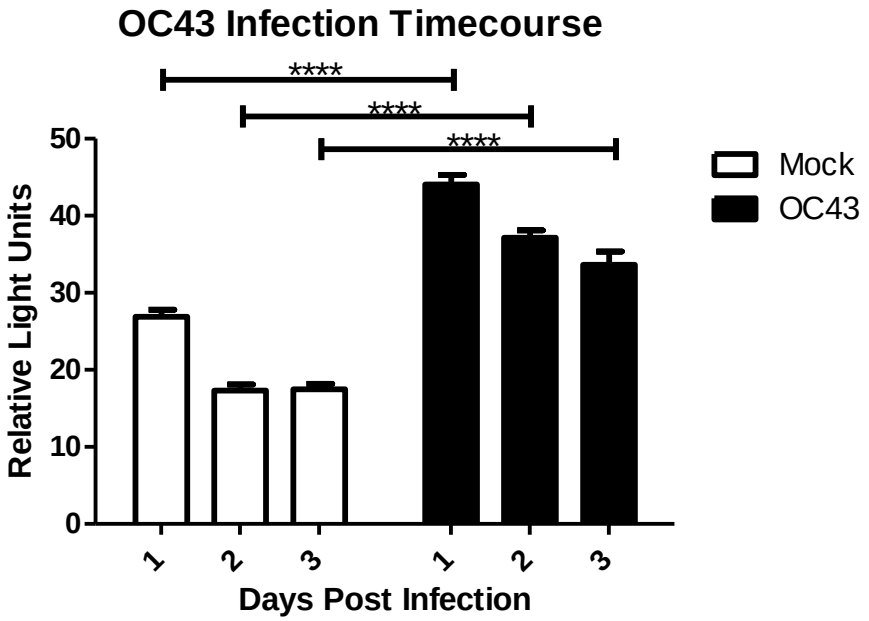
OC43 Infection Timecourse
****
****
****
Relative Light Units
50
40
30
20
10
0
1
2
3
1
2
3
Days Post Infection
Mock
OC43

Figure 42. Infection with OC43 results in activation of NF-kB.

HCT-8 cells were transfected with reporter plasmid NF-kB-luc and were subsequently infected with OC43. A significant increase in luciferase activity was observed in OC43 infected cells as compared to mock infected. Error bars represent standard error of the mean. **** $p < 0.0001$.

It was remarked, however, that the perpetuation of NF-κB activation by N solely occurred when the cells were stimulated. This indicated that the cell could not effectively turn off activated NF-κB when N was present and suggested that the point of interference was a negative regulator of NF-κB. Preliminary pursuit of this mechanism of NF-κB activation potentiation began with examination of the NF-κB subunit p65 and its inhibitor IκBα. These were the obvious candidates and points in the pathway at which many other viruses interfere (267, 386, 387). While anticipating that N perhaps prolonged IκBα degradation and allowed for potentiated p65 activation, the data indicated that neither protein was affected by the presence of N. Despite the elimination of these candidates, the hypothesis that OC43 N was affecting a negative regulator of NF-κB was maintained. It was possible that OC43 N was binding to a protein responsible for negatively regulating NF-κB activation and we sought to identify cellular proteins with which N interacts.

Many published studies have explored interactions between various nidovirus nucleocapsids and cellular proteins. It has been well established that there are many interactions with nuclear and nucleolar proteins, such as fibrillarin and nucleolin though none have reported these interactions for OC43 N (106, 116, 388). Additionally, no previously identified interacting partners were directly involved in the regulation of NF-κB activation and thus proteins that interacted with OC43 N were investigated. Numerous cellular proteins that interacted with N were identified, among them nucleolin, and upon further scrutiny, it was noted that the majority of them were RNA binding proteins. The nucleocapsid itself is a known RNA-binding protein, as its main function in viral replication is to complex with the RNA genome and additionally, other coronaviral N proteins have been found to be RNA chaperone proteins (114). Taken together, this led to the suspicion that the identified protein interactions were RNA-dependent. With RNase treatment, these interactions were revealed to be RNA-dependent, which to our knowledge, has not been previously recognized for other nidoviral nucleocapsid interactions including the binding to nucleolin.

The revelation that these were indirect interactions via RNA gave rise to the prospect that the N protein could be binding to regulatory RNAs such as microRNAs. These small, non-coding RNAs have come to light as extremely important regulators of gene expression and play an important role in the regulation of the innate immune response (reviewed in 389, 390, 391). Through

a large genome wide qPCR-based screen of miRNAs, a multitude of miRNAs which were upregulated with OC43-N expression and TNF-α treatment were identified. One of these miRNAs with increased expression that also had links to NF-κB was miR-9. Multiple studies, as well as predictive software, have implicated miR-9 in the prevention of NFKB1 translation by targeting the 3'UTR (259, 260, 381, 383). Additionally, miR-9 expression is inducible by TNF-α as well as TLR2 signalling pathways (259, 260).

Subsequent experiments illustrated that not only did the OC43 nucleocapsid bind miR-9, but prevented its functionality via this interaction. RNA-immunoprecipitation of N-transfected cells revealed that miR-9 co-immunoprecipitated with N, indicating binding. As would be expected if miR-9 was prevented from NFKB1 negative regulation, when OC43 N was expressed in cells, elevated protein levels of both NFKB1 subunits were observed, demonstrating that the negative regulation of NFKB1 had been disrupted. The luciferase assay confirmed that N was functionally interfering with miR-9 function, as mir-9 suppression of luciferase via the NFKB1 3'UTR was reversed when N was present. In examining protein levels of NFKB1 via western blot and flow cytometry, cells treated with TNF-α did not show a significant difference in p105/p50 intensity compared to untreated cells. NFKB1 levels do not fluctuate greatly from basal levels due to the tightly regulated expression of these proteins. This important negative feedback loop is significantly disrupted by the N protein, as observed by the increase in both steady state and stimulated levels of NFKB1.

It was important to confirm these phenomena in the context of a coronaviral infection, as while transient transfection reveals the impact of an individual protein, there are a multitude of other factors during a viral infection that could lessen or negate the effects. Once OC43 growth in human colorectal carcinoma cell line, HCT-8, was established and optimized, similar interactions with miR-9 were observed. Interactions between N and miR-9 were confirmed, as miR-9 was co-immunoprecipitated with N from OC43 infected cells. The level of detection was lower, as evidenced by the 8 to 10-fold difference from control as compared to RNA immunoprecipitated from N-FL VSV infected cells, which was 30-fold higher than the control. A factor affecting these data is the differing method of immunoprecipitation; one employed a commercial FLAG immunoprecipitation kit with high efficiency, and the other employed the traditional method of conjugating a nucleocapsid antibody which was a great deal less efficient. The other possible factor leading to a lesser amount of immunoprecipitated miR-9 may have been OC43 genomic RNA, which could

have bound competitively to N. This was supported by the inverse relationship between N protein levels and precipitated miR-9. Though the amount of N detected at 20 h.p.i. is higher than 8 h.p.i., the quantity of miR-9 detected is lower. As N has been shown to bind viral RNA more efficiently than non-viral RNA, this discrepancy is not necessarily surprising as more viral RNA is present at later time points during infection (392).

As expected with miR-9 sequestration, an increase in NFKB1 protein expression was seen in OC43 infected cells as compared to mock. An increase in NFKB1 mRNA was also observed in OC43 infected cells as was in the N-transfected scenario. Lastly, activation of NF-κB was also observed in OC43 infected cells via luciferase assay. These data combined support the hypothesis that during OC43 infection, the nucleocapsid protein binds miR-9 and prevents the negative regulation of NFKB1. Unfortunately, stimulation of OC43 infected HCT-8 cells with TNF-α or TLR-2 ligand Pam3CSK4 was not possible to compare to N-transfected data. HCT-8 cells were unresponsive to both stimulants as NF-κB activation by luciferase assay was not achieved. This is a possible explanation as to why although activation of NF-κB by luciferase was detected in OC43 infected cells, super activation of NF-κB as observed in transfected cells did not occur. Few cell lines are permissive to OC43 infection and this restricted the ability to directly compare transfection and infection scenarios (393).

Taken together, the data has aided in the creation of a proposed mechanistic model of how OC43-N is interacting with the NF-κB pathway. As seen in Figure 43A, in resting, unstimulated cells, p105 is processed into p50, which then can homodimerize and act as a transcriptional repressor or activator depending on co-factors. p50 also dimerizes with other NF-κB members such as p65 and remains in the cytoplasm in an inhibitory state. There is also a basal level of expression of NFKB1 mRNA and miR-9 in order to regulate NFKB1 translation. Upon stimulation, p50-p65 heterodimers are released from the control of IκBα and are able to translocate to the nucleus where again, depending on whether they are bound to co-activators or co-repressors, they activate or inhibit transcription (Figure 43B). There is also a marked increase in NFKB1 mRNA and miR-9 upon stimulation. Figure 43C shows what is proposed to be occurring when OC43-N is expressed in resting cells. OC43-N binds miR-9, which is basally expressed, and prevents its control of NFKB1 mRNA. With a stimulus such as TNF-α, both miR-9 and NFKB1 mRNA increase, but OC43 N continues to bind miR-9, preventing inhibition of NFKB1 translation (Figure 43D). This interference in the negative feedback mechanism of p105/p50 expression

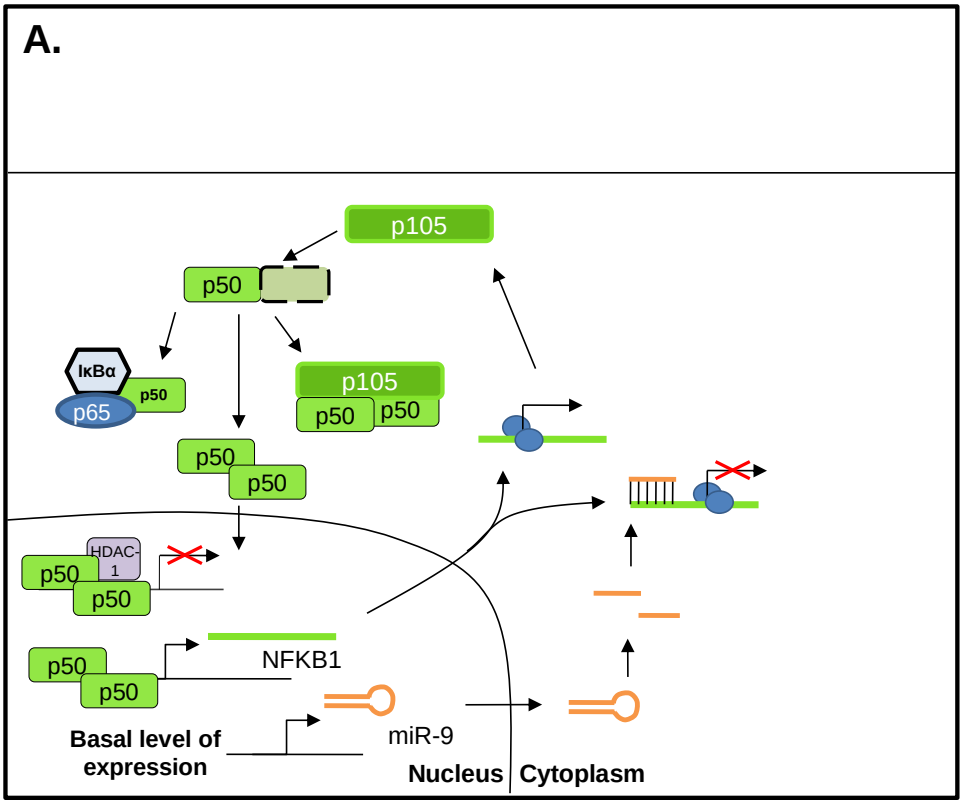
A.
p105
p50
IκBα
p65
p50
p105
p50
p50
p50
p50
HDAC-1
p50
p50
NFKB1
p50
p50
Basal level of expression
miR-9
Nucleus
Cytoplasm

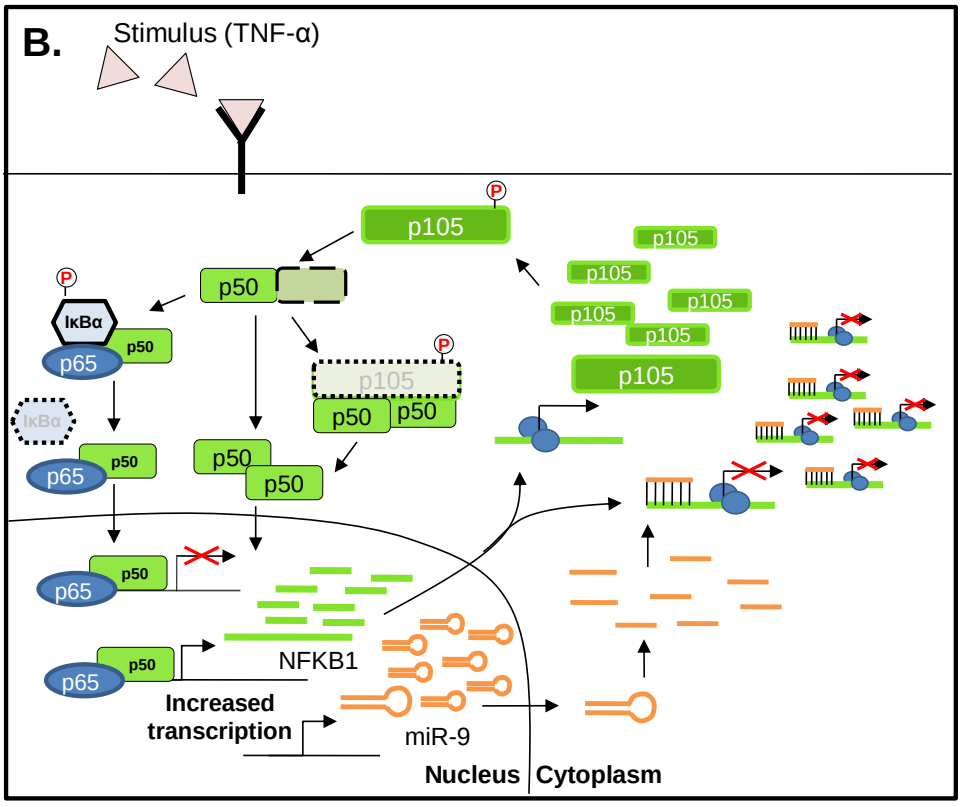
B.
Stimulus (TNF-α)
P
p105
p105
p105
p105
p105
p105
p105
p105
IκBα
p65
p50
p105
p50
p50
IκBα
p65
p50
p50
p50
p65
p50
p65
p50
NFKB1
Increased transcription
miR-9
Nucleus
Cytoplasm

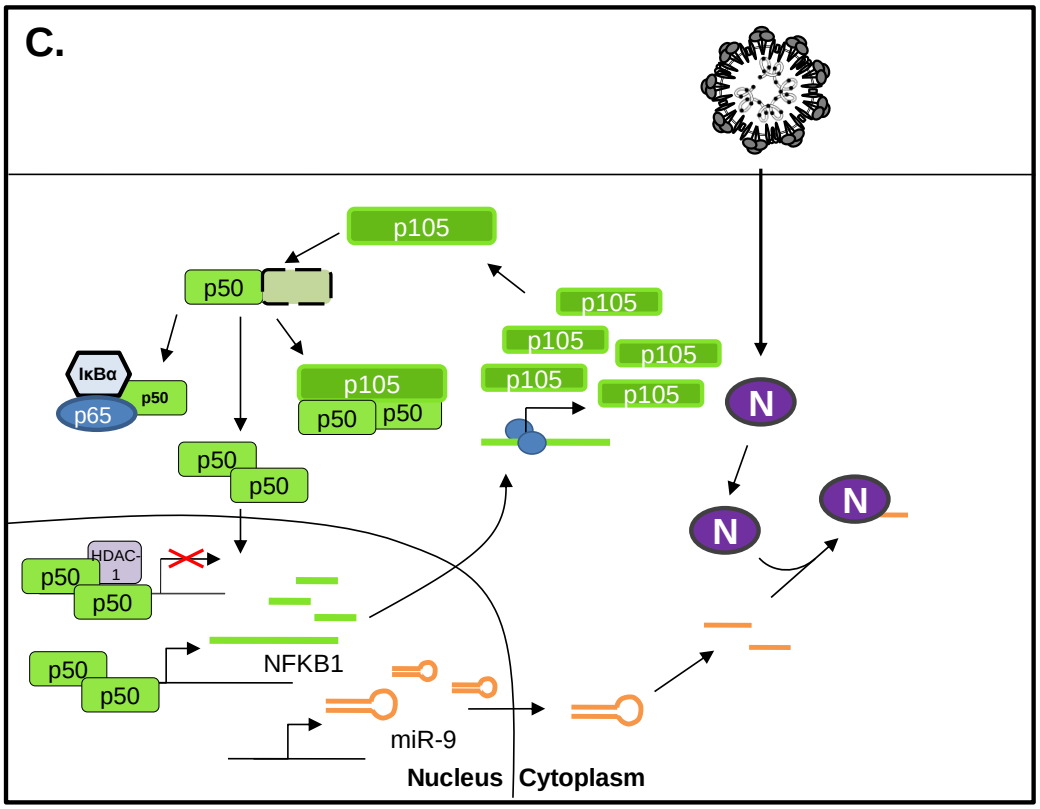
C.
p105
p50
p105
p105
p105
p105
p105
IκBα
p50
p65
p105
p50
p50
p50
p50
N
N
N
HDAC-1
p50
p50
p50
p50
NFKB1
miR-9
Nucleus
Cytoplasm

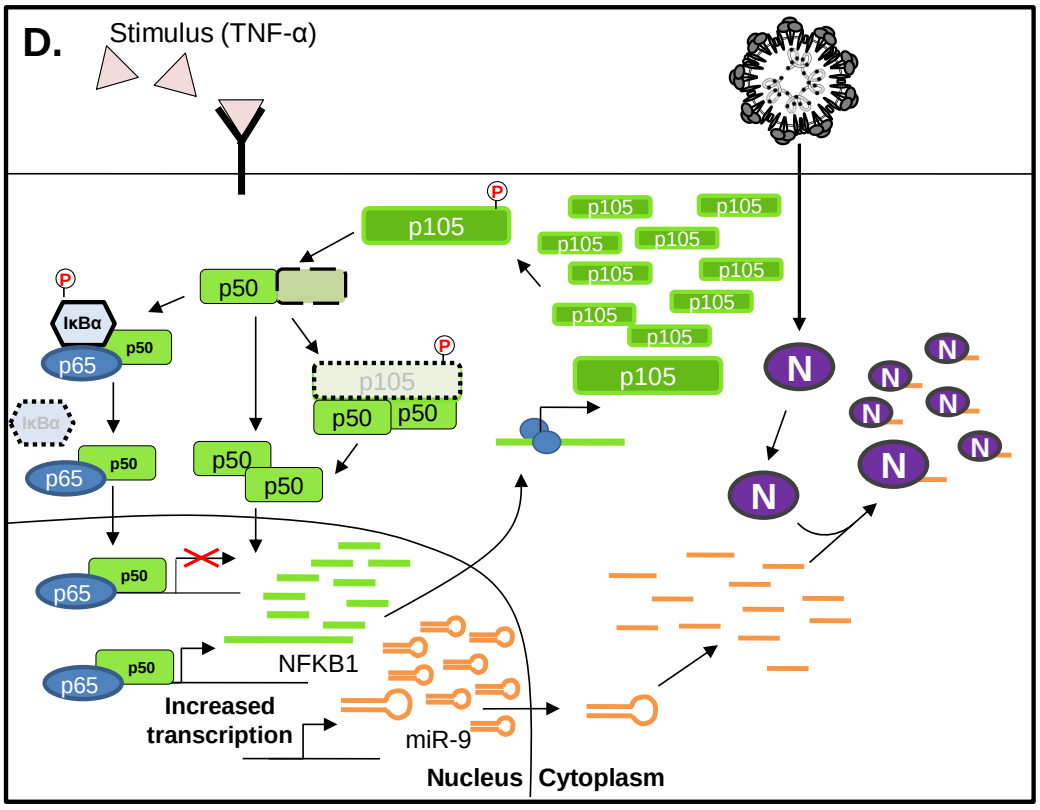
D.
Stimulus (TNF-α)
P
p105
p105
p105
p105
p105
p105
p105
p105
p105
p105
p105
IκBα
p50
p65
p50
p105
p50
p50
IκBα
p65
p50
p50
p50
N
N
N
N
N
N
N
N
p65
p50
p65
p50
NFKB1
Increased transcription
miR-9
Nucleus
Cytoplasm

Figure 43. Proposed mechanism of HCoV N interference with NFKB1.

(A) In resting cells, basal levels of NFKB1 and miR-9 are expressed. miR-9 negatively regulates NFKB1 expression. (B) With stimulus, a signalling cascade is initiated, resulting in increased transcription of both NFKB1 and miR-9. (C) Upon OC43 infection of cells, miR-9 is bound by the N protein, allowing for increased translation of NFKB1. (D) Addition of stimulus to OC43 infected cells further increases both NFKB1 and miR-9 transcription, but miR-9 is unable to act negatively in NFKB1 expression as it is bound by OC43 N.

leads to increased NFKB1 mRNA and therefore protein expression. This last scenario presented in Figure 43D is purely speculative, as HCT-8 cells were not responsive to TNF-α and NFKB1 could not be assessed in cells both infected with OC43 and treated with TNF-α.

As to why OC43 potentiates NFKB1 activation, a few scenarios can be theorized. The first possibility is that this is merely an unintentional side-effect of its RNA-binding nucleocapsid protein. In the context of an infection, there may be other viral proteins that aid in controlling the inflammatory response. As OC43 does not generally manifest in fatal infections, it is feasible that this is the key difference between OC43 and its fellow betacoronavirus, SARS-CoV. The latter causes immense levels of inflammation in the lungs of patients that does not resolve, resulting in high mortality. We also recognize that N is binding other miRNAs, and that its interaction with cellular RNAs is not limited to miR-9, indicating that this contact may be inadvertent.

The second possibility is that there is an advantage for OC43 to increase activated NFKB1. Although the subunit p50 can form dimers with other NF-κB subunits like p65, it may also form homodimers which can function as transcriptional repressors. Because p50 lacks transactivation domains (TAD), when homodimerized it binds consensus sequences in the promoter region and prevents transcription of various genes. When complexed with many of its co-activators of transcription, p50 homodimers also initiate transcription of anti-inflammatory genes. It is this property as well as the inhibitory IκB properties of precursor p105 that renders NFKB1 primarily anti-inflammatory. The full-length subunit p105 is also an inhibitor of NF-κB subunits which can retain them in the cytoplasm. An excess of both p50 and p105 subunits may lead to a state of repression within the cell, whereas normally in the context of a viral infection, a state of activation is desirable. This may also possibly have an impact on the interferon response. p50 homodimers have been shown to bind guanine-rich interferon response elements in the IFN-β enhancer region, effectively preventing transcription of IFN-β (394).

OC43 is by no means the only RNA virus with an RNA-binding protein, and this could be a common function across different genera of RNA viruses. Viruses such as influenza A, hepatitis C virus, and rubella virus all possess nucleocapsid proteins that complex with genomic RNA (395-397). Although several studies have shown that nucleocapsid recognizes viral RNA specifically,

it is not necessarily surprising that a viral RNA binding protein is able to bind cellular RNA (49, 117). miRNAs are an extremely important subset of cellular RNAs and have been the focus of a large volume of research since their discovery in the early 1990's (284). Many groups have shown anti-viral effects of miRNAs as well as viral manipulations of the miRNA pathways, including the encoding of viral miRNA mimics. This strategy is thought to be mainly a DNA virus specialty, as they typically have much larger genomes to encode extraneous virulence factors. RNA viruses must, as with other evasion tactics, be mutationally creative and utilize what little genomic space they possess. This often means multitasking of their encoded proteins. This novel mechanism of binding miRNAs to prevent function is a prime demonstration of how RNA viruses are constantly evolving to best the host immune system.

Chapter 5
Final Conclusions

Due to low rates and severity of morbidity and mortality, human coronaviruses were understudied until the beginning of the 21st century. With the emergence of SARS-CoV and MERS-CoV, it appears increasingly imperative that we understand the biology of coronaviruses, as cross-species transmission continues to occur. In this body of work, the nucleocapsid protein of HCoVs was shown to be an inhibitor of the innate interferon response and to deregulate NFKB1.

The nucleocapsid proteins of HCoVs were able to block IFN-initiated signalling. Although we were not able to elucidate the mechanism of interference, this property of human CoV N proteins has not been previously shown. It is important to ascertain that this essential protein of HCoV may be a main contributor to innate immune suppression in infections. This is most likely a common feature of coronaviruses, as our investigations show three HCoV N proteins possess abilities to block IFN signalling and in previous publications, SARS-CoV N as well as MHV N were also capable of antagonizing IFN.

Most intriguingly, the nucleocapsid interfered with the negative regulation of NFKB1. This ability has not been shown previously in any coronavirus. The elucidated mechanism is attributed to the RNA binding properties of the nucleocapsid, which has widespread implications for coronaviruses, as RNA binding is a common attribute among CoV N proteins.

Taken together, it is tempting to speculate that one of the consequences to increasing the amount of NFKB1 is the reduction of IFN-β and other ISGs. In addition to recognizing and binding to κB promoter sequences, homodimers of p50 also show a high affinity for guanine-rich interferon response elements (IRE) (394). p50 homodimers bind to these guanine-rich IREs in the promoter of IFN-β and other ISGs, repressing the transcription of these antiviral genes (394). As one of the most abundant NF-κB dimers in mammals, it is thought that these p50 homodimers act as competitive repressors and is speculated to primarily function as a competitor of IRF3, which preferentially binds a similar IRE sequence (394, 398). If expression of CoV N is able to promote p50 homodimer formation as a result of increased NFKB1 expression, this may be a mechanism by which CoV suppresses IFN.

Further research is necessary to test whether N is capable of promoting p50 homodimer formation and subsequent binding to IFN promoters. The abundance of p50 homodimers in a cell expressing N could be compared to untransfected cells, indicating whether N has the capability to positively skew the

formation of p50 homodimers. The DNA binding preferences of these homodimers in N expressing cells could also be examined via chromatin immunoprecipitation and determination of whether there is an increase in p50 homodimer binding to the IFN-β promoter could be examined. IFN-β transcript levels could also be examined in N expressing cells via quantitative PCR. These aspects should also be investigated in the context of OC43 infection. As we observed with miR-9 binding in Chapter 4, it seems that there is an inverse relationship between N-miR-9 binding and infection progression. This is likely due to competitive binding of the viral genome as the abundance of the genome is higher later in infection. It could then be speculated that this mechanism described above is dependent on the progression of OC43 infection, where N-miR-9 binding and its subsequent consequences occurs early in infection, but is lessened at later time points. This avenue would be important to explore in the future.

Zoonotic transmission of coronaviruses has been proven to possess the potential to be deadly. Evidence suggests that OC43 originated from BCoV, citing a deletion of two BCoV accessory proteins, and it is speculated that a pandemic between 1889 and 1890 coincided with this zoonotic transmission and genetic divergence (7). This outbreak was characterized by increased fatalities in the elderly and along with more typical symptoms such as malaise and fever, severe neurological symptoms were observed, supporting the line of evidence that the neurotropic OC43 was responsible (7). Although this speculated initial zoonotic transmission was fatal, OC43 has since become an infection that results in mild illness in the majority of populations. Both SARS-CoV and MERS-CoV have bat origins and although SARS-CoV was quickly controlled and has faded from the population, only time will tell if MERS-CoV will follow suit (399). Knowing this, it is valuable to learn as much as possible from non-pathogenic or non-fatal viruses, as much can be inferred from these viruses and implicated in related, more severe disease-causing viruses. RNA viruses are known to be highly mutable and coronaviruses are no exception. This research contributes to the understanding of the molecular biology of coronaviruses, particularly human CoV, and expands on the knowledge of coronavirus-host interactions. We hope that these studies have aided in furthering the discipline of human coronavirus research and have helped to additionally equip the field with knowledge for zoonotic coronavirus transmissions yet to come.

References

1. **Gonzalez JM, Gomez-Puertas P, Cavanagh D, Gorbalenya AE, Enjuanes L.** 2003. A comparative sequence analysis to revise the current taxonomy of the family Coronaviridae. Archives of virology **148:**2207-2235.
2. **Weiss SR, Navas-Martin S.** 2005. Coronavirus pathogenesis and the emerging pathogen severe acute respiratory syndrome coronavirus. Microbiology and Molecular Biology Reviews **69:**635-664.
3. **Woo PCY, Lau SKP, Lam CSF, Lau CCY, Tsang AKL, Lau JHN, Bai R, Teng JLL, Tsang CCC, Wang M, Zheng B-J, Chan K-H, Yuen K-Y.** 2012. Discovery of Seven Novel Mammalian and Avian Coronaviruses in the Genus Deltacoronavirus Supports Bat Coronaviruses as the Gene Source of Alphacoronavirus and Betacoronavirus and Avian Coronaviruses as the Gene Source of Gammacoronavirus and Deltacoronavirus. Journal of Virology **86:**3995-4008.
4. **Becker WB, McIntosh K, Dees JH, Chanock RM.** 1967. Morphogenesis of avian infectious bronchitis virus and a related human virus (strain 229E). Journal of virology **1:**1019-1027.
5. **McIntosh K, Becker WB, Chanock RM.** 1967. Growth in suckling-mouse brain of "IBV-like" viruses from patients with upper respiratory tract disease. Proceedings of the National Academy of Sciences of the United States of America **58:**2268-2273.
6. **Hamre D, Procknow JJ.** 1966. A New Virus Isolated from the Human Respiratory Tract. Proceedings of the Society for Experimental Biology and Medicine. Society for Experimental Biology and Medicine (New York, N.Y.) **121:**190-193.
7. **Vijgen L, Keyaerts E, Moes E, Thoelen I, Wollants E, Lemey P, Vandamme AM, Van Ranst M.** 2005. Complete genomic sequence of human coronavirus OC43: molecular clock analysis suggests a relatively recent zoonotic coronavirus transmission event. Journal of Virology **79:**1595-1604.
8. **Ksiazek TG, Erdman D, Goldsmith CS, Zaki SR, Peret T, Emery S, Tong S, Urbani C, Comer JA, Lim W, Rollin PE, Dowell SF, Ling AE, Humphrey CD, Shieh WJ, Guarner J, Paddock CD, Rota P, Fields B, DeRisi J, Yang JY, Cox N, Hughes JM, LeDuc JW, Bellini WJ, Anderson LJ.** 2003. A novel coronavirus associated with severe acute respiratory syndrome. The New England journal of medicine **348:**1953-1966.
9. **Drosten C, Gunther S, Preiser W, van der Werf S, Brodt HR, Becker S, Rabenau H, Panning M, Kolesnikova L, Fouchier RA, Berger A, Burguiere AM, Cinatl J, Eickmann M, Escriou N, Grywna K, Kramme S, Manuguerra JC, Muller S, Rickerts V, Sturmer M, Vieth S, Klenk**

HD, Osterhaus AD, Schmitz H, Doerr HW. 2003. Identification of a novel coronavirus in patients with severe acute respiratory syndrome. The New England journal of medicine **348:**1967-1976.

10. **Li W, Shi Z, Yu M, Ren W, Smith C, Epstein JH, Wang H, Crameri G, Hu Z, Zhang H, Zhang J, McEachern J, Field H, Daszak P, Eaton BT, Zhang S, Wang L-F.** 2005. Bats Are Natural Reservoirs of SARS-Like Coronaviruses. Science **310:**676-679.
11. **Zhong NS, Zheng BJ, Li YM, Poon LLM, Xie ZH, Chan KH, Li PH, Tan SY, Chang Q, Xie JP, Liu XQ, Xu J, Li DX, Yuen KY, Peiris JSM, Guan Y.** 2003. Epidemiology and cause of severe acute respiratory syndrome (SARS) in Guangdong, People's Republic of China, in February, 2003. The Lancet **362:**1353-1358.
12. **Pyrc K, Berkhout B, van der Hoek L.** 2007. The novel human coronaviruses NL63 and HKU1. Journal of virology **81:**3051-3057.
13. **van der Hoek L, Pyrc K, Jebbink MF, Vermeulen-Oost W, Berkhout RJ, Wolthers KC, Wertheim-van Dillen PM, Kaandorp J, Spaargaren J, Berkhout B.** 2004. Identification of a new human coronavirus. Nature Medicine **10:**368-373.
14. **Woo PC, Lau SK, Chu CM, Chan KH, Tsoi HW, Huang Y, Wong BH, Poon RW, Cai JJ, Luk WK, Poon LL, Wong SS, Guan Y, Peiris JS, Yuen KY.** 2005. Characterization and complete genome sequence of a novel coronavirus, coronavirus HKU1, from patients with pneumonia. Journal of Virology **79:**884-895.
15. **Zaki AM, van Boheemen S, Bestebroer TM, Osterhaus ADME, Fouchier RAM.** 2012. Isolation of a Novel Coronavirus from a Man with Pneumonia in Saudi Arabia. New England Journal of Medicine **367:**1814-1820.
16. **van Boheemen S, de Graaf M, Lauber C, Bestebroer TM, Raj VS, Zaki AM, Osterhaus ADME, Haagmans BL, Gorbalenya AE, Snijder EJ, Fouchier RAM.** 2012. Genomic Characterization of a Newly Discovered Coronavirus Associated with Acute Respiratory Distress Syndrome in Humans. mBio **3**.
17. **C.D.C.** 2013. Update: Severe Respiratory Illness Associated with Middle East Respiratory Syndrome Coronavirus (MERS-CoV) — Worldwide, 2012–2013. Morbidity and Mortality Weekly Report **62**.
18. **W.H.O.** June 14 2013 2013, posting date. Middle East respiratory syndrome coronavirus (MERS-CoV) - update. [Online.]
19. **Risco C, Anton IM, Enjuanes L, Carrascosa JL.** 1996. The transmissible gastroenteritis coronavirus contains a spherical core shell consisting of M and N proteins. Journal of Virology **70:**4773-4777.
20. 2007. Fields' virology, 5th ed. ed. Philadelphia, Wolters kluwer/Lippincott Williams & Wilkins.
21. **Perlman S, Netland J.** 2009. Coronaviruses post-SARS: update on replication and pathogenesis. Nature Reviews Microbiology **7:**439-450.

22. **Delmas B, Laude H.** 1990. Assembly of coronavirus spike protein into trimers and its role in epitope expression. Journal of Virology **64:**5367-5375.
23. **Belouzard S, Millet JK, Licitra BN, Whittaker GR.** 2012. Mechanisms of Coronavirus Cell Entry Mediated by the Viral Spike Protein. Viruses **4:**1011-1033.
24. **Casais R, Dove B, Cavanagh D, Britton P.** 2003. Recombinant Avian Infectious Bronchitis Virus Expressing a Heterologous Spike Gene Demonstrates that the Spike Protein Is a Determinant of Cell Tropism. Journal of Virology **77:**9084-9089.
25. **Navas S, Seo S-H, Chua MM, Sarma JD, Lavi E, Hingley ST, Weiss SR.** 2001. Murine Coronavirus Spike Protein Determines the Ability of the Virus To Replicate in the Liver and Cause Hepatitis. Journal of Virology **75:**2452-2457.
26. **Hodgson T, Casais R, Dove B, Britton P, Cavanagh D.** 2004. Recombinant Infectious Bronchitis Coronavirus Beaudette with the Spike Protein Gene of the Pathogenic M41 Strain Remains Attenuated but Induces Protective Immunity. Journal of Virology **78:**13804-13811.
27. **Bosch BJ, van der Zee R, de Haan CAM, Rottier PJM.** 2003. The Coronavirus Spike Protein Is a Class I Virus Fusion Protein: Structural and Functional Characterization of the Fusion Core Complex. Journal of Virology **77:**8801-8811.
28. **Kawase M, Shirato K, Matsuyama S, Taguchi F.** 2009. Protease-Mediated Entry via the Endosome of Human Coronavirus 229E. Journal of Virology **83:**712-721.
29. **Sainz B, Rausch JM, Gallaher WR, Garry RF, Wimley WC.** 2004. The Aromatic Domain of the Coronavirus Class I Viral Fusion Protein Induces Membrane Permeabilization: Putative Role during Viral Entry†. Biochemistry **44:**947-958.
30. **Mounir S, Talbot PJ.** 1992. Sequence analysis of the membrane protein gene of human coronavirus OC43 and evidence for O-glycosylation. Journal of General Virology **73:**2731-2736.
31. **Locker JK, Rose JK, Horzinek MC, Rottier PJ.** 1992. Membrane assembly of the triple-spanning coronavirus M protein. Individual transmembrane domains show preferred orientation. Journal of Biological Chemistry **267:**21911-21918.
32. **de Haan CAM, Kuo L, Masters PS, Vennema H, Rottier PJM.** 1998. Coronavirus Particle Assembly: Primary Structure Requirements of the Membrane Protein. Journal of Virology **72:**6838-6850.
33. **de Haan CAM, Smeets M, Vernooij F, Vennema H, Rottier PJM.** 1999. Mapping of the Coronavirus Membrane Protein Domains Involved in Interaction with the Spike Protein. Journal of Virology **73:**7441-7452.

34. **de Haan CAM, Vennema H, Rottier PJM.** 2000. Assembly of the Coronavirus Envelope: Homotypic Interactions between the M Proteins. Journal of Virology **74:**4967-4978.
35. **Narayanan K, Maeda A, Maeda J, Makino S.** 2000. Characterization of the Coronavirus M Protein and Nucleocapsid Interaction in Infected Cells. Journal of Virology **74:**8127-8134.
36. **Ruch TR, Machamer CE.** 2012. The Coronavirus E Protein: Assembly and Beyond. Viruses **4:**363-382.
37. **Wilson L, McKinlay C, Gage P, Ewart G.** 2004. SARS coronavirus E protein forms cation-selective ion channels. Virology **330:**322-331.
38. **Wilson L, Gage P, Ewart G.** 2006. Hexamethylene amiloride blocks E protein ion channels and inhibits coronavirus replication. Virology **353:**294-306.
39. **Ortego J, Ceriani JE, Patiño C, Plana J, Enjuanes L.** 2007. Absence of E protein arrests transmissible gastroenteritis coronavirus maturation in the secretory pathway. Virology **368:**296-308.
40. **DeDiego ML, Álvarez E, Almazán F, Rejas MT, Lamirande E, Roberts A, Shieh W-J, Zaki SR, Subbarao K, Enjuanes L.** 2007. A Severe Acute Respiratory Syndrome Coronavirus That Lacks the E Gene Is Attenuated In Vitro and In Vivo. Journal of Virology **81:**1701-1713.
41. **Yokomori K, Banner LR, Lai MMC.** 1991. Heterogeneity of gene expression of the hemagglutinin-esterase (HE) protein of murine coronaviruses. Virology **183:**647-657.
42. **Hogue BG, Kienzle TE, Brian DA.** 1989. Synthesis and Processing of the Bovine Enteric Coronavirus Haemagglutinin Protein. Journal of General Virology **70:**345-352.
43. **Popova R, Zhang X.** 2002. The Spike but Not the Hemagglutinin/Esterase Protein of Bovine Coronavirus Is Necessary and Sufficient for Viral Infection. Virology **294:**222-236.
44. **Desforges M, Desjardins J, Zhang C, Talbot PJ.** 2013. The Acetyl-Esterase Activity of the Hemagglutinin-Esterase Protein of Human Coronavirus OC43 Strongly Enhances the Production of Infectious Virus. Journal of Virology **87:**3097-3107.
45. **Lissenberg A, Vrolijk MM, van Vliet ALW, Langereis MA, de Groot-Mijnes JDF, Rottier PJM, de Groot RJ.** 2005. Luxury at a Cost? Recombinant Mouse Hepatitis Viruses Expressing the Accessory Hemagglutinin Esterase Protein Display Reduced Fitness In Vitro. Journal of Virology **79:**15054-15063.
46. **Luytjes W, Bredenbeek PJ, Noten AF, Horzinek MC, Spaan WJ.** 1988. Sequence of mouse hepatitis virus A59 mRNA 2: indications for RNA recombination between coronaviruses and influenza C virus. Virology **166:**415-422.
47. **Zeng Q, Langereis MA, van Vliet ALW, Huizinga EG, de Groot RJ.** 2008. Structure of coronavirus hemagglutinin-esterase offers insight into

corona and influenza virus evolution. Proceedings of the National Academy of Sciences **105:**9065-9069.

48. **Vlasak R, Luytjes W, Spaan W, Palese P.** 1988. Human and bovine coronaviruses recognize sialic acid-containing receptors similar to those of influenza C viruses. Proceedings of the National Academy of Sciences **85:**4526-4529.
49. **Stohlman SA, Baric RS, Nelson GN, Soe LH, Welter LM, Deans RJ.** 1988. Specific interaction between coronavirus leader RNA and nucleocapsid protein. Journal of Virology **62:**4288-4295.
50. **Surjit M, Lal SK.** 2008. The SARS-CoV nucleocapsid protein: A protein with multifarious activities. Infection, Genetics and Evolution **8:**397-405.
51. **Brierley I, Digard P, Inglis SC.** 1989. Characterization of an efficient coronavirus ribosomal frameshifting signal: requirement for an RNA pseudoknot. Cell **57:**537-547.
52. **Chen Z, Wang Y, Ratia K, Mesecar AD, Wilkinson KD, Baker SC.** 2007. Proteolytic processing and deubiquitinating activity of papain-like proteases of human coronavirus NL63. Journal of Virology **81:**6007-6018.
53. **Ziebuhr J, Thiel V, Gorbalenya AE.** 2001. The Autocatalytic Release of a Putative RNA Virus Transcription Factor from Its Polyprotein Precursor Involves Two Paralogous Papain-like Proteases That Cleave the Same Peptide Bond. Journal of Biological Chemistry **276:**33220-33232.
54. **Harcourt BH, Jukneliene D, Kanjanahaluethai A, Bechill J, Severson KM, Smith CM, Rota PA, Baker SC.** 2004. Identification of Severe Acute Respiratory Syndrome Coronavirus Replicase Products and Characterization of Papain-Like Protease Activity. Journal of Virology **78:**13600-13612.
55. **Rota PA, Oberste MS, Monroe SS, Nix WA, Campagnoli R, Icenogle JP, Penaranda S, Bankamp B, Maher K, Chen MH, Tong S, Tamin A, Lowe L, Frace M, DeRisi JL, Chen Q, Wang D, Erdman DD, Peret TC, Burns C, Ksiazek TG, Rollin PE, Sanchez A, Liffick S, Holloway B, Limor J, McCaustland K, Olsen-Rasmussen M, Fouchier R, Gunther S, Osterhaus AD, Drosten C, Pallansch MA, Anderson LJ, Bellini WJ.** 2003. Characterization of a novel coronavirus associated with severe acute respiratory syndrome. Science **300:**1394-1399.
56. **Putics Á, Filipowicz W, Hall J, Gorbalenya AE, Ziebuhr J.** 2005. ADP-Ribose-1"-Monophosphatase: a Conserved Coronavirus Enzyme That Is Dispensable for Viral Replication in Tissue Culture. Journal of Virology **79:**12721-12731.
57. **Putics Á, Gorbalenya AE, Ziebuhr J.** 2006. Identification of protease and ADP-ribose 1″-monophosphatase activities associated with transmissible gastroenteritis virus non-structural protein 3. Journal of General Virology **87:**651-656.
58. **Snijder EJ, Bredenbeek PJ, Dobbe JC, Thiel V, Ziebuhr J, Poon LLM, Guan Y, Rozanov M, Spaan WJM, Gorbalenya AE.** 2003. Unique and

Conserved Features of Genome and Proteome of SARS-coronavirus, an Early Split-off From the Coronavirus Group 2 Lineage. Journal of Molecular Biology **331:**991-1004.

59. **Lee H-J, Shieh C-K, Gorbalenya AE, Koonin EV, La Monica N, Tuler J, Bagdzhadzhyan A, Lai MMC.** 1991. The complete sequence (22 kilobases) of murine coronavirus gene 1 encoding the putative proteases and RNA polymerase. Virology **180:**567-582.
60. **Brockway SM, Clay CT, Lu XT, Denison MR.** 2003. Characterization of the Expression, Intracellular Localization, and Replication Complex Association of the Putative Mouse Hepatitis Virus RNA-Dependent RNA Polymerase. Journal of Virology **77:**10515-10527.
61. **Bhardwaj K, Guarino L, Kao CC.** 2004. The Severe Acute Respiratory Syndrome Coronavirus Nsp15 Protein Is an Endoribonuclease That Prefers Manganese as a Cofactor. Journal of Virology **78:**12218-12224.
62. **Ivanov KA, Ziebuhr J.** 2004. Human Coronavirus 229E Nonstructural Protein 13: Characterization of Duplex-Unwinding, Nucleoside Triphosphatase, and RNA 5′-Triphosphatase Activities. Journal of Virology **78:**7833-7838.
63. **Minskaia E, Hertzig T, Gorbalenya AE, Campanacci V, Cambillau C, Canard B, Ziebuhr J.** 2006. Discovery of an RNA virus 3′→5′ exoribonuclease that is critically involved in coronavirus RNA synthesis. Proceedings of the National Academy of Sciences of the United States of America **103:**5108-5113.
64. **Decroly E, Imbert I, Coutard B, Bouvet M, Selisko B, Alvarez K, Gorbalenya AE, Snijder EJ, Canard B.** 2008. Coronavirus Nonstructural Protein 16 Is a Cap-0 Binding Enzyme Possessing (Nucleoside-2′O)-Methyltransferase Activity. Journal of Virology **82:**8071-8084.
65. **Yount B, Roberts RS, Sims AC, Deming D, Frieman MB, Sparks J, Denison MR, Davis N, Baric RS.** 2005. Severe acute respiratory syndrome coronavirus group-specific open reading frames encode nonessential functions for replication in cell cultures and mice. Journal of virology **79:**14909-14922.
66. **de Haan CA, Masters PS, Shen X, Weiss S, Rottier PJ.** 2002. The group-specific murine coronavirus genes are not essential, but their deletion, by reverse genetics, is attenuating in the natural host. Virology **296:**177-189.
67. **Pewe L, Zhou H, Netland J, Tangudu C, Olivares H, Shi L, Look D, Gallagher T, Perlman S.** 2005. A severe acute respiratory syndrome-associated coronavirus-specific protein enhances virulence of an attenuated murine coronavirus. Journal of virology **79:**11335-11342.
68. **Tangudu C, Olivares H, Netland J, Perlman S, Gallagher T.** 2007. Severe acute respiratory syndrome coronavirus protein 6 accelerates murine coronavirus infections. Journal of virology **81:**1220-1229.

69. **Ortego J, Sola I, Almazan F, Ceriani JE, Riquelme C, Balasch M, Plana J, Enjuanes L.** 2003. Transmissible gastroenteritis coronavirus gene 7 is not essential but influences in vivo virus replication and virulence. Virology **308:**13-22.
70. **Haijema BJ, Volders H, Rottier PJ.** 2004. Live, attenuated coronavirus vaccines through the directed deletion of group-specific genes provide protection against feline infectious peritonitis. Journal of virology **78:**3863-3871.
71. **Tan Y-J, Lim SG, Hong W.** 2006. Understanding the accessory viral proteins unique to the severe acute respiratory syndrome (SARS) coronavirus. Antiviral Research **72:**78-88.
72. **Narayanan K, Huang C, Makino S.** 2008. SARS coronavirus accessory proteins. Virus Research **133:**113-121.
73. **Yuan X, Wu J, Shan Y, Yao Z, Dong B, Chen B, Zhao Z, Wang S, Chen J, Cong Y.** 2006. SARS coronavirus 7a protein blocks cell cycle progression at G0/G1 phase via the cyclin D3/pRb pathway. Virology **346:**74-85.
74. **Kopecky-Bromberg SA, Martinez-Sobrido L, Palese P.** 2006. 7a protein of severe acute respiratory syndrome coronavirus inhibits cellular protein synthesis and activates p38 mitogen-activated protein kinase. Journal of Virology **80:**785-793.
75. **Yuan X, Shan Y, Zhao Z, Chen J, Cong Y.** 2005. G0/G1 arrest and apoptosis induced by SARS-CoV 3b protein in transfected cells. Virology journal **2:**66.
76. **Geng H, Liu YM, Chan WS, Lo AW, Au DM, Waye MM, Ho YY.** 2005. The putative protein 6 of the severe acute respiratory syndrome-associated coronavirus: expression and functional characterization. FEBS Letters **579:**6763-6768.
77. **Law PY, Liu YM, Geng H, Kwan KH, Waye MM, Ho YY.** 2006. Expression and functional characterization of the putative protein 8b of the severe acute respiratory syndrome-associated coronavirus. FEBS Letters **580:**3643-3648.
78. **Tan YJ, Tham PY, Chan DZ, Chou CF, Shen S, Fielding BC, Tan TH, Lim SG, Hong W.** 2005. The severe acute respiratory syndrome coronavirus 3a protein up-regulates expression of fibrinogen in lung epithelial cells. Journal of Virology **79:**10083-10087.
79. **Hofmann H, Pyrc K, van der Hoek L, Geier M, Berkhout B, Pöhlmann S.** 2005. Human coronavirus NL63 employs the severe acute respiratory syndrome coronavirus receptor for cellular entry. Proceedings of the National Academy of Sciences **102:**7988-7993.
80. **Li W, Moore MJ, Vasilieva N, Sui J, Wong SK, Berne MA, Somasundaran M, Sullivan JL, Luzuriaga K, Greenough TC, Choe H, Farzan M.** 2003. Angiotensin-converting enzyme 2 is a functional receptor for the SARS coronavirus. Nature **426:**450-454.

81. **Chan CM, Lau SKP, Woo PCY, Tse H, Zheng B-J, Chen L, Huang J-D, Yuen K-Y.** 2009. Identification of Major Histocompatibility Complex Class I C Molecule as an Attachment Factor That Facilitates Coronavirus HKU1 Spike-Mediated Infection. Journal of Virology **83:**1026-1035.
82. **Yeager CL, Ashmun RA, Williams RK, Cardellichio CB, Shapiro LH, Look AT, Holmes KV.** 1992. Human aminopeptidase N is a receptor for human coronavirus 229E. Nature **357:**420-422.
83. **Sawicki SG, Sawicki DL, Siddell SG.** 2007. A Contemporary View of Coronavirus Transcription. Journal of Virology **81:**20-29.
84. **Gaunt ER, Hardie A, Claas ECJ, Simmonds P, Templeton KE.** 2010. Epidemiology and Clinical Presentations of the Four Human Coronaviruses 229E, HKU1, NL63, and OC43 Detected over 3 Years Using a Novel Multiplex Real-Time PCR Method. Journal of Clinical Microbiology **48:**2940-2947.
85. **McIntosh K, Chao RK, Krause HE, Wasil R, Mocega HE, Mufson MA.** 1974. Coronavirus Infection in Acute Lower Respiratory Tract Disease of Infants. The Journal of Infectious Diseases **130:**502-507.
86. **Leung WK, To KF, Chan PK, Chan HL, Wu AK, Lee N, Yuen KY, Sung JJ.** 2003. Enteric involvement of severe acute respiratory syndrome-associated coronavirus infection. Gastroenterology **125:**1011-1017.
87. **Birch CJ, Clothier HJ, Seccull A, Tran T, Catton MC, Lambert SB, Druce JD.** 2005. Human coronavirus OC43 causes influenza-like illness in residents and staff of aged-care facilities in Melbourne, Australia. Epidemiology and Infection **133:**273-277.
88. **Patrick DM, Petric M, Skowronski DM, Guasparini R, Booth TF, Krajden M, McGeer P, Bastien N, Gustafson L, Dubord J, Macdonald D, David ST, Srour LF, Parker R, Andonov A, Isaac-Renton J, Loewen N, McNabb G, McNabb A, Goh SH, Henwick S, Astell C, Guo JP, Drebot M, Tellier R, Plummer F, Brunham RC.** 2006. An Outbreak of Human Coronavirus OC43 Infection and Serological Cross-reactivity with SARS Coronavirus. Canadian Journal of Infectious Diseases and Medical Microbiology **17:**330-336.
89. **Vabret A, Mourez T, Gouarin S, Petitjean J, Freymuth F.** 2003. An Outbreak of Coronavirus OC43 Respiratory Infection in Normandy, France. Clinical Infectious Diseases **36:**985-989.
90. **Dijkman R, Jebbink MF, Gaunt E, Rossen JWA, Templeton KE, Kuijpers TW, van der Hoek L.** 2012. The dominance of human coronavirus OC43 and NL63 infections in infants. Journal of Clinical Virology **53:**135-139.
91. **Butler N, Pewe L, Trandem K, Perlman S.** 2006. Murine encephalitis caused by HCoV-OC43, a human coronavirus with broad species specificity, is partly immune-mediated. Virology **347:**410-421.

92. **McIntosh K, Becker WB, Chanock RM.** 1967. Growth in suckling-mouse brain of "IBV-like" viruses from patients with upper respiratory tract disease. Proceedings of the National Academy of Sciences **58:**2268-2273.
93. **Arbour N, Day R, Newcombe J, Talbot PJ.** 2000. Neuroinvasion by Human Respiratory Coronaviruses. Journal of Virology **74:**8913-8921.
94. **Dessau R, Lisby G, Frederiksen J.** 2001. Coronaviruses in brain tissue from patients with multiple sclerosis. Acta Neuropathol **101:**601-604.
95. **Stewart JN, Mounir S, Talbot PJ.** 1992. Human coronavirus gene expression in the brains of multiple sclerosis patients. Virology **191:**502-505.
96. **Lassnig C, Sanchez CM, Egerbacher M, Walter I, Majer S, Kolbe T, Pallares P, Enjuanes L, Müller M.** 2005. Development of a transgenic mouse model susceptible to human coronavirus 229E. Proceedings of the National Academy of Sciences of the United States of America **102:**8275-8280.
97. **Roberts A, Subbarao K.** 2006. Animal models for SARS. Advances in Experimental Medicine and Biology **581:**463-471.
98. **Smits SL, de Lang A, van den Brand JM, Leijten LM, van IWF, Eijkemans MJ, van Amerongen G, Kuiken T, Andeweg AC, Osterhaus AD, Haagmans BL.** 2010. Exacerbated innate host response to SARS-CoV in aged non-human primates. PLoS Pathogens **6:**e1000756.
99. **Roberts A, Paddock C, Vogel L, Butler E, Zaki S, Subbarao K.** 2005. Aged BALB/c Mice as a Model for Increased Severity of Severe Acute Respiratory Syndrome in Elderly Humans. Journal of Virology **79:**5833-5838.
100. **Bradburne AF, Somerset BA.** 1972. Coronative antibody tires in sera of healthy adults and experimentally infected volunteers. Journal of Hygiene (London) **70:**235-244.
101. **Callow KA.** 1985. Effect of specific humoral immunity and some non-specific factors on resistance of volunteers to respiratory coronavirus infection. Journal of Hygiene (London) **95:**173-189.
102. **Callow KA, Parry HF, Sergeant M, Tyrrell DA.** 1990. The time course of the immune response to experimental coronavirus infection of man. Epidemiology and Infection **105:**435-446.
103. **Reghunathan R, Jayapal M, Hsu LY, Chng HH, Tai D, Leung BP, Melendez AJ.** 2005. Expression profile of immune response genes in patients with Severe Acute Respiratory Syndrome. BMC Immunology **6:**2.
104. **Totura AL, Baric RS.** 2012. SARS coronavirus pathogenesis: host innate immune responses and viral antagonism of interferon. Current Opinion in Virology **2:**264-275.
105. **Hiscox JA, Wurm T, Wilson L, Britton P, Cavanagh D, Brooks G.** 2001. The coronavirus infectious bronchitis virus nucleoprotein localizes to the nucleolus. Journal of Virology **75:**506-512.

106. **Wurm T, Chen H, Hodgson T, Britton P, Brooks G, Hiscox JA.** 2001. Localization to the nucleolus is a common feature of coronavirus nucleoproteins, and the protein may disrupt host cell division. Journal of Virology **75:**9345-9356.
107. **Rowland RR, Kervin R, Kuckleburg C, Sperlich A, Benfield DA.** 1999. The localization of porcine reproductive and respiratory syndrome virus nucleocapsid protein to the nucleolus of infected cells and identification of a potential nucleolar localization signal sequence. Virus Research **64:**1-12.
108. **Rowland RR, Chauhan V, Fang Y, Pekosz A, Kerrigan M, Burton MD.** 2005. Intracellular localization of the severe acute respiratory syndrome coronavirus nucleocapsid protein: absence of nucleolar accumulation during infection and after expression as a recombinant protein in vero cells. Journal of Virology **79:**11507-11512.
109. **You J, Dove BK, Enjuanes L, DeDiego ML, Alvarez E, Howell G, Heinen P, Zambon M, Hiscox JA.** 2005. Subcellular localization of the severe acute respiratory syndrome coronavirus nucleocapsid protein. Journal of General Virology **86:**3303-3310.
110. **You JH, Reed ML, Hiscox JA.** 2007. Trafficking motifs in the SARS-coronavirus nucleocapsid protein. Biochemical and Biophysical Research Communications **358:**1015-1020.
111. **Cawood R, Harrison SM, Dove BK, Reed ML, Hiscox JA.** 2007. Cell cycle dependent nucleolar localization of the coronavirus nucleocapsid protein. Cell Cycle **6:**863-867.
112. **Zhao X, Nicholls JM, Chen YG.** 2008. Severe acute respiratory syndrome-associated coronavirus nucleocapsid protein interacts with Smad3 and modulates transforming growth factor-beta signaling. Journal of Biological Chemistry **283:**3272-3280.
113. **Luo C, Luo H, Zheng S, Gui C, Yue L, Yu C, Sun T, He P, Chen J, Shen J, Luo X, Li Y, Liu H, Bai D, Shen J, Yang Y, Li F, Zuo J, Hilgenfeld R, Pei G, Chen K, Shen X, Jiang H.** 2004. Nucleocapsid protein of SARS coronavirus tightly binds to human cyclophilin A. Biochemical and Biophysical Research Communications **321:**557-565.
114. **Zuniga S, Sola I, Moreno JL, Sabella P, Plana-Duran J, Enjuanes L.** 2007. Coronavirus nucleocapsid protein is an RNA chaperone. Virology **357:**215-227.
115. **Zeng Y, Ye L, Zhu S, Zheng H, Zhao P, Cai W, Su L, She Y, Wu Z.** 2008. The nucleocapsid protein of SARS-associated coronavirus inhibits B23 phosphorylation. Biochemical and Biophysical Research Communications **369:**287-291.
116. **Chen H, Wurm T, Britton P, Brooks G, Hiscox JA.** 2002. Interaction of the coronavirus nucleoprotein with nucleolar antigens and the host cell. Journal of Virology **76:**5233-5250.
117. **Chen H, Gill A, Dove BK, Emmett SR, Kemp CF, Ritchie MA, Dee M, Hiscox JA.** 2005. Mass spectroscopic characterization of the coronavirus

infectious bronchitis virus nucleoprotein and elucidation of the role of phosphorylation in RNA binding by using surface plasmon resonance. Journal of Virology **79:**1164-1179.

118. **Spencer KA, Dee M, Britton P, Hiscox JA.** 2008. Role of phosphorylation clusters in the biology of the coronavirus infectious bronchitis virus nucleocapsid protein. Virology **370:**373-381.
119. **Surjit M, Kumar R, Mishra RN, Reddy MK, Chow VT, Lal SK.** 2005. The severe acute respiratory syndrome coronavirus nucleocapsid protein is phosphorylated and localizes in the cytoplasm by 14-3-3-mediated translocation. Journal of Virology **79:**11476-11486.
120. **Wu CH, Yeh SH, Tsay YG, Shieh YH, Kao CL, Chen YS, Wang SH, Kuo TJ, Chen DS, Chen PJ.** 2009. Glycogen synthase kinase-3 regulates the phosphorylation of severe acute respiratory syndrome coronavirus nucleocapsid protein and viral replication. Journal of Biological Chemistry **284:**5229-5239.
121. **Okuda M, Horn HF, Tarapore P, Tokuyama Y, Smulian AG, Chan PK, Knudsen ES, Hofmann IA, Snyder JD, Bove KE, Fukasawa K.** 2000. Nucleophosmin/B23 is a target of CDK2/cyclin E in centrosome duplication. Cell **103:**127-140.
122. **Chang C-K, Hsu Y-L, Chang Y-H, Chao F-A, Wu M-C, Huang Y-S, Hu C-K, Huang T-H.** 2009. Multiple Nucleic Acid Binding Sites and Intrinsic Disorder of Severe Acute Respiratory Syndrome Coronavirus Nucleocapsid Protein: Implications for Ribonucleocapsid Protein Packaging. Journal of Virology **83:**2255-2264.
123. **Huang C-Y, Hsu Y-L, Chiang W-L, Hou M-H.** 2009. Elucidation of the stability and functional regions of the human coronavirus OC43 nucleocapsid protein. Protein Science **18:**2209-2218.
124. **Huang Q, Yu L, Petros AM, Gunasekera A, Liu Z, Xu N, Hajduk P, Mack J, Fesik SW, Olejniczak ET.** 2004. Structure of the N-terminal RNA-binding domain of the SARS CoV nucleocapsid protein. Biochemistry **43:**6059-6063.
125. **Saikatendu KS, Joseph JS, Subramanian V, Neuman BW, Buchmeier MJ, Stevens RC, Kuhn P.** 2007. Ribonucleocapsid formation of severe acute respiratory syndrome coronavirus through molecular action of the N-terminal domain of N protein. Journal of Virology **81:**3913-3921.
126. **Zhou M, Collisson EW.** 2000. The amino and carboxyl domains of the infectious bronchitis virus nucleocapsid protein interact with 3' genomic RNA. Virus Research **67:**31-39.
127. **Timani KA, Liao Q, Ye L, Zeng Y, Liu J, Zheng Y, Ye L, Yang X, Lingbao K, Gao J, Zhu Y.** 2005. Nuclear/nucleolar localization properties of C-terminal nucleocapsid protein of SARS coronavirus. Virus Research **114:**23-34.
128. **Peng TY, Lee KR, Tarn WY.** 2008. Phosphorylation of the arginine/serine dipeptide-rich motif of the severe acute respiratory syndrome coronavirus

nucleocapsid protein modulates its multimerization, translation inhibitory activity and cellular localization. FEBS Journal **275:**4152-4163.

129. **He R, Dobie F, Ballantine M, Leeson A, Li Y, Bastien N, Cutts T, Andonov A, Cao J, Booth TF, Plummer FA, Tyler S, Baker L, Li X.** 2004. Analysis of multimerization of the SARS coronavirus nucleocapsid protein. Biochemical and Biophysical Research Communications **316:**476-483.
130. **Luo H, Ye F, Chen K, Shen X, Jiang H.** 2005. SR-rich motif plays a pivotal role in recombinant SARS coronavirus nucleocapsid protein multimerization. Biochemistry **44:**15351-15358.
131. **Tylor S, Andonov A, Cutts T, Cao J, Grudesky E, Van Domselaar G, Li X, He R.** 2009. The SR-rich motif in SARS-CoV nucleocapsid protein is important for virus replication. Canadian Journal of Microbiology **55:**254-260.
132. **Lo Y-S, Lin S-Y, Wang S-M, Wang C-T, Chiu Y-L, Huang T-H, Hou M-H.** 2013. Oligomerization of the carboxyl terminal domain of the human coronavirus 229E nucleocapsid protein. FEBS Letters **587:**120-127.
133. **Surjit M, Liu B, Kumar P, Chow VTK, Lal SK.** 2004. The nucleocapsid protein of the SARS coronavirus is capable of self-association through a C-terminal 209 amino acid interaction domain. Biochemical and Biophysical Research Communications **317:**1030-1036.
134. **Yu IM, Gustafson CL, Diao J, Burgner JW, 2nd, Li Z, Zhang J, Chen J.** 2005. Recombinant severe acute respiratory syndrome (SARS) coronavirus nucleocapsid protein forms a dimer through its C-terminal domain. Journal of Biological Chemistry **280:**23280-23286.
135. **Fan H, Ooi A, Tan YW, Wang S, Fang S, Liu DX, Lescar J.** 2005. The Nucleocapsid Protein of Coronavirus Infectious Bronchitis Virus: Crystal Structure of Its N-Terminal Domain and Multimerization Properties. Structure **13:**1859-1868.
136. **Hurst KR, Kuo L, Koetzner CA, Ye R, Hsue B, Masters PS.** 2005. A major determinant for membrane protein interaction localizes to the carboxy-terminal domain of the mouse coronavirus nucleocapsid protein. Journal of Virology **79:**13285-13297.
137. **Isaacs A, Lindenmann J.** 1957. Virus interference. I. The interferon. Proceedings of the Royal Society B: Biological Sciences **147:**258-267.
138. **Isaacs A, Lindenmann J, Valentine RC.** 1957. Virus interference. II. Some properties of interferon. Proceedings of the Royal Society B: Biological Sciences **147:**268-273.
139. **Lindenmann J, Burke DC, Isaacs A.** 1957. Studies on the production, mode of action and properties of interferon. British Journal of Experimental Pathology **38:**551-562.
140. **Ho M, Enders JF.** 1959. Further studies on an inhibitor of viral activity appearing in infected cell cultures and its role in chronic viral infections. Virology **9:**446-477.

141. **Ho M, Enders JF.** 1959. An Inhibitor of Viral Activity Appearing in Infected Cell Cultures. Proceedings of the National Academy of Sciences **45:**385-389.
142. **Kotenko SV, Gallagher G, Baurin VV, Lewis-Antes A, Shen M, Shah NK, Langer JA, Sheikh F, Dickensheets H, Donnelly RP.** 2003. IFN-[lambda]s mediate antiviral protection through a distinct class II cytokine receptor complex. Nature Immunology **4:**69-77.
143. **Pestka S, Krause CD, Walter MR.** 2004. Interferons, interferon-like cytokines, and their receptors. Immunological Reviews **202:**8-32.
144. **de Weerd NA, Nguyen T.** 2012. The interferons and their receptors[mdash]distribution and regulation. Immunology and Cell Biology **90:**483-491.
145. **Pitha PM, Kunzi MS.** 2007. Type I Interferon: The Ever Unfolding Story, p. 41-70. *In* Pitha P (ed.), Interferon: The 50th Anniversary, vol. 316. Springer Berlin Heidelberg.
146. **Cavlar T, Ablasser A, Hornung V.** 2012. Induction of type I IFNs by intracellular DNA-sensing pathways. Immunology and Cell Biology **90:**474-482.
147. **Rock FL, Hardiman G, Timans JC, Kastelein RA, Bazan JF.** 1998. A family of human receptors structurally related to Drosophila Toll. Proceedings of the National Academy of Sciences **95:**588-593.
148. **Medzhitov R, Preston-Hurlburt P, Janeway CA.** 1997. A human homologue of the Drosophila Toll protein signals activation of adaptive immunity. Nature **388:**394-397.
149. **Chuang TH, Ulevitch RJ.** 2000. Cloning and characterization of a sub-family of human toll-like receptors: hTLR7, hTLR8 and hTLR9. European Cytokine Network **11:**372-378.
150. **Chuang T-H, Ulevitch RJ.** 2001. Identification of hTLR10: a novel human Toll-like receptor preferentially expressed in immune cells. Biochimica et Biophysica Acta (BBA) - Gene Structure and Expression **1518:**157-161.
151. **Du X, Poltorak A, Wei Y, Beutler B.** 2000. Three novel mammalian toll-like receptors: gene structure, expression, and evolution. European Cytokine Network **11:**362-371.
152. **Takeuchi O, Kawai T, Sanjo H, Copeland NG, Gilbert DJ, Jenkins NA, Takeda K, Akira S.** 1999. TLR6: A novel member of an expanding Toll-like receptor family. Gene **231:**59-65.
153. **Medzhitov R, Preston-Hurlburt P, Kopp E, Stadlen A, Chen C, Ghosh S, Janeway Jr CA.** 1998. MyD88 Is an Adaptor Protein in the hToll/IL-1 Receptor Family Signaling Pathways. Molecular Cell **2:**253-258.
154. **Ozinsky A, Underhill DM, Fontenot JD, Hajjar AM, Smith KD, Wilson CB, Schroeder L, Aderem A.** 2000. The repertoire for pattern recognition of pathogens by the innate immune system is defined by cooperation between Toll-like receptors. Proceedings of the National Academy of Sciences **97:**13766-13771.

155. **Takeuchi O, Sato S, Horiuchi T, Hoshino K, Takeda K, Dong Z, Modlin RL, Akira S.** 2002. Cutting Edge: Role of Toll-Like Receptor 1 in Mediating Immune Response to Microbial Lipoproteins. The Journal of Immunology **169:**10-14.
156. **Honda K, Takaoka A, Taniguchi T.** 2006. Type I Inteferon Gene Induction by the Interferon Regulatory Factor Family of Transcription Factors. Immunity **25:**349-360.
157. **Cui Y, Li M, Walton KD, Sun K, Hanover JA, Furth PA, Hennighausen L.** 2001. The Stat3/5 Locus Encodes Novel Endoplasmic Reticulum and Helicase-like Proteins That Are Preferentially Expressed in Normal and Neoplastic Mammary Tissue. Genomics **78:**129-134.
158. **Kang D-c, Gopalkrishnan RV, Wu Q, Jankowsky E, Pyle AM, Fisher PB.** 2002. mda-5: An interferon-inducible putative RNA helicase with double-stranded RNA-dependent ATPase activity and melanoma growth-suppressive properties. Proceedings of the National Academy of Sciences **99:**637-642.
159. **Yoneyama M, Kikuchi M, Matsumoto K, Imaizumi T, Miyagishi M, Taira K, Foy E, Loo Y-M, Gale M, Akira S, Yonehara S, Kato A, Fujita T.** 2005. Shared and Unique Functions of the DExD/H-Box Helicases RIG-I, MDA5, and LGP2 in Antiviral Innate Immunity. The Journal of Immunology **175:**2851-2858.
160. **Saito T, Hirai R, Loo YM, Owen D, Johnson CL, Sinha SC, Akira S, Fujita T, Gale M, Jr.** 2007. Regulation of innate antiviral defenses through a shared repressor domain in RIG-I and LGP2. Proceedings of the National Academy of Sciences **104:**582-587.
161. **Kato H, Takeuchi O, Sato S, Yoneyama M, Yamamoto M, Matsui K, Uematsu S, Jung A, Kawai T, Ishii KJ, Yamaguchi O, Otsu K, Tsujimura T, Koh C-S, Reis e Sousa C, Matsuura Y, Fujita T, Akira S.** 2006. Differential roles of MDA5 and RIG-I helicases in the recognition of RNA viruses. Nature **441:**101-105.
162. **Kato H, Takeuchi O, Mikamo-Satoh E, Hirai R, Kawai T, Matsushita K, Hiiragi A, Dermody TS, Fujita T, Akira S.** 2008. Length-dependent recognition of double-stranded ribonucleic acids by retinoic acid–inducible gene-I and melanoma differentiation–associated gene 5. The Journal of Experimental Medicine **205:**1601-1610.
163. **Kawai T, Takahashi K, Sato S, Coban C, Kumar H, Kato H, Ishii KJ, Takeuchi O, Akira S.** 2005. IPS-1, an adaptor triggering RIG-I- and Mda5-mediated type I interferon induction. Nature Immunology **6:**981-988.
164. **Meylan E, Curran J, Hofmann K, Moradpour D, Binder M, Bartenschlager R, Tschopp J.** 2005. Cardif is an adaptor protein in the RIG-I antiviral pathway and is targeted by hepatitis C virus. Nature **437:**1167-1172.

165. **Seth RB, Sun L, Ea C-K, Chen ZJ.** 2005. Identification and Characterization of MAVS, a Mitochondrial Antiviral Signaling Protein that Activates NF-κB and IRF3. Cell **122:**669-682.
166. **Xu L-G, Wang Y-Y, Han K-J, Li L-Y, Zhai Z, Shu H-B.** 2005. VISA Is an Adapter Protein Required for Virus-Triggered IFN-β Signaling. Molecular Cell **19:**727-740.
167. **Schoggins JW, Rice CM.** 2011. Interferon-stimulated genes and their antiviral effector functions. Current Opinion in Virology **1:**519-525.
168. **Sato M, Hata N, Asagiri M, Nakaya T, Taniguchi T, Tanaka N.** 1998. Positive feedback regulation of type I IFN genes by the IFN-inducible transcription factor IRF-7. FEBS Letters **441:**106-110.
169. **Ning S, Pagano JS, Barber GN.** 2011. IRF7: activation, regulation, modification and function. Genes & Immunity **12:**399-414.
170. **Hervas-Stubbs S, Perez-Gracia JL, Rouzaut A, Sanmamed MF, Le Bon A, Melero I.** 2011. Direct Effects of Type I Interferons on Cells of the Immune System. Clinical Cancer Research **17:**2619-2627.
171. **Nguyen KB, Salazar-Mather TP, Dalod MY, Van Deusen JB, Wei X-q, Liew FY, Caligiuri MA, Durbin JE, Biron CA.** 2002. Coordinated and Distinct Roles for IFN-αβ, IL-12, and IL-15 Regulation of NK Cell Responses to Viral Infection. The Journal of Immunology **169:**4279-4287.
172. **Durbin JE, Fernandez-Sesma A, Lee C-K, Rao TD, Frey AB, Moran TM, Vukmanovic S, García-Sastre A, Levy DE.** 2000. Type I IFN Modulates Innate and Specific Antiviral Immunity. The Journal of Immunology **164:**4220-4228.
173. **Bogdan C, Mattner J, Schleicher U.** 2004. The role of type I interferons in non-viral infections. Immunological Reviews **202:**33-48.
174. **Santini SM, Lapenta C, Logozzi M, Parlato S, Spada M, Di Pucchio T, Belardelli F.** 2000. Type I Interferon as a Powerful Adjuvant for Monocyte-Derived Dendritic Cell Development and Activity in Vitro and in Hu-Pbl-Scid Mice. The Journal of Experimental Medicine **191:**1777-1788.
175. **Gallucci S, Lolkema M, Matzinger P.** 1999. Natural adjuvants: Endogenous activators of dendritic cells. Nature Medicine **5:**1249-1255.
176. **Montoya M, Schiavoni G, Mattei F, Gresser I, Belardelli F, Borrow P, Tough DF.** 2002. Type I interferons produced by dendritic cells promote their phenotypic and functional activation. Blood **99:**3263-3271.
177. **Ozato K, Shin D-M, Chang T-H, Morse HC.** 2008. TRIM family proteins and their emerging roles in innate immunity. Nature Reviews Immunology **8:**849-860.
178. **Williams BR.** 1999. PKR; a sentinel kinase for cellular stress. Oncogene **18:**6112-6120.
179. **Schulz O, Pichlmair A, Rehwinkel J, Rogers NC, Scheuner D, Kato H, Takeuchi O, Akira S, Kaufman RJ, Reis e Sousa C.** 2010. Protein Kinase R Contributes to Immunity against Specific Viruses by Regulating Interferon mRNA Integrity. Cell Host & Microbe **7:**354-361.

180. **Espert L, Degols G, Gongora C, Blondel D, Williams BR, Silverman RH, Mechti N.** 2003. ISG20, a New Interferon-induced RNase Specific for Single-stranded RNA, Defines an Alternative Antiviral Pathway against RNA Genomic Viruses. Journal of Biological Chemistry **278:**16151-16158.
181. **Haller O, Staeheli P, Kochs G.** 2007. Interferon-induced Mx proteins in antiviral host defense. Biochimie **89:**812-818.
182. **Haller O, Stertz S, Kochs G.** 2007. The Mx GTPase family of interferon-induced antiviral proteins. Microbes and Infection **9:**1636-1643.
183. **Skaug B, Chen ZJ.** 2010. Emerging Role of ISG15 in Antiviral Immunity. Cell **143:**187-190.
184. **Shi H-X, Yang K, Liu X, Liu X-Y, Wei B, Shan Y-F, Zhu L-H, Wang C.** 2010. Positive Regulation of Interferon Regulatory Factor 3 Activation by Herc5 via ISG15 Modification. Molecular and Cellular Biology **30:**2424-2436.
185. **Pfaller CK, Li Z, George CX, Samuel CE.** 2011. Protein kinase PKR and RNA adenosine deaminase ADAR1: new roles for old players as modulators of the interferon response. Current Opinion in Immunology **23:**573-582.
186. **Chiu Y-L, Greene WC.** 2006. Multifaceted antiviral actions of APOBEC3 cytidine deaminases. Trends in Immunology **27:**291-297.
187. **Diamond MS, Farzan M.** 2013. The broad-spectrum antiviral functions of IFIT and IFITM proteins. Nature Reviews Immunology **13:**46-57.
188. **Raychoudhuri A, Shrivastava S, Steele R, Kim H, Ray R, Ray RB.** 2011. ISG56 and IFITM1 Proteins Inhibit Hepatitis C Virus Replication. Journal of Virology **85:**12881-12889.
189. **Wang C, Pflugheber J, Sumpter R, Sodora DL, Hui D, Sen GC, Gale M.** 2003. Alpha Interferon Induces Distinct Translational Control Programs To Suppress Hepatitis C Virus RNA Replication. Journal of Virology **77:**3898-3912.
190. **Daffis S, Szretter KJ, Schriewer J, Li J, Youn S, Errett J, Lin T-Y, Schneller S, Zust R, Dong H, Thiel V, Sen GC, Fensterl V, Klimstra WB, Pierson TC, Buller RM, Gale Jr M, Shi P-Y, Diamond MS.** 2010. 2[prime]-O methylation of the viral mRNA cap evades host restriction by IFIT family members. Nature **468:**452-456.
191. **Szretter KJ, Daniels BP, Cho H, Gainey MD, Yokoyama WM, Gale M, Jr., Virgin HW, Klein RS, Sen GC, Diamond MS.** 2012. 2′-<italic>O</italic> Methylation of the Viral mRNA Cap by West Nile Virus Evades Ifit1-Dependent and -Independent Mechanisms of Host Restriction In Vivo. PLoS Pathogens **8:**e1002698.
192. **Zust R, Cervantes-Barragan L, Habjan M, Maier R, Neuman BW, Ziebuhr J, Szretter KJ, Baker SC, Barchet W, Diamond MS, Siddell SG, Ludewig B, Thiel V.** 2011. Ribose 2'-O-methylation provides a molecular signature for the distinction of self and non-self mRNA dependent on the RNA sensor Mda5. Nature Immunology **12:**137-143.

193. **Pichlmair A, Lassnig C, Eberle C-A, Gorna MW, Baumann CL, Burkard TR, Burckstummer T, Stefanovic A, Krieger S, Bennett KL, Rulicke T, Weber F, Colinge J, Muller M, Superti-Furga G.** 2011. IFIT1 is an antiviral protein that recognizes 5[prime]-triphosphate RNA. Nature Immunology **12:**624-630.
194. **Saikia P, Fensterl V, Sen GC.** 2010. The Inhibitory Action of P56 on Select Functions of E1 Mediates Interferon's Effect on Human Papillomavirus DNA Replication. Journal of Virology **84:**13036-13039.
195. **Terenzi F, Saikia P, Sen GC.** 2008. Interferon-inducible protein, P56, inhibits HPV DNA replication by binding to the viral protein E1. EMBO Journal **27:**3311-3321.
196. **Hatada E, Fukuda R.** 1992. Binding of influenza A virus NS1 protein to dsRNA in vitro. Journal of General Virology **73:**3325-3329.
197. **Li S, Min J-Y, Krug RM, Sen GC.** 2006. Binding of the influenza A virus NS1 protein to PKR mediates the inhibition of its activation by either PACT or double-stranded RNA. Virology **349:**13-21.
198. **Taguchi T, Nagano-Fujii M, Akutsu M, Kadoya H, Ohgimoto S, Ishido S, Hotta H.** 2004. Hepatitis C virus NS5A protein interacts with 2′,5′-oligoadenylate synthetase and inhibits antiviral activity of IFN in an IFN sensitivity-determining region-independent manner. Journal of General Virology **85:**959-969.
199. **Gale Jr MJ, Korth MJ, Tang NM, Tan S-L, Hopkins DA, Dever TE, Polyak SJ, Gretch DR, Katze MG.** 1997. Evidence That Hepatitis C Virus Resistance to Interferon Is Mediated through Repression of the PKR Protein Kinase by the Nonstructural 5A Protein. Virology **230:**217-227.
200. **Abe T, Kaname Y, Hamamoto I, Tsuda Y, Wen X, Taguwa S, Moriishi K, Takeuchi O, Kawai T, Kanto T, Hayashi N, Akira S, Matsuura Y.** 2007. Hepatitis C Virus Nonstructural Protein 5A Modulates the Toll-Like Receptor-MyD88-Dependent Signaling Pathway in Macrophage Cell Lines. Journal of Virology **81:**8953-8966.
201. **Li K, Foy E, Ferreon JC, Nakamura M, Ferreon ACM, Ikeda M, Ray SC, Gale M, Lemon SM.** 2005. Immune evasion by hepatitis C virus NS3/4A protease-mediated cleavage of the Toll-like receptor 3 adaptor protein TRIF. Proceedings of the National Academy of Sciences of the United States of America **102:**2992-2997.
202. **Otsuka M, Kato N, Moriyama M, Taniguchi H, Wang Y, Dharel N, Kawabe T, Omata M.** 2005. Interaction between the HCV NS3 protein and the host TBK1 protein leads to inhibition of cellular antiviral responses. Hepatology **41:**1004-1012.
203. **Lin R, Lacoste J, Nakhaei P, Sun Q, Yang L, Paz S, Wilkinson P, Julkunen I, Vitour D, Meurs E, Hiscott J.** 2006. Dissociation of a MAVS/IPS-1/VISA/Cardif-IKKε Molecular Complex from the Mitochondrial Outer Membrane by Hepatitis C Virus NS3-4A Proteolytic Cleavage. Journal of Virology **80:**6072-6083.

204. **Melroe GT, Silva L, Schaffer PA, Knipe DM.** 2007. Recruitment of activated IRF-3 and CBP/p300 to herpes simplex virus ICP0 nuclear foci: Potential role in blocking IFN-β induction. Virology **360:**305-321.
205. **Paladino P, Collins SE, Mossman KL.** 2010. Cellular Localization of the Herpes Simplex Virus ICP0 Protein Dictates Its Ability to Block IRF3-Mediated Innate Immune Responses. PLoS ONE **5:**e10428.
206. **Okumura A, Alce T, Lubyova B, Ezelle H, Strebel K, Pitha PM.** 2008. HIV-1 accessory proteins VPR and Vif modulate antiviral response by targeting IRF-3 for degradation. Virology **373:**85-97.
207. **Barro M, Patton JT.** 2005. Rotavirus nonstructural protein 1 subverts innate immune response by inducing degradation of IFN regulatory factor 3. Proceedings of the National Academy of Sciences of the United States of America **102:**4114-4119.
208. **Barro M, Patton JT.** 2007. Rotavirus NSP1 Inhibits Expression of Type I Interferon by Antagonizing the Function of Interferon Regulatory Factors IRF3, IRF5, and IRF7. Journal of Virology **81:**4473-4481.
209. **Graff JW, Mitzel DN, Weisend CM, Flenniken ML, Hardy ME.** 2002. Interferon Regulatory Factor 3 Is a Cellular Partner of Rotavirus NSP1. Journal of Virology **76:**9545-9550.
210. **Symons JA, Alcamí A, Smith GL.** 1995. Vaccinia virus encodes a soluble type I interferon receptor of novel structure and broad species soecificity. Cell **81:**551-560.
211. **Horvath CM.** 2004. Weapons of STAT destruction. European Journal of Biochemistry **271:**4621-4628.
212. **Ramachandran A, Parisien J-P, Horvath CM.** 2008. STAT2 Is a Primary Target for Measles Virus V Protein-Mediated Alpha/Beta Interferon Signaling Inhibition. Journal of Virology **82:**8330-8338.
213. **Rodriguez JJ, Parisien J-P, Horvath CM.** 2002. Nipah Virus V Protein Evades Alpha and Gamma Interferons by Preventing STAT1 and STAT2 Activation and Nuclear Accumulation. Journal of Virology **76:**11476-11483.
214. **Bowie AG, Unterholzner L.** 2008. Viral evasion and subversion of pattern-recognition receptor signalling. Nature Reviews Immunology **8:**911-922.
215. **García-Sastre A, Biron CA.** 2006. Type 1 Interferons and the Virus-Host Relationship: A Lesson in Détente. Science **312:**879-882.
216. **Haller O, Kochs G, Weber F.** 2006. The interferon response circuit: induction and suppression by pathogenic viruses. Virology **344:**119-130.
217. **Haller O, Weber F.** 2007. Pathogenic Viruses: Smart Manipulators of the Interferon System, p. 315-334. *In* Pitha P (ed.), Interferon: The 50th Anniversary, vol. 316. Springer Berlin Heidelberg.
218. **Loo YM, Gale M, Jr.** 2007. Viral Regulation and Evasion of the Host Response, p. 295-313. *In* Pitha P (ed.), Interferon: The 50th Anniversary, vol. 316. Springer Berlin Heidelberg.

219. **Taylor KE, Mossman KL.** 2013. Recent advances in understanding viral evasion of type I interferon. Immunology **138:**190-197.
220. **Hayden MS, Ghosh S.** 2004. Signaling to NF-kappaB. Genes & Development **18:**2195-2224.
221. **Perkins ND.** 2007. Integrating cell-signalling pathways with NF-kappaB and IKK function. Nature reviews **8:**49-62.
222. **Hayden MS, Ghosh S.** 2012. NF-κB, the first quarter-century: remarkable progress and outstanding questions. Genes & Development **26:**203-234.
223. **Ghosh S, May MJ, Kopp EB.** 1998. NF-{kappa}B AND REL PROTEINS: Evolutionarily Conserved Mediators of Immune Responses. Annual Review of Immunology **16:**225-260.
224. **Senftleben U, Cao Y, Xiao G, Greten FR, Krähn G, Bonizzi G, Chen Y, Hu Y, Fong A, Sun S-C, Karin M.** 2001. Activation by IKKα of a Second, Evolutionary Conserved, NF-κB Signaling Pathway. Science **293:**1495-1499.
225. **Razani B, Reichardt AD, Cheng G.** 2011. Non-canonical NF-κB signaling activation and regulation: principles and perspectives. Immunological Reviews **244:**44-54.
226. **Moorthy AK, Savinova OV, Ho JQ, Wang VY, Vu D, Ghosh G.** 2006. The 20S proteasome processes NF-kappaB1 p105 into p50 in a translation-independent manner. EMBO Journal **25:**1945-1956.
227. **Cohen S, Lahav-Baratz S, Ciechanover A.** 2006. Two distinct ubiquitin-dependent mechanisms are involved in NF-kappaB p105 proteolysis. Biochemical and Biophysical Research Communications **345:**7-13.
228. **Coux O, Goldberg AL.** 1998. Enzymes catalyzing ubiquitination and proteolytic processing of the p105 precursor of nuclear factor kappaB1. Journal of Biological Chemistry **273:**8820-8828.
229. **Orian A, Whiteside S, Israel A, Stancovski I, Schwartz AL, Ciechanover A.** 1995. Ubiquitin-mediated processing of NF-kappa B transcriptional activator precursor p105. Reconstitution of a cell-free system and identification of the ubiquitin-carrier protein, E2, and a novel ubiquitin-protein ligase, E3, involved in conjugation. Journal of Biological Chemistry **270:**21707-21714.
230. **Palombella VJ, Rando OJ, Goldberg AL, Maniatis T.** 1994. The ubiquitin-proteasome pathway is required for processing the NF-kappa B1 precursor protein and the activation of NF-kappa B. Cell **78:**773-785.
231. **Kravtsova-Ivantsiv Y, Cohen S, Ciechanover A.** 2009. Modification by Single Ubiquitin Moieties Rather Than Polyubiquitination Is Sufficient for Proteasomal Processing of the p105 NF-κB Precursor. Molecular Cell **33:**496-504.
232. **Lin L, Ghosh S.** 1996. A glycine-rich region in NF-kappaB p105 functions as a processing signal for the generation of the p50 subunit. Molecular and Cellular Biology **16:**2248-2254.

233. **Orian A, Schwartz AL, Israel A, Whiteside S, Kahana C, Ciechanover A.** 1999. Structural motifs involved in ubiquitin-mediated processing of the NF-kappaB precursor p105: roles of the glycine-rich region and a downstream ubiquitination domain. Molecular and Cellular Biology **19:**3664-3673.
234. **Heissmeyer V, Krappmann D, Hatada EN, Scheidereit C.** 2001. Shared pathways of IkappaB kinase-induced SCF(betaTrCP)-mediated ubiquitination and degradation for the NF-kappaB precursor p105 and IkappaBalpha. Molecular and Cellular Biology **21:**1024-1035.
235. **Lang V, Janzen J, Fischer GZ, Soneji Y, Beinke S, Salmeron A, Allen H, Hay RT, Ben-Neriah Y, Ley SC.** 2003. betaTrCP-mediated proteolysis of NF-kappaB1 p105 requires phosphorylation of p105 serines 927 and 932. Molecular and Cellular Biology **23:**402-413.
236. **Cohen S, Achbert-Weiner H, Ciechanover A.** 2004. Dual effects of IkappaB kinase beta-mediated phosphorylation on p105 Fate: SCF(beta-TrCP)-dependent degradation and SCF(beta-TrCP)-independent processing. Molecular and Cellular Biology **24:**475-486.
237. **Liou HC, Nolan GP, Ghosh S, Fujita T, Baltimore D.** 1992. The NF-kappa B p50 precursor, p105, contains an internal I kappa B-like inhibitor that preferentially inhibits p50. EMBO Journal **11:**3003-3009.
238. **Hoberg JE, Yeung F, Mayo MW.** 2004. SMRT derepression by the IkappaB kinase alpha: a prerequisite to NF-kappaB transcription and survival. Molecular Cell **16:**245-255.
239. **Watanabe N, Iwamura T, Shinoda T, Fujita T.** 1997. Regulation of NFKB1 proteins by the candidate oncoprotein BCL-3: generation of NF-kappaB homodimers from the cytoplasmic pool of p50-p105 and nuclear translocation. EMBO Journal **16:**3609-3620.
240. **Motoyama M, Yamazaki S, Eto-Kimura A, Takeshige K, Muta T.** 2005. Positive and negative regulation of nuclear factor-kappaB-mediated transcription by IkappaB-zeta, an inducible nuclear protein. Journal of Biological Chemistry **280:**7444-7451.
241. **Huang WC, Ju TK, Hung MC, Chen CC.** 2007. Phosphorylation of CBP by IKKalpha promotes cell growth by switching the binding preference of CBP from p53 to NF-kappaB. Molecular Cell **26:**75-87.
242. **Ten RM, Paya CV, Israel N, Le Bail O, Mattei MG, Virelizier JL, Kourilsky P, Israel A.** 1992. The characterization of the promoter of the gene encoding the p50 subunit of NF-kappa B indicates that it participates in its own regulation. EMBO Journal **11:**195-203.
243. **Cogswell PC, Scheinman RI, Baldwin AS.** 1993. Promoter of the human NF-kappa B p50/p105 gene. Regulation by NF-kappa B subunits and by c-REL. The Journal of Immunology **150:**2794-2804.
244. **Bonizzi G, Karin M.** 2004. The two NF-κB activation pathways and their role in innate and adaptive immunity. Trends in Immunology **25:**280-288.

245. **Dinarello CA.** 2009. Immunological and Inflammatory Functions of the Interleukin-1 Family. Annual Review of Immunology **27:**519-550.
246. **Aggarwal BB.** 2000. Tumour necrosis factors receptor associated signalling molecules and their role in activation of apoptosis, JNK and NF-κB. Annals of the Rheumatic Diseases **59:**i6-i16.
247. **Wang L, Du F, Wang X.** 2008. TNF-α Induces Two Distinct Caspase-8 Activation Pathways. Cell **133:**693-703.
248. **Wang C-Y, Mayo MW, Korneluk RG, Goeddel DV, Baldwin AS.** 1998. NF-κB Antiapoptosis: Induction of TRAF1 and TRAF2 and c-IAP1 and c-IAP2 to Suppress Caspase-8 Activation. Science **281:**1680-1683.
249. **Neurath MF, Finotto S.** 2011. IL-6 signaling in autoimmunity, chronic inflammation and inflammation-associated cancer. Cytokine & Growth Factor Reviews **22:**83-89.
250. **Gerszten RE, Garcia-Zepeda EA, Lim Y-C, Yoshida M, Ding HA, Gimbrone MA, Luster AD, Luscinskas FW, Rosenzweig A.** 1999. MCP-1 and IL-8 trigger firm adhesion of monocytes to vascular endothelium under flow conditions. Nature **398:**718-723.
251. **Rot A, Krieger M, Brunner T, Bischoff SC, Schall TJ, Dahinden CA.** 1992. RANTES and macrophage inflammatory protein 1 alpha induce the migration and activation of normal human eosinophil granulocytes. The Journal of Experimental Medicine **176:**1489-1495.
252. **Schall TJ, Bacon K, Toy KJ, Goeddel DV.** 1990. Selective attraction of monocytes and T lymphocytes of the memory phenotype by cytokine RANTES. Nature **347:**669-671.
253. **Werner SL, Kearns JD, Zadorozhnaya V, Lynch C, O'Dea E, Boldin MP, Ma A, Baltimore D, Hoffmann A.** 2008. Encoding NF-kappaB temporal control in response to TNF: distinct roles for the negative regulators IkappaBalpha and A20. Genes & Development **22:**2093-2101.
254. **Wan F, Lenardo MJ.** 2010. The nuclear signaling of NF-kappaB: current knowledge, new insights, and future perspectives. Cell Research **20:**24-33.
255. **Krikos A, Laherty CD, Dixit VM.** 1992. Transcriptional activation of the tumor necrosis factor alpha-inducible zinc finger protein, A20, is mediated by kappa B elements. Journal of Biological Chemistry **267:**17971-17976.
256. **Boone DL, Turer EE, Lee EG, Ahmad R-C, Wheeler MT, Tsui C, Hurley P, Chien M, Chai S, Hitotsumatsu O, McNally E, Pickart C, Ma A.** 2004. The ubiquitin-modifying enzyme A20 is required for termination of Toll-like receptor responses. Nature Immunology **5:**1052-1060.
257. **Mauro C, Pacifico F, Lavorgna A, Mellone S, Iannetti A, Acquaviva R, Formisano S, Vito P, Leonardi A.** 2006. ABIN-1 Binds to NEMO/IKKγ and Co-operates with A20 in Inhibiting NF-κB. Journal of Biological Chemistry **281:**18482-18488.
258. **Wertz IE, O'Rourke KM, Zhou H, Eby M, Aravind L, Seshagiri S, Wu P, Wiesmann C, Baker R, Boone DL, Ma A, Koonin EV, Dixit VM.** 2004.

De-ubiquitination and ubiquitin ligase domains of A20 downregulate NF-[kappa]B signalling. Nature **430:**694-699.

259. **Bazzoni F, Rossato M, Fabbri M, Gaudiosi D, Mirolo M, Mori L, Tamassia N, Mantovani A, Cassatella MA, Locati M.** 2009. Induction and regulatory function of miR-9 in human monocytes and neutrophils exposed to proinflammatory signals. Proceedings of the National Academy of Sciences **106:**5282-5287.
260. **Guo LM, Pu Y, Han Z, Liu T, Li YX, Liu M, Li X, Tang H.** 2009. MicroRNA-9 inhibits ovarian cancer cell growth through regulation of NF-kappaB1. FEBS Journal **276:**5537-5546.
261. **Upton C, Macen JL, Schreiber M, McFaddeni G.** 1991. Myxoma virus expresses a secreted protein with homology to the tumor necrosis factor receptor gene family that contributes to viral virulence. Virology **184:**370-382.
262. **DiPerna G, Stack J, Bowie AG, Boyd A, Kotwal G, Zhang Z, Arvikar S, Latz E, Fitzgerald KA, Marshall WL.** 2004. Poxvirus Protein N1L Targets the I-κB Kinase Complex, Inhibits Signaling to NF-κB by the Tumor Necrosis Factor Superfamily of Receptors, and Inhibits NF-κB and IRF3 Signaling by Toll-like Receptors. Journal of Biological Chemistry **279:**36570-36578.
263. **Shisler JL, Jin X-L.** 2004. The Vaccinia Virus K1L Gene Product Inhibits Host NF-κB Activation by Preventing IκBα Degradation. Journal of Virology **78:**3553-3560.
264. **Kim JC, Lee SY, Kim SY, Kim JK, Kim HJ, Lee HM, Choi MS, Min JS, Kim MJ, Choi HS, Ahn JK.** 2008. HSV-1 ICP27 suppresses NF-κB activity by stabilizing IκBα. FEBS Letters **582:**2371-2376.
265. **Bour S, Perrin C, Akari H, Strebel K.** 2001. The Human Immunodeficiency Virus Type 1 Vpu Protein Inhibits NF-κB Activation by Interfering with βTrCP-mediated Degradation of IκB. Journal of Biological Chemistry **276:**15920-15928.
266. **Chang S-J, Hsiao J-C, Sonnberg S, Chiang C-T, Yang M-H, Tzou D-L, Mercer AA, Chang W.** 2009. Poxvirus Host Range Protein CP77 Contains an F-Box-Like Domain That Is Necessary To Suppress NF-κB Activation by Tumor Necrosis Factor Alpha but Is Independent of Its Host Range Function. Journal of Virology **83:**4140-4152.
267. **Mansur DS, Maluquer de Motes C, Unterholzner L, Sumner RP, Ferguson BJ, Ren H, Strnadova P, Bowie AG, Smith GL.** 2013. Poxvirus Targeting of E3 Ligase β-TrCP by Molecular Mimicry: A Mechanism to Inhibit NF-κB Activation and Promote Immune Evasion and Virulence. PLoS Pathogens **9:**e1003183.
268. **Graff JW, Ettayebi K, Hardy ME.** 2009. Rotavirus NSP1 Inhibits NFκB Activation by Inducing Proteasome-Dependent Degradation of β-TrCP: A Novel Mechanism of IFN Antagonism. PLoS Pathogens **5:**e1000280.

269. **Taylor SL, Frias-Staheli N, García-Sastre A, Schmaljohn CS.** 2009. Hantaan Virus Nucleocapsid Protein Binds to Importin α Proteins and Inhibits Tumor Necrosis Factor Alpha-Induced Activation of Nuclear Factor Kappa B. Journal of Virology **83:**1271-1279.
270. **Taylor SL, Krempel RL, Schmaljohn CS.** 2009. Inhibition of TNF-α-induced Activation of NF-κB by Hantavirus Nucleocapsid Proteins. Annals of the New York Academy of Sciences **1171:**E86-E93.
271. **Wilson JR, de Sessions PF, Leon MA, Scholle F.** 2008. West Nile Virus Nonstructural Protein 1 Inhibits TLR3 Signal Transduction. Journal of Virology **82:**8262-8271.
272. **Camus-Bouclainville C, Fiette L, Bouchiha S, Pignolet B, Counor D, Filipe C, Gelfi J, Messud-Petit F.** 2004. A Virulence Factor of Myxoma Virus Colocalizes with NF-κB in the Nucleus and Interferes with Inflammation. Journal of Virology **78:**2510-2516.
273. **Mohamed MR, Rahman MM, Lanchbury JS, Shattuck D, Neff C, Dufford M, van Buuren N, Fagan K, Barry M, Smith S, Damon I, McFadden G.** 2009. Proteomic screening of variola virus reveals a unique NF-κB inhibitor that is highly conserved among pathogenic orthopoxviruses. Proceedings of the National Academy of Sciences **106:**9045-9050.
274. **Mohamed MR, Rahman MM, Rice A, Moyer RW, Werden SJ, McFadden G.** 2009. Cowpox Virus Expresses a Novel Ankyrin Repeat NF-κB Inhibitor That Controls Inflammatory Cell Influx into Virus-Infected Tissues and Is Critical for Virus Pathogenesis. Journal of Virology **83:**9223-9236.
275. **Rahman MM, Mohamed MR, Kim M, Smallwood S, McFadden G.** 2009. Co-Regulation of NF-κB and Inflammasome-Mediated Inflammatory Responses by Myxoma Virus Pyrin Domain-Containing Protein M013. PLoS Pathogens **5:**e1000635.
276. **Weil R, Sirma H, Giannini C, Kremsdorf D, Bessia C, Dargemont C, Bréchot C, Israël A.** 1999. Direct Association and Nuclear Import of the Hepatitis B Virus X Protein with the NF-κB Inhibitor IκBα. Molecular and Cellular Biology **19:**6345-6354.
277. **Hiscott J, Kwon H, xE, nin P.** 2001. Hostile takeovers: viral appropriation of the NF-kB pathway. The Journal of Clinical Investigation **107:**143-151.
278. **Devergne O, Hatzivassiliou E, Izumi KM, Kaye KM, Kleijnen MF, Kieff E, Mosialos G.** 1996. Association of TRAF1, TRAF2, and TRAF3 with an Epstein-Barr virus LMP1 domain important for B-lymphocyte transformation: role in NF-kappaB activation. Molecular and Cellular Biology **16:**7098-7108.
279. **Mosialos G, Birkenbacht M, Yalamanchill R, Van Arsdale T, Ware C, Kleff E.** 1995. The Epstein-Barr virus transforming protein LMP1 engages signaling proteins for the tumor necrosis factor receptor family. Cell **80:**389-399.

280. **You L-R, Chen C-M, Lee Y-HW.** 1999. Hepatitis C Virus Core Protein Enhances NF-κB Signal Pathway Triggering by Lymphotoxin-β Receptor Ligand and Tumor Necrosis Factor Alpha. Journal of Virology **73:**1672-1681.
281. **Fiedler MA, Wernke-Dollries K.** 1999. Incomplete Regulation of NF-κB by IκBα during Respiratory Syncytial Virus Infection in A549 Cells. Journal of Virology **73:**4502-4507.
282. **Pahl HL.** 1999. Activators and target genes of Rel/NF-kappaB transcription factors. Oncogene **18:**6853-6866.
283. **Yurochko AD, Mayo MW, Poma EE, Baldwin AS, Huang ES.** 1997. Induction of the transcription factor Sp1 during human cytomegalovirus infection mediates upregulation of the p65 and p105/p50 NF-kappaB promoters. Journal of Virology **71:**4638-4648.
284. **Lee RC, Feinbaum RL, Ambros V.** 1993. The C. elegans heterochronic gene lin-4 encodes small RNAs with antisense complementarity to lin-14. Cell **75:**843-854.
285. **Han J, Lee Y, Yeom K-H, Nam J-W, Heo I, Rhee J-K, Sohn SY, Cho Y, Zhang B-T, Kim VN.** 2006. Molecular Basis for the Recognition of Primary microRNAs by the Drosha-DGCR8 Complex. Cell **125:**887-901.
286. **Khvorova A, Reynolds A, Jayasena SD.** 2003. Functional siRNAs and miRNAs Exhibit Strand Bias. Cell **115:**209-216.
287. **Schwarz DS, Hutvágner G, Du T, Xu Z, Aronin N, Zamore PD.** 2003. Asymmetry in the Assembly of the RNAi Enzyme Complex. Cell **115:**199-208.
288. **Rivas FV, Tolia NH, Song J-J, Aragon JP, Liu J, Hannon GJ, Joshua-Tor L.** 2005. Purified Argonaute2 and an siRNA form recombinant human RISC. Nature Structural & Molecular Biology **12:**340-349.
289. **Filipowicz W, Bhattacharyya SN, Sonenberg N.** 2008. Mechanisms of post-transcriptional regulation by microRNAs: are the answers in sight? Nature Reviews Genetics **9:**102-114.
290. **Wu L, Fan J, Belasco JG.** 2006. MicroRNAs direct rapid deadenylation of mRNA. Proceedings of the National Academy of Sciences of the United States of America **103:**4034-4039.
291. **Behm-Ansmant I, Rehwinkel J, Doerks T, Stark A, Bork P, Izaurralde E.** 2006. mRNA degradation by miRNAs and GW182 requires both CCR4:NOT deadenylase and DCP1:DCP2 decapping complexes. Genes & Development **20:**1885-1898.
292. **Pillai RS, Bhattacharyya SN, Filipowicz W.** 2007. Repression of protein synthesis by miRNAs: how many mechanisms? Trends in Cell Biology **17:**118-126.
293. **Pfeffer S, Zavolan M, Grässer FA, Chien M, Russo JJ, Ju J, John B, Enright AJ, Marks D, Sander C, Tuschl T.** 2004. Identification of Virus-Encoded MicroRNAs. Science **304:**734-736.

294. **Carl JW, Jr., Trgovcich J, Hannenhalli S.** 2013. Widespread evidence of viral miRNAs targeting host pathways. BMC Bioinformatics **14 Suppl 2:**S3.
295. **Grundhoff A, Sullivan CS.** 2011. Virus-encoded microRNAs. Virology **411:**325-343.
296. **Cullen BR.** 2013. MicroRNAs as mediators of viral evasion of the immune system. Nature Immunology **14:**205-210.
297. **Abend JR, Ramalingam D, Kieffer-Kwon P, Uldrick TS, Yarchoan R, Ziegelbauer JM.** 2012. Kaposi's Sarcoma-Associated Herpesvirus MicroRNAs Target IRAK1 and MYD88, Two Components of the Toll-Like Receptor/Interleukin-1R Signaling Cascade, To Reduce Inflammatory-Cytokine Expression. Journal of Virology **86:**11663-11674.
298. **O'Connell RM, Taganov KD, Boldin MP, Cheng G, Baltimore D.** 2007. MicroRNA-155 is induced during the macrophage inflammatory response. Proceedings of the National Academy of Sciences **104:**1604-1609.
299. **O'Connell RM, Rao DS, Chaudhuri AA, Boldin MP, Taganov KD, Nicoll J, Paquette RL, Baltimore D.** 2008. Sustained expression of microRNA-155 in hematopoietic stem cells causes a myeloproliferative disorder. The Journal of Experimental Medicine **205:**585-594.
300. **Gottwein E, Mukherjee N, Sachse C, Frenzel C, Majoros WH, Chi J-TA, Braich R, Manoharan M, Soutschek J, Ohler U, Cullen BR.** 2007. A viral microRNA functions as an orthologue of cellular miR-155. Nature **450:**1096-1099.
301. **Skalsky RL, Samols MA, Plaisance KB, Boss IW, Riva A, Lopez MC, Baker HV, Renne R.** 2007. Kaposi's Sarcoma-Associated Herpesvirus Encodes an Ortholog of miR-155. Journal of Virology **81:**12836-12845.
302. **Gatto G, Rossi A, Rossi D, Kroening S, Bonatti S, Mallardo M.** 2008. Epstein–Barr virus latent membrane protein 1 trans-activates miR-155 transcription through the NF-κB pathway. Nucleic Acids Research **36:**6608-6619.
303. **Linnstaedt SD, Gottwein E, Skalsky RL, Luftig MA, Cullen BR.** 2010. Virally Induced Cellular MicroRNA miR-155 Plays a Key Role in B-Cell Immortalization by Epstein-Barr Virus. Journal of Virology **84:**11670-11678.
304. **Chiang K, Liu H, Rice AP.** 2013. miR-132 enhances HIV-1 replication. Virology **438:**1-4.
305. **Jopling CL, Yi M, Lancaster AM, Lemon SM, Sarnow P.** 2005. Modulation of Hepatitis C Virus RNA Abundance by a Liver-Specific MicroRNA. Science **309:**1577-1581.
306. **Machlin ES, Sarnow P, Sagan SM.** 2011. Masking the 5′ terminal nucleotides of the hepatitis C virus genome by an unconventional microRNA-target RNA complex. Proceedings of the National Academy of Sciences **108:**3193-3198.
307. **Shimakami T, Yamane D, Jangra RK, Kempf BJ, Spaniel C, Barton DJ, Lemon SM.** 2012. Stabilization of hepatitis C virus RNA by an Ago2–miR-

122 complex. Proceedings of the National Academy of Sciences **109:**941-946.
308. **Li Y, Masaki T, Yamane D, McGivern DR, Lemon SM.** 2013. Competing and noncompeting activities of miR-122 and the 5′ exonuclease Xrn1 in regulation of hepatitis C virus replication. Proceedings of the National Academy of Sciences **110:**1881-1886.
309. **Buck AH, Perot J, Chisholm MA, Kumar DS, Tuddenham L, Cognat V, Marcinowski L, Dölken L, Pfeffer S.** 2010. Post-transcriptional regulation of miR-27 in murine cytomegalovirus infection. RNA **16:**307-315.
310. **Cazalla D, Yario T, Steitz JA.** 2010. Down-Regulation of a Host MicroRNA by a Herpesvirus saimiri Noncoding RNA. Science **328:**1563-1566.
311. **Backes S, Shapiro Jillian S, Sabin Leah R, Pham Alissa M, Reyes I, Moss B, Cherry S, tenOever Benjamin R.** 2012. Degradation of Host MicroRNAs by Poxvirus Poly(A) Polymerase Reveals Terminal RNA Methylation as a Protective Antiviral Mechanism. Cell Host & Microbe **12:**200-210.
312. **Lu S, Cullen BR.** 2004. Adenovirus VA1 Noncoding RNA Can Inhibit Small Interfering RNA and MicroRNA Biogenesis. Journal of Virology **78:**12868-12876.
313. **Andersson MG, Haasnoot PCJ, Xu N, Berenjian S, Berkhout B, Akusjärvi G.** 2005. Suppression of RNA Interference by Adenovirus Virus-Associated RNA. Journal of Virology **79:**9556-9565.
314. **Fabozzi G, Nabel CS, Dolan MA, Sullivan NJ.** 2011. Ebolavirus Proteins Suppress the Effects of Small Interfering RNA by Direct Interaction with the Mammalian RNA Interference Pathway. Journal of Virology **85:**2512-2523.
315. **Haasnoot J, de Vries W, Geutjes E-J, Prins M, de Haan P, Berkhout B.** 2007. The Ebola Virus VP35 Protein Is a Suppressor of RNA Silencing. PLoS Pathogens **3:**e86.
316. **Lin J, Cullen BR.** 2007. Analysis of the Interaction of Primate Retroviruses with the Human RNA Interference Machinery. Journal of Virology **81:**12218-12226.
317. **Holland B, Wong J, Li M, Rasheed S.** 2013. Identification of Human MicroRNA-Like Sequences Embedded within the Protein-Encoding Genes of the Human Immunodeficiency Virus. PLoS ONE **8:**e58586.
318. **Candiano G, Bruschi M, Musante L, Santucci L, Ghiggeri GM, Carnemolla B, Orecchia P, Zardi L, Righetti PG.** 2004. Blue silver: a very sensitive colloidal Coomassie G-250 staining for proteome analysis. Electrophoresis **25:**1327-1333.
319. **Spiegel M, Pichlmair A, Martinez-Sobrido L, Cros J, Garcia-Sastre A, Haller O, Weber F.** 2005. Inhibition of Beta interferon induction by severe acute respiratory syndrome coronavirus suggests a two-step model for

activation of interferon regulatory factor 3. Journal of Virology **79:**2079-2086.

320. **Kopecky-Bromberg SA, Martinez-Sobrido L, Frieman M, Baric RA, Palese P.** 2007. Severe acute respiratory syndrome coronavirus open reading frame (ORF) 3b, ORF 6, and nucleocapsid proteins function as interferon antagonists. Journal of Virology **81:**548-557.
321. **Frieman M, Yount B, Heise M, Kopecky-Bromberg SA, Palese P, Baric RS.** 2007. Severe Acute Respiratory Syndrome Coronavirus ORF6 Antagonizes STAT1 Function by Sequestering Nuclear Import Factors on the Rough Endoplasmic Reticulum/Golgi Membrane. Journal of Virology **81:**9812-9824.
322. **Minakshi R, Padhan K, Rani M, Khan N, Ahmad F, Jameel S.** 2009. The SARS Coronavirus 3a Protein Causes Endoplasmic Reticulum Stress and Induces Ligand-Independent Downregulation of the Type 1 Interferon Receptor. PLoS ONE **4:**e8342.
323. **Kamitani W, Narayanan K, Huang C, Lokugamage K, Ikegami T, Ito N, Kubo H, Makino S.** 2006. Severe acute respiratory syndrome coronavirus nsp1 protein suppresses host gene expression by promoting host mRNA degradation. Proceedings of the National Academy of Sciences **103:**12885-12890.
324. **Narayanan K, Huang C, Lokugamage K, Kamitani W, Ikegami T, Tseng CT, Makino S.** 2008. Severe acute respiratory syndrome coronavirus nsp1 suppresses host gene expression, including that of type I interferon, in infected cells. Journal of Virology **82:**4471-4479.
325. **Wathelet MG, Orr M, Frieman MB, Baric RS.** 2007. Severe acute respiratory syndrome coronavirus evades antiviral signaling: role of nsp1 and rational design of an attenuated strain. Journal of Virology **81:**11620-11633.
326. **Devaraj SG, Wang N, Chen Z, Chen Z, Tseng M, Barretto N, Lin R, Peters CJ, Tseng C-TK, Baker SC, Li K.** 2007. Regulation of IRF-3-dependent Innate Immunity by the Papain-like Protease Domain of the Severe Acute Respiratory Syndrome Coronavirus. Journal of Biological Chemistry **282:**32208-32221.
327. **Frieman M, Ratia K, Johnston RE, Mesecar AD, Baric RS.** 2009. Severe acute respiratory syndrome coronavirus papain-like protease ubiquitin-like domain and catalytic domain regulate antagonism of IRF3 and NF-kappaB signaling. Journal of Virology **83:**6689-6705.
328. **Siu K-L, Kok K-H, Ng M-HJ, Poon VKM, Yuen K-Y, Zheng B-J, Jin D-Y.** 2009. Severe Acute Respiratory Syndrome Coronavirus M Protein Inhibits Type I Interferon Production by Impeding the Formation of TRAF3·TANK·TBK1/IKKε Complex. Journal of Biological Chemistry **284:**16202-16209.
329. **Lu X, Pan Ja, Tao J, Guo D.** 2011. SARS-CoV nucleocapsid protein antagonizes IFN-β response by targeting initial step of IFN-β induction

pathway, and its C-terminal region is critical for the antagonism. Virus Genes **42:**37-45.

330. **Versteeg GA, Bredenbeek PJ, van den Worm SH, Spaan WJ.** 2007. Group 2 coronaviruses prevent immediate early interferon induction by protection of viral RNA from host cell recognition. Virology **361:**18-26.
331. **Koetzner CA, Kuo L, Goebel SJ, Dean AB, Parker MM, Masters PS.** 2010. Accessory Protein 5a Is a Major Antagonist of the Antiviral Action of Interferon against Murine Coronavirus. Journal of Virology **84:**8262-8274.
332. **Zheng D, Chen G, Guo B, Cheng G, Tang H.** 2008. PLP2, a potent deubiquitinase from murine hepatitis virus, strongly inhibits cellular type I interferon production. Cell Research **18:**1105-1113.
333. **Wang G, Chen G, Zheng D, Cheng G, Tang H.** 2011. PLP2 of Mouse Hepatitis Virus A59 (MHV-A59) Targets TBK1 to Negatively Regulate Cellular Type I Interferon Signaling Pathway. PLoS ONE **6:**e17192.
334. **Ye Y, Hauns K, Langland JO, Jacobs BL, Hogue BG.** 2007. Mouse hepatitis coronavirus A59 nucleocapsid protein is a type I interferon antagonist. Journal of Virology **81:**2554-2563.
335. **Funk CJ, Wang J, Ito Y, Travanty EA, Voelker DR, Holmes KV, Mason RJ.** 2012. Infection of human alveolar macrophages by human coronavirus strain 229E. Journal of General Virology **93:**494-503.
336. **Clementz MA, Chen Z, Banach BS, Wang Y, Sun L, Ratia K, Baez-Santos YM, Wang J, Takayama J, Ghosh AK, Li K, Mesecar AD, Baker SC.** 2010. Deubiquitinating and Interferon Antagonism Activities of Coronavirus Papain-Like Proteases. Journal of Virology **84:**4619-4629.
337. **Letchworth GJ, Rodriguez LL, Del cbarrera J.** 1999. Vesicular stomatitis. Vet J **157:**239-260.
338. **Johnson KM, Vogel JE, Peralta PH.** 1966. Clinical and Serological Response to Laboratory-Acquired Human Infection by Indiana Type Vesicular Stomatitis Virus (VSV). The American Journal of Tropical Medicine and Hygiene **15:**244-246.
339. **Flint S.J. LWE, V.R. Racaniello, and A.M. Skalka.** 2004. Principles of Virology: molecular biology, pathogenesis, and control of animal viruses., 2nd Edition ed. ASM Press, Washington D.C.
340. **Lichty BD, Power AT, Stojdl DF, Bell JC.** 2004. Vesicular stomatitis virus: re-inventing the bullet. Trends in molecular medicine **10:**210-216.
341. **Ferran MC, Lucas-Lenard JM.** 1997. The vesicular stomatitis virus matrix protein inhibits transcription from the human beta interferon promoter. Journal of Virology **71:**371-377.
342. **Faria PA, Chakraborty P, Levay A, Barber GN, Ezelle HJ, Enninga J, Arana C, van Deursen J, Fontoura BM.** 2005. VSV disrupts the Rae1/mrnp41 mRNA nuclear export pathway. Molecular cell **17:**93-102.
343. **Her LS, Lund E, Dahlberg JE.** 1997. Inhibition of Ran guanosine triphosphatase-dependent nuclear transport by the matrix protein of vesicular stomatitis virus. Science (New York, N.Y **276:**1845-1848.

344. **Petersen JM, Her LS, Varvel V, Lund E, Dahlberg JE.** 2000. The matrix protein of vesicular stomatitis virus inhibits nucleocytoplasmic transport when it is in the nucleus and associated with nuclear pore complexes. Molecular and Cellular Biology **20:**8590-8601.
345. **Coulon P, Deutsch V, Lafay F, Martinet-Edelist C, Wyers F, Herman RC, Flamand A.** 1990. Genetic evidence for multiple functions of the matrix protein of vesicular stomatitis virus. The Journal of general virology **71 (Pt 4):**991-996.
346. **Petersen JM, Her LS, Dahlberg JE.** 2001. Multiple vesiculoviral matrix proteins inhibit both nuclear export and import. Proceedings of the National Academy of Sciences of the United States of America **98:**8590-8595.
347. **Petersen JM, Her LS, Varvel V, Lund E, Dahlberg JE.** 2000. The matrix protein of vesicular stomatitis virus inhibits nucleocytoplasmic transport when it is in the nucleus and associated with nuclear pore complexes. Molecular and cellular biology **20:**8590-8601.
348. **Kim GN, Kang CY.** 2007. Matrix protein of VSV New Jersey serotype containing methionine to arginine substitutions at positions 48 and 51 allows near-normal host cell gene expression. Virology **357:**41-53.
349. **Stojdl DF, Lichty BD, tenOever BR, Paterson JM, Power AT, Knowles S, Marius R, Reynard J, Poliquin L, Atkins H, Brown EG, Durbin RK, Durbin JE, Hiscott J, Bell JC.** 2003. VSV strains with defects in their ability to shutdown innate immunity are potent systemic anti-cancer agents. Cancer Cell **4:**263-275.
350. **Lai F, Kazdhan N, Lichty BD.** 2008. Using G-deleted vesicular stomatitis virus to probe the innate anti-viral response. Journal of virological methods.
351. **Emeny JM, Morgan MJ.** 1979. Regulation of the Interferon System: Evidence that Vero Cells have a Genetic Defect in Interferon Production. Journal of General Virology **43:**247-252.
352. **Mosca JD, Pitha PM.** 1986. Transcriptional and posttranscriptional regulation of exogenous human beta interferon gene in simian cells defective in interferon synthesis. Molecular and Cellular Biology **6:**2279-2283.
353. **Kim O, Sun Y, Lai FW, Song C, Yoo D.** 2010. Modulation of type I interferon induction by porcine reproductive and respiratory syndrome virus and degradation of CREB-binding protein by non-structural protein 1 in MARC-145 and HeLa cells. Virology **402:**315-326.
354. **Luo R, Xiao S, Jiang Y, Jin H, Wang D, Liu M, Chen H, Fang L.** 2008. Porcine reproductive and respiratory syndrome virus (PRRSV) suppresses interferon-β production by interfering with the RIG-I signaling pathway. Molecular Immunology **45:**2839-2846.
355. **Patel D, Nan Y, Shen M, Ritthipichai K, Zhu X, Zhang Y-J.** 2010. Porcine Reproductive and Respiratory Syndrome Virus Inhibits Type I

Interferon Signaling by Blocking STAT1/STAT2 Nuclear Translocation. Journal of Virology **84:**11045-11055.

356. **Sagong M, Lee C.** 2011. Porcine reproductive and respiratory syndrome virus nucleocapsid protein modulates interferon-β production by inhibiting IRF3 activation in immortalized porcine alveolar macrophages. Archives of virology **156:**2187-2195.
357. **van Kasteren PB, Bailey-Elkin BA, James TW, Ninaber DK, Beugeling C, Khajehpour M, Snijder EJ, Mark BL, Kikkert M.** 2013. Deubiquitinase function of arterivirus papain-like protease 2 suppresses the innate immune response in infected host cells. Proceedings of the National Academy of Sciences **110:**E838-E847.
358. **Palosaari H, Parisien JP, Rodriguez JJ, Ulane CM, Horvath CM.** 2003. STAT protein interference and suppression of cytokine signal transduction by measles virus V protein. Journal of Virology **77:**7635-7644.
359. **Pfaller CK, Conzelmann KK.** 2008. Measles virus V protein is a decoy substrate for IkappaB kinase alpha and prevents Toll-like receptor 7/9-mediated interferon induction. Journal of Virology **82:**12365-12373.
360. **Takeuchi K, Kadota SI, Takeda M, Miyajima N, Nagata K.** 2003. Measles virus V protein blocks interferon (IFN)-alpha/beta but not IFN-gamma signaling by inhibiting STAT1 and STAT2 phosphorylation. FEBS Letters **545:**177-182.
361. **Yoneyama M, Kikuchi M, Natsukawa T, Shinobu N, Imaizumi T, Miyagishi M, Taira K, Akira S, Fujita T.** 2004. The RNA helicase RIG-I has an essential function in double-stranded RNA-induced innate antiviral responses. Nature Immunology **5:**730-737.
362. **Lin R, Heylbroeck C, Pitha PM, Hiscott J.** 1998. Virus-Dependent Phosphorylation of the IRF-3 Transcription Factor Regulates Nuclear Translocation, Transactivation Potential, and Proteasome-Mediated Degradation. Molecular and Cellular Biology **18:**2986-2996.
363. **Butash KA, Natarajan P, Young A, Fox DK.** 2000. Reexamination of the effect of endotoxin on cell proliferation and transfection efficiency. Biotechniques **29:**610-614, 616, 618-619.
364. **Weber M, Moller K, Welzeck M, Schorr J.** 1995. Short technical reports. Effects of lipopolysaccharide on transfection efficiency in eukaryotic cells. Biotechniques **19:**930-940.
365. **Chen IJ, Chou CC, Liu CL, Lee CC, Kan LS, Hou MH.** 2010. Crystallization and preliminary X-ray diffraction analysis of the N-terminal domain of human coronavirus OC43 nucleocapsid protein. Acta Crystallographica Section F Structural Biology and Crystallization Communications **66:**815-818.
366. **Chen IJ, Yuann J-MP, Chang Y-M, Lin S-Y, Zhao J, Perlman S, Shen Y-Y, Huang T-H, Hou M-H.** 2013. Crystal structure-based exploration of the important role of Arg106 in the RNA-binding domain of human

coronavirus OC43 nucleocapsid protein. Biochimica et Biophysica Acta (BBA) - Proteins and Proteomics.

367. **Chen CY, Chang CK, Chang YW, Sue SC, Bai HI, Riang L, Hsiao CD, Huang TH.** 2007. Structure of the SARS coronavirus nucleocapsid protein RNA-binding dimerization domain suggests a mechanism for helical packaging of viral RNA. Journal of Molecular Biology **368:**1075-1086.
368. **Chang C-k, Sue S-C, Yu T-h, Hsieh C-M, Tsai C-K, Chiang Y-C, Lee S-j, Hsiao H-h, Wu W-J, Chang W-L, Lin C-H, Huang T-h.** 2006. Modular organization of SARS coronavirus nucleocapsid protein. J Biomed Sci **13:**59-72.
369. **Dosch SF, Mahajan SD, Collins AR.** 2009. SARS coronavirus spike protein-induced innate immune response occurs via activation of the NF-kappaB pathway in human monocyte macrophages in vitro. Virus Research **142:**19-27.
370. **Wang W, Ye L, Ye L, Li B, Gao B, Zeng Y, Kong L, Fang X, Zheng H, Wu Z, She Y.** 2007. Up-regulation of IL-6 and TNF-α induced by SARS-coronavirus spike protein in murine macrophages via NF-κB pathway. Virus Research **128:**1-8.
371. **Fang X, Gao J, Zheng H, Li B, Kong L, Zhang Y, Wang W, Zeng Y, Ye L.** 2007. The membrane protein of SARS-CoV suppresses NF-kappaB activation. Journal of Medical Virology **79:**1431-1439.
372. **Law AH, Lee DC, Cheung BK, Yim HC, Lau AS.** 2007. Role for nonstructural protein 1 of severe acute respiratory syndrome coronavirus in chemokine dysregulation. Journal of Virology **81:**416-422.
373. **Kanzawa N, Nishigaki K, Hayashi T, Ishii Y, Furukawa S, Niiro A, Yasui F, Kohara M, Morita K, Matsushima K, Le MQ, Masuda T, Kannagi M.** 2006. Augmentation of chemokine production by severe acute respiratory syndrome coronavirus 3a/X1 and 7a/X4 proteins through NF-κB activation. FEBS Letters **580:**6807-6812.
374. **Eleouet J-F, Chilmonczyk S, Besnardeau L, Laude H.** 1998. Transmissible Gastroenteritis Coronavirus Induces Programmed Cell Death in Infected Cells through a Caspase-Dependent Pathway. Journal of Virology **72:**4918-4924.
375. **Yu D, Zhu H, Liu Y, Cao J, Zhang X.** 2009. Regulation of Proinflammatory Cytokine Expression in Primary Mouse Astrocytes by Coronavirus Infection. Journal of Virology **83:**12204-12214.
376. **Zhou H, Perlman S.** 2007. Mouse hepatitis virus does not induce Beta interferon synthesis and does not inhibit its induction by double-stranded RNA. Journal of Virology **81:**568-574.
377. **Liao QJ, Ye LB, Timani KA, Zeng YC, She YL, Ye L, Wu ZH.** 2005. Activation of NF-kappaB by the full-length nucleocapsid protein of the SARS coronavirus. Acta Biochim Biophys Sin (Shanghai) **37:**607-612.

378. **Zhang X, Wu K, Wang D, Yue X, Song D, Zhu Y, Wu J.** 2007. Nucleocapsid protein of SARS-CoV activates interleukin-6 expression through cellular transcription factor NF-kappaB. Virology **365:**324-335.
379. **Yan X, Hao Q, Mu Y, Timani KA, Ye L, Zhu Y, Wu J.** 2006. Nucleocapsid protein of SARS-CoV activates the expression of cyclooxygenase-2 by binding directly to regulatory elements for nuclear factor-kappa B and CCAAT/enhancer binding protein. International Journal of Biochemistry & Cell Biology **38:**1417-1428.
380. **He R, Leeson A, Andonov A, Li Y, Bastien N, Cao J, Osiowy C, Dobie F, Cutts T, Ballantine M, Li X.** 2003. Activation of AP-1 signal transduction pathway by SARS coronavirus nucleocapsid protein. Biochemical and Biophysical Research Communications **311:**870-876.
381. **Wan HY, Guo LM, Liu T, Liu M, Li X, Tang H.** 2010. Regulation of the transcription factor NF-kappaB1 by microRNA-9 in human gastric adenocarcinoma. Molecular Cancer **9:**16.
382. **Liu S, Kumar SM, Lu H, Liu A, Yang R, Pushparajan A, Guo W, Xu X.** 2012. MicroRNA-9 up-regulates E-cadherin through inhibition of NF-κB1–Snail1 pathway in melanoma. The Journal of Pathology **226:**61-72.
383. **Arora H, Qureshi R, Jin S, Park AK, Park WY.** 2011. miR-9 and let-7g enhance the sensitivity to ionizing radiation by suppression of NFkappaB1. Experimental and Molecular Medicine **43:**298-304.
384. **Aliprantis AO, Yang R-B, Mark MR, Suggett S, Devaux B, Radolf JD, Klimpel GR, Godowski P, Zychlinsky A.** 1999. Cell Activation and Apoptosis by Bacterial Lipoproteins Through Toll-like Receptor-2. Science **285:**736-739.
385. **Rahman MM, McFadden G.** 2011. Modulation of NF-kappaB signalling by microbial pathogens. Nature Reviews Microbiology **9:**291-306.
386. **Petropoulos L, Lin R, Hiscott J.** 1996. Human T Cell Leukemia Virus Type 1 Tax Protein Increases NF-κB Dimer Formation and Antagonizes the Inhibitory Activity of the IκBα Regulatory Protein. Virology **225:**52-64.
387. **Ning Z, Zheng Z, Hao W, Duan C, Li W, Wang Y, Li M, Luo S.** 2013. The N Terminus of Orf Virus-Encoded Protein 002 Inhibits Acetylation of NF-κB p65 by Preventing Ser²⁷⁶ Phosphorylation. PLoS ONE **8:**e58854.
388. **Yoo D, Wootton SK, Li G, Song C, Rowland RR.** 2003. Colocalization and interaction of the porcine arterivirus nucleocapsid protein with the small nucleolar RNA-associated protein fibrillarin. Journal of Virology **77:**12173-12183.
389. **Gantier MP.** 2010. New perspectives in MicroRNA regulation of innate immunity. Journal of Interferon & Cytokine Research **30:**283-289.
390. **O'Neill LA, Sheedy FJ, McCoy CE.** 2011. MicroRNAs: the fine-tuners of Toll-like receptor signalling. Nature Reviews Immunology **11:**163-175.
391. **Ambros V.** 2004. The functions of animal microRNAs. Nature **431:**350-355.

392. **Cologna R, Spagnolo JF, Hogue BG.** 2000. Identification of nucleocapsid binding sites within coronavirus-defective genomes. Virology **277:**235-249.
393. **St-Jean JR, Desforges M, Talbot PJ.** 2006. Genetic evolution of human coronavirus OC43 in neural cell culture. Advances in Experimental Medicine and Biology **581:**499-502.
394. **Cheng CS, Feldman KE, Lee J, Verma S, Huang DB, Huynh K, Chang M, Ponomarenko JV, Sun SC, Benedict CA, Ghosh G, Hoffmann A.** 2011. The specificity of innate immune responses is enforced by repression of interferon response elements by NF-kappaB p50. Science Signaling **4:**ra11.
395. **Law LMJ, Everitt JC, Beatch MD, Holmes CFB, Hobman TC.** 2003. Phosphorylation of Rubella Virus Capsid Regulates Its RNA Binding Activity and Virus Replication. Journal of Virology **77:**1764-1771.
396. **Ye Q, Krug RM, Tao YJ.** 2006. The mechanism by which influenza A virus nucleoprotein forms oligomers and binds RNA. Nature **444:**1078-1082.
397. **Santolini E, Migliaccio G, La Monica N.** 1994. Biosynthesis and biochemical properties of the hepatitis C virus core protein. Journal of Virology **68:**3631-3641.
398. **Phelps CB, Sengchanthalangsy LL, Malek S, Ghosh G.** 2000. Mechanism of κB DNA binding by Rel/NF-κB dimers. Journal of Biological Chemistry **275:**24392-24399.
399. **Lau SKP, Li KSM, Tsang AKL, Lam CSF, Ahmed S, Chen H, Chan K-H, Woo PCY, Yuen K-Y.** 2013. Genetic characterization of Betacoronavirus lineage C viruses in bats revealed marked sequence divergence in the spike protein of Pipistrellus bat coronavirus HKU5 in Japanese pipistrelle: implications on the origin of the novel Middle East Respiratory Syndrome Coronavirus. Journal of Virology.